2011

Evaluation of Effects of Super-Heavy Loading on the US 41 Bridge Over the White River

Ryan J. Sherman
Purdue University, rjsherma@purdue.edu

Joseph M. Mueller
Purdue University, jmmuelle@purdue.edu

Robert J. Connor
Purdue University, rconnor@purdue.edu

Mark D. Bowman
Purdue University, bowmanmd@purdue.edu

JOINT TRANSPORTATION RESEARCH PROGRAM

INDIANA DEPARTMENT OF TRANSPORTATION
AND PURDUE UNIVERSITY

EVALUATION OF EFFECTS OF SUPER-HEAVY LOADING ON THE US-41 BRIDGE OVER THE WHITE RIVER

Ryan J. Sherman
Graduate Research Assistant
School of Civil Engineering
Purdue University

Joseph M. Mueller
Field and Lab Engineer Technician
School of Civil Engineering
Purdue University

Robert J. Connor
Professor of Civil Engineering
Purdue University

Mark D. Bowman
Professor of Civil Engineering
Purdue University
Corresponding Author

SPR-3472
Report Number: FHWA/IN/JTRP-2011/15
DOI: 10.5703/1288284314645

This page intentionally left blank.

RECOMMENDED CITATION

Sherman, R. J., Mueller, J. M., Connor, R. J., Bowman, M. D. *Evaluation of Effects of Super-Heavy Loading on the US-41 Bridge over the White River*. Publication FHWA/IN/JTRP-2011/15. Joint Transportation Research Program, Indiana Department of Transportation and Purdue University, West Lafayette, Indiana, 2012. DOI: 10.5703/1288284314645

CORRESPONDING AUTHORS

Prof. Mark D. Bowman
School of Civil Engineering
Purdue University
(765) 494-2220
bowmanmd@purdue.edu

ACKNOWLEDGMENTS

This project was financially supported by the Indiana Department of Transportation (INDOT) in cooperation with Joint Transportation Research Program. Special thanks are extended to all individuals associated with both of these organizations for making this research possible. Thank you to all of the members of the project's Study Advisory Committee, including Bill Dittrich, Khalil Dughaish, Joe Gustin, Brian Harvey, Victor Hong, Tommy Nantung, and Robert Turner of the Indiana Department of Transportation, and Keith Hoernschemeyer of the FHWA for their guidance and input throughout the project. The experimental part of this study could not be possible without the help and assistance of several from the Vincennes District during the inspection, instrumentation, load testing, and continuous monitoring of the US-41 White River Bridge.

Finally, the authors would like to thank Civil Engineering graduate students Allen DeSchepper, Sorin Marcu and Jason Provines for their help. Without their assistance, the rapid instrumentation would not have been as successful as it was. Thank you also to Brian Santosuosso and his associates from WJE for their assistance during the rivet removal and inspection phase of the project.

This page intentionally left blank.

TECHNICAL REPORT STANDARD TITLE PAGE

1. Report No.	2. Government Accession No.	3. Recipient's Catalog No.
FHWA/IN/JTRP-2011/15		

4. Title and Subtitle	5. Report Date
Evaluation of Effects of Super-Heavy Loading on the US 41 Bridge Over the White River	2011
	6. Performing Organization Code

7. Author(s)	8. Performing Organization Report No.
Ryan J. Sherman , Joseph M. Mueller , Robert J. Connor , Mark D. Bowman	FHWA/IN/JTRP-2011/15

9. Performing Organization Name and Address	10. Work Unit No.
Joint Transportation Research Program Purdue University 550 Stadium Mall Drive West Lafayette, IN 47907-2051	
	11. Contract or Grant No. SPR-3472

12. Sponsoring Agency Name and Address	13. Type of Report and Period Covered
Indiana Department of Transportation State Office Building 100 North Senate Avenue Indianapolis, IN 46204	
	14. Sponsoring Agency Code

15. Supplementary Notes

Prepared in cooperation with the Indiana Department of Transportation and Federal Highway Administration.

16. Abstract

Built in 1958, the US-41 White River Bridge is a two-girder, riveted steel structure located in Hazelton, IN. The bridge is comprised of two, sixteen span superstructures sharing a common substructure. Each superstructure also contains four pin and hanger expansion joint assemblies. Over a period from August 2009 to August 2010 a series of nearly one hundred super-heavy loads ranging in weight from 200,000 lbs to up over 1,000,000 lbs crossed the northbound superstructure of the bridge. The loads were moved to support the construction of a new power plant facility located in Edwardsport, IN. It was unknown what effect this number of super-heavy loading events, over a relatively short period, would have on the long-term performance of the US-41 White River Bridge. Therefore, long-term remote monitoring was used to quantify any negative effects due to the series of superloads. Five primary tasks were undertaken as part of this study:

1. Perform controlled load testing to gain insight on the typical behavior of the bridge.
2. Monitor the effect of individual superloads on the bridge structure to detect any notable damage.
3. Perform an in-depth fracture evaluation.
4. Evaluate the effects of multiple super-heavy loading events on the bridge.
5. Collect stress range histograms to be used as part of a fatigue life evaluation.

The results of this study confirmed the US-41 White River Bridge is an excellent structure. The series of superloads had negligible long-term effects. Low material toughness was found during the material testing; however, based on the analysis performed, fracture is of little concern. Also, from the stress range histograms produced during the long-term monitoring, sufficient remaining fatigue life was calculated for all critical details. Thus, based on these results, only two actions items were suggested: 1.) Perform an in-depth inspection of the pin and hanger assemblies; and 2.) Lubricate all pin and hanger expansion joints.

17. Key Words	18. Distribution Statement
Superload, fatigue, fracture, remote monitoring, long-term monitoring	No restrictions. This document is available to the public through the National Technical Information Service, Springfield, VA 22161

19. Security Classif. (of this report)	20. Security Classif. (of this page)	21. No. of Pages	22. Price
Unclassified	Unclassified		

Form DOT F 1700.7 (8-69)

This page intentionally left blank.

EXECUTIVE SUMMARY

EVALUATION OF EFFECTS OF SUPER-HEAVY LOADING ON THE US-41 BRIDGE OVER THE WHITE RIVER

Introduction

Built in 1958, the US-41 White River Bridge is a two-girder, riveted steel structure located near Hazelton, IN. The bridge is comprised of two, sixteen span superstructures sharing a common substructure. Each superstructure also contains four pin and hanger expansion joint assemblies. Over a period from August 2009 to August 2010 a series of nearly one hundred super-heavy loads ranging in weight from 200,000 lbs. to up over 1,000,000 lbs. crossed the northbound superstructure of the bridge. The loads were moved to support the construction of a new power plant facility located in Edwardsport, IN. It was unknown what effect this number of super-heavy loading events, over a relatively short period, would have on the long-term performance of the US-41 White River Bridge. Therefore, long-term remote monitoring was used to quantify any negative effects due to the series of superloads. Five primary tasks were undertaken as part of this study:

1. Perform controlled load testing to gain insight on the typical behavior of the bridge.
2. Monitor the effect of individual superloads on the bridge structure to detect any notable damage.
3. Perform an in-depth fracture evaluation.
4. Evaluate the effects of multiple super-heavy loading events on the bridge.
5. Collect stress range histograms to be used as part of a fatigue life evaluation.

Findings

The results presented in this report show the following:

- The series of superloads had negligible long-term negative effects on the bridge.
- The CVN test results indicated the bridge material has very low fracture toughness.
- Fracture is unlikely to occur based on the in-depth fracture evaluation.
- If one of the components of the built-up member fractured, there is sufficient reserve capacity in the remaining components to carry the increase in stress.
- Sufficient remaining fatigue life was calculated for all critical details.

Implementation

Based on the results of the study, only two actions items were suggested: 1.) Perform an in-depth inspection of the pin and hanger assemblies; and 2.) Lubricate all pin and hanger expansion joints. This study was not able to evaluate the pins of these joints directly; therefore, an in-depth inspection of the pins by a qualified inspector is advisable in response to this series of super-heavy loadings. Also, during the long-term monitoring, bending was measured in the four hangers instrumented; thus, lubricating the joints should allow for better movement and in turn less bending.

Results of the fatigue evaluation indicated sufficient remaining fatigue life for all critical details. This was largely due to the low live load stress ranges measured during normal daily traffic. Similar monitoring could be performed on other bridges to accurately establish their remaining fatigue life. This is especially true for those bridges currently showing a finite or negative fatigue life. Accurately quantifying the live load stress range of these bridges will not only provide for a much more accurate estimation of the remaining fatigue life but may show many of these bridge have very low live load stresses resulting in infinite or at a minimum sufficient remaining life.

CONTENTS

LIST OF TABLES

LIST OF FIGURES

Figure 1.1: Aerial view of bridge area from Google Maps

1. INTRODUCTION

1.1 Bridge Description

Built in 1958, Bridge 41-26-03917E (NBI#14560) is comprised of two, sixteen span, two-girder riveted superstructures sharing a single substructure. Each superstructure carries two lanes of either northbound or southbound US-41 traffic over the White River and adjacent north and south floodplains. The bridge is located near Hazleton, IN. Figure 1.1 shows an aerial view taken from Google Maps of the bridge and surrounding area. The US-41 White River Bridge is symmetric about its midpoint and has a total length of 2403 feet. The sixteen spans of each superstructure consist of equal end spans of 111 feet 3 inches and fourteen interior spans of 155 feet 9 inches. Both superstructures have a width of 32 feet 6 inches. The bridge also has four pin and hanger expansion joints spread throughout the length. Photographs of the bridge are included below. Figure 1.2 shows a partial elevation of the northbound bridge and Figure 1.3 shows the underside of the superstructure and the shared substructure.

1.2 Objective

Approximately 100 super-heavy loads ranging in weight from 200,000 lbs. up to over 1,000,000 lbs. crossed the US-41 White River Bridge in a period from August 2009 to August 2010. These loads were moved to support the construction of a new power plant facility in Edwardsport, IN. The objective of this study was to assess the effects of this series of super-heavy loads on the US-41 White River Bridge. Specifically, the goal was to ensure the loads had no negative effects on the overall bridge performance. This was

Figure 1.2: Elevation view of the northern half of the US-41 White River Bridge

Figure 1.3: View of twin structures looking north

accomplished through remote long-term monitoring of the structure. Critical details were identified and instrumented with strain gages to measure stress ranges and maximum stress events due to the heavy loading. Strain gage locations were specifically selected to capture the maximum response of the bridge to the superloads. Additionally, controlled load testing was performed to gain insight on the typical response of the bridge and rainflow cycle counting was performed to construct histograms used in a fatigue analysis of the structure. All field work and strain gage monitoring was conducted over the period between August 2009 and August 2010 by personnel from the Bowen Laboratory at Purdue University, West Lafayette, IN. It should also be noted that the maximum bridge deflections during the larger superloads were measured by surveyors from Bernardin, Lochmueller & Associates (BLA). These deflections were included during inspection reports submitted by BLA.

2. INSTRUMENTATION PLAN AND DATA ACQUISITION

On the week of August 16, 2009 long-term monitoring instrumentation was installed by the Purdue Research Team on the US-41 White River Bridge. Instrumentation was solely focused on the northbound superstructure. The primary intent of the monitoring was to capture live load stress ranges in predetermined areas of interest. These areas included the main girders, floor beams, stringers, cross-bracing, and pin and hanger assemblies. Using the live load stress measurements it could be determined if the bridge was experiencing any negative effects from the passage of multiple super-heavy loads. Additionally, stress ranges were used to evaluate the fatigue performance of the structure and to estimate the remaining fatigue life.

2.1 Instrumentation and Data Acquisition

In order to monitor the live load stress ranges remotely over an extended period of time, various instrumentation and data acquisition equipment is required. The following section briefly describes the key components of the long-term monitoring system used on the US-41 White River Bridge.

2.1.1 Strain Gages

Strain gages were installed to understand both the local response of specific details as well as the global response of the entire bridge. The particular strain gages used were produced by Vishay Micro-Measurements model LWK-06-W250B-350 with an active grid length of 0.25 inches and a resistance of 350 ohms. These are uni-axial weldable resistance-type strain gages and were selected to be used at this site for their ease of installation in the field. The selected strain gages are also temperature compensated for use on structural steel and perform very well when accurate strain measurements are required over long periods of time (anywhere from months to years). Additionally, an excitation voltage of 10 volts was used for the strain gages at the site.

The strain gages come pre-bonded to a metal strip by the manufacturer. To attach them to the component in the field, numerous pinprick sized resistance spot welds are used. The spot welds pose no concern with respect

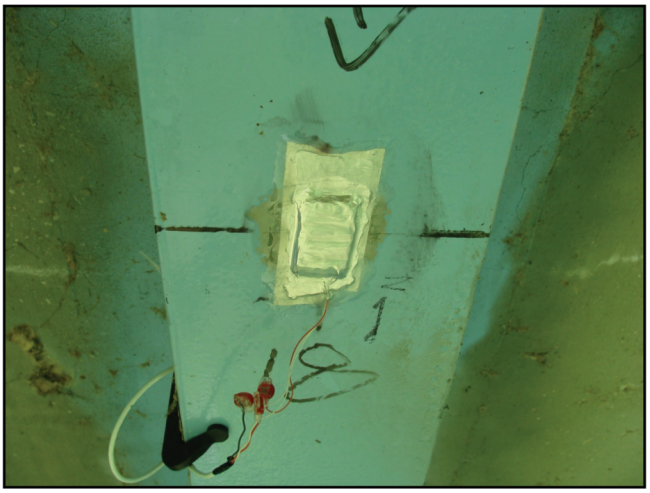

Figure 2.1: Installed strain gage

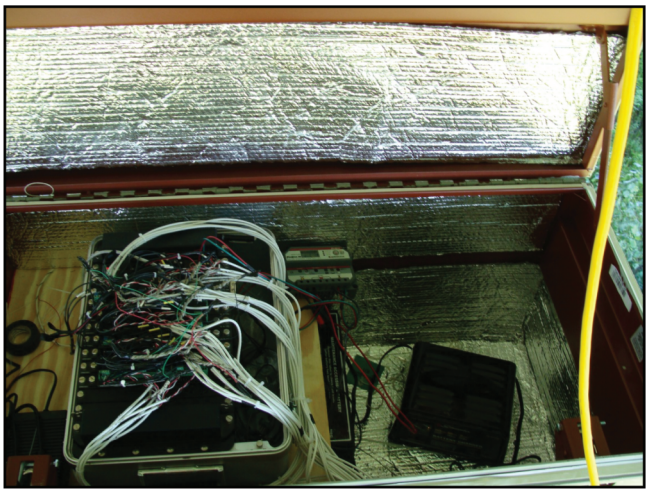

Figure 2.2: Data acquisition equipment

to fatigue. To prepare the surface for installation the base metal is ground smooth and cleaned with degreaser. The final step in the installation process involves covering the strain gage with a proven multi-layer weatherproofing system to protect it against the extreme outdoor conditions. Figure 2.1 shows the final condition of the strain gage after installation and sealing.

2.1.2 Data Acquisition

The data acquisition system used on the US-41 White River Bridge was very straight forward consisting of only a data logger, modem, and antenna. A Campbell Scientific CR9000X data logger was used to collect the data throughout the duration of the remote monitoring. The CR9000X is a high-speed, multi-channel, 16-bit system that uses analog and digital filters to guarantee noise free signals. An attractive feature of the CR9000X is its ease of programming, making it a very flexible platform that is easily adapted to a specific experiment. Another notable aspect is the ability of the data logger to develop stress-range histograms using the rainflow cycle counting method. Lastly, the CR9000X has the capability for live data viewing allowing the Research Team to quickly give data a preliminary review for any standout observations.

To communicate with the CR9000X a high-speed cellular modem was used. The modem used onsite was an 882-EVDO CDMA Data Modem and IP Router, manufactured by CalAmp/LandCell. This particular modem is an external 3G cellular broadband router with an integrated DHCP server as well as port forwarding and port mapping capabilities. The high-speed cellular modem installed served several purposes. The first of which is to retrieve data remotely. Data are initially collected locally and stored onsite. Then using specialized software installed on a server residing at Purdue University the data are automatically downloaded at a predefined interval. The second purpose of the cellular modem is to view live data in real time. This allows the Research Team to verify that the monitoring system is still functional as well as remotely view any live events. One final attractive feature of the cellular modem is the ability to reprogram the data logger remotely through the cellular connection. This allows the Research Team to update and change the program based on the review of prior data. Figure 2.2 shows the data acquisition equipment that was used on site.

All of the required equipment was enclosed in a weather-tight steel box that was installed on top of Pier 13. Even though the box was on top of the pier it was still locked to prevent anyone from tampering with the data acquisition equipment. Figure 2.3 shows the weather-tight enclosure. It should also be noted that power was supplied by a new service drop installed in the early going of the project. Prior to the installation of the permanent power the data acquisition system was powered by generators when the Research Team was onsite.

Figure 2.3: Weather-tight enclosure

Figure 2.4: Video camera installation

2.1.3 Video Recording

The Research Team has been experimenting with video recording to help verify that the information recorded by the data logger was actually caused by a real truck and not noise. Video recording also permits for the accurate identification of the configuration, position, and the number of trucks that produced a given response. Thus, a video camera was installed on the parapet above Pier 13 in a weather-tight enclosure that is heated and cooled as necessary. Figure 2.4 depicts of the video camera installation. The camera was programmed to start recording at the same trigger levels as the data logger. Once triggered, the video camera captures images for several seconds before and after an event. Aside from recording triggered video, the camera can be controlled remotely and take still images.

2.2 Summary of Instrumentation Layout

Two types of tests were performed during the monitoring of the US-41 White River Bridge: controlled load testing and in-service long-term monitoring (this includes the effects of the super-heavy loads). Similar instrumentation plans were used for both types of tests. The controlled load test utilized all forty-eight (48) strain gages originally installed on the bridge. After reviewing the controlled load test data, the original forty-eight (48) strain gages was reduced to twenty-four (24) strain gages for long-term monitoring. The following section summarizes the instrumentation plan that was implemented on the US-41 White River Bridge for both sets of tests. These sections are only intended as a brief summary of the key locations. A detailed as-built instrumentation plan is provided in Appendix A for further review.

2.2.1 Strain Gages on Main Girders

During the original installation, twelve (12) strain gages were installed on the northbound main girders, Girder G1 (west main girder) and Girder G2 (east main girder). The main girder strain gages were installed in sets (top and bottom); thus, a total of six main girder locations were instrumented. These locations included the location of maximum positive moment, dead load inflection point, and location of maximum negative moment. Table 2.1 is a summary of the main girder strain gages detailing the specific location of each channel. The table also indicates the tests for which the strain gages were used.

The goal of the Research Team was to install the strain gages at the extreme-most fiber of the element. Thus, for the main girder this typically resulted in the strain gages being placed on the bottom of the bottom flange cover plate and bottom of the top flange angle. Due to the concrete deck being in contact with the top of the top flange cover plate, the strain gages had to be placed on the bottom of the angle. Also, it is worth mentioning that the strain gages were installed as close to the centerline of the element as was permitted. For the bottom strain gage this was right on the centerline; however, the top strain gage typically was a few inches off of the web. Figure 2.5 and Figure 2.6 are photographs of typical main girder bottom and top strain gage locations, respectively.

TABLE 2.1:
Main girder strain gage summary

		Location		
Channel	Girder	Global	Local	Test(s)
CH_1	G2	Maximum positive moment Span N	Top	Controlled load tests
CH_2	G2	Maximum positive moment Span N	Bottom	Controlled load tests/Long-term monitoring
CH_3	G2	Inflection point Span N	Top	Controlled load tests
CH_4	G2	Inflection point Span N	Bottom	Controlled load tests/Long-term monitoring
CH_5	G2	Maximum negative moment near Pier 13	Top	Controlled load tests/Long-term monitoring
CH_6	G2	Maximum negative moment near Pier 13	Bottom	Controlled load tests/Long-term monitoring
CH_11	G1	Maximum negative moment near Pier 13	Top	Controlled load tests
CH_12	G1	Maximum negative moment near Pier 13	Bottom	Controlled load tests/Long-term monitoring
CH_23	G2	Maximum positive moment Span P	Top	Controlled load tests
CH_24	G2	Maximum positive moment Span P	Bottom	Controlled load tests/Long-term monitoring
CH_25	G1	Maximum positive moment Span P	Top	Controlled load tests
CH_26	G1	Maximum positive moment Span P	Bottom	Controlled load tests/Long-term monitoring

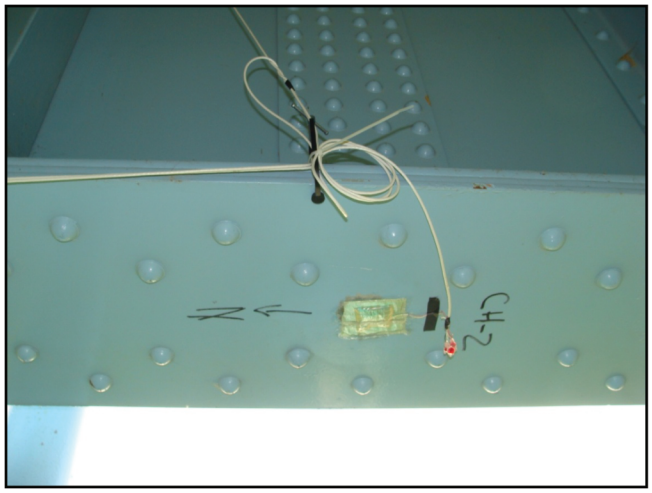

Figure 2.5: Typical main girder bottom flange strain gage location

2.2.2 Strain Gages on Floor Beams

A total of six (6) strain gages were installed on floor beams throughout the US-41 White River Bridge. Floor beam strain gages were installed in top and bottom sets; therefore, a total of three locations were instrumented. Areas of interest on the floor beams included the locations of both maximum positive moment and maximum negative moment. It should also be noted that a total of eight different floor beam geometries were used on the US-41 White River Bridge. Only two of eight most common floor beams were selected for instrumentation. Table 2.2 is a summary of the floor beam strain gages. Included in the table are the location of each strain gage and a summary of tests for which each strain gage was used. Also, photographs of typical maximum positive and negative moment locations can be seen in Figure 2.7.

All the floor beam strain gages were installed at the extreme-most fiber possible in an attempt to capture the greatest response possible. Unlike the main girders, the top of the top flange was accessible on the floor beams; thus, the strain gages could be installed on the top and bottom of the upper and lower flanges respectively. However, as the floor beams are built-up sections the strain gages could not be placed perfectly on the centerline of the section. Thus, the strain gages were slightly offset from center. Figure 2.8 is a photograph of a typical floor beam strain gage installation.

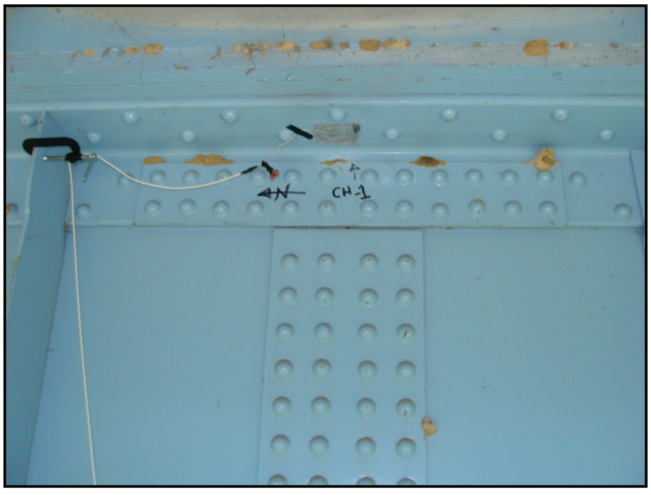

Figure 2.6: Typical main girder top flange strain gage location

TABLE 2.2:
Floor beam strain gage summary

		Location		
Channel	Floor Beam	Global	Local	Test(s)
CH_7	Over Pier 13 (FB-3)	Maximum negative moment	Top	Controlled load tests
CH_8	Over Pier 13 (FB-3)	Maximum negative moment	Bottom	Controlled load tests
CH_9	Over Pier 13 (FB-3)	Maximum positive moment	Top	Controlled load tests
CH_10	Over Pier 13 (FB-3)	Maximum positive moment	Bottom	Controlled load tests/ Long-term monitoring
CH_21	3rd FB north of hanger (FB-2)	Maximum positive moment	Top	Controlled load tests
CH_22	3rd FB north of hanger (FB-2)	Maximum positive moment	Bottom	Controlled load tests/ Long-term monitoring

2.2.3 Strain Gages on Stringers

A total of ten (10) strain gages were installed on stringers throughout the US-41 White River Bridge. Like the main girders and floor beams, the stringer strain gages were installed as top and bottom sets. Thus, five stringer locations were instrumented. These five sets of strain gages include locations of maximum positive moment and locations of maximum negative moment. Table 2.3 is a summary of the stringer strain gage locations as well as the tests for which each strain gage was used. Also, photographs of typical positive and negative moment locations are included in Figure 2.9 and Figure 2.10, respectively. As can be seen in the figures, the location of the top strain gages of the stringers is similar to those of the main girder. Due to the top of the stringer being in contact with the deck, the upper strain gages must be attached on the underside of the top flange.

2.2.4 Strain Gages on Pin and Hangers

The pin and hanger assemblies were of great interest during this study. Historically, problems have occurred in other bridges when the pin and hanger elements seize up as a result of corrosion. The fixity that results from the corrosion can introduce bi-axial bending that was

Figure 2.7: Floor beam over Pier 13 maximum positive and negative moment locations

not accounted for during the original design. In some cases, this bi-axial bending has led to the development of fatigue cracks. Thus, sixteen (16) strain gages were installed on four hangers to determine if bi-axial bending is present in the pin and hanger assemblies. One of the four hangers (east hanger Girder G2) was heavily instrumented with eight strain gages. This hanger had gages installed on the sides of the hanger (top, middle and bottom) and on the face of the hanger (centerline). The location of these gages can be seen in Figure 2.11. *(Note: some of the strain gages in the photograph were moved due to a preliminary data review during the installation. Please consult the as-built instrumentation plans attached in the appendices for final strain gage locations.)* The remaining four hangers had either two or four strain gages each. Table 2.4 is a summary of the pin and hanger strain gages including the tests for which each strain gage was used.

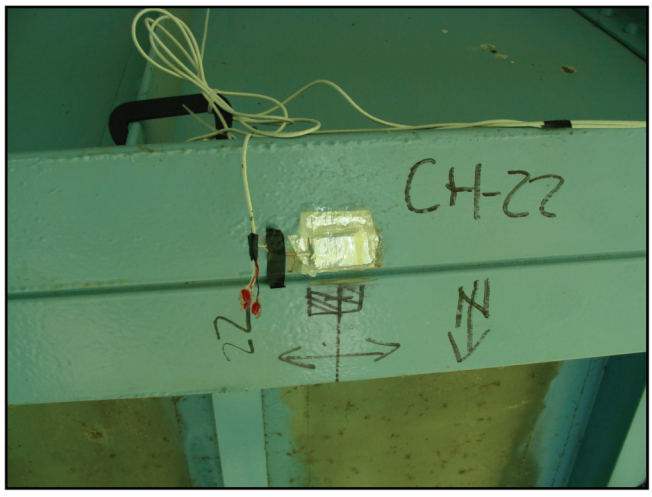

Figure 2.8: Typical strain gage location on a floor beam

2.2.5 Strain Gages on Cross-Bracing

Strain gages were also installed on the cross-bracing of the US-41 White River Bridge. Only one set of cross-bracing was instrumented. A total of four (4) strain gages were used at this location. The cross-bracing is made from WT sections. Two of the strain gages were placed back-to-back on the web of the WT section near the gusset plate connection. The remaining two strain gages were installed on the bottom side of the flange of the WT section. These were installed in the same vertical plane as the web strain gages. Figure 2.12 is a photograph of the cross-bracing flange strain gages. Table 2.5 is a summary of the cross-bracing strain gages including the tests for which each channel was used.

2.3 Remote Long-Term Monitoring

Two types of data were collected during the remote long-term monitoring period of the US-41 White River Bridge. These included triggered data and stress-range histograms. What follows is a brief description of both types of data.

2.3.1 Triggered Data

To limit the amount of data collected and transmitted, time-history data was not recorded continuously for the duration of monitoring. Rather, trigger events were used to start and stop data collection. The trigger events were based on predefined stress levels measured in the bottom flange of the main girder at the midspan of Span P. When this strain gage exceeded the

TABLE 2.3:
Stringer strain gage summary

Channel	Stringer	Location		Test(s)
		Global	Local	
CH_13	Center stringer Over Pier 13	Maximum negative moment	Top	Controlled load tests/Long-term monitoring
CH_14	Center stringer Over Pier 13	Maximum negative moment	Bottom	Controlled load tests/Long-term monitoring
CH_15	East stringer Simple span	Maximum positive moment	Bottom	Controlled load tests/Long-term monitoring
CH_16	East stringer Simple span	Maximum positive moment	Top	Controlled load tests/Long-term monitoring
CH_17	East stringer 0.4 point	Maximum positive moment	Top	Controlled load tests/Long-term monitoring
CH_18	East stringer 0.4 point	Maximum positive moment	Bottom	Controlled load tests/Long-term monitoring
CH_19	East stringer 0.4 point	Maximum negative moment	Top	Controlled load tests
CH_20	East stringer 0.4 point	Maximum negative moment	Bottom	Controlled load tests
CH_27	Center stringer 4th FB north of hanger	Maximum negative moment	Top	Controlled load tests
CH_28	Center stringer 4th FB north of hanger	Maximum negative moment	Bottom	Controlled load tests/ Long-term monitoring

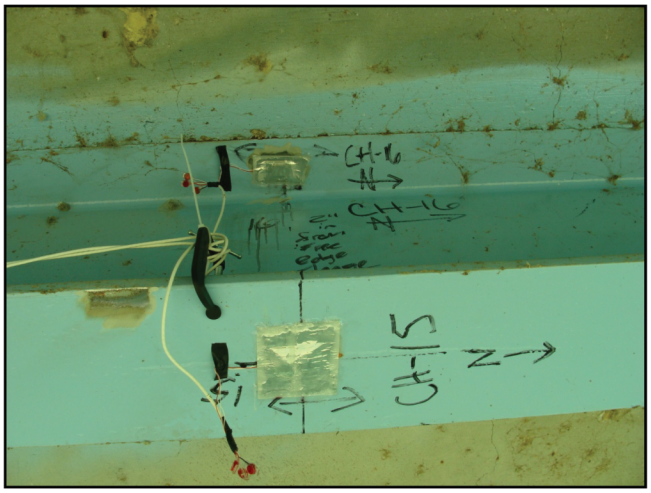

Figure 2.9: Typical positive moment stringer strain gage location

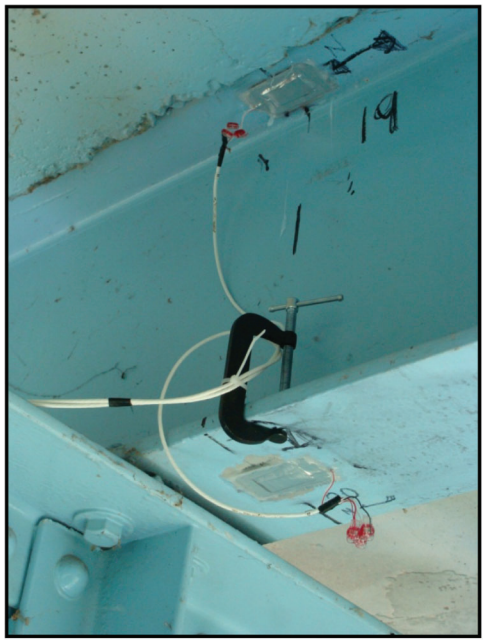

Figure 2.10: Typical negative moment stringer strain gage location

predefined strain level, data was recorded for a defined period of time before and after the trigger event.

The data logger was programmed with two separate triggers. The first, and more common, trigger captured a heavily loaded truck found in normal day-to-day traffic. This trigger value was set at a stress level of 1.8 ksi and recorded for four seconds before and after the event. The second trigger was intended to capture the super-heavy loads. This trigger value was set at a stress of 4.0 ksi and recorded data 160 seconds before the event and 180 seconds after an event. All trigger durations were set such that an entire loading event

Figure 2.11: East pin and hanger on G2

TABLE 2.4:
Pin and hanger strain gage summary

Channel	Girder	Face	Test(s)
CH_29	G2	East	Controlled load tests/Long-term monitoring
CH_30	G2	East	Controlled load tests
CH_31	G2	East	Controlled load tests/Long-term monitoring
CH_32	G2	East	Controlled load tests/Long-term monitoring
CH_33	G2	East	Controlled load tests
CH_34	G2	East	Controlled load tests/Long-term monitoring
CH_35	G2	East	Controlled load tests
CH_36	G2	East	Controlled load tests
CH_37	G2	West	Controlled load tests
CH_38	G2	West	Controlled load tests/Long-term monitoring
CH_39	G1	East	Controlled load tests
CH_40	G1	East	Controlled load tests
CH_41	G1	West	Controlled load tests
CH_42	G1	West	Controlled load tests
CH_43	G1	West	Controlled load tests/Long-term monitoring
CH_44	G1	West	Controlled load tests/Long-term monitoring

could be seen in the data. These durations as well as stress levels were established by the Research Team based on a preliminary review of data collected during the start of the long-term monitoring.

2.3.2 Stress-Range Histograms

Stress-range histograms were generated by the data logger using a rainflow cycle counting algorithm for the remaining twenty-four strain gages after the controlled load testing. The rainflow cycle counting algorithm was programmed to place all cycles from selected channels in equally divided 0.5 ksi bins. The exception to the 0.5 ksi bin size is the first bin which holds cycles between 0.25 ksi and 0.5 ksi. Cycles less than the 0.25 ksi thresholds were neglected in the bin counts. The histograms were used in the fatigue analysis of the US-41 White River Bridge.

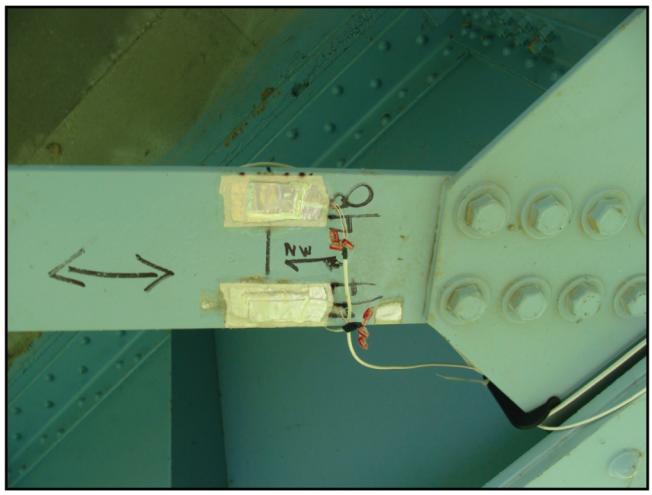

Figure 2.12: Cross-bracing bottom flange strain gages

TABLE 2.5:
Cross-bracing strain gage summary

Channel	Location	Direction	Test(s)
CH_45	Web	South	Controlled load tests
CH_46	Web	North	Controlled load tests
CH_47	Bottom Flange	South	Controlled load tests
CH_48	Bottom Flange	North	Controlled load tests/Long-term monitoring

3. CONTROLLED LOAD TESTING

A series of controlled load tests were conducted to verify measurements obtained during in-service testing and to determine the specific areas of the US-41 White River Bridge of greatest interest for long-term monitoring. The controlled tests were performed using four loaded tandem axle plow trucks provided by INDOT of known load and geometry. These tests were conducted on the morning of Tuesday November 24, 2009. Testing began shortly after the morning rush hour and was completed in approximately one hour. This was done to limit the impact on US-41 traffic as both of the northbound lanes of the US-41 White River Bridge were closed periodically throughout the controlled load testing.

3.1 Test Trucks

INDOT provided the Research Team with four loaded tandem axle plow trucks for the controlled load testing. Figure 3.1 is an example photograph of one of the trucks used for testing. Three of the four trucks provided were identical while the fourth had different axle spacing than the rest. Figure 3.2 through Figure 3.5 are drawings detailing the geometry, weight, and number for each truck. All weights and measurements were provided to the Research Team courtesy of INDOT on the day of testing.

3.2 Static Tests

A series of four park tests were performed for the static testing portion of the controlled load tests. All four plow

Figure 3.1: Example truck used for controlled load testing

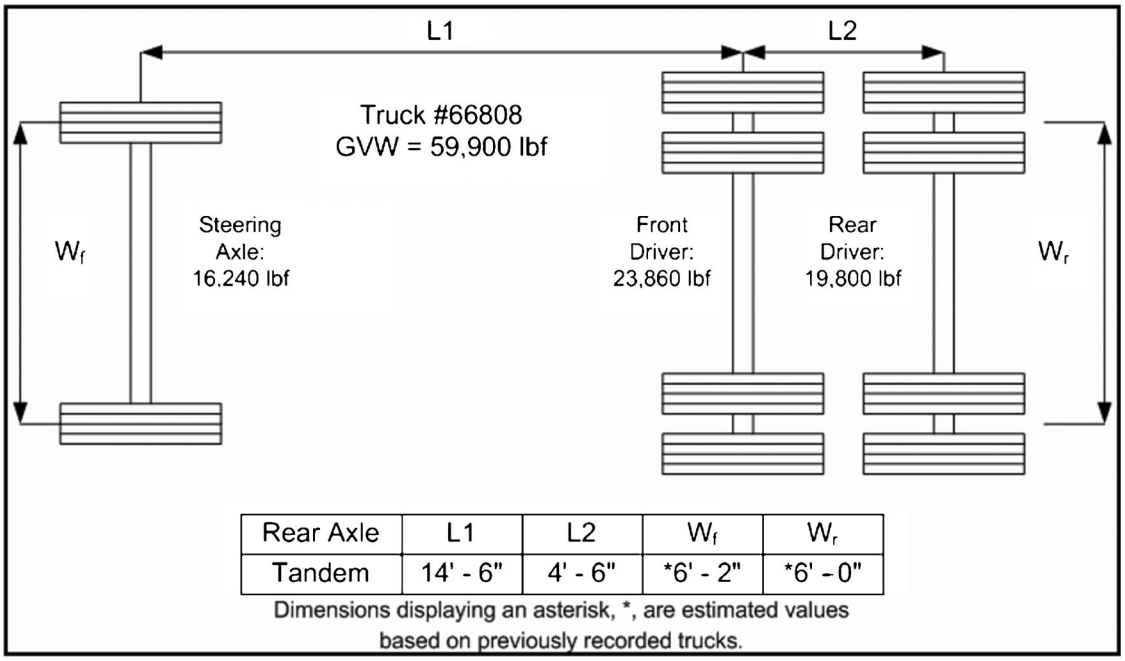

Figure 3.2: Geometry and weight of Truck #66808

trucks were used for each of the four park tests. Two trucks were put front to back in both northbound lanes to maximize the bridge load, which in turn maximizes the response of the bridge. Figure 3.6 is a photograph of one of the truck configurations for the static tests. The four park tests consisted of parking the block of trucks as described above in four different longitudinal positions on the bridge. Longitudinal positions were selected to maximize the bridge response at selected strain gage locations. The strain gages selected to have a maximized response were CH_2, CH_4, CH_6, and CH_24. All of these strain gages are on the outside girder of the northbound lane. CH_2 and CH_24 are located at mid-span of span N and P, respectively, at the region of maximum positive moment. CH_4 is located at the dead load inflection point south of Pier 13 and is the location of the greatest stress range. CH_6 is located at Pier 13 and is the position of the maximum negative moment.

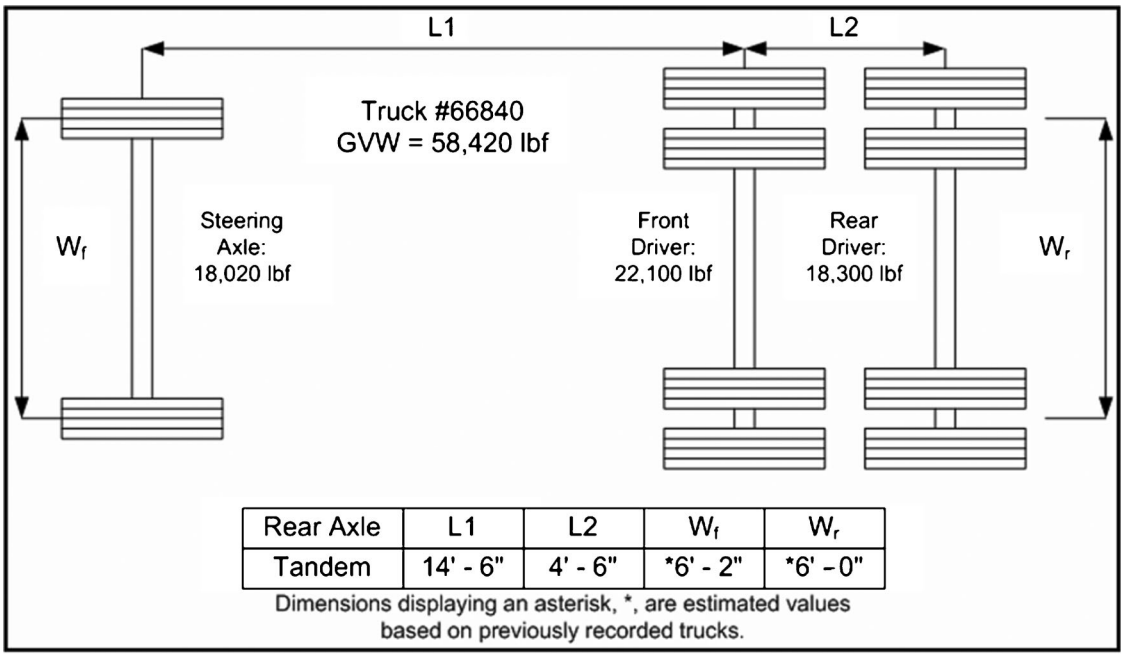

Figure 3.3: Geometry and weight of Truck #66840

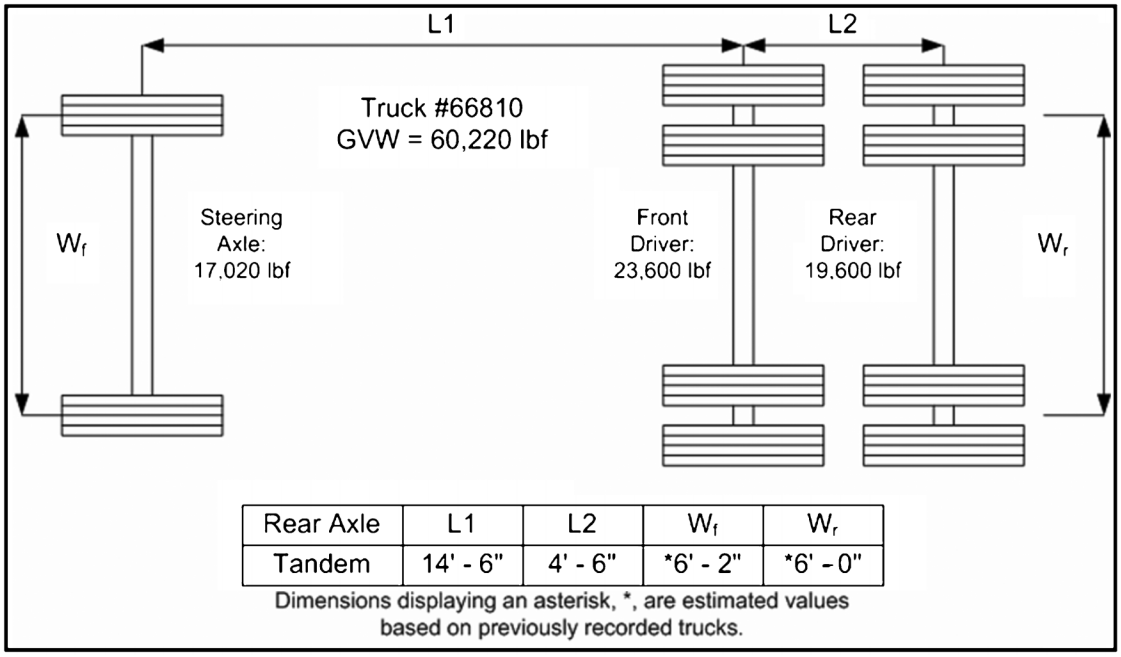

Rear Axle	L1	L2	W_f	W_r
Tandem	14' - 6"	4' - 6"	*6' - 2"	*6' – 0"

Dimensions displaying an asterisk, *, are estimated values based on previously recorded trucks.

Figure 3.4: Geometry and weight of Truck #66810

3.3 Crawl Tests

Crawl tests were also performed as part of the controlled load testing. The trucks crossed the bridge at five miles per hour or less. A total of two crawl tests were performed. Both tests again used all four trucks; however, the position of the trucks was not the same for both crawls. The first crawl test used positioning similar to that used for the static tests, as pictured in Figure 3.6, but not identical. Identical positions were not able to be used because when the trucks were parked front to back they were only a few inches apart. When moving at five miles per hour, the trucks had to be several feet apart at a minimum. This crawl test configuration will be referred to as the side-by-side crawl test. The second crawl test position consisted of all four trucks in the east lane of the northbound bridge. Like the first crawl test, the trucks were several feet apart when moving. A

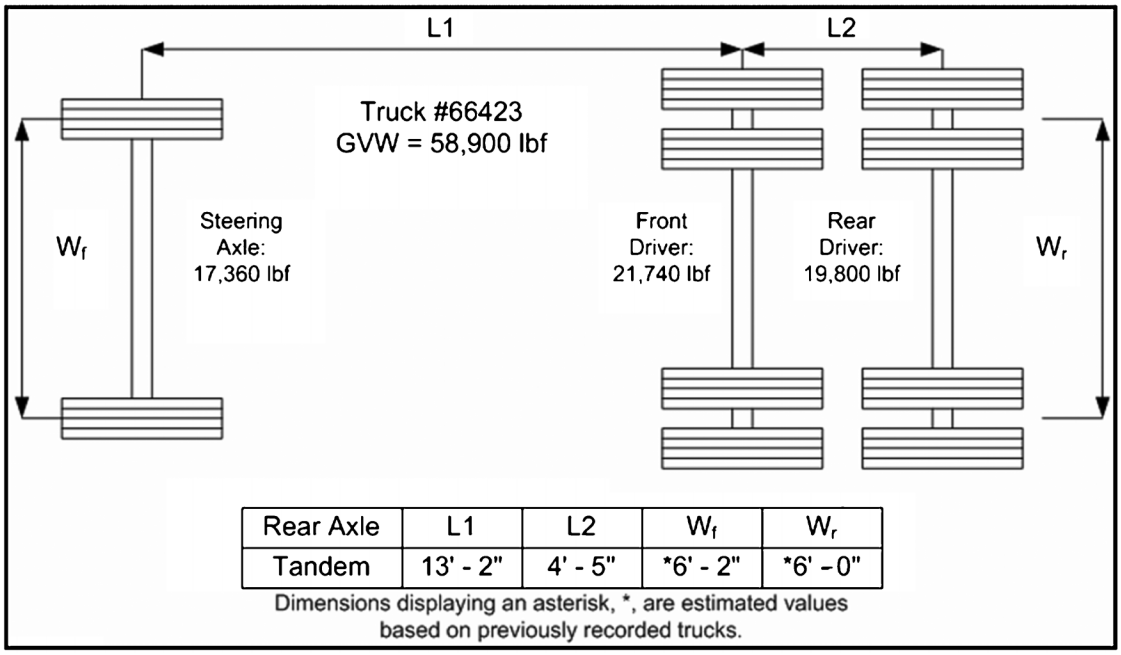

Rear Axle	L1	L2	W_f	W_r
Tandem	13' - 2"	4' - 5"	*6' - 2"	*6' – 0"

Dimensions displaying an asterisk, *, are estimated values based on previously recorded trucks.

Figure 3.5: Geometry and weight of Truck #66423

Figure 3.6: Photograph of static test configuration

Figure 3.7: Photograph of the single-line crawl test

photograph of this configuration can be seen in Figure 3.7. This crawl test configuration will be referred to as the single-line crawl test.

4. RESULTS OF CONTROLLED LOAD TESTS

Controlled load testing was performed to quantify the response of the US-41 White River Bridge to a known loading. Four fully loaded tandem axle plow trucks were provided by INDOT for the testing. In total, four static park tests and two crawl tests were performed. The four static tests targeted four primary locations of interest on the primary girder, while the crawl tests indicated the maximum response to the test trucks at all strain gage locations. A more detailed description of the test trucks and specific tests can be found in Chapter 3. What follows is a discussion of the results obtained from the controlled load testing.

4.1 General Response

The overall response of the bridge was very common to that of a continuous two-girder, riveted, stringer and floor beam structure with pin and hanger assemblies. Load transferred well from the deck down to the stringers, over to the floor beams, and out the primary girders. This is clearly demonstrated by the measured data. For both crawl tests the maximum and minimum stress as well as the resulting stress range at each strain gage was tabulated. A summary of these stresses and stress ranges can be found in Table 4.1. Also included in the table is a general location for each strain gage (i.e., main girder, floor beam, etc.). It should be noted that the stress range given in the table might not be the difference of the maximum and minimum stresses shown in the table due to rounding. All values in the table are rounded to the nearest tenth, but have additional significant digits associated with them in the spreadsheet from which the table was constructed. What follows is a specific section for each of the elements of primary interest: main girders, floor beams, stringers, and pin and hanger assemblies. These sections will discuss any interesting observations made during the controlled tests.

4.2 Stresses in Main Girders

Four static tests were performed as part of the controlled load testing. Each static test was targeted at

TABLE 4.1:
Summary of crawl test stresses

		SIDE-BY-SIDE			SINGLE-LINE		
CHANNEL	POSITION	MIN	MAX	RANGE	MIN	MAX	RANGE
CH_1	Main Girder	−0.4	0.2	0.6	−0.4	0.2	0.6
CH_2	Main Girder	−1.5	4.3	5.8	−1.1	3.6	4.7
CH_3	Main Girder	−0.7	0.9	1.6	−0.5	0.8	1.3
CH_4	Main Girder	−5.4	4.5	9.9	−4.1	3.4	7.5
CH_5	Main Girder	−0.1	0.8	0.9	−0.1	0.7	0.8
CH_6	Main Girder	−2.5	0.4	2.9	−2.2	0.4	2.6
CH_7	Floor Beam	−0.2	0.7	0.8	−0.2	0.4	0.6
CH_8	Floor Beam	N/A	N/A	N/A	N/A	N/A	N/A
CH_9	Floor Beam	−2.0	0.0	2.1	−1.0	0.1	1.1
CH_10	Floor Beam	−0.1	2.3	2.3	−0.1	1.3	1.3
CH_11	Main Girder	−0.1	0.7	0.7	−0.1	0.2	0.2
CH_12	Main Girder	−2.6	0.3	2.9	−1.0	0.4	1.5
CH_13	Stringer	−0.2	2.8	3.0	−0.1	1.2	1.3
CH_14	Stringer	−3.5	0.1	3.6	−1.6	0.1	1.7
CH_15	Stringer	−0.2	2.5	2.6	0.0	2.0	2.0
CH_16	Stringer	−1.6	0.0	1.7	−1.3	0.1	1.3
CH_17	Stringer	−2.0	0.2	2.2	−1.5	0.2	1.7
CH_18	Stringer	−0.1	2.9	3.0	−0.1	2.2	2.3
CH_19	Stringer	−0.5	1.5	2.0	−0.2	1.6	1.8
CH_20	Stringer	−1.4	0.3	1.7	−1.5	0.1	1.5
CH_21	Floor Beam	−1.9	0.1	2.1	−0.9	0.0	1.0
CH_22	Floor Beam	−0.3	2.7	3.0	0.0	1.3	1.4
CH_23	Main Girder	−0.2	0.1	0.3	−0.1	0.1	0.2
CH_24	Main Girder	−1.1	4.0	5.2	−1.0	3.3	4.3
CH_25	Main Girder	−2.9	0.1	3.0	−0.1	0.1	0.2
CH_26	Main Girder	−1.0	3.4	4.4	−0.1	1.4	1.5
CH_27	Stringer	−0.2	2.3	2.5	−0.2	0.9	1.2
CH_28	Stringer	−1.8	0.4	2.2	−0.6	0.4	1.0
CH_29	Pin and Hanger	−0.6	2.7	3.3	−0.7	3.0	3.7
CH_30	Pin and Hanger	N/A	N/A	N/A	N/A	N/A	N/A
CH_31	Pin and Hanger	−0.7	2.5	3.2	−0.6	2.1	2.7
CH_32	Pin and Hanger	−1.8	2.5	4.3	−1.3	2.4	3.7
CH_33	Pin and Hanger	−0.2	0.6	0.7	−0.2	0.6	0.8
CH_34	Pin and Hanger	−0.8	1.4	2.2	−0.9	1.1	2.0
CH_35	Pin and Hanger	−0.6	1.0	1.5	−0.6	1.0	1.6
CH_36	Pin and Hanger	−0.6	1.6	2.2	−0.7	1.1	1.8
CH_37	Pin and Hanger	N/A	N/A	N/A	N/A	N/A	N/A
CH_38	Pin and Hanger	−1.9	3.1	5.0	−1.3	2.9	4.1
CH_39	Pin and Hanger	−0.7	2.6	3.3	−0.9	0.8	1.6
CH_40	Pin and Hanger	−0.5	1.7	2.2	−0.6	0.4	1.0
CH_41	Pin and Hanger	−0.7	2.3	3.0	−0.5	0.4	0.9
CH_42	Pin and Hanger	−0.3	2.3	2.6	−0.8	0.8	1.6
CH_43	Pin and Hanger	−0.6	1.5	2.1	−0.7	0.5	1.2
CH_44	Pin and Hanger	−0.8	2.6	3.4	−1.0	0.9	1.9
CH_45	Cross-Bracing	−0.6	0.2	0.9	−0.4	0.4	0.7
CH_46	Cross-Bracing	−0.5	0.2	0.7	−0.2	0.3	0.6
CH_47	Cross-Bracing	−0.7	2.4	3.2	−1.1	1.1	2.2
CH_48	Cross-Bracing	−0.9	2.9	3.8	−1.3	1.5	2.8

maximizing the response of a specific set of strain gages on the main girder. A total of twelve (12) strain gages were installed on the main girders, targeting four locations. The four strain gage locations targeted on the main girder include the location of maximum positive moment in Span P, the dead load inflection point south of Pier 13, the location of maximum negative moment near Pier 13, and the location of maximum moment in Span N. Results obtained from the static tests were then compared to those obtained during the crawl tests. The following paragraphs will discuss general results obtained from the four targeted locations.

4.2.1 Static Test: Span N Location of Maximum Positive Moment

The four test trucks crossed the northbound superstructure from south to north. In doing so the first park

location was located such that the strain gages at the midspan of Span N, CH_1 and CH_2, were maximized. This is the location of maximum positive moment for Span N. Both strain gages are located on Girder G2. CH_1 is located on the underside of the top flange and CH_2 is located on the underside of the bottom flange. A plot of the data obtained during this test for CH_1 and CH_2 can be seen in Figure 4.1. It is important to note that this is a snapshot of the data obtained and therefore the reason the traces do not start at zero. If the entire data file was plotted the traces would start and end at zero stress.

Several observations can be made from the plot. First, the global bending response of the bridge is as expected for the location of maximum positive moment; tension in bottom of the beam (CH_2) and compression in the top (CH_1). Thus, the response is opposite; however, it is quite clearly not equal (i.e., not the same magnitude). For a standard non-composite beam, as the US-41 White River Bridge was designed, the response at the location of maximum positive moment should be stresses of equal magnitude, but opposite sign (positive and negative). Clearly in Figure 4.1 the magnitude of the tensile and compressive stresses are not equal. There is a maximum tensile stress of approximately 4.5 ksi for CH_2 but only a maximum compressive stress of approximately −0.5 ksi for CH_1. Therefore, some other element of the bridge is carrying this additional compressive force. This element is the deck. *(It should be noted that when referring to the 'maximum stress values' during a static test, the peak stress value is not actually recorded. Rather, the maximum stress value is an average taken over the flat-line portion of the data. This is done to remove the measured effects of the bridge vibrating.)*

It is worth taking a moment to briefly discuss composite action. Composite action is developed when two load carrying structural members, such as a concrete deck and supporting steel beam, are integrally connected and deflect as a single unit. Without an integral connection, horizontal slippage will occur at the interface between the two members as they each deflect individually. However, when a system is integrally connected and acts compositely no relative slip occurs and the two elements deflect as single unit. This results in a single neutral axis for the two members. The resulting neutral axis is located between the individual neutral axis of each element. Figure 4.2 illustrates the strain variation in composite beams.

Even though the US-41 White River Bridge was not designed to be composite, the data suggests the structure is acting compositely. This greatly increases

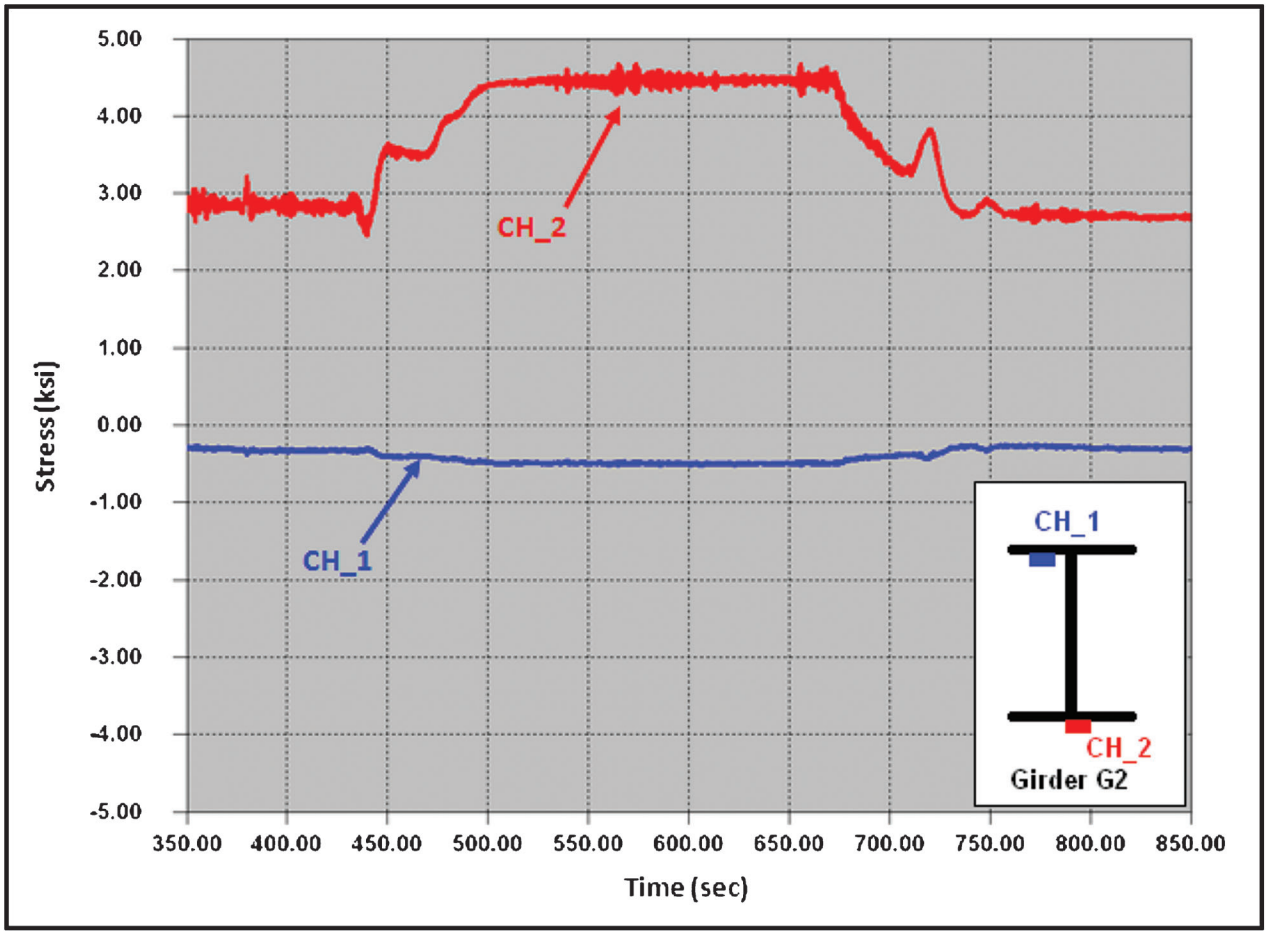

Figure 4.1: Response from park test at midspan of Span N

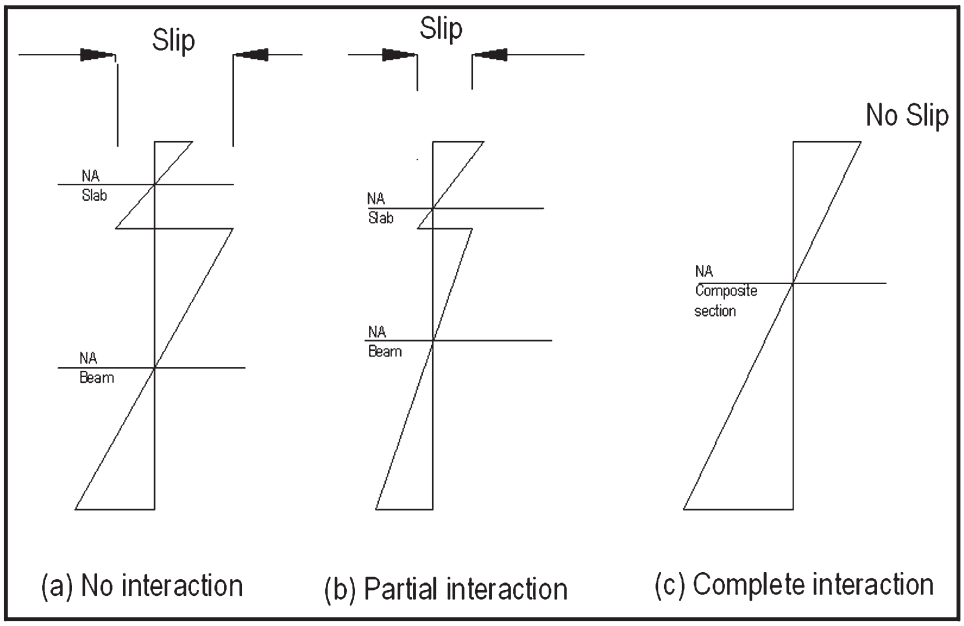

Figure 4.2: Composite action

the load carrying capacity of the structure. Typically, composite action is created by welding headed shear connectors to the top flange of the steel beam. No such connectors exist on the US-41 White River Bridge; however, the bridge is a riveted structure. Since the top flange of the main girders is in contact with the concrete deck, the rivets are acting as the shear connector between the steel girder and concrete deck, eliminating the horizontal slippage.

Using the strain gage measurements and an assumed linear stress distribution, the position of the neutral axis can be calculated. Figure 4.3 shows the stresses, section height, and resulting neutral axis. It should also be noted that the upper flange strain gage (CH_1) is on the bottom face of the flange. Thus, linear interpolation was used to calculate the stress on the top of the top flange.

For composite action to exist between the steel girder and concrete deck, the location of the neutral axis from the field measured stresses must be between the neutral axis of each individual element. Figure 4.4 plots the location of the neutral axis for the steel, concrete, and field measured stresses. As can be seen in the plot, the neutral axis calculated using the field measured stresses is between that of the steel and concrete. This confirms that some level of composite interaction exists between the girder and deck.

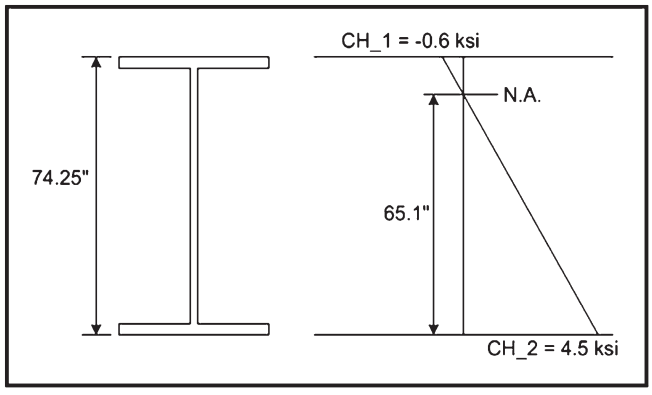

Figure 4.3: Neutral axis for park test at midspan of Span N

Also included in Figure 4.4 is the location of the neutral axis as calculated using AASHTO 2010 requirements for a fully composite section in the positive moment region. Using AASHTO, an effective width of participating concrete is calculated based on the girder spacing and deck overhang. The concrete width is then converted to an equivalent width of steel by taking a ratio of the steel and concrete modulus of elasticity (modular ratio). Once the materials have been converted, the AASHTO neutral axis can be calculated. Since the AASHTO neutral axis assumes full composite behavior, if the neutral axis calculated from the field measured stresses is between the ASSHTO neutral axis and the concrete deck neutral axis, the section can be assumed to be fully composite. This is the case for midspan of Span N. The neutral axis from the field measured stresses is between that of the ASSHTO calculation and concrete deck. Thus, full composite action can be assumed for this section of the US-41 White River Bridge.

Additional factors are also involved that account for the difference between the AASHTO neutral axis value and the value calculated from the field measured stresses. The AASHTO value only assumes the concrete deck is contributing to the composite action and load distribution. However, this is not the case. For the actual bridge there are additional elements beyond the girder and deck that transfer load. These include elements such as the concrete barrier wall and steel

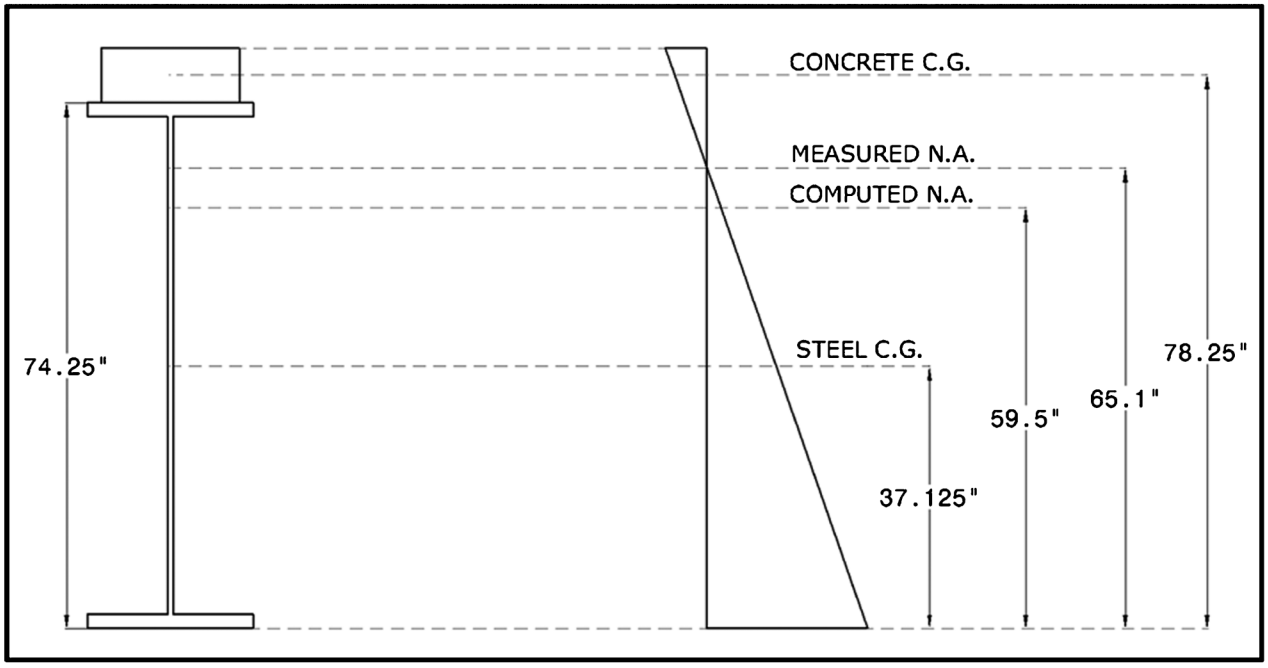

Figure 4.4: Neutral axis comparison for park test at midspan of Span N

stringers. Secondly, the AASHTO calculation relies on an assumed concrete compressive strength. If the concrete compressive strength is different than the assumed value, the location of the AASHTO neutral axis can shift. Both of these are reasons explaining why the measurements indicated that the bridge is acting more composite than what is assumed in standard composite design.

4.2.2 Static Test: Inflection Point South of Pier 13 in Span N

The second position the parked test trucks reached as they crossed the US-41 White River Bridge was the dead load inflection point south of Pier 13 in Span N. This was the location that maximized CH_3 and CH_4, top and bottom strain gages respectively, on Girder G2. The dead load inflection point is the location of a beam where the moment due to dead load switches from positive to negative; thus, in theory, this is typically a location of zero moment for dead load. However, oftentimes the dead load inflection point is actually the point of greatest live load stress range. This will be addressed later in the report when the crawl test results are presented. Figure 4.5 shows a plot of CH_3 and CH_4 when the test trucks were parked at the position maximizing the response at the inflection point south of Pier 13 in Span N. It is important to note that this is a snapshot of the data obtained and therefore the reason the traces do not start at zero. If the entire data file was plotted the traces would start and end at zero stress.

As can be seen in the plot this location resulted in a maximum tensile response of approximately 4.6 ksi for CH_4 and a maximum compressive response of approximately −0.7 ksi for CH_3. These stresses indicate that positive bending is occurring at the dead load inflection point. Additionally, the plot shows a much greater tensile response than compressive response indicating the beam is acting compositely. To verify if composite action exists, the position of the neutral axis was calculated using strain gage measurements recorded during the test. Figure 4.6 shows the stresses, section height, and resulting neutral axis. It should also be noted that the upper flange strain gage (CH_3) is on the bottom face of the flange. Thus, linear interpolation was used to calculate the stress on the top of the top flange.

The neutral axis calculated from the field measured stresses was then plotted with that of the steel girder, concrete deck, and AASHTO computation. This is shown in Figure 4.7. As can be seen in the figure the neutral axis of the composite section is located between that of the concrete slab and steel girder confirming that some level of composite interaction between the two elements. Comparing the AASHTO neutral axis to the neutral axis from field measured stresses, remarkable agreement is found. A minor difference of only 0.3 inches separates the two values. The neutral axis from the field measured stresses is slightly greater than the neutral axis calculated from AASHTO. This indicates that full composite behavior exists between the girder and deck.

4.2.3 Static Test: Pier 13 Location of Maximum Negative Moment

The third position for the parked trucks was such that the strain gages near Pier 13 were maximized. This is the location of maximum negative moment on the US-41 White River Bridge. Due to the support being

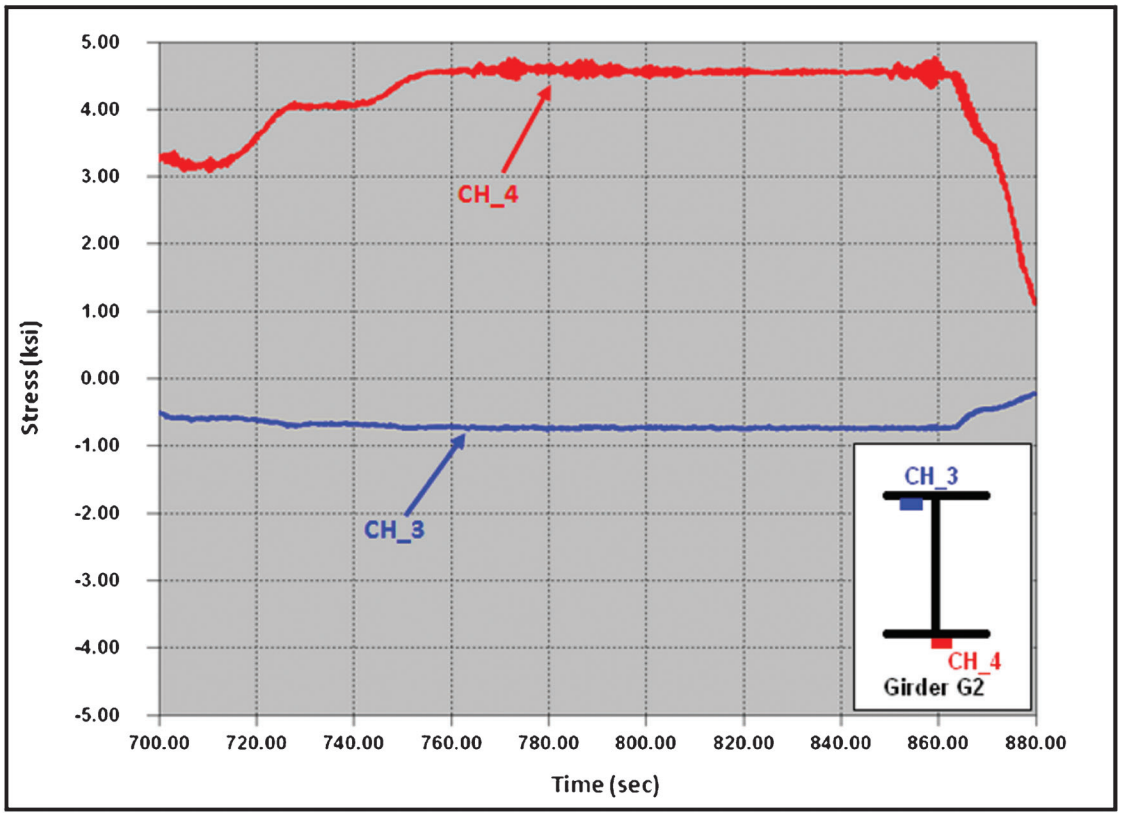

Figure 4.5: Response from park test at inflection point south of Pier 13 in Span N

located at the exact position of maximum negative moment the strain gages at Pier 13 were installed two feet to the south of the centerline of the support. At this location both Girder G1 and Girder G2 were instrumented. Girder G1 had CH_11 installed on the underside of the top flange and CH_12 on the underside of the bottom flange. Identical locations on Girder G2 were instrumented with CH_5 and CH_6, top and bottom respectively. The response of all four strain gages to the park test can be seen in Figure 4.6. It is important to note that this is a snapshot of the data obtained and therefore the reason the traces do not start at zero. If the entire data file was plotted the traces would start and end at zero stress.

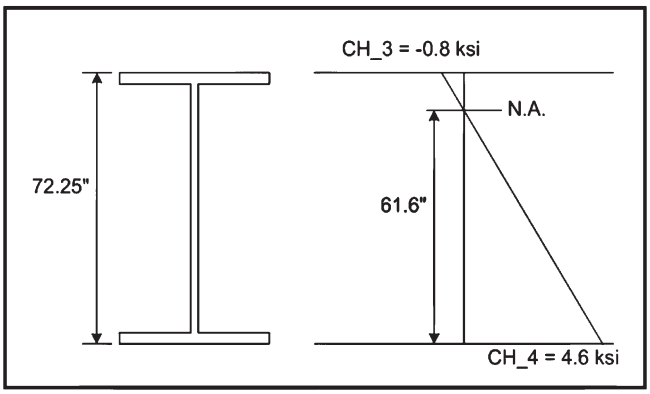

Figure 4.6: Neutral axis for park test at inflection point south of Pier 13 in Span N

As would be expected for the location of maximum negative moment (i.e., negative bending) the top flange strain gages (CH_5 and CH_11) indicate a tensile response and the bottom flange strain gages (CH_6 and CH_12) indicate a compressive response. The strain gages also show that both girders have nearly identical responses. This is expected as the trucks are parked side-by-side in two rows. Any small differences between the stresses in the two girders are easily attributed to the location in the grouping of the truck with the different axle spacing and/or the slightly varying weight of each truck. Overall this plot shows great load distribution between the two primary girders.

As mentioned above, the US-41 White River Bridge was designed non-composite. Thus, it would be expected that the response of a pair of strain gages installed top and bottom on a girder would be equal and opposite. Like the positive moment regions presented above, Figure 4.8 shows that this is not the case for the negative moment region. The strain gages indicate that the response is opposite (i.e., tensile and compressive) but not of equal magnitude. Therefore, some other element in the bridge is carrying the additional tensile load. In the case of the negative moment region the reinforcing steel in the concrete deck is carrying the additional tensile load. Again, this is due to the rivets acting as a shear connector between the main girder and deck.

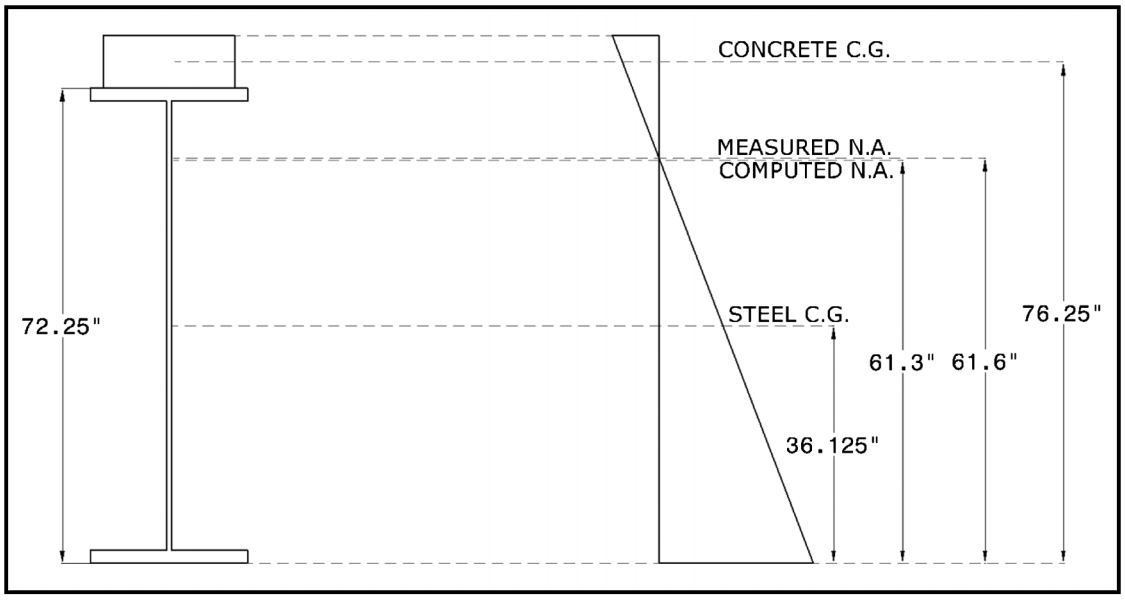

Figure 4.7: Neutral axis comparison for park test at inflection point south of Pier 13 in Span N

To verify if composite action exists, the position of the neutral axis was calculated using strain gage measurements recorded during the test. Figure 4.9 shows the stresses, section height, and resulting neutral axis. It should also be noted that the upper flange strain gages (CH_5 and CH_11) are on the bottom face of the flange. Thus, linear interpolation was used to calculate the stress on the top of the flange for both girders.

The neutral axis calculated from the field measured stresses was then compared to the neutral axis of the steel, concrete, and AASHTO computation. This was done by plotting them on a stress diagram as shown in

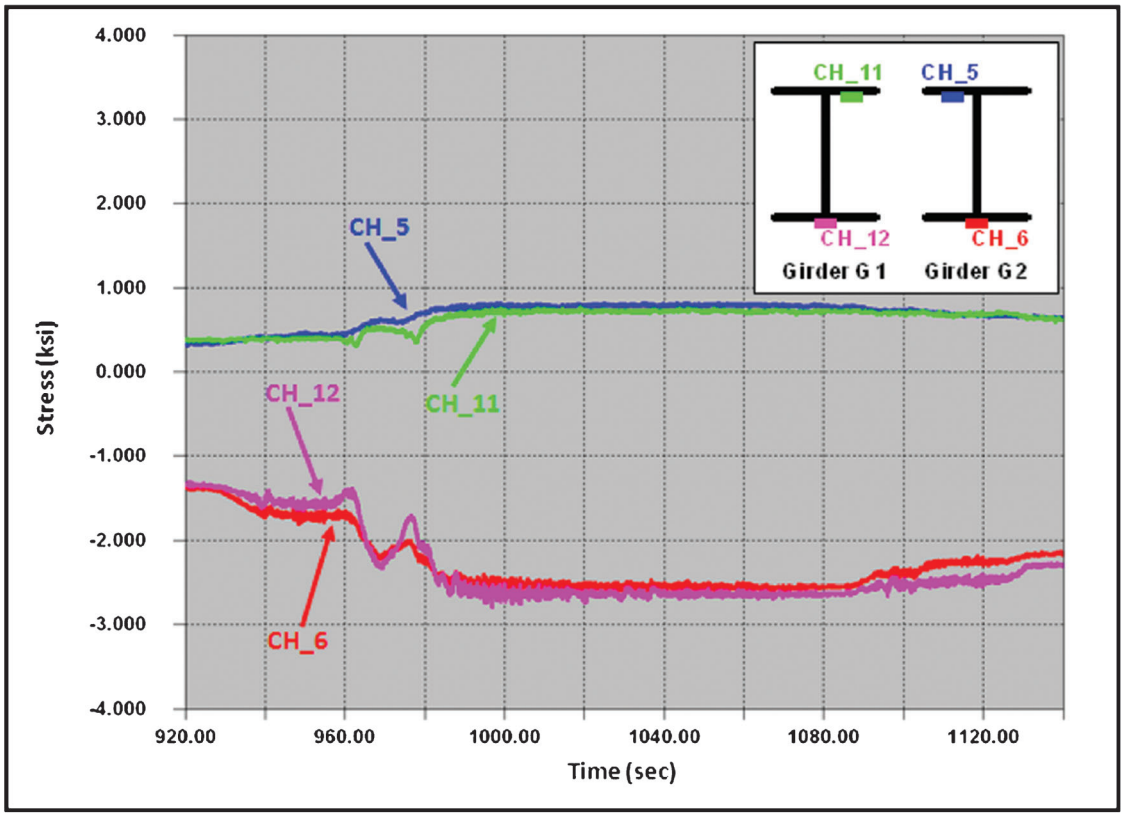

Figure 4.8: Response from park test at Pier 13

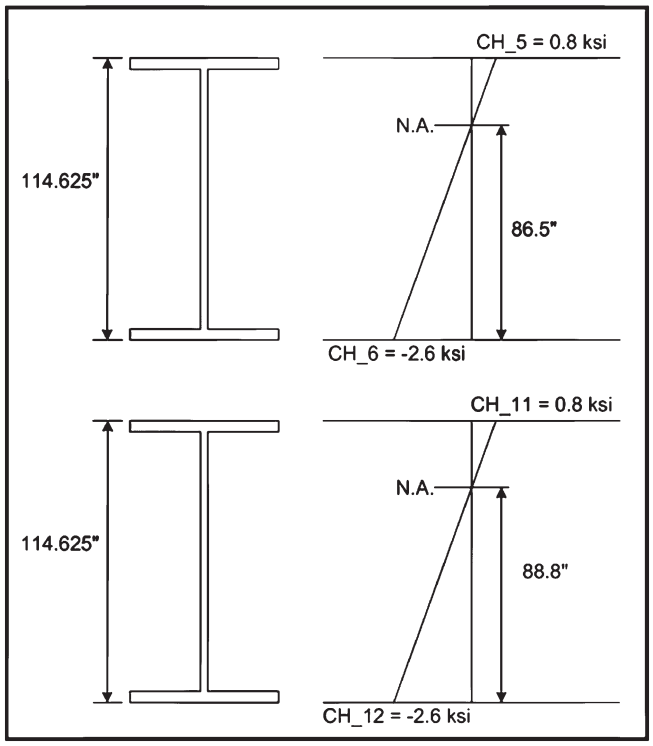

Figure 4.9: Neutral axis for park test at Pier 13

Figure 4.10 and Figure 4.11. As can be seen in the figure the neutral axis of the composite section is located between that of the concrete slab and steel girder confirming that some level of composite interaction exists between the two elements. The neutral axis computed from the field measured stresses is also between that of the concrete deck and ASSHTO calculation indicating full composite behavior. This is the case for both sets of strain gages at the Pier 13 location.

As can be seen in the plot there appears to be a larger difference between the AASHTO calculated neutral axis and the measured value. It is important to keep in mind that the park test at Pier 13 is in the negative moment region of the bridge. The AASHTO calculation for composite behavior in the negative moment region differs greatly compared to the calculation for the positive moment region. In the positive moment region the concrete carries a large portion of the compressive force. However, for the negative moment region there is now tension where the concrete is located. As concrete is very poor in tension, any tension carried by the concrete is actually carried by the longitudinal reinforcing steel. Longitudinal reinforcing steel in the concrete barriers as well as the steel stringers are not accounted for in the AASHTO calculation of the neutral axis. These additional load carrying members can help explain the difference between the neutral axis calculated by AASHTO and the neutral

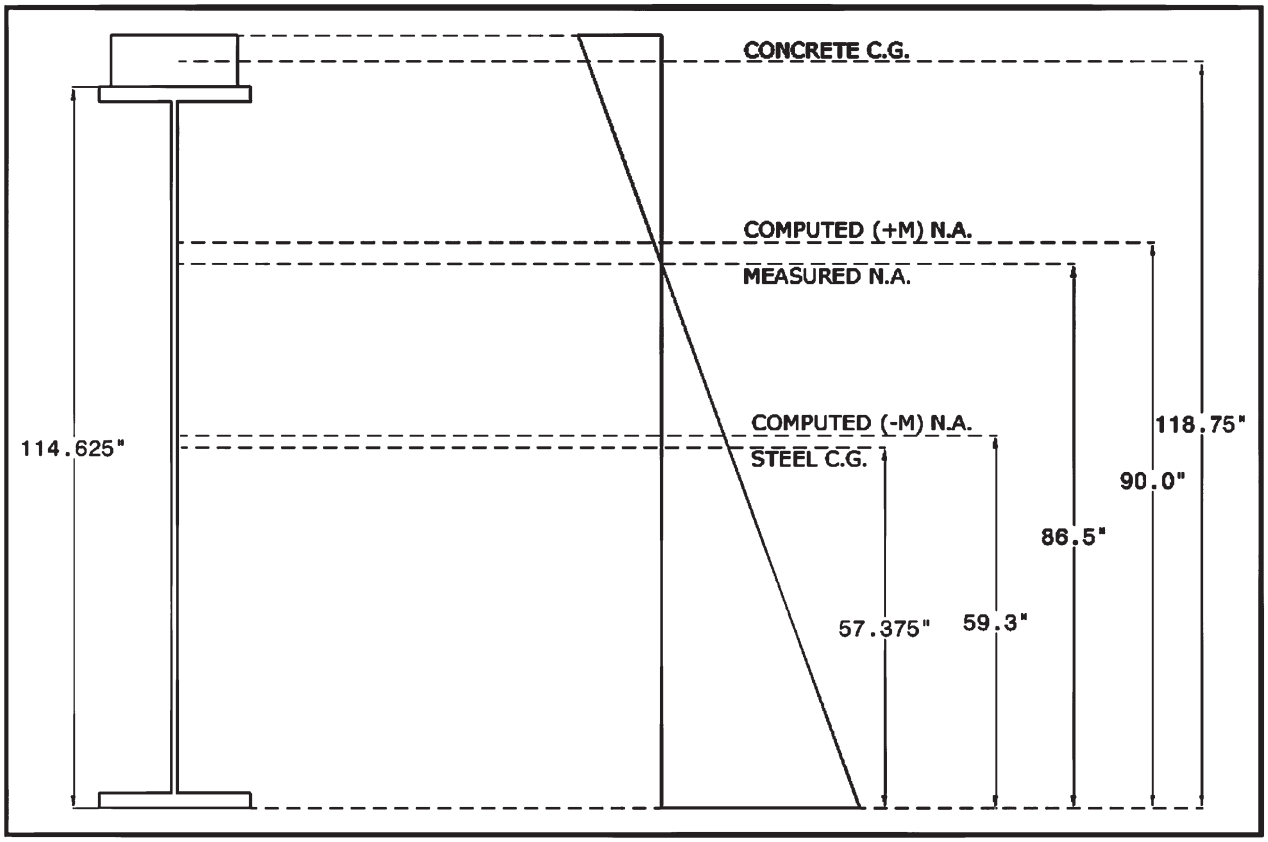

Figure 4.10: Neutral axis comparison for park test at Pier 13 Girder G2

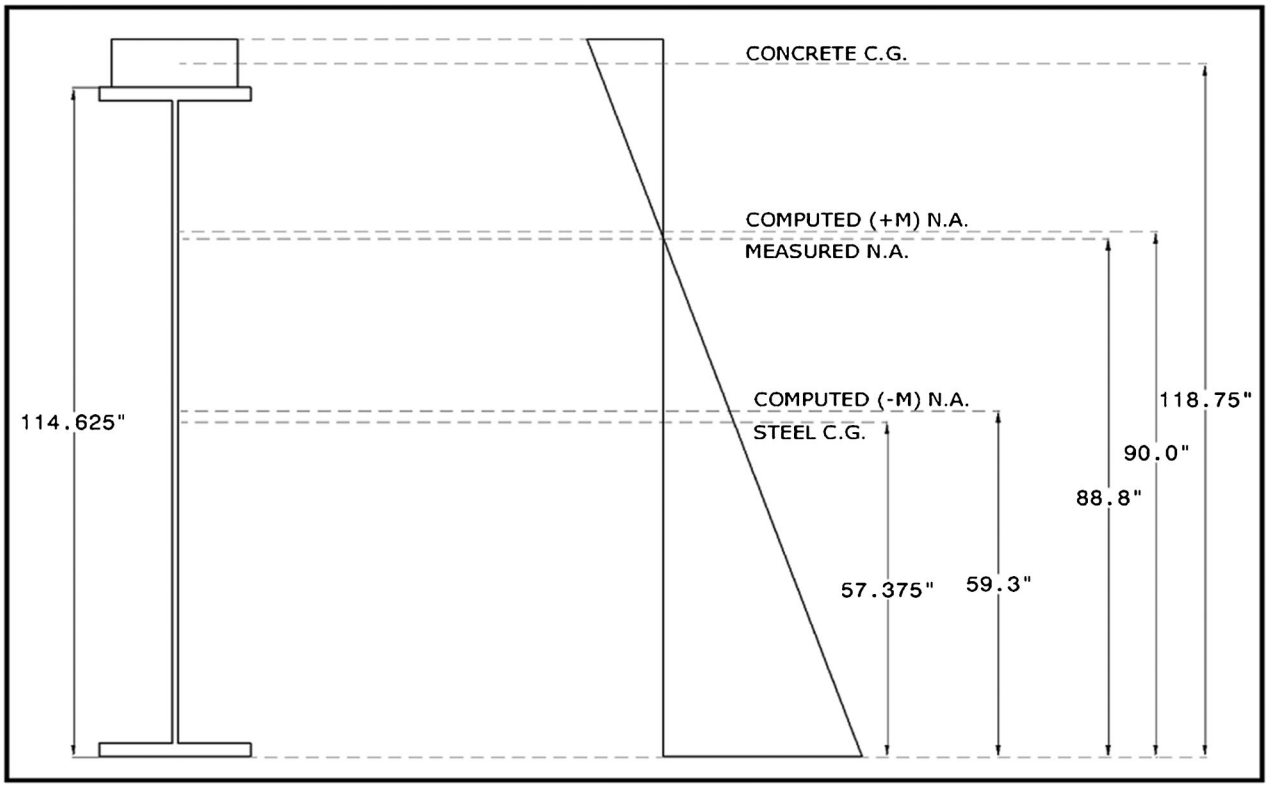

Figure 4.11: Neutral axis comparison for park test at Pier 13 Girder G1

axis computed from the field measured stresses. One thing that is remarkable is the agreement between he measured neutral axis location and the computation for the neutral axis based on a positive moment region. The nearly identical values suggest the composite action at the Pier 13 strain gage location has the behavior of positive moment composite section.

4.2.4 Static Test: Span P Location of Maximum Positive Moment

The fourth position for the parked trucks was located such that the strain gages at the midspan of Span P were maximized. This was the location of maximum positive moment of Span P. Both Girder G1 and Girder G2 were instrumented at this location. CH_23 and CH_25 were located on the underside of the top flange on Girder G2 and Girder G1 respectively. Likewise, CH_24 and CH_26 were located on the underside of the bottom flange of Girder G2 and Girder G1 respectively. The responses for all channels at the midspan of Span P are plotted in Figure 4.12. It is important to note that this is a snapshot of the data obtained and therefore the reason the traces do not start at zero. If the entire data file was plotted the traces would start and end at zero stress.

As expected, tension was measured in the bottom flange (CH_24 and CH_26) and compression in the top flange (CH_23 and CH_25). Since strain gages were installed on both main girders the load distribution could be evaluated at this position. As seen in the plot, both girders approximately carried the same amount of load. The bottom flange stresses were nearly identical between the girders, −0.1 ksi for CH_23 and −0.2 ksi for CH_25. However, there was a 0.5 ksi difference in the top flange stresses. The maximum response measured at CH_24 was 3.8 ksi whereas the maximum response measured at CH_26 was only 3.3 ksi. Overall this shows a fairly equal load distribution between the girders. The small difference between the values can likely be attributed to the location of the truck with the different axle spacing and/or the varying weights of each individual truck.

The compressive response was significantly smaller than the tensile response; thus, once again indicating the girders and deck are acting compositely. Using the strain gage measurements the location of the neutral axis was calculated to verify if composite action exists. Figure 4.13 shows the stresses, section height, and resulting neutral axis. It should also be noted that the upper flange strain gages (CH_23 and CH_25) is on the bottom face of the top flange. Thus, linear interpolation was used to calculate the stress on the top of the flange.

The neutral axis calculated from the field measured stresses was then plotted with that of the steel girder, concrete deck, and AASHTO computation as shown in Figure 4.14 and Figure 4.15. The plot shows the neutral axis of the composite section located between that of the concrete slab and steel girder. This confirms that some level of composite action exists between the two elements. When comparing the AASHTO neutral axis to the neutral axis from field measured stresses, an

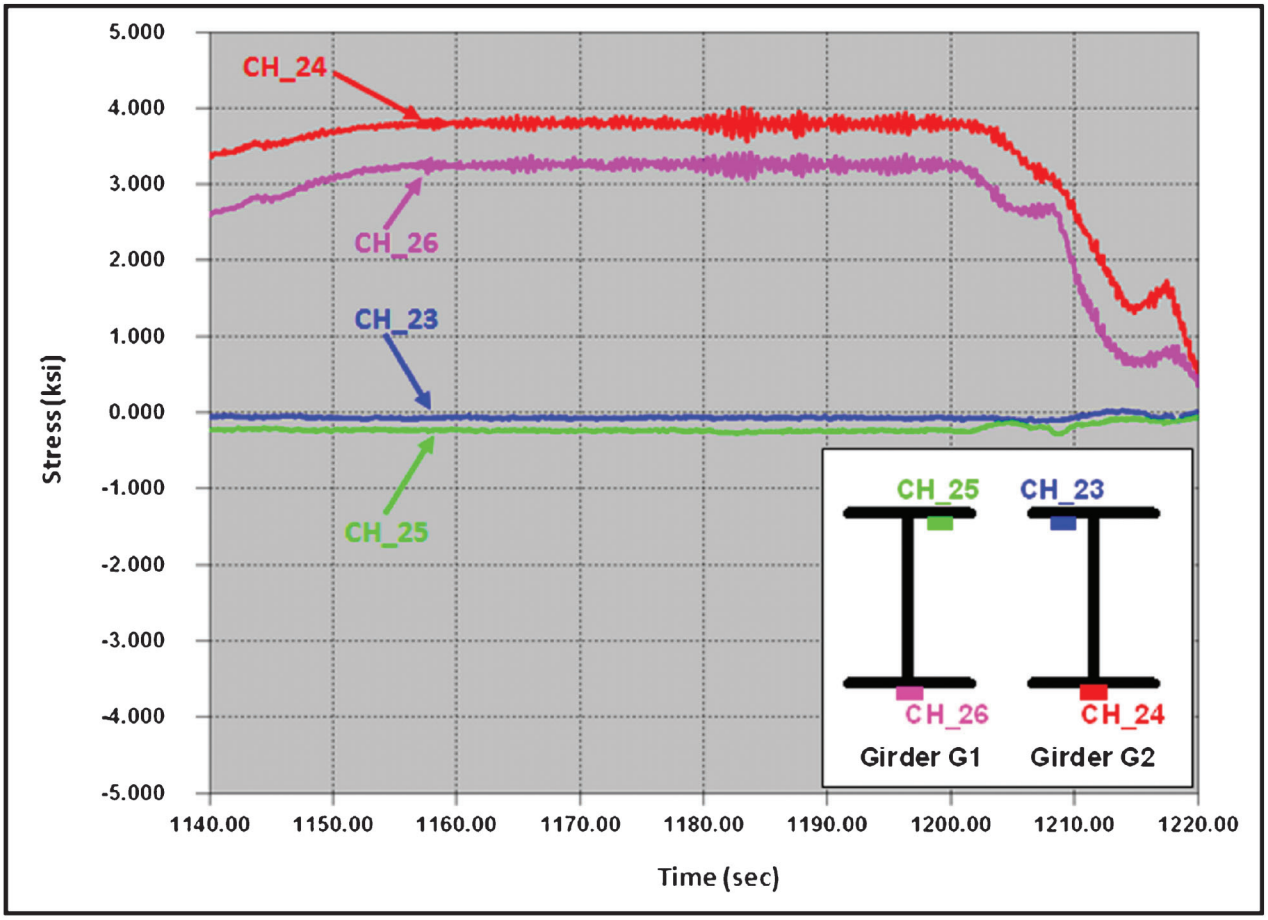

Figure 4.12: Response from park test at midspan of Span P

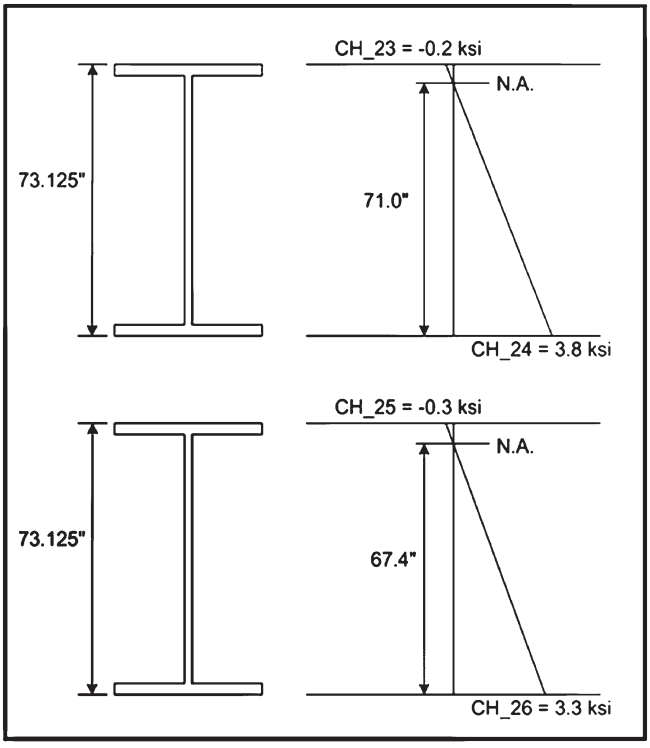

Figure 4.13: Neutral axis for park test at midspan of Span P

average difference of nine inches is observed. The neutral axis from the field measured stresses is greater than the neutral axis calculated from AASHTO indicating full composite behavior. The difference between the two values can be attributed to load distribution not accounted for in the AASHTO computation such as the effect of concrete barriers and steel stringers. Additionally, the concrete in the bridge may have a greater compressive strength than what is assumed for the AASHTO calculation.

4.2.5 Crawl Tests

After completing the four static controlled load tests, two crawl tests were performed. One of the two crawl tests had a nearly identical side-by-side truck configuration as the static tests. The results from this crawl test were compared to those obtained during the static tests. However, before discussing the comparison, it should be noted that it is not uncommon for the results between identically configured crawl tests and static tests to vary slightly. Differences in the responses between the tests occur for a variety of reasons. These include differences in the transverse location of the trucks on the bridge, difference in the longitudinal spacing of the trucks, and any added effects from

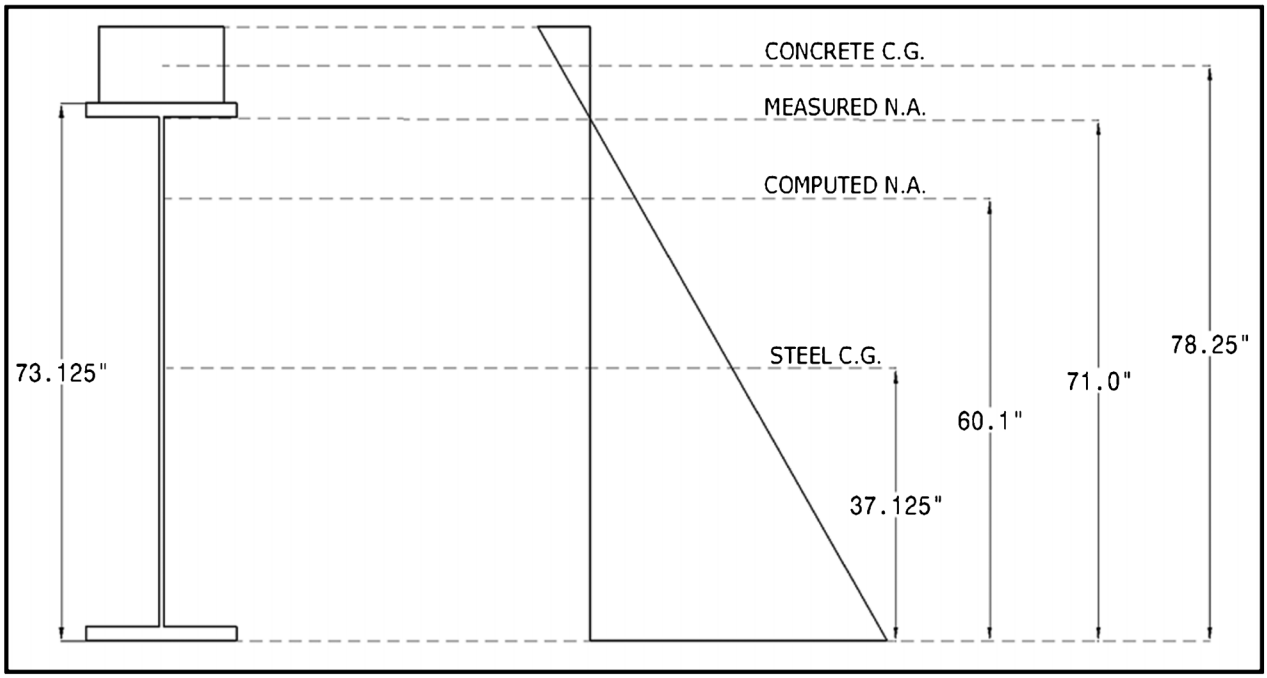

Figure 4.14: Neutral axis comparison for park test at midspan of Span P Girder G2

impact loading and general bridge vibration. Any single one of these reasons or a combination of multiple ones could slightly alter the stresses up or down for either test. One other important thing to note about the crawl test is the length of an event. For the static test, only a snapshot of the crawl test was shown for the maximum response at a given location. Conversely, when viewing a plot of crawl test data an entire event can easily be displayed. Thus, the crawl tests help to illustrate the global response of the structure. Specifically, the resulting stress range from the test trucks can be observed.

The first main girder strain gage location encountered when crossing the bridge is the midspan of Span

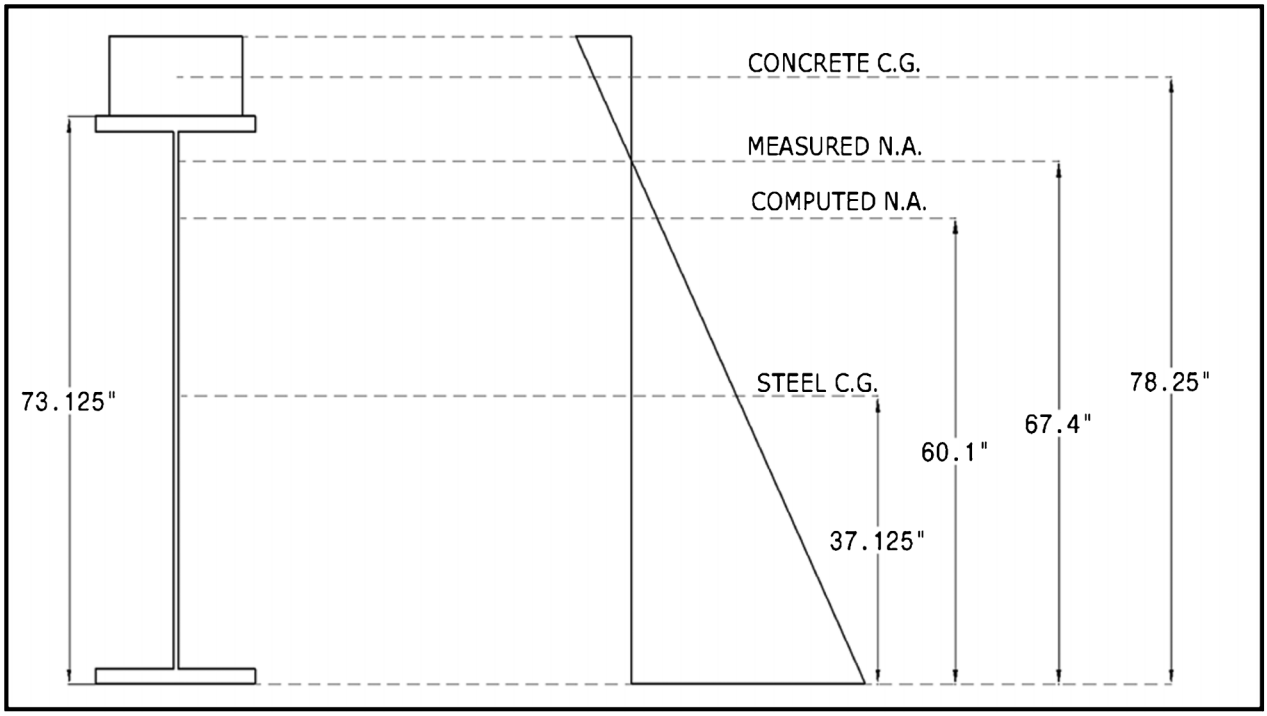

Figure 4.15: Neutral axis comparison for park test at midspan of Span P Girder G1

N. Plotted in Figure 4.16 is the response from the side-by-side crawl test at this location. To begin, this plot can be used to illustrate the difference between data from a static test and data from a crawl test. The static test plot was a snapshot of the peak positive bending response of this figure. Conversely, the crawl test plots show the response as the test trucks crossed over the spans of the US-41 White River Bridge adjacent to the instrumented span. As would be expected, when the trucks are in the directly adjacent spans a negative bending response is measured. Furthermore, when the test trucks are two spans away a positive bending response is recorded. As mentioned previously, the maximum stress range can also be taken from a crawl test plot. The maximum stress range from the plot is the difference between the peak positive and peak negative stress values for a given channel as the truck crosses the bridge.

Comparing the maximum responses from the crawl test to those from the static test for the instrumented span, similar results are found. The maximum stresses from the static test were −0.5 ksi and 4.5 ksi for CH_1 and CH_2 respectively. For the crawl test, the maximum stresses were −0.4 ksi and 4.3 ksi for CH_1 and CH_2 respectively. These are remarkably similar results. The minor differences can be attributed to the reasons discussed above. However, since the crawl test response is smaller than the static test response the most likely reason for the difference is truck spacing. During the crawl test the trucks were several feet apart as opposed to being several inches apart as there were during the static test. This helped to greater distribute the load, likely resulting in a smaller maximum response.

Taking the entire response from the crawl test into consideration, the maximum stress range for each channel can be measured. The maximum stress ranges recorded during the side-by-side crawl test at midspan of Span N was 0.6 ksi and 5.8 ksi for CH_1 and CH_2 respectively. These stress ranges occurred as the trucks passed through multiple spans. For example, in Figure 4.16 it can be seen that the maximum stress range occurred as the trucks passed from the instrumented span (location of maximum tensile response) to the adjacent span to the north (location of maximum compressive response).

The second main girder strain gage location encountered as the test trucks crossed the US-41 White River Bridge was the dead load inflection point south of Pier 13 in Span N. Figure 4.17 is a plot of the side-by-side

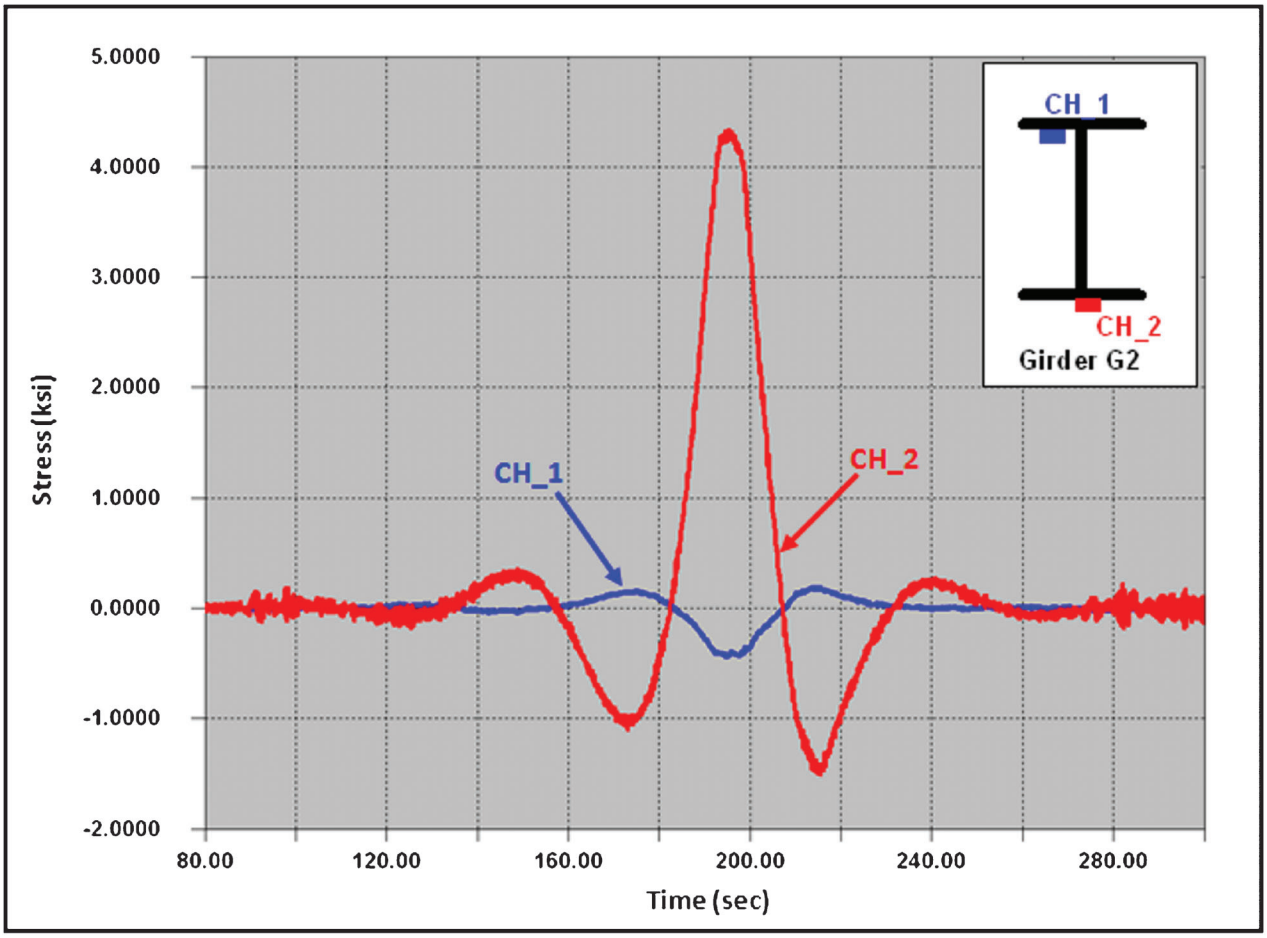

Figure 4.16: Response from side-by-side crawl test at midspan of Span N

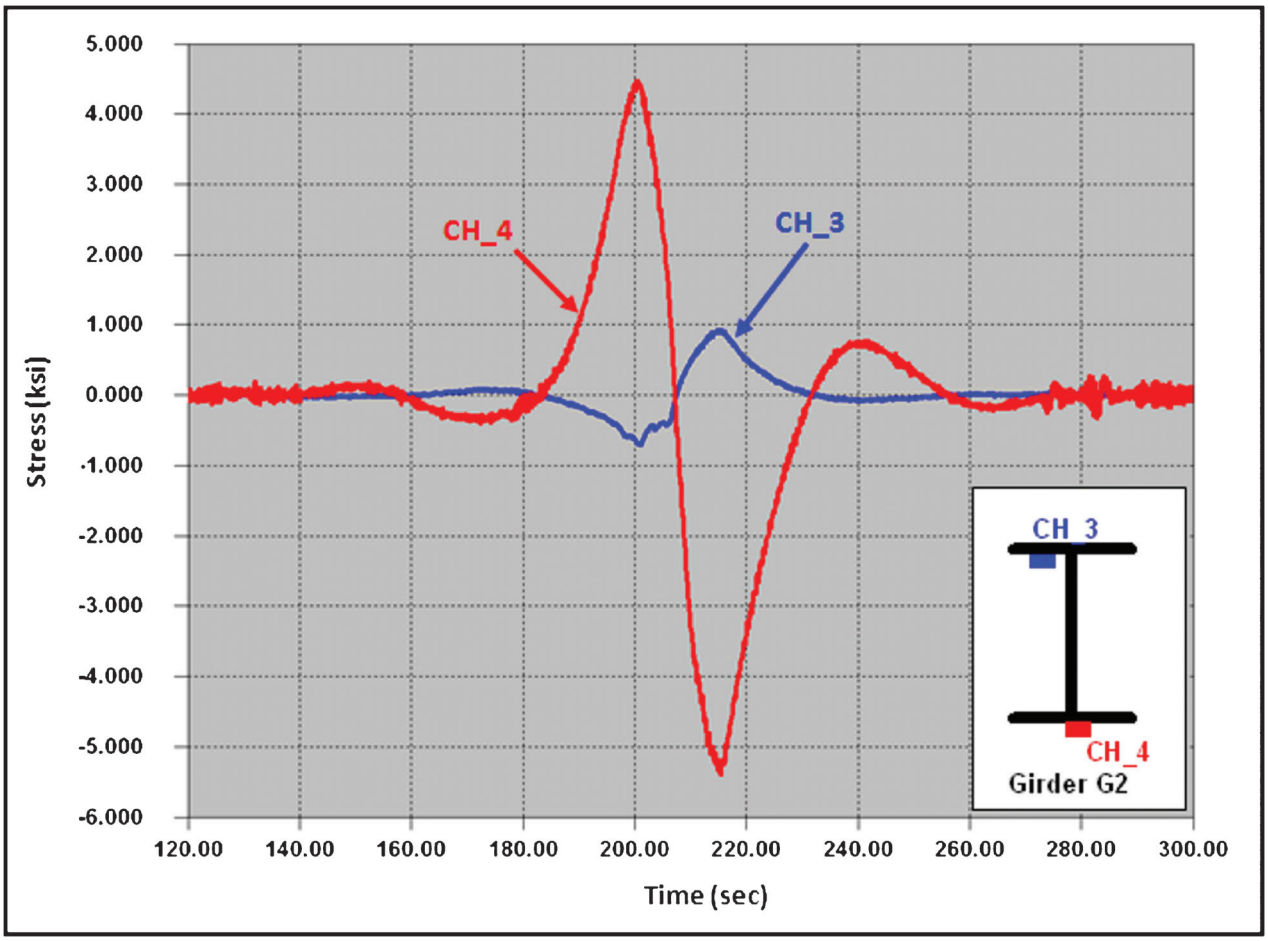

Figure 4.17: Response from side-by-side crawl test at Girder G2 inflection point south of Pier 13

crawl test for CH_3 and CH_4 located at the dead load inflection point. At this location the static test measurements and crawl test measurements had great agreement. During the static test, the maximum stresses recorded were −0.7 ksi and 4.6 ksi for CH_3 and CH_4 respectively. These compare quite well with the stresses of −0.7 ksi and 4.5 ksi recorded for the same span during the crawl test. Here again, the difference between the static and crawl tests can likely be attributed to the spacing of the test trucks as they crossed the strain gage location.

As briefly mentioned during the static response discussion of the dead load inflection point, this location often has the greatest live load stress range. Just as anticipated, this was the case of the US-41 White River Bridge. The maximum stress range recorded for the controlled load tests was 9.9 ksi at CH_4. This was over 4 ksi greater than the next nearest maximum stress range measured at any strain gage during the controlled load tests. Due to the composite nature of the main girders, the top flange strain gage (CH_3) only had a maximum stress range of 1.6 ksi for the side-by-side controlled load test.

The third main girder strain gage position crossed as the test trucks crawled across the bridge was the location of maximum negative moment. This was located at Pier 13. Figure 4.18 is a plot of the response at these strain gages during the side-by-side crawl test. The maximum stress values for this test are nearly identical to those obtained during the static tests. Maximum stress values of 0.8 ksi, −2.6 ksi, 0.7 ksi, and −2.6 ksi were recorded during the static test for CH_5, CH_6, CH_11, and CH_12 respectively. These were all the same during the crawl test expect for CH_6 which was −2.5 ksi. It should be noted that all stress values recorded are rounded to the nearest tenth; therefore, these stresses are not truly identical, but close enough for all practical purposes.

Like the static test, the load distribution between the girders for the crawl test at this location is phenomenal. For both the compressive and tensile responses, the difference in magnitude between the two girders was approximately 0.1 ksi. This type of load distribution would be expected based on the configuration of the test trucks. Also, the maximum stress range between the girders for the crawl test was fairly similar. The top flange strain gages measured stress ranges of 0.9 ksi and 0.7 ksi for CH_5 (Girder G2) and CH_11 (Girder G1) respectively. Likewise, the bottom flange strain gages had similar results measuring 2.5 ksi and 2.6 ksi for

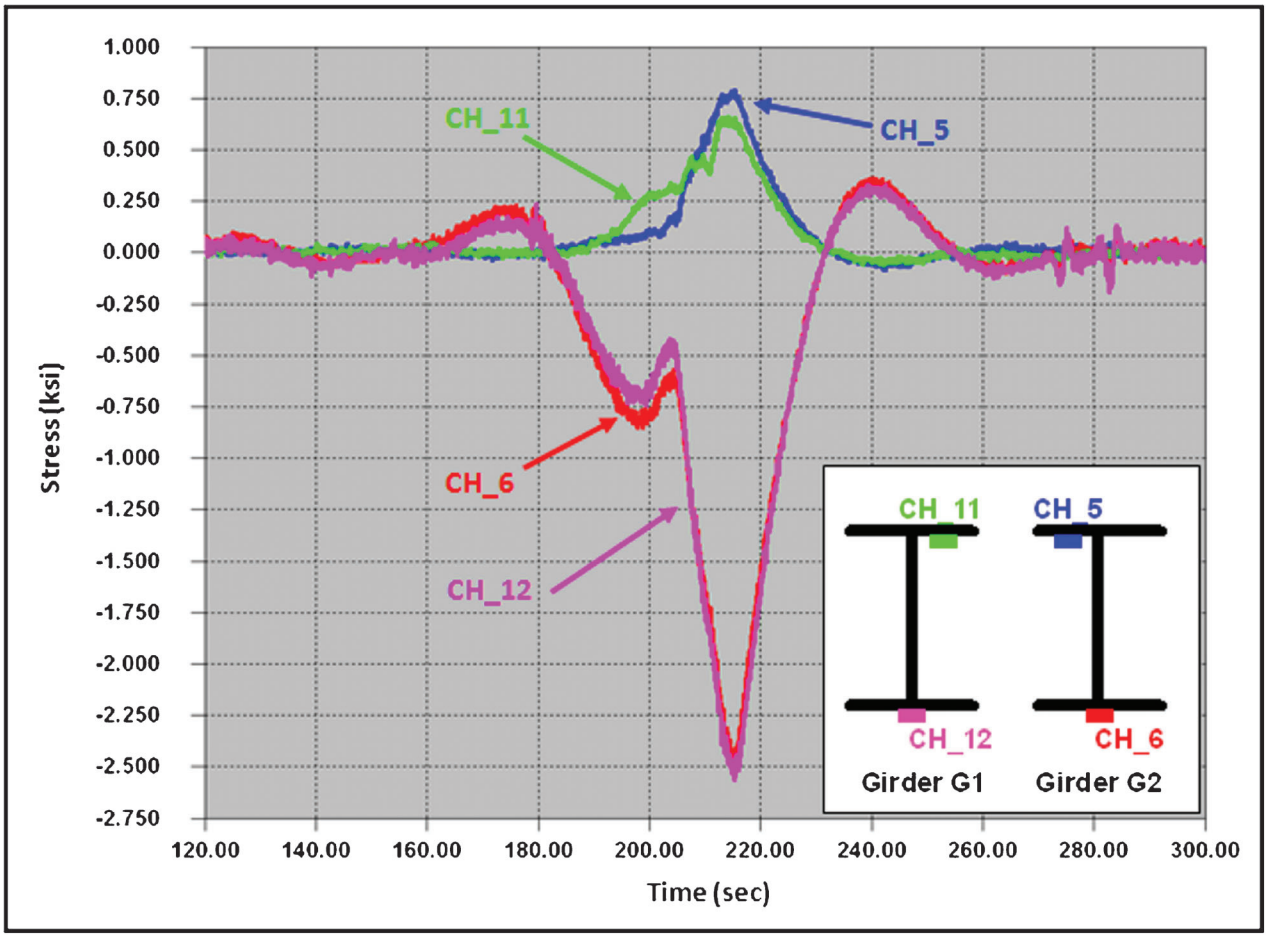

Figure 4.18: Response from side-by-side crawl test at Pier 13 girders

CH_6 (Girder G2) and CH_12 (Girder G1), respectively.

The fourth and final strain gage location is the midspan of Span P. This is the location of maximum positive moment in Span P. Plotted in Figure 4.19 is the strain gage response from the side-by-side crawl test. At this location, the crawl tests had a slightly greater response than the static test. During the static test CH_23 through CH_26 had stresses of −0.1 ksi, 3.8 ksi, −0.2 ksi, and 3.3 ksi, respectively. However, during the crawl test these same strain gages had stresses of −0.2 ksi, 4.0 ksi, −0.3 ksi, and 3.4 ksi. The minor difference of 0.2 ksi or less can easily be attributed to bridge vibrations that amplified the response during the crawl test.

Similar to the static response, the strain gages at the midspan of Span P did not show a perfectly equal load distribution like the strain gages at Pier 13. Rather, as shown in the plot, Girder G2 appeared to carry more of the moment at the midspan of Span P. However, it should be noted that the load distribution between the main girders at this location was reasonable nevertheless. The difference is likely due to the transverse locations of the test trucks as they crossed over the midspan of Span P. Also, the amount of load being carried by additional bridge components such as the concrete barrier or steel stringers is unknown which may also account for the difference between girders.

This difference in magnitude is also seen in the maximum stress range measured in the top flange of the main girder for the side-by-side crawl test. Girder G1 (CH_26) had a maximum stress range of 4.4 ksi whereas Girder G2 (CH_24) had a maximum stress range of 5.2 ksi. This difference was only noticed for the top flange. The magnitude of the stress range in the top flange is so small that it would be unlikely to ever generate a difference of such magnitude (0.3 ksi for CH_23 and 0.4 ksi for CH_25).

4.2.6 Live Load Distribution

Some minor discussion of load distribution was presented during the sections on the static controlled load test and side-by-side crawl controlled test. From that analysis it was found that the negative moment region over Pier 13 had balanced load distribution, both girders had nearly identical stresses. It was also found that there was reasonable load distribution in the positive moment region at the midspan of Span P. This location did not have a perfect fifty-fifty split between the girders; however, the stresses did not indicate anything too out of the ordinary. To further evaluate

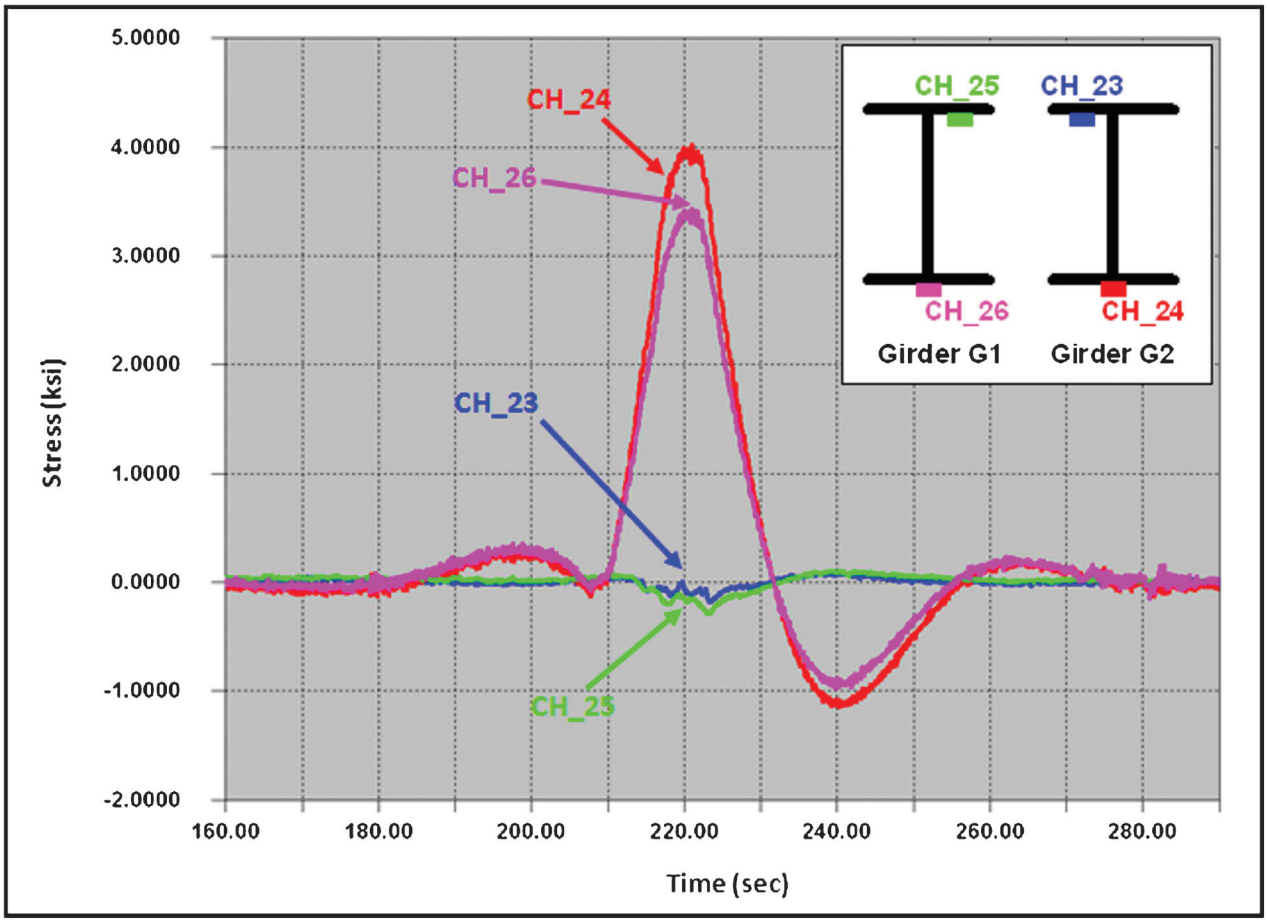

Figure 4.19: Response from side-by-side crawl test at midspan of Span P girders

the load distribution an analysis of the single-line crawl test was performed on the main girder strain gage locations. Specifically, the evaluation will focus on the two main girder strain gage locations where both girders were instrumented: over Pier 13 and midspan of Span P.

Calculating the percent of live load distributed to each main girder for the side-by-side crawl test was simple. Since the US-41 White River Bridge is a two girder bridge and the load is symmetric, half the load went to Girder G1 and half the load went to Girder G2. This is not the case with the single-line crawl test because all the trucks are in the right lane. To determine the theoretical amount of live load distributed to each girder the lever rule is used. Figure 4.20 is an illustration showing how the lever rule was used to compute the load distribution between the two girders. The illustration is based on a total unit load of one kip, the actual bridge dimensions, and approximate locations of the trucks during the test. Based on the results from the lever rule, the theoretical live load distribution for the single-line crawl test should be 18.4% for Girder G1 and 81.6% for Girder G2.

The strain gage location over Pier 13 had both main girders instrumented during the controlled load tests. Perfect load distribution was observed at this location for both the static controlled load test and side-by-side crawl controlled load test. To evaluate the results of the single-line crawl controlled load test, the data recorded during this test was plotted in Figure 4.21. As would be expected, Girder G2 has a larger stress and carries a greater portion of the load than Girder G1 for both the tensile and compressive responses. The live load distribution factor for each girder can be calculated by dividing the response from a single strain gage by the sum of both, top flange or bottom flange, strain gages.

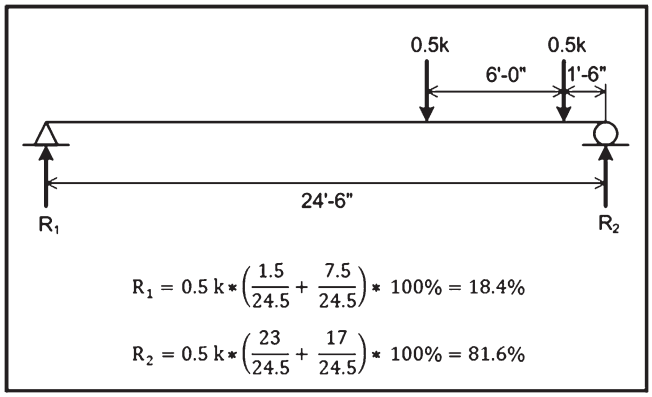

Figure 4.20: Single lane crawl test load distribution

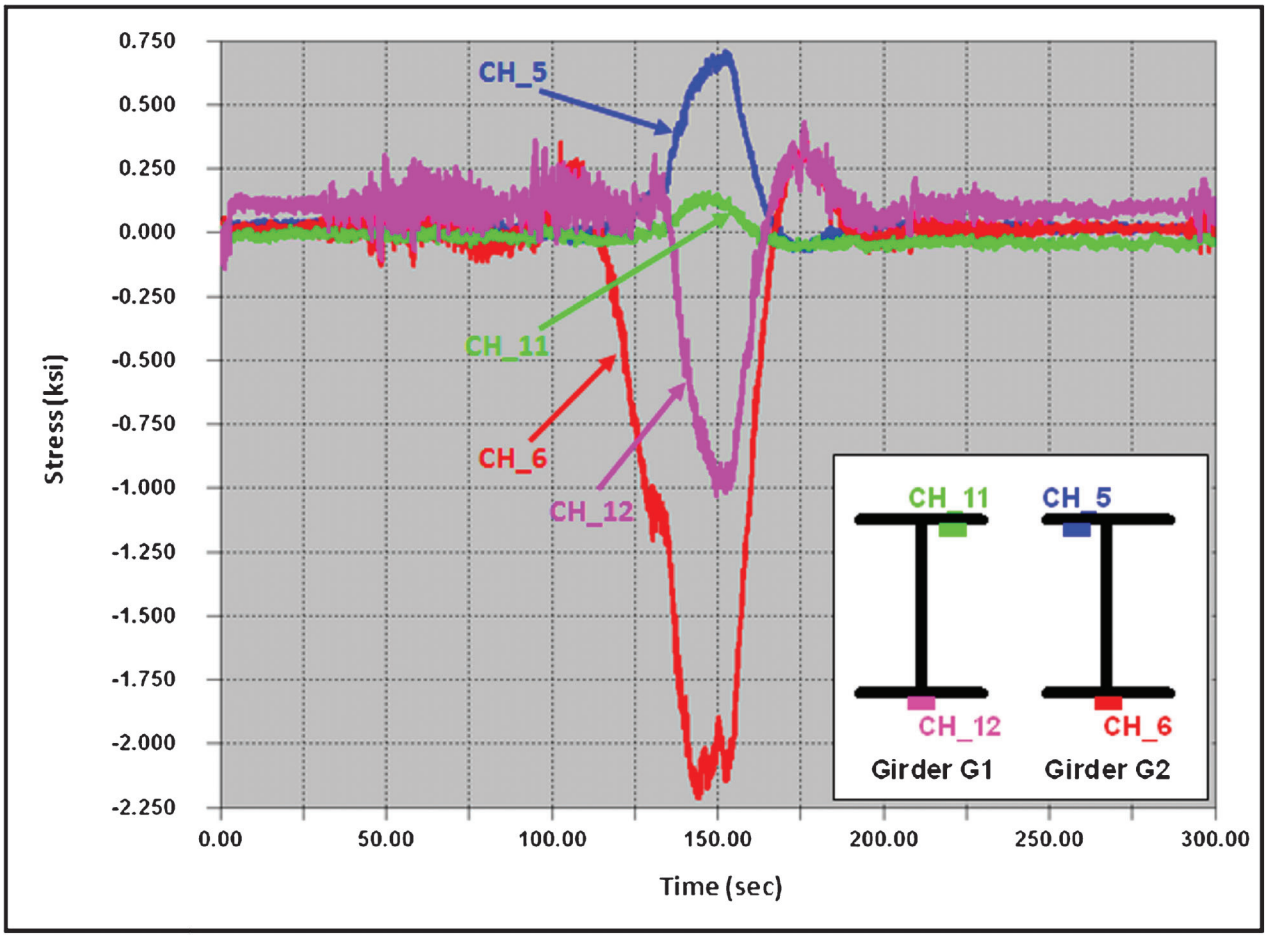

Figure 4.21: Response from single-line crawl test at Pier 13 girders

Looking first at the compressive response (bottom flange strain gages), the live load distribution factors are calculated as 30.4% and 69.6% for Girder G1 and Girder G2, respectively. The difference between the measured and theoretical distribution factors can be attributed to a variety of reasons. The most likely reason for the difference between the distribution factors is the additional structural elements not accounted for in the simple model used for the level rule. Elements such as the concrete deck and steel stringers help to distribute the load out away from the exact area of the strain gages both transversely and longitudinally; hence, resulting in difference live load distribution factors.

At the Pier 13 location live load distribution factors were also calculated for the top flange strain gages. Calculating the percentage of load distributed to each of these strain gages, better agreement is found. The top flange strain gages have live load distribution of factors of 18.1% for Girder G1 (CH_26) and 81.9% for Girder G2 (CH_24). These distribution factors are near perfect matches to those calculated by the lever rule.

Live load distribution factors could also be calculated for the single-line crawl test at the midspan of Span P. The data used to calculate the live load distribution factors at this location is plotted in Figure 4.22. As seen in the figure, the compressive response is very minimal; thus, distribution factors will only be calculated for the tensile, bottom flange, strain gages. The resulting live load distribution factors for the bottom flange strain gages are 31.8% for Girder G1 (CH_26) and 68.2% for Girder G2 (CH_24). These are not the same as the theoretical distribution factors calculated by the lever rule. The difference between the measured distribution factors and theoretical distribution factors can once again be attributed to the additional load carrying elements not accounted for in the lever rule computation. Therefore, it is not a surprise that the measured live load distribution factors indicate better load distribution than the theoretical distribution factors calculated by the lever rule.

One notable observation is made when comparing the live load distribution factors measured for the bottom flange at the Pier 13 strain gage location to those measured at the midspan of Span P strain gage location. There is less than a one percent difference between the factors measured at these two positions. Both locations likely have similar elements distributing the load, resulting in similar values. Had more than one girder been instrumented in the other two main girder

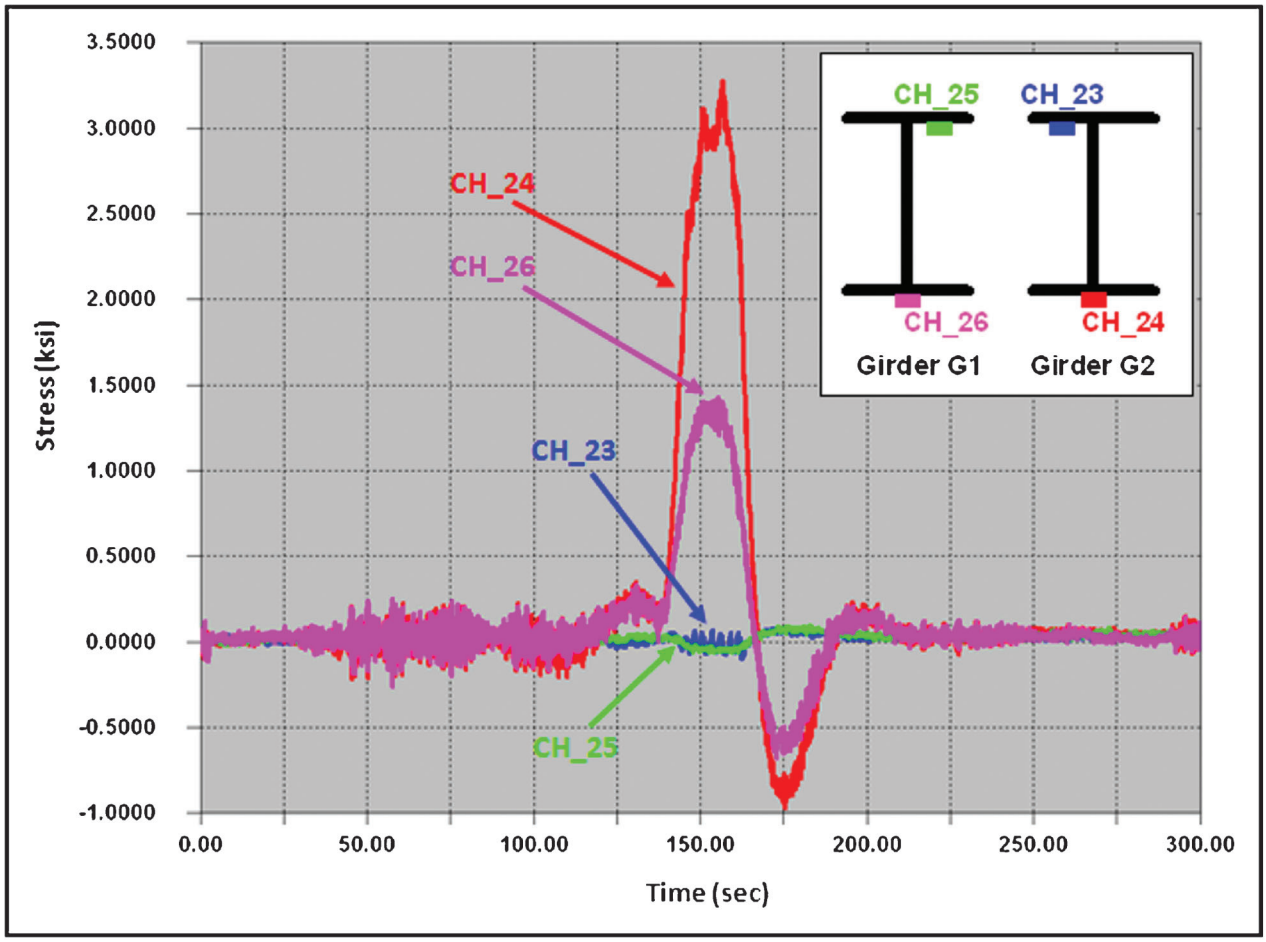

Figure 4.22: Response from single-line crawl test at midspan of Span P

strain gage locations, it would not have been uncommon to find those locations also having similar live load distribution factors.

4.3 Stresses in Floor Beams

Three floor beam locations (top and bottom) were instrumented with strain gages. Two sets of the strain gages were installed on the floor beam over Pier 13; two near the center of the floor beam and two near the edge. The third set of strain gages were installed near the centerline of the third floor beam north of the pin and hanger assembly. Exact locations for all floor beam strain gages can be found in the attached as-built instrumentation plans. It should be noted that the data from the side-by-side controlled load test were used for the discussion of the stresses in the floor beams.

The floor beams instrumented responded very similar to a single span beam with fixed ends; specifically, the floor beam over Pier 13 responded in this fashion. Figure 4.23 is a plot of the four strain gages installed on the floor beam over Pier 13. Before discussing the response of this floor beam, it should be noted that CH_8 (red trace) stopped functioning in the period between the installation and the controlled load testing; however, it is still shown for completeness sake. As can be seen in the plot, the strain gages near midspan of the floor beam respond equal and opposite. This is the expected response as there is no interaction with the concrete deck that would cause a composite response. Also, as expected, the strain gage on the bottom of the floor beam, CH_10 (pink trace), has a tensile response while the strain gage on the top of the floor beam, CH_9 (green trace), has a compressive response. This is typical of a single span beam with fixed ends.

Looking at the strain gages out near the edge of the floor beam, the typical response of a fixed end beam is observed. For a fixed end beam under the load conditions present, it would be expected to experience negative bending. Negative bending should result in tension on the top and compression on the bottom of the floor beam. In the plot, the top strain gage, CH_7 (blue trace), experiences tension as predicted. Unfortunately, the bottom strain gage, CH_8 (red trace), is not functional; however, it can be assumed that it would indicate compression on the bottom of the floor beam.

The second floor beam instrumented had a very similar response to the floor beam over Pier 13, with

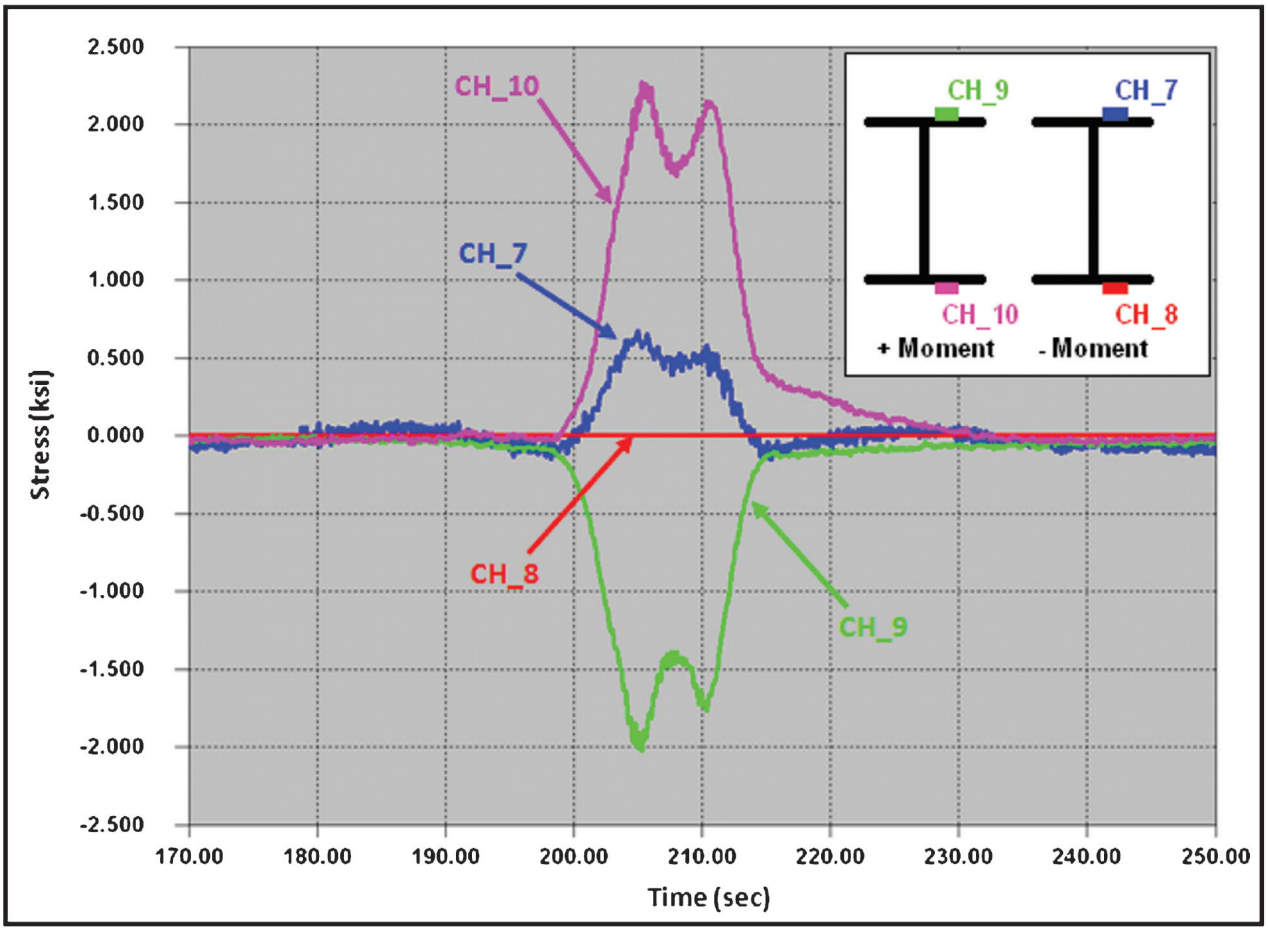

Figure 4.23: Response from floor beam at Pier 13

two mirror differences. One difference was the magnitude of the stress. The maximum stress of the floor beam north of the pin and hanger assembly was approximately 0.5 ksi greater than the stress in the floor beam over Pier 13. Secondly, the response of the floor beam north of the pin and hanger was approximately, but not exactly, equal and opposite. There was a greater tensile stress measured from the top flange than compressive force measured from the bottom flange. A plot of the stresses from the strain gages installed on the third floor beam north of the pin and hanger assembly can be found in Figure 4.24.

4.4 Stresses in Stringers

Five stringer locations (top and bottom) were outfitted with strain gages at the time of the controlled load testing. Three locations were in regions of negative moment. These include the center stringer over Pier 13, the east stringer at the 0.4 point, and the center stringer near midspan of Span P. The other two stringer locations with strain gages were in regions of positive moment. One of the locations of positive moment is on the same center stringer near midspan as one of the negative moment gages. The second positive moment strain gage is located at midspan of the simply supported stringer north of the pin and hanger assembly. Exact locations for all stringer strain gages can be found in the attached as-built instrumentation plans.

4.4.1 Composite Action

The stringers were designed to carry the loads from the deck to the supporting floor beams. Like the main girders, analysis was performed to determine if the stringers were acting compositely with the deck. To determine if the stringers and deck were acting compositely the neutral axis was calculated for the two locations in positive moment using the strain gage measurements and an assumed linear stress distribution. For the comparison the maximum stress from the side-by-side crawl test was used for both sets of gages. Plots of these data can be seen in Figure 4.25 and Figure 4.26. It should also be noted that the upper flange gages (CH_16 and CH_17) are on the bottom face of the flange. Thus, linear interpolation was used to calculate the stress on the top flange of the stringers. Figure 4.27 displays the two resulting stress diagrams and calculated neutral axis for both locations.

As can be seen in Figure 4.27, the calculated neutral axis is slightly above the neutral of the plain section

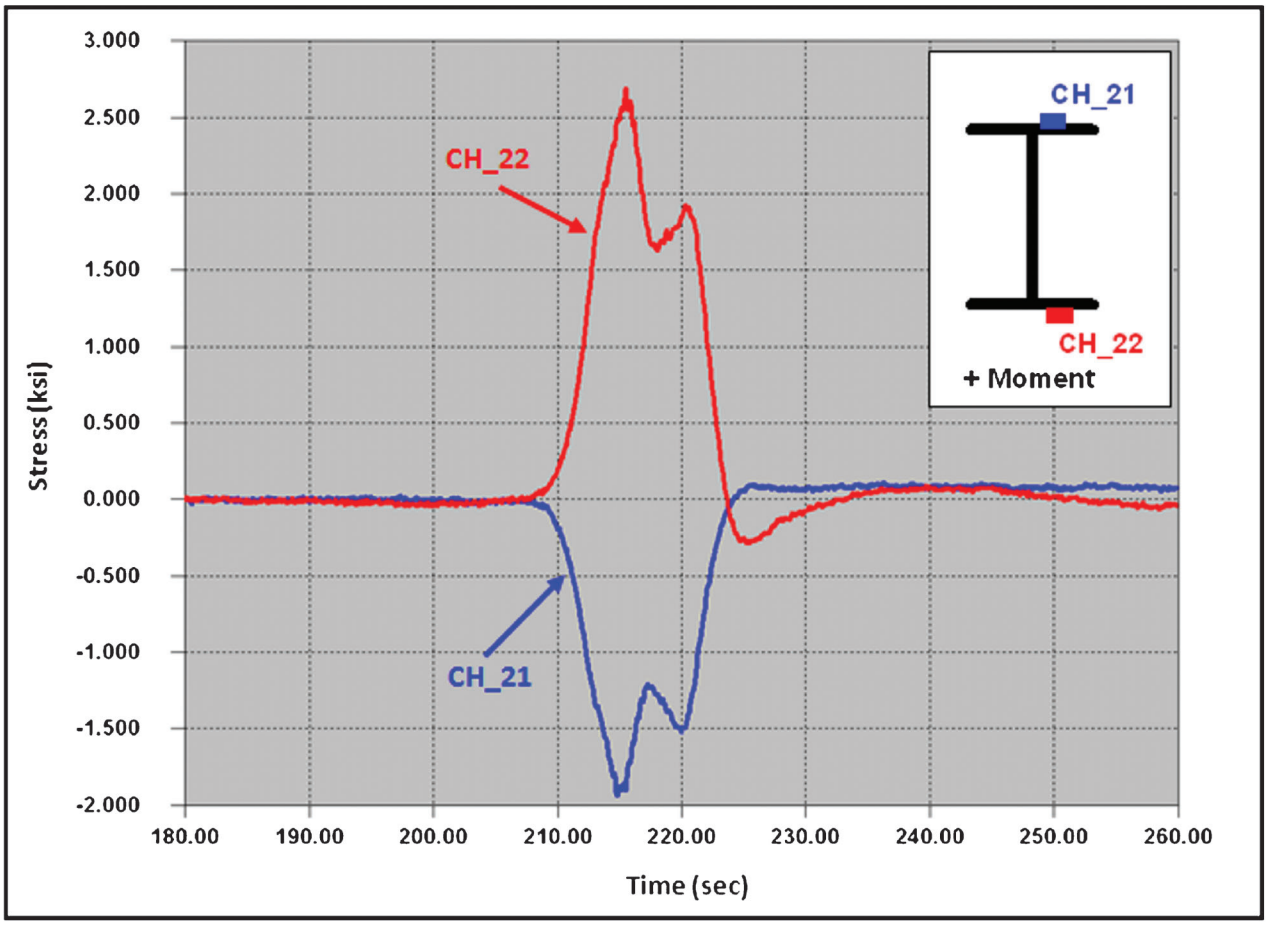

Figure 4.24: Response from floor beam north of pin and hanger assembly

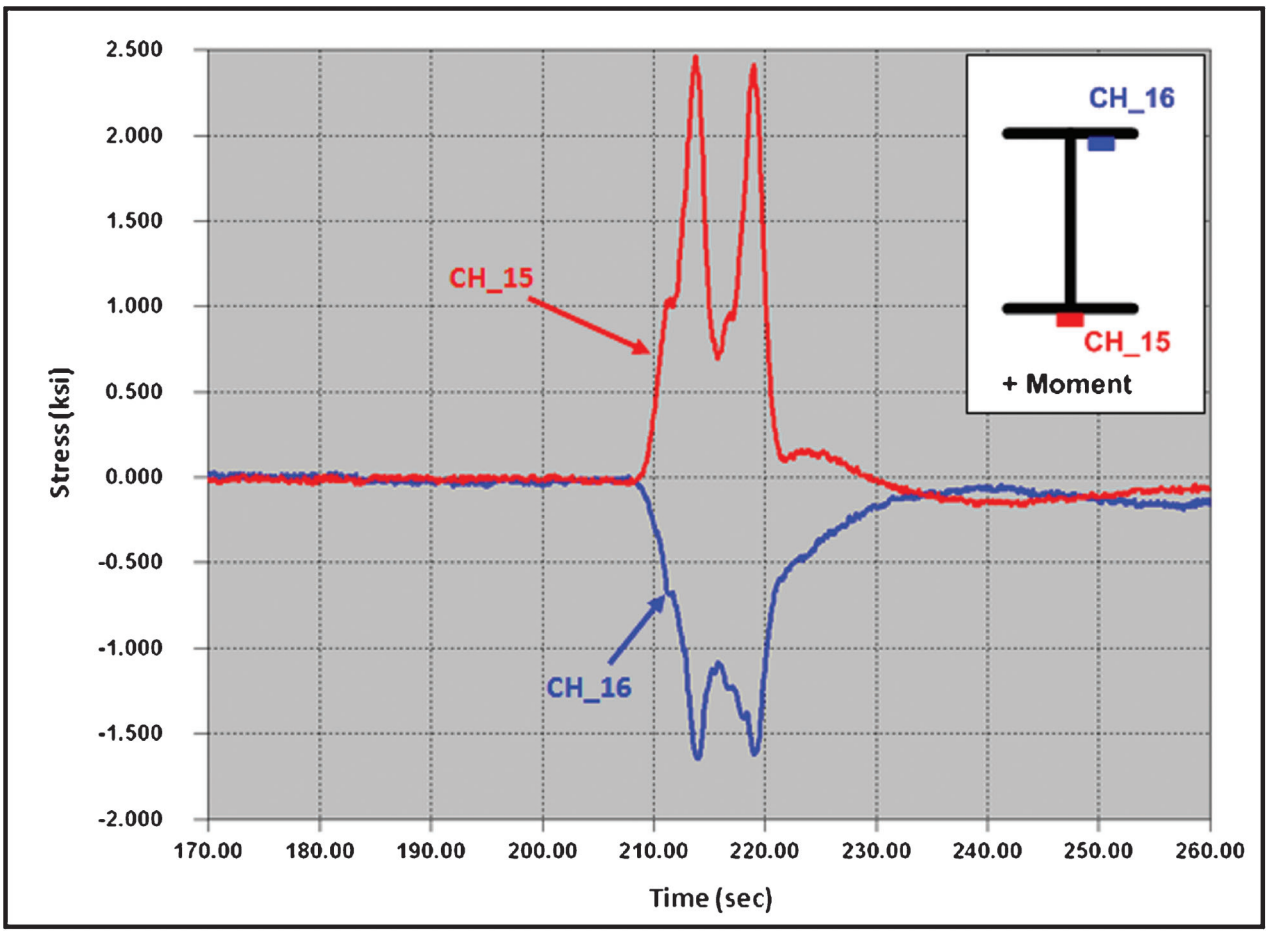

Figure 4.25: Maximum stress at CH_15 and CH_16 for side-by-side crawl test

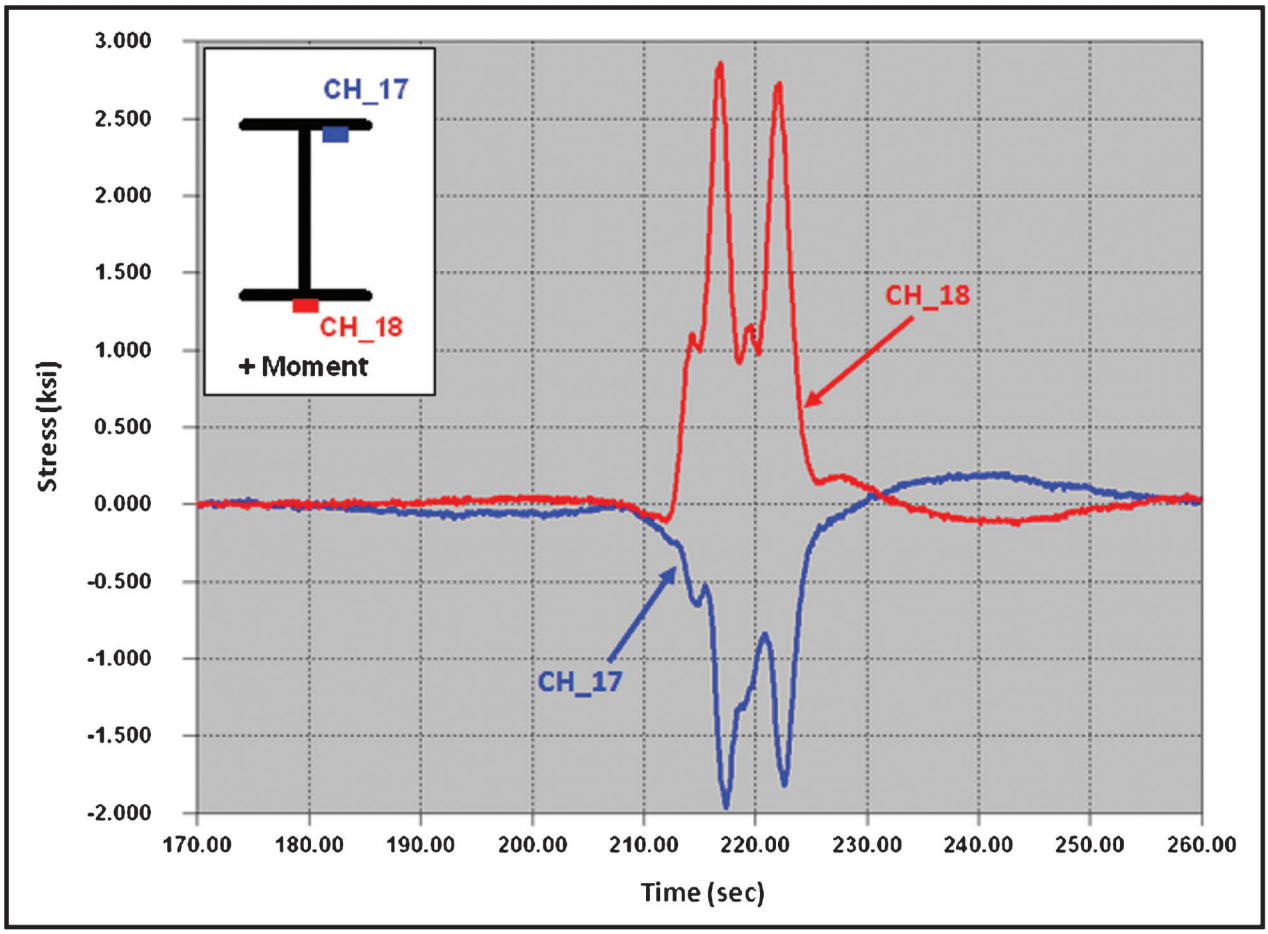

Figure 4.26: Maximum stress at CH_17 and CH_18 for side-by-side crawl test

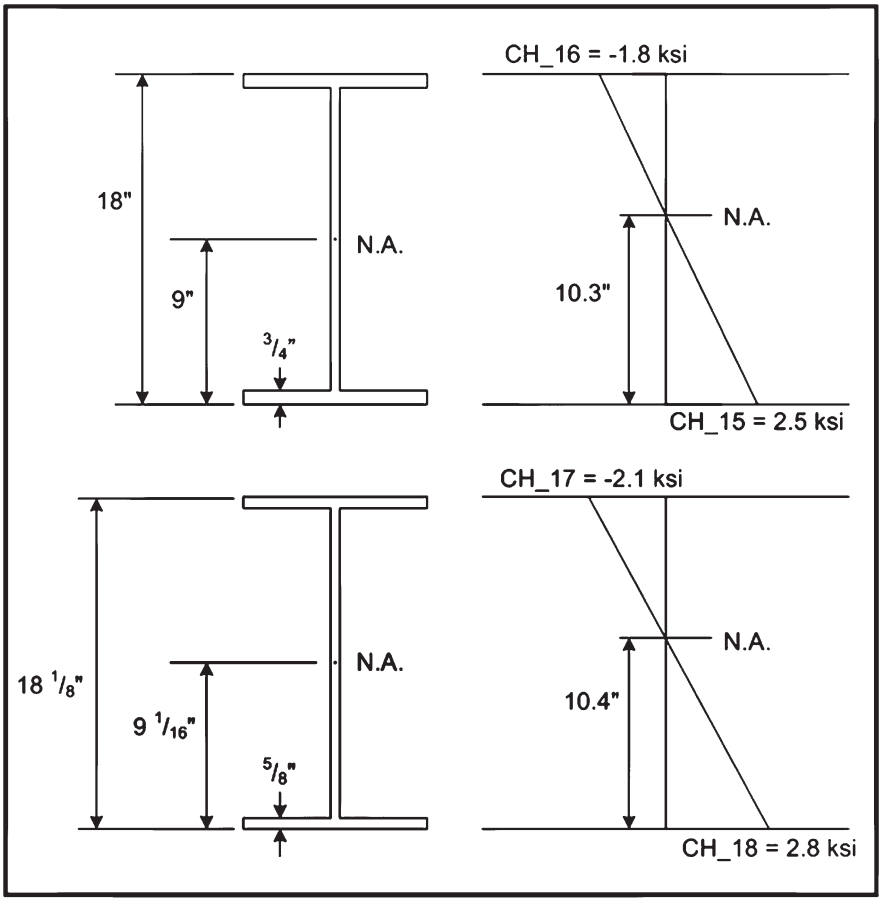

Figure 4.27: Neutral axis for positive moment region stringer locations from side-by-side crawl test

indicating the section is acting slightly composite. This can also be seen when looking at both data plots. The stresses in the data plots are not equal and opposite; specifically, the tensile stress is greater than the compressive stress. This suggests that some other element, most likely the deck, is carrying a portion of the compressive force. However, when viewing these plots it is important to remember that the stresses from the strain gages will not be perfectly equal and opposite because the top strain gage is on the bottom side of the top flange.

As stated above, slight composite action was observed between the steel stringers and concrete deck. However, the magnitude and consistency in which the composite action was observed is not enough to consider it in design or analysis. For all practical purposes the stringers acts independent of the concrete deck. The lack of consistency in the composite action is most likely attributed to the fact there is no positive connection between the deck and stringers; therefore, nothing to limit slip between the surface.

4.4.2 Local Bending Effects

Local bending effects can often be observed in the stringers of a bridge. These local bending effects are typically the direct result of tire loads and are most often observed in elements that are in direct contact with the deck, such as stringers. The magnitude of the local bending is a direct result of the location of the element to the travel lane. For instance, a stringer at the center of the driving lane will be less affected by tire loads than a stringer out toward the edge of a lane where the wheels travel. Figure 4.28 is a diagram of the local bending effect observed during the controlled load testing. As can be seen in the diagram the stringer has a global negative bending response. However, as the tire load passes over the stringer a local positive bending response is observed.

The local bending of the stringers was observed through strain gage measurements. Figure 4.29 is an example of such a response. The two plotted channels,

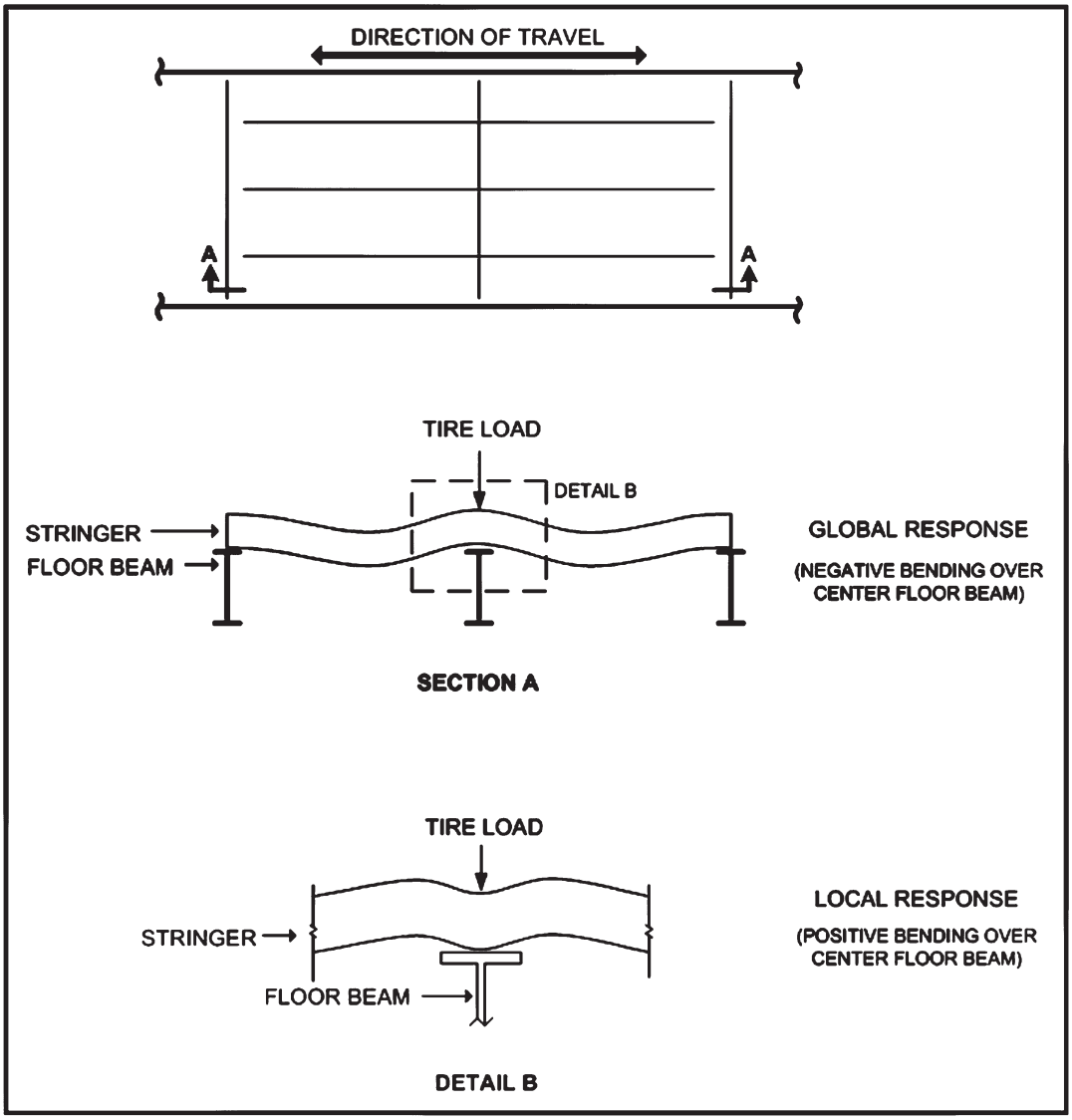

Figure 4.28: Diagram of local bending due to tire load

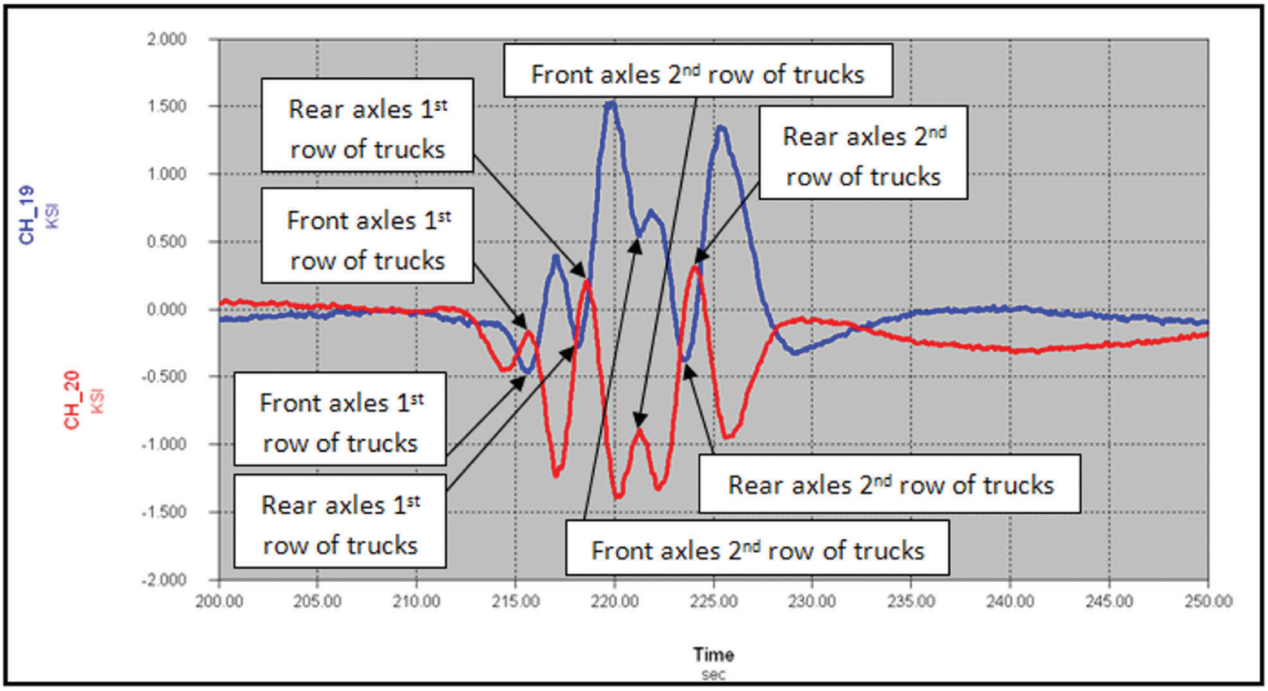

Figure 4.29: Example of local bending in a stringer

CH_19 and CH_20, are located in the negative moment region of the east stringer at the 0.4 point north of Pier 13. The blue trace is CH_19 and is located on the bottom side of the upper flange of the stringer. At the negative moment region, this gage should show a global tensile response. Conversely, CH_20 is located on the bottom of the bottom flange of the stringer and in the negative moment region should show a global compressive response. This is exactly what is seen when looking at the plot. However, as individual axles cross directly over the strain gage there is a local response, compressive for CH_19 and tensile for CH_20. The locations of the axle crossings are indicated on Figure 4.29. When evaluating the response of the stringers this local bending effect must be ignored.

4.5 Stresses at Pin and Hangers

On the northbound superstructure of the US-41 White River Bridge there are four locations with pin and hanger expansion joints. Pin and hangers have a history of seizing up due to corrosion. This results in bi-axial bending in the hanger which in some cases has lead to the development of fatigue cracks. Therefore, to verify that the pin and hanger assemblies were still acting as designed, the joint in Span P was instrumented. A total of sixteen (16) strain gages were installed on the four hangers at this location. One of the four hangers (east hanger on Girder G2) was heavily instrumented with eight strain gages. This hanger had gages installed on the side of the hanger (top, middle and bottom) and on the face of the hanger (centerline). Each of the remaining three hangers had either two or four strain gages installed on the side of the hanger. The exact locations for all pin and hanger strain gages can be found in the attached as-built instrumentation plans.

It should also be noted that for the discussion of the pin and hanger results from the controlled load test, the data from side-by-side crawl test was used. Results from the controlled load test for each of the pin and hanger locations will be discussed in the following sections. Since Girder G2 had the majority of the pin and hanger strain gages it will be the first discussed with Girder G1 to follow.

4.5.1 Girder G2 East Hanger

The east hanger on Girder G2 was the most instrumented hanger of the four monitored. Seven strain gages were installed on the side of the hanger and a single strain gage was installed on the east face. Originally, more than one strain gage was installed on the east face of the hanger. However, while collecting data during the installation it was determined moving these additional gages to the side of the hanger would be more beneficial. Therefore, CH_33 was the lone strain gage left on the face. A plot of the response from CH_33 during the side-by-side crawl test can be seen in Figure 4.30.

It can be seen in the plot that a very minimal response was measured at CH_33 during the controlled test. The peak stress was only 0.6 ksi. This occurred as the trucks crossed over the hanger onto the 'hung' span. Figure 4.31 is a photograph of the pin and hanger illustrating this concept. As can be seen in the photo, the traffic in the northbound lane crosses over Pier 13, onto the cantilevered span, and then onto the hanging span. Once the test trucks are on the suspended span, the

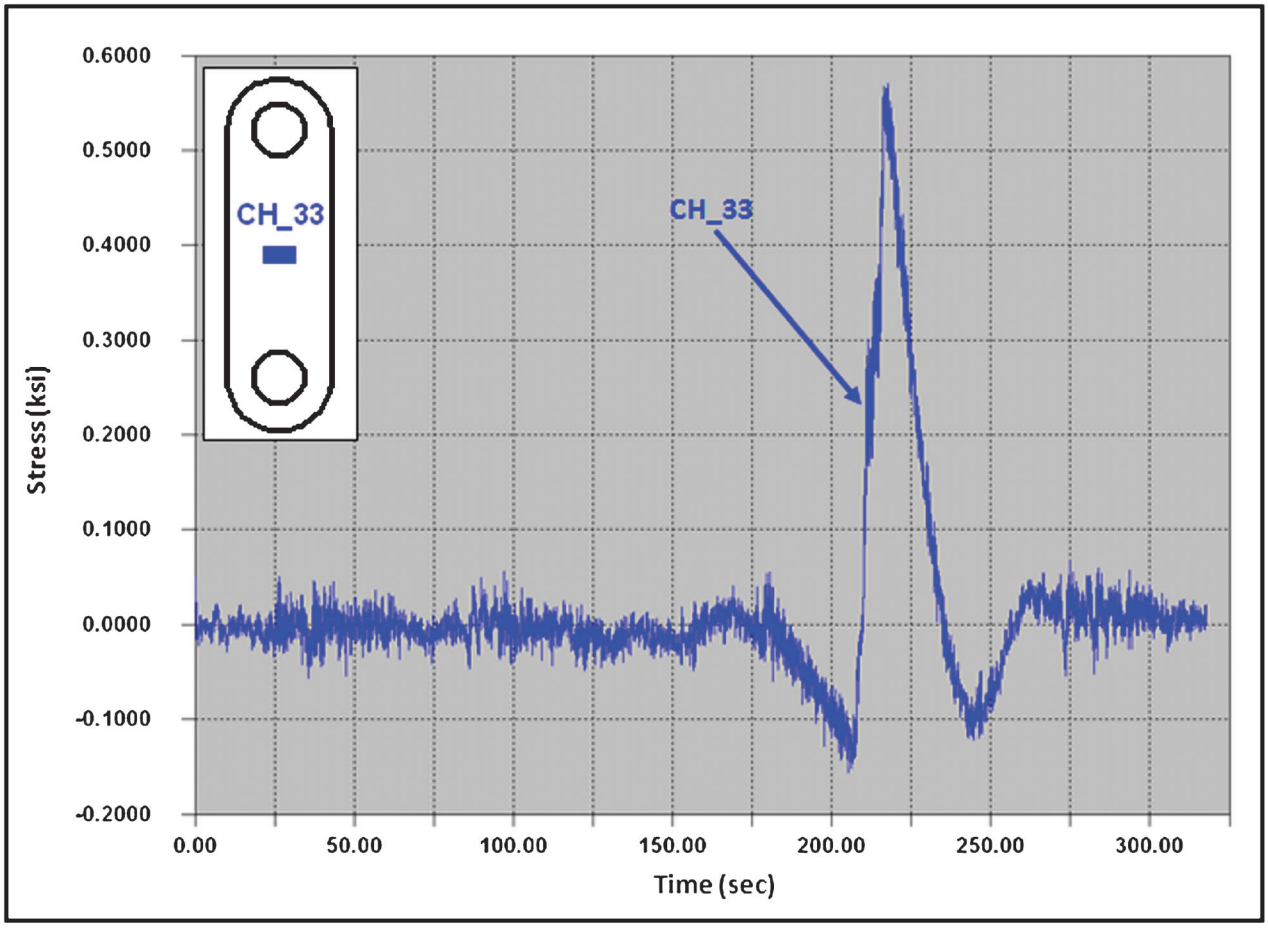

Figure 4.30: Hanger face strain gage response from side-by side crawl test at Girder G2 east hanger

hanger goes into tension to support the hanging span. It should be noted that the photograph in Figure 4.31 was taken prior to the installation of instrumentation on the US-41 White River Bridge; therefore, no strain gages are present in the photograph.

Some minor compression was also measured at CH_33. The compressive response occurred when the test trucks were in the adjacent spans to the pin and hanger. This sort of response is extremely common in continuous structures. Typically, as a load moves

Figure 4.31: Photograph of pin and hanger

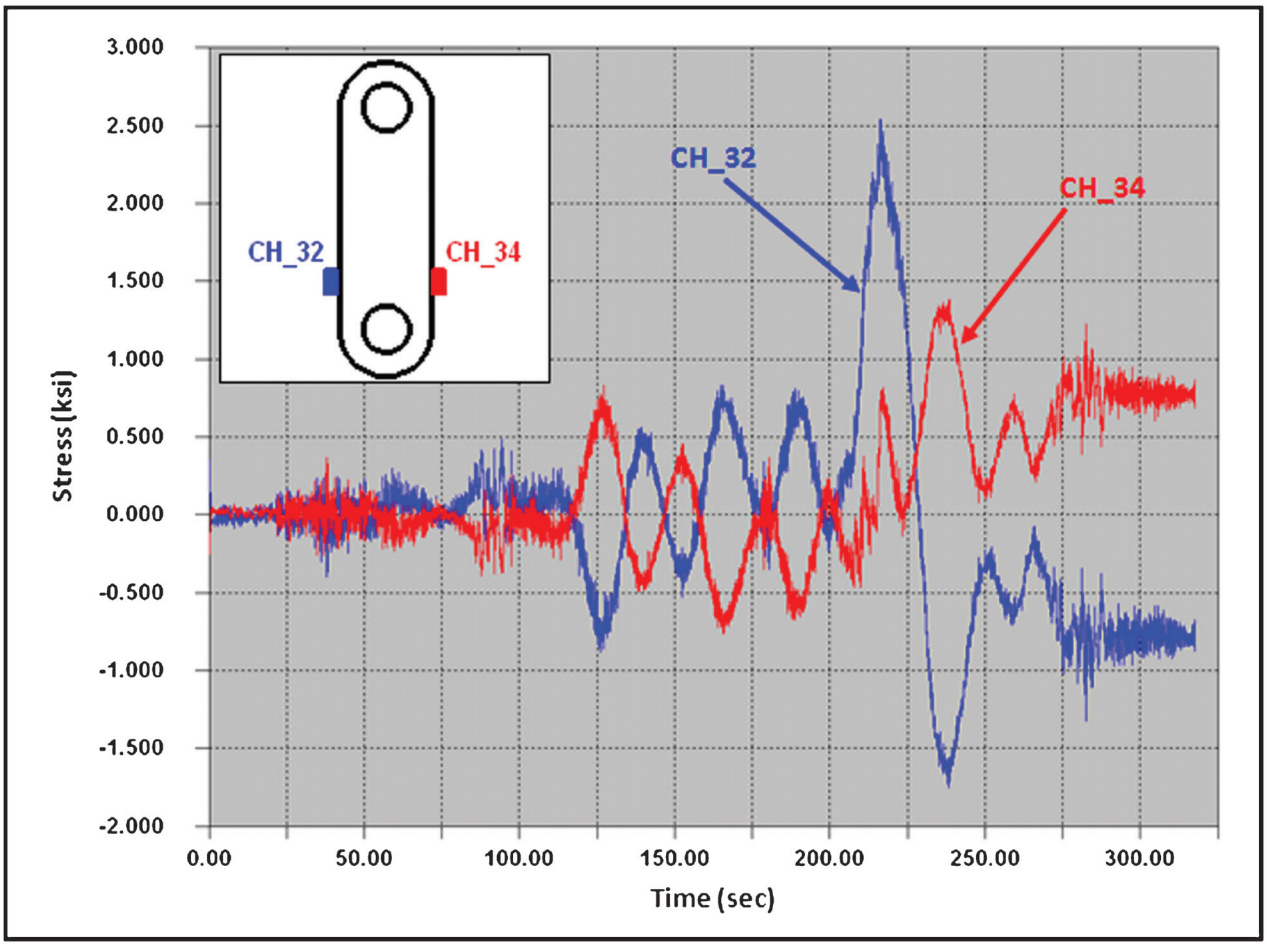

Figure 4.32: Maximum response from side-by-side crawl test at Girder G2 east hanger

through successive spans of a continuous structure a strain gage alternates between tension and compression.

The strain gages mounted on the edge of the hangers were the ones of greatest interest. These gages can be used to determine the degree to which bi-axial bending is occurring. Theoretically, all the force in a hanger should be strictly axial. A hanger is an element commonly referred to in structural engineering as a two-force member. Hence, strain gages mounted in the same location on opposite faces should experience the same stress. Plotted in Figure 4.32 are channels CH_32 and CH_34. These strain gages are located across from each other on the lower half of the Girder G2 east hanger. They have the greatest response of the Girder G2 east hanger side strain gages.

The plot indicates that some minor bending is occurring in the hanger. Bending is signified by the opposite response of the strain gages (i.e., one is in tension while the other is compression). This is seen in every span. As discussed above, for a continuous structure a strain gage will alternate between tension and compression as a load moves through successive spans. Such a response is noted at the Girder G2 east hanger for the side-by-side crawl test. The way in which the hanger is bending is as predicted. When the trucks are in the directly adjacent spans the north strain gage (CH_34) is in tension and the south strain gage (CH_32) is in compression. Conversely, when the trucks are in the span with the strain gage or any even span away the response is reversed (compression in the north strain gage and tension in the south).

Figure 4.33 is an illustration showing how the pin and hanger is bending as a load moves across the bridge. The sketch illustrates the predominant tension or compression stress induced in the hanger as a result of the deformation caused by the applied truck load. The direction of the bending is related to the resistance provide by the hanger to the relative displacement.

The only time the strain gages do not indicate bending is directly after the trucks cross the pin and hanger expansion joint. At this point both strain gages have a large tensile response. As discussed above, the reason for the all tensile response is due to the vertical support provided by the hanger for the heavy load on the hanging span. Once the load crosses Pier 14 and is no longer in the hanging span, the strain gages once again indicate bending.

One final interesting observation made from Figure 4.32 is the final displacement of the hanger. Since the stress does not come back to zero after the

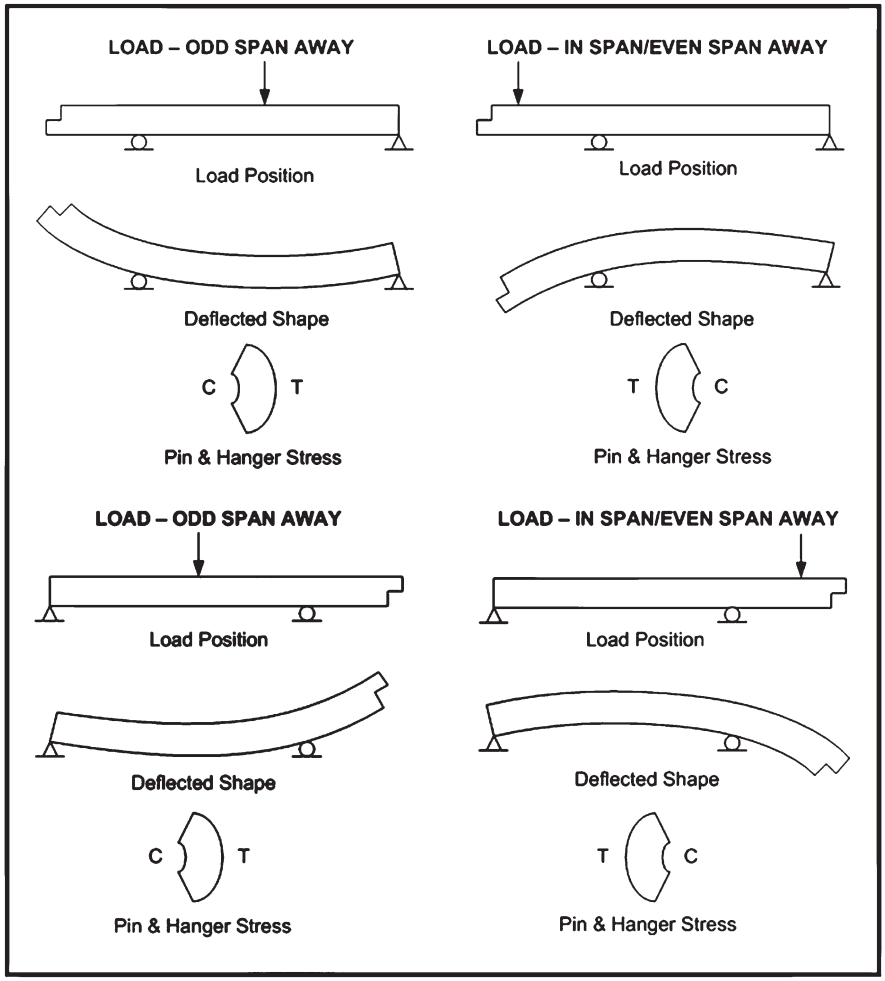

Figure 4.33: Hanger bending

trucks exit the bridge, a displacement has resulted. A permanent displacement in the pin and hangers would be of concern; however, what is shown in the plot is not permanent. Based on data recorded longer than the above plot, the pin and hanger assemblies exhibit some minor temporary displacement after a heavy loading. Over time the pin and hangers slowly vibrate back to their original position. This behavior is not uncommon with pin and hanger assemblies and, therefore, is of little concern. Based on the data presented above, the Girder G2 east hanger is not moving completely freely because bending is occurring; however, since the hanger does return to its original position there is not a large concern with the functionality of this element.

4.5.2 Girder G2 West Hanger

Each pin and hanger assembly is made of two hangers. Therefore, one would expect both hangers in an assembly to have very similar responses to a given loading; however, this is not always the case. Thus, the response from both hangers is reviewed. Girder G2 west hanger is the adjacent hanger to Girder G2 east hanger. Plotted in Figure 4.34 is the response from Girder G2 west hanger. It should be noted that only CH_38 is plotted as the opposite channel, CH_37, was not functional at the time of controlled load testing.

Comparing the plot of CH_38 with the corresponding strain gage on the adjacent hanger, CH_32, similarities are found. Both plots have the same general shape. The hanger experienced bending as the trucks crossed through the adjacent spans. Comparing the two hangers, Girder G2 west hanger has a larger overall response. The maximum tensile stress in Girder G2 west hanger was 0.6 ksi greater than that of Girder G2 east hanger. On the other hand, the compressive response was only 0.1 ksi different. One other notable feature is observed; the stress did not return to zero when the trucks exited the bridge. All three functional strain gages had readings of approximately 0.7 ksi when the trucks exited. It was found that over a period of time the hangers slowly vibrated back to their original position. Thus, the temporary displacement caused by the passage of the trucks was not of great concern. Based on the data presented above, the Girder G2 west hanger is not moving completely freely; however, since the hanger does return to its original position there is not a large concern with the functionality of this element.

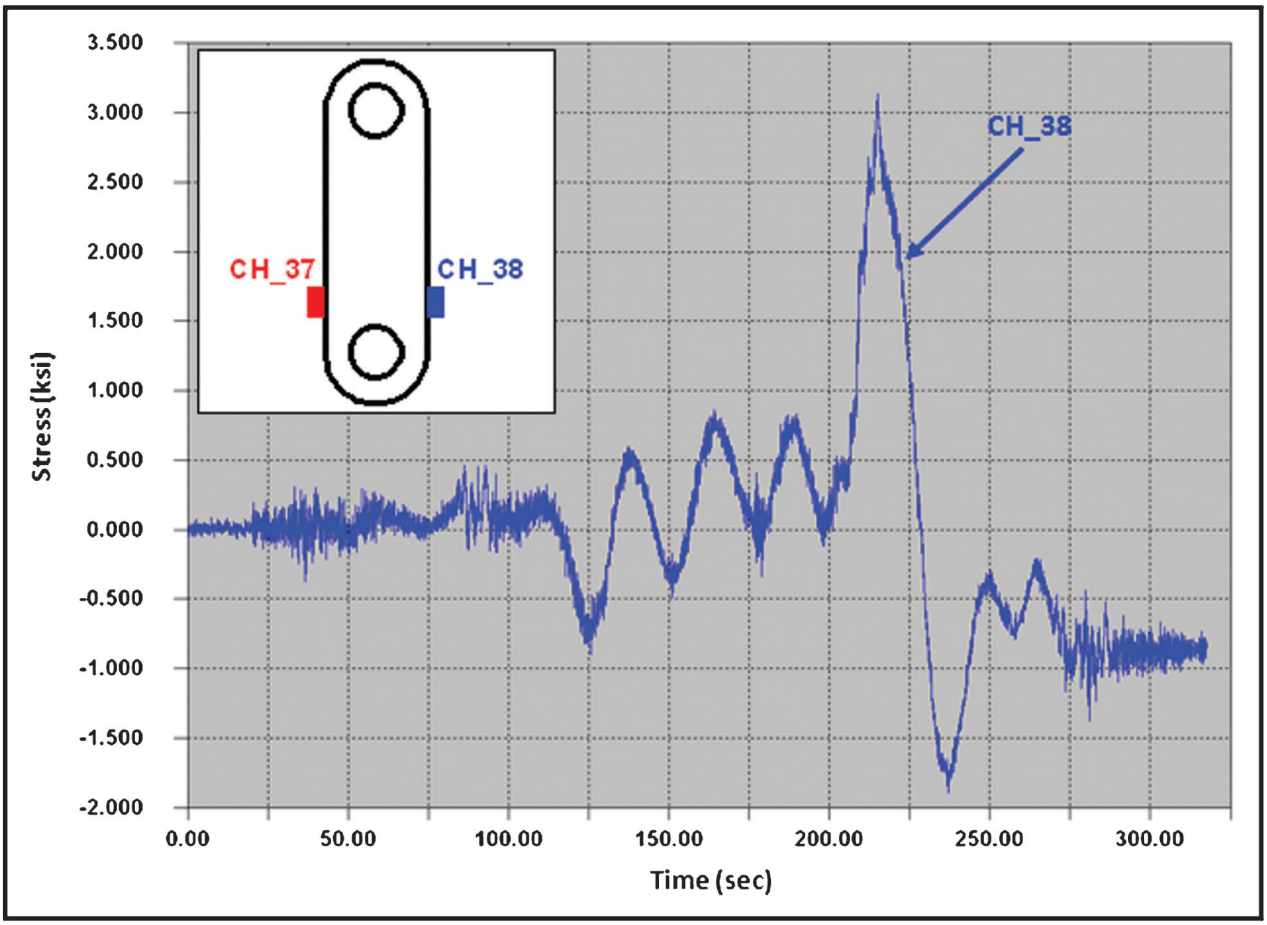

Figure 4.34: Response from side-by-side crawl test at Girder G2 west hanger

4.5.3 Girder G1 East Hanger

The pin and hanger assembly on Girder G1 is independent from the assembly on Girder G2. Therefore, the response from each hanger needs to be reviewed independently. Plotted in Figure 4.35 is the response of Girder G1 east hanger during the side-by-side crawl test. Both strain gages are installed on the sides of the hanger, six inches above the lower pin. CH_40 is on the north side and CH_39 is on the south side.

The above plot indicates that some minor bending is occurring. This again is signified by the two strain gages having opposite responses as the test trucks pass through successive spans. However, the amount of bending measured at this pin and hanger is less than the bending that was recorded in either Girder G2 hangers. As is typical with a pin and hanger, both strain gages indicate a large tensile stress as the trucks cross over the pin and hanger into the suspended span. A maximum stress of 2.6 ksi was recorded for CH_39 and 1.7 ksi for CH_40. It is also important to note that both strain gages returned to near zero stress after the loading event. This indicates that the pin and hanger assembly returned nearly back to the original starting position. Based on the data presented above, the Girder G1 west hanger is moving relatively freely and acting as designed.

4.5.4 Girder G1 West Hanger

Four strain gages were located on the Girder G1 west hanger. All strain gages were on the side of the hanger: two on the top half and two bottom half. Both sets of strain gages produced similar results. Since the lower strain gages are in the exact same position as the plots from the other hangers, they will be used to evaluate the response of the Girder G1 west hanger. Plotted in Figure 4.36 are the results from the lower two strain gages (CH_43 and CH_44) from the side-by-side crawl test.

Girder G1 west hanger exhibited some minor bending during the controlled load testing. This is noted by the opposite stress response in the strain gages shown in the plot of the data recorded during the side-by-side crawl test. This response is very similar to that of Girder G1 east hanger. Again, a tensile response was recorded for both hangers as the truck crossed into the hung span. Upon exiting the hung span; however, the response switched back to conflicting stresses. Lastly, the Girder G1 west hanger had some, but very little, final displacement at the end of the event as the stress

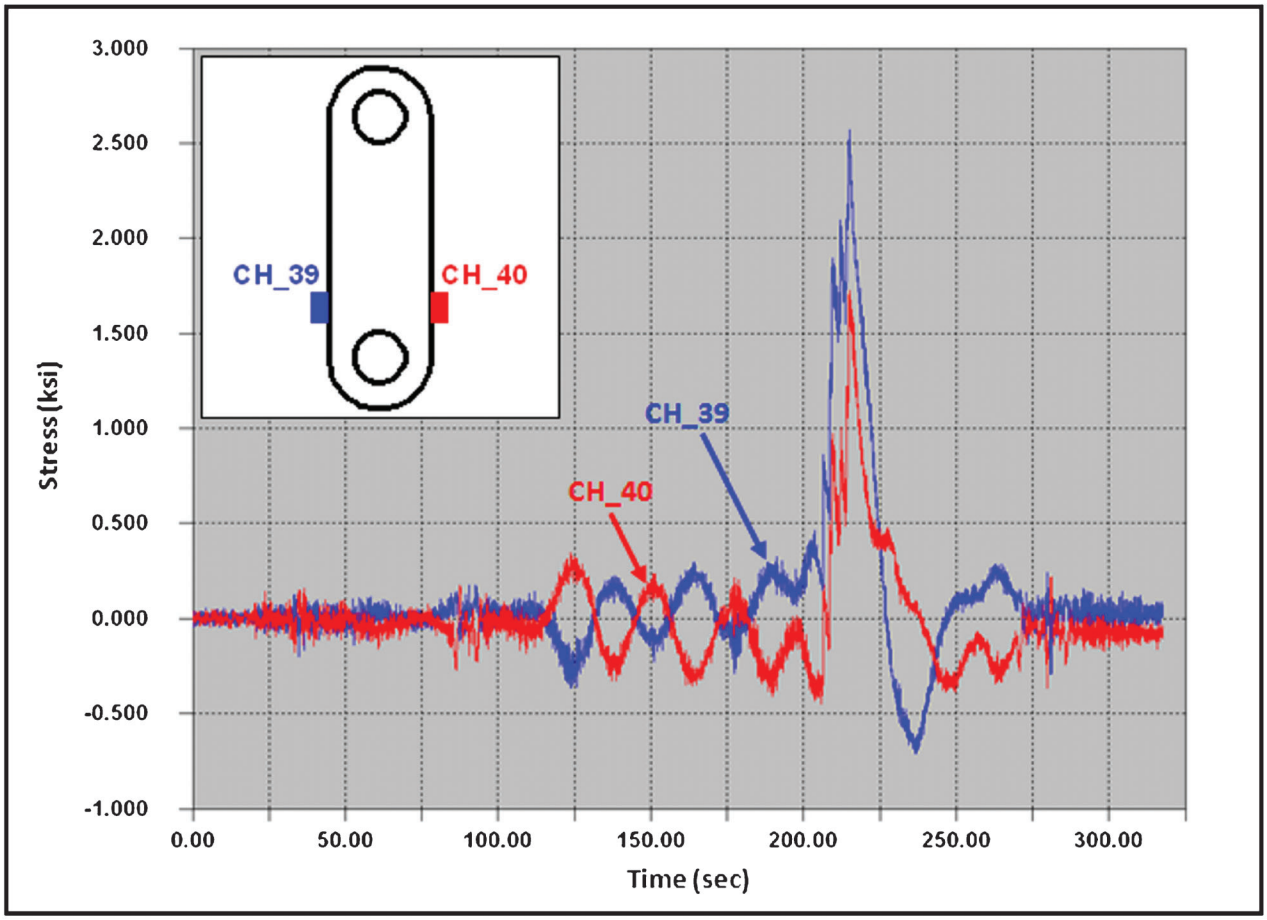

Figure 4.35 Response from side-by-side crawl test at Girder G1 east hanger

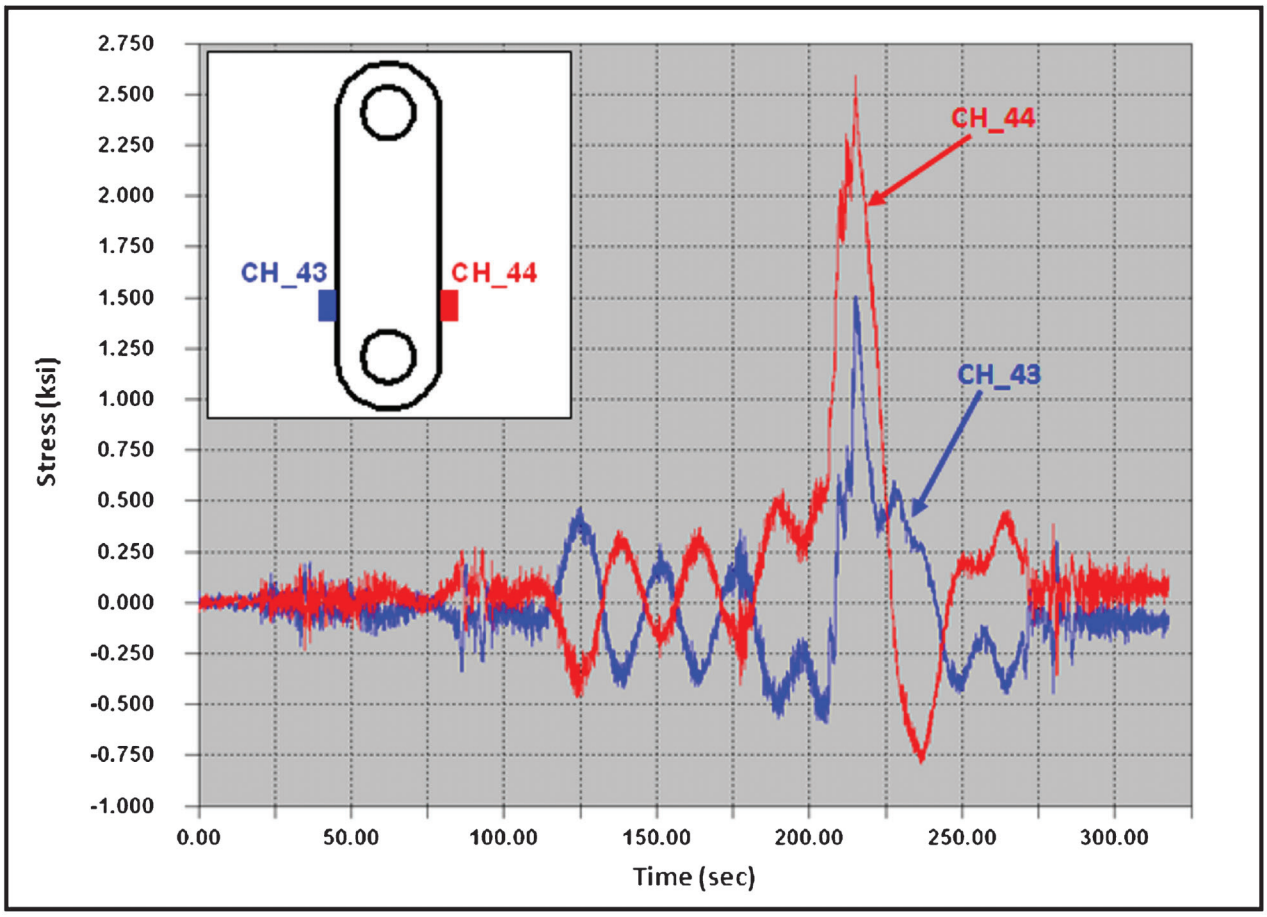

Figure 4.36: Response from side-by-side crawl test at Girder G1 west hanger

did not return perfectly to zero. Based on the data presented above, the Girder G1 east hanger is moving relatively freely and mostly acting as designed.

5. ANALYTICAL WORK

5.1 General Description

Structural analysis of the US-41 White River Bridge was performed using SAP2000. A basic two-dimensional model of the bridge was developed using frame elements. The model was created for two primary purposes: determine the critical locations of the test trucks for the static controlled load testing and verify the results obtained during the controlled load testing. At each of the four main girder strain gage locations, the influence line was calculated using SAP2000. The influence line for each location was used to determine the test truck layout that would maximize the response at a given strain gage. After the controlled load testing, point loads were added for each axle location of the test trucks. The stress at each strain gage location was then calculated using the moments produced by SAP2000 due to the test trucks. This was done for all four parked truck locations. Finally, the stresses computed using SAP2000 were compared to the field measured values obtained during testing. The following sections discuss how the model was created, present the influence lines for each parked truck location, and compare the calculated stresses to the field measured values.

5.2 Analytical Model

The US-41 White River Bridge consists of two superstructures that share a common substructure and are made up of sixteen spans each. Only half of the northbound superstructure of the bridge was included in the SAP2000 model. Since the US-41 White River Bridge is symmetric about its midpoint and the area of interest was located several spans away from the center of the bridge, modeling only half the bridge was the most efficient way to obtain a reasonably accurate model. Thus, the model included spans J, K, L, M, N, P, R, and S. All instrumentation was installed in spans N and P; therefore, these were the primary spans of interest during the modeling. Nevertheless, all eight spans were included in the model for accuracy.

A simple two-dimensional model was created for the analysis. The model was made of multiple frame section elements each having a different stiffness. All seven of the interior spans of the bridge were broken into seven segments. Additionally, the end span was split into five

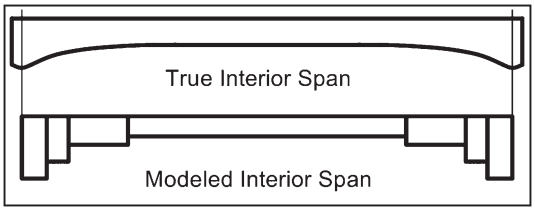

Figure 5.1: Comparison of actual bridge to model

segments. At each of the strain gage locations as well as at the pin and hanger assemblies an additional node was added giving the appearance that these spans were broken into more than seven segments. The frame sections on either side of these elements are identical; thus, each span was only broken into seven different stiffness segments.

To define the stiffness of a given frame section, the moment of inertia for each individual segment was input into SAP2000. The moment of inertia for each segment was calculated based on the gross area of the steel girder as detailed in the original design drawings. It should be noted that the moment of inertia for a given frame section is an estimate of the average moment of inertia over the length of the segment. Figure 5.1 depicts the difference between a true interior span and the way in which the interior spans were modeled. The stiffness of an element was not only averaged due to the haunch detail at the supports, but also due to the varying cover plate thickness as well. An example section of the SAP2000 model is provided in Figure 5.2. The span depicted in Figure 5.2 is Span N and contains three of the four stain gage locations of interest.

The exact truck locations were documented during the controlled load testing. Using these locations along with the test truck weights and dimensions presented during Chapter 3 (Figure 3.2 through Figure 3.5), the SAP2000 model was updated to analyze the stresses at the four strain gage locations of interest. Based on the field measured stress data, it was found that the steel girder and concrete deck were acting compositely. Thus, the moment of inertia for each of the frame sections was updated in the model for the stress analysis to reflect the increased stiffness due to the composite section. The weight of each axle was represented with point loads on the two-dimensional model. When adding the axle loads to the model, the lever rule was used to establish the amount of each tire load going to either girder. For a given horizontal position, all the axle loads were summed up and added as a single point load to the model. Figure 5.3 through Figure 5.6

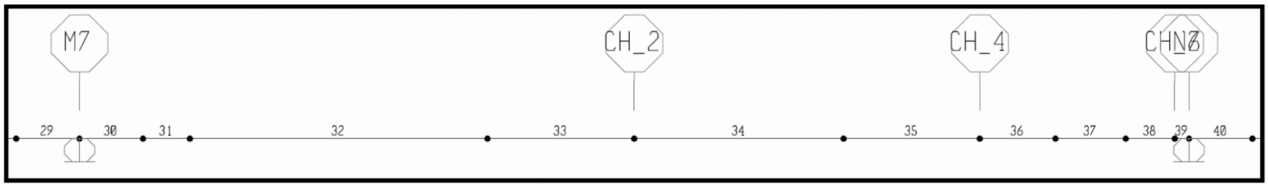

Figure 5.2: Example section of SAP2000 model

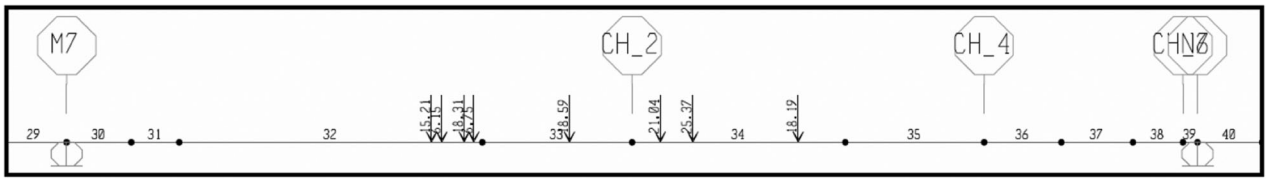

Figure 5.3: Load configuration for CH_2

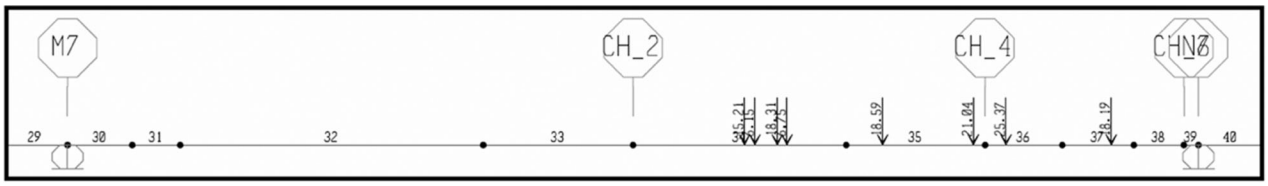

Figure 5.4: Load configuration for CH_4

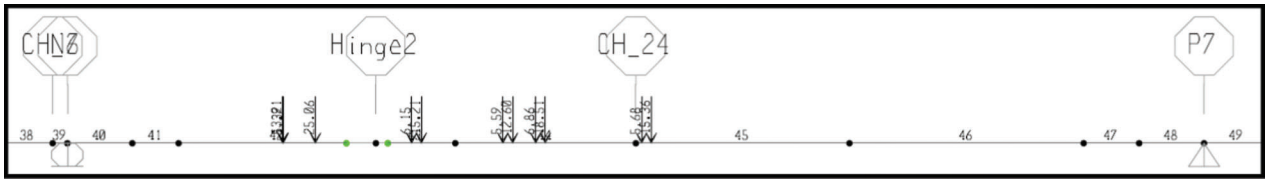

Figure 5.5: Load configuration for CH_6

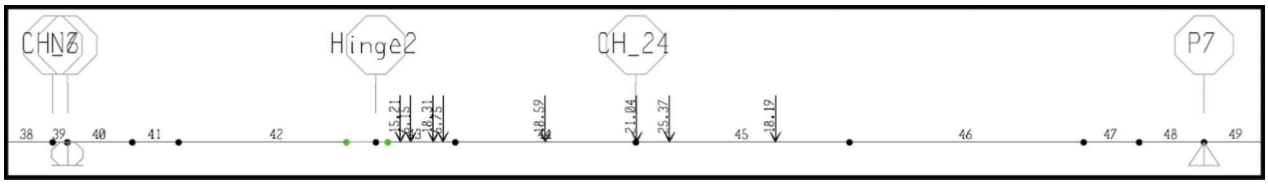

Figure 5.6: Load configuration for CH_24

display the loaded span for each parked truck position. Additionally, Figure 5.7 presents how the lever rule was used to determine the amount of load carried by Girder G2.

5.3 Influence Line Results

Prior to the controlled load testing, modeling was performed to determine the ideal locations for the parked test trucks that would maximize the response from the bridge. Influence lines were created to determine these locations. Using influence lines allows the stress at a given location on the bridge to be quantified based on a load at any location along the length of the bridge. For instance, if the moment or shear at the midspan of a continuous two span structure is desired when a point load is at midspan of the opposite span, an influence line of the structure could be used to directly determine the desired parameter by multiplying the load by the influence coefficient (moment or shear). Hence, an influence line is simply a plot of coefficients for a given location that when are multiplied by an applied load will produce the moment or shear at the location of interest.

When modeled correctly, SAP2000 can easily output the influence line at any location along the length of a

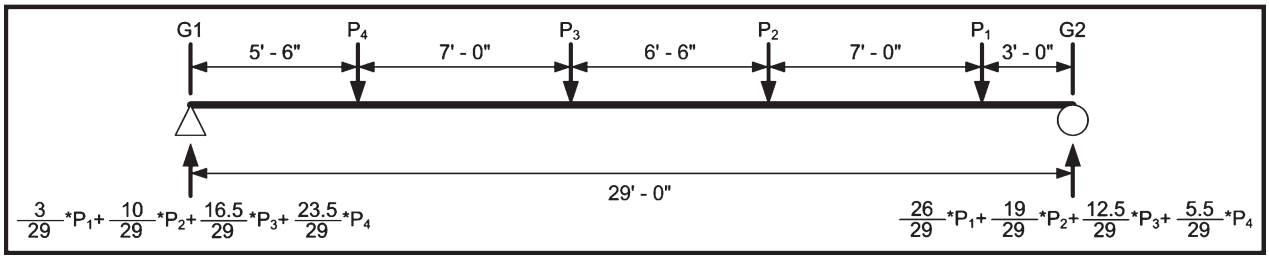

Figure 5.7: Lever rule graphic

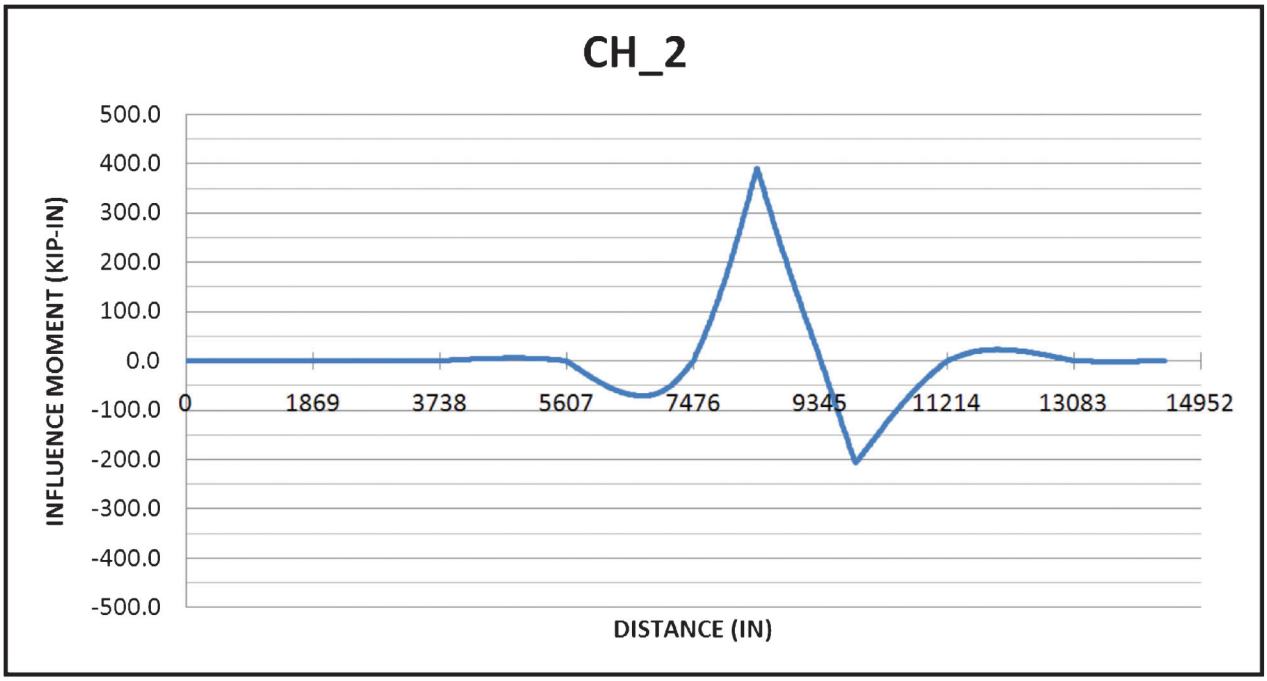

Figure 5.8: CH_2 strain gage location influence line

member. The influence lines for CH_2, CH_4, CH_6, and CH_24 are presented in Figure 5.8 through Figure 5.11, respectively. Using the table output from SAP2000 the influence lines were plotted in MS Excel. SAP2000 also plots the influence lines directly; however, MS Excel provided for a cleaner presentation of the analysis. It should be noted that the horizontal divisions of the plots are the location of the bridge piers in inches from the midpoint of the bridge. This is true except for the last division (14952) which is beyond the end of the bridge. Due to the shorter end span the bridge ends at the completion of the trace (14418 inches).

Using the above plots the trucks were placed at the peak influence moments. For instance, in the case of CH_2 the test trucks were placed at the midspan of

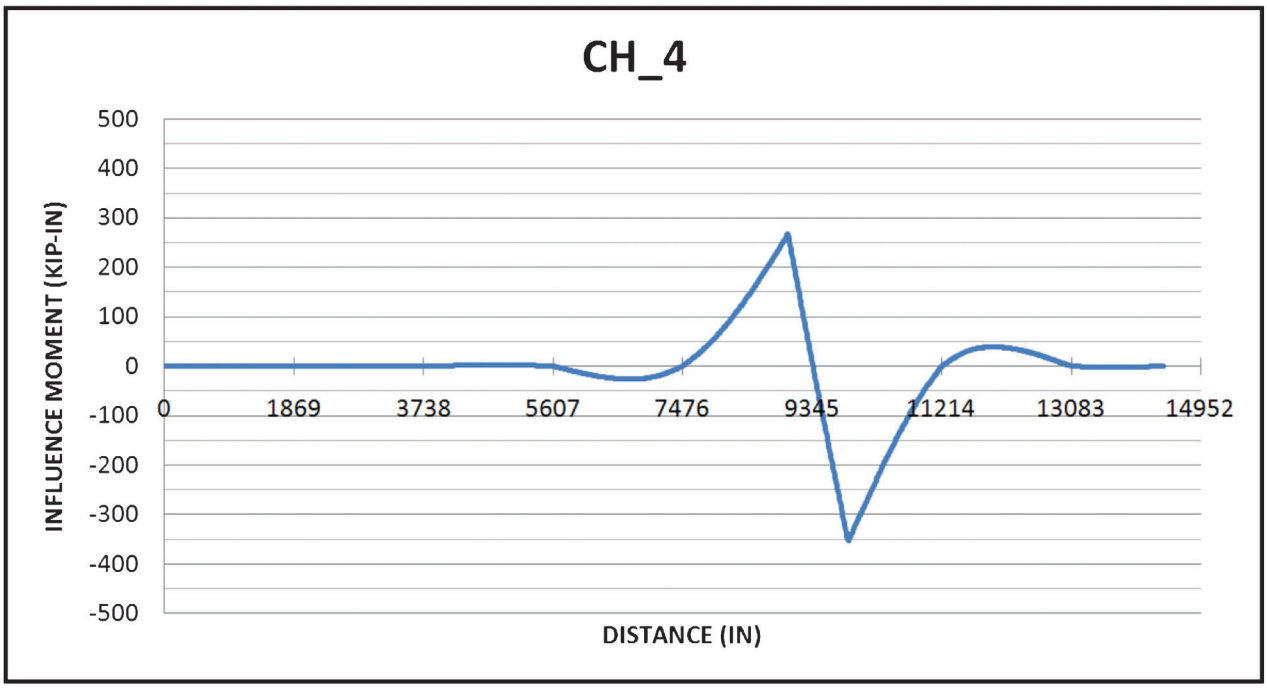

Figure 5.9: CH_4 strain gage location influence line

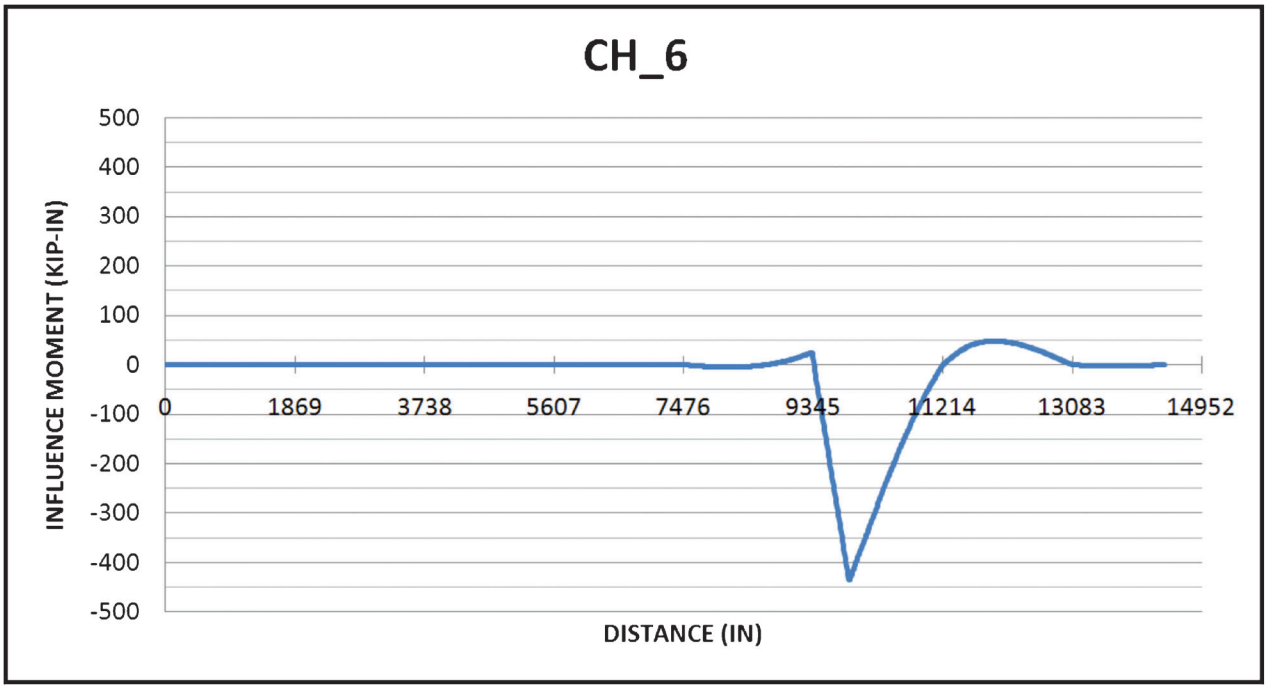

Figure 5.10: CH_6 strain gage location influence line

Span N. This created the greatest positive moment at CH_2 and hence the peak stress due to positive bending. Conversely, if the maximum negative bending stress was desired at CH_2 the test trucks would be parked near the pin and hanger expansion joint north of 9345 (Pier 13). For the park tests performed on the US-41 White River Bridge four locations were used. The negative bending response was maximized for CH_24 and the positive bending response was maximized for CH_2, CH_4, and CH_24.

5.4 Comparison to Controlled Load Tests

The maximum moment at each of the four strain gage locations was taken from the SAP2000 model and used to calculate the peak stress due to the test trucks.

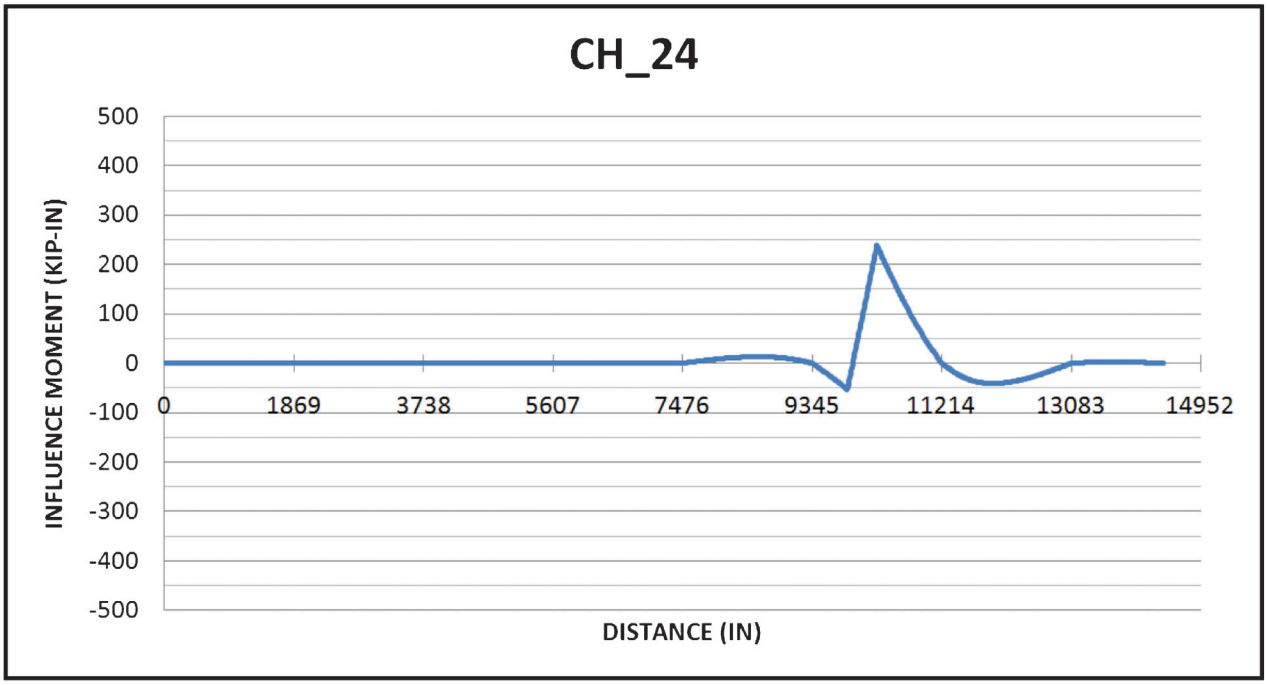

Figure 5.11: CH_24 strain gage location influence line

TABLE 5.1:
Comparison of analytical and field measured stresses

	BOTTOM		TOP	
CHANNEL	MEASURED (ksi)	CALCULATED (ksi)	MEASURED (ksi)	CALCULATED (ksi)
CH_2	4.5	8.0	−0.5	−1.6
CH_4	4.6	6.8	−0.7	−1.2
CH_6	−2.5	−6.1	0.8	1.5
CH_24	3.8	3.8	−0.1	−0.7

To compute stress from the moment output, the maximum moment at each strain gage location was divided by the section modulus at that location. These stress values were then compared to field measured stress values. Table 5.1 displays the measured and calculated stresses for the controlled load testing at the four main girder strain gage locations on the US-41 White River Bridge.

As can be seen in the table, the model typically over predicted the stress by approximately a factor between two and three. It is not uncommon for a two-dimensional frame section model to over predict the stress at a given location of a bridge by this amount. Compared to the actual bridge, the two-dimensional model of the primary girders is very simple. It does not account for other elements of the bridge that carry load out longitudinally away from the strain gage location. For example, elements such as the stringers and parapets help to distribute the load but are not included in the basic two-dimensional model. A more detailed three-dimensional model would undoubtedly more accurately account for the effects of these additional load carrying elements. However, since such minimal stresses were measured in the bridge due to the controlled load testing it was not deemed necessary to refine the analysis further.

One interesting point to note about the comparison, the bottom flange stress at the main girder strain gage in Span P was predicted exactly correct in the model. This was also the only strain gage location included in the analysis that was located in the span with the pin and hanger assembly. To accommodate the longitudinal movement due to the pin and hanger assembly there is a discontinuity in elements such as the concrete deck and parapet wall. These elements contribute to the longitudinal load distribution. Due to the discontinuity, these elements are no longer carrying any of the load. Thus, the main girder is left to carry the entire load; hence, the analytical model agrees perfectly with the field measured stresses.

6. FRACTURE ANALYSIS

One part of the evaluation performed on the US-41 White River Bridge consisted of determining the material properties of the bridge steel. Both toughness and hardness testing were performed on material samples removed from various structural elements of the bridge. Test results indicated the bridge had extremely low toughness values making the steel very brittle and hence susceptible to brittle fracture. Thus, a complete fracture evaluation was performed as part of the US-41 White River Bridge study. The following section describes the material testing and resulting fracture analysis in detail.

6.1 Material Testing

Steel samples were removed from the US-41 White River Bridge to perform material testing. The samples were extracted from a main girder angle and cover plate as well as the flange angle of a transverse floor beam. Upon receiving the floor beam specimen, a significant amount of pitting due to corrosion was noted. The samples were sent to be machined and tested. During this process, the floor beam sample was found to be too pitted with corrosion to manufacture a valid Charpy V-Notch (CVN) test specimen; thus, an additional floor beam sample was removed during the controlled load testing on November 24, 2009. A photograph of an example material sample removed from the cover plate can be seen in Figure 6.1.

INDOT extracted the samples from the bridge under the direction of the Purdue Research Team. The specimens were taken from areas of low stress (e.g., at the end of a member) with the consideration of the difficulty of removal. To remove each sample, a hole was first drilled at the corner of the specimen. This was done to create a smooth transition to the removed section for improved fatigue resistance. Likewise, after each sample was removed the cut surface was ground smooth to improve the fatigue resistance. Finally, all bare surfaces were painted to reduce the effects of corrosion. Figure 6.2 is an example location where a material specimen was removed from the US-41 White River Bridge. The area in the photo is at a cover plate termination.

Figure 6.1: Example material sample

Figure 6.2: Example location of removed material sample

6.1.1 Rockwell Hardness Testing

Hardness testing was performed on the steel samples removed from the US-41 White River Bridge. From the hardness data, estimates of the ultimate strength (F_u) of the steel were made according to ASTM A370. Testing was done using an Instron automated testing machine and Rockwell Hardness Scale 'B' (HRB). Results of the hardness testing for the cover plate, main girder angle, and floor beam angle are summarized in Table 6.1 through Table 6.3, respectively.

The original design drawings indicated the steel girders were made from ASTM A7 steel. Based on the ASTM specifications at the time period the US-41 White River Bridge was constructed, the ultimate strength of A7 steel was permitted to be between 60 ksi and 72 ksi. Table 6.4 presents the estimated ultimate strength based on the average hardness of each element.

TABLE 6.1:
Cover plate hardness testing results

COVER PLATE (HRB)				
	Sample Number			
Piece	1	2	3	Average
70 F #2	69.0	72.5	70.0	70.5
0 F #3	72.5	77.5	74.5	74.8
−30 F #1	69.0	66.5	71.0	68.8
Average of all tests:				71.4

TABLE 6.2:
Main girder angle hardness testing results

MAIN GIRDER ANGLE (HRB)				
	Sample Number			
Piece	1	2	3	Average
0 F #3	66.5	66.5	67.0	66.7
40 F #3	69.0	70.5	69.5	69.7
−30 F #3	69.5	68.5	69.0	69.0
Average of all tests:				68.4

TABLE 6.3:
Floor beam angle hardness testing results

FLOOR BEAM ANGLE (HRB)				
	Sample Number			
Piece	1	2	3	Average
−30 F #1	69.0	66.0	67.0	67.3
0 F #2	63.0	64.0	63.0	63.3
40 F #3	63.0	67.5	64.0	64.8
Average of all tests:				65.2

TABLE 6.4:
Estimated ultimate strength based on ASTM A370

ELEMENT	ESTIMATED ULTIMATE STRENGTH (ksi)
Cover plate	63
Main girder angle	59
Floor beam angle	56

As can be seen in the table, only the cover plate meets the ASTM specification. Both the main girder and floor beam angle have values slightly below the bottom end of the permitted range. Thus, since the values provided in ASTM A370 are only estimated values, the actual values might be within the acceptable range. To verify if these values truly fall outside the ASTM limits tensile coupons would need to be tested.

6.1.2 Charpy V-Notch Testing (CVN)

CVN testing of all three specimens was performed to determine the toughness of the US-41 White River Bridge material. The testing was completed by Laboratory Testing Inc. in Hatfield, PA. Results were originally only received for the cover plate and main girder angle. Due to the corrosion on the first floor beam sample a valid CVN sample was not able to be obtained. At a later time, CVN results for the floor beam were also obtained. A total of twelve tests were acquired for each member location. The twelve total tests were comprised of sets of three tests each at −30 °F, 0 °F, 40 °F, and 70 °F. The results are shown in Table 6.5 and plotted in Figure 6.3 through Figure 6.5 for the cover plate, main girder, and floor beam, respectively. Also shown in each of the plots are the AASHTO CVN impact energy minimum limits for non-fracture critical and fracture critical members in a Zone 2 temperature environment (Indiana is classified as Zone 2): 15 ft-lbs at 40 °F and 25 ft-lbs at 40 °F, respectively.

As can be observed in the plots of the test results, the impact toughness for all three elements is extremely poor. The CVN values for the US-41 White River Bridge do not meet the current requirements for a fracture critical bridge. Furthermore, of all nine specimens tested at 40 °F only one of the floor beam specimens exceeded the non-fracture critical requirement. It should be noted that the US-41 White River

TABLE 6.5:
CVN results

COVER PLATE		MAIN GIRDER ANGLE		FLOOR BEAM ANGLE	
TEMP (℉)	CVN (ft-lbs)	TEMP (℉)	CVN (ft-lbs)	TEMP (℉)	CVN (ft-lbs)
	2		2		3
−30	3	−30	2	−30	4
	2		3		3
	3		4		6
0	4	0	3	0	4
	6		3		5
	7		8		16
40	7	40	10	40	12
	7		13		14
	18		29		60
70	26	70	31	70	43
	14		25		55

Bridge was constructed in 1958 at a time when there were no CVN impact energy requirements for bridge steel materials; thus, it is not surprising the bridge does not meet these requirements. With that said, the requirements were set for a reason and therefore the extremely low values were of great concern to the Research Team leading to a complete fracture analysis.

6.2 Fracture Analysis

In an effort to assess the influence of the low CVN impact values, a full fracture analysis was performed on the US-41 White River Bridge after receiving CVN results for the main girder angle and cover plate. The fracture analysis began by determining the critical crack length based on the CVN results, loading measurements, and assumed dead load stresses. From this analysis it was determined the critical flaw size was nearly identical to the amount of material covered by a rivet head. Thus, Wiss, Janney, Elstner, Inc. (WJE) was contracted to remove rivets from selected regions of high stress and inspect the base metal for any cracks or defects using magnetic particle inspection techniques. No cracks were found as a result of the investigation performed by WJE. Therefore, it was determined fracture is not likely to occur for the US-41 White River Bridge. Additionally, an after fracture redundancy study was performed to determine the result of fracture in one of the main girder angles or cover plates. The study indicated sufficient reserve capacity would remain in the girder if fracture of one of these elements occurred. The following sections discuss each component of the fracture analysis in greater detail.

6.2.1 Critical Flaw Size

To determine the critical flaw size a quick evaluation was first performed to determine the smallest flaw detectable during a routine bridge inspection. It was determined that a 3/8 inch long crack emanating from the edge of a rivet hole would remain hidden under the head of the rivet and therefore would not be detectable during a routine visual inspection. An illustration of this concept is presented in Figure 6.6. Thus, it was first evaluated if a 3/8″ flaw had the potential for fracture. (It is noted that cracks extending past the head of the rivet (i.e., larger cracks) could also be missed; however, if a 3/8 inch defect is large enough to lead to fracture a larger

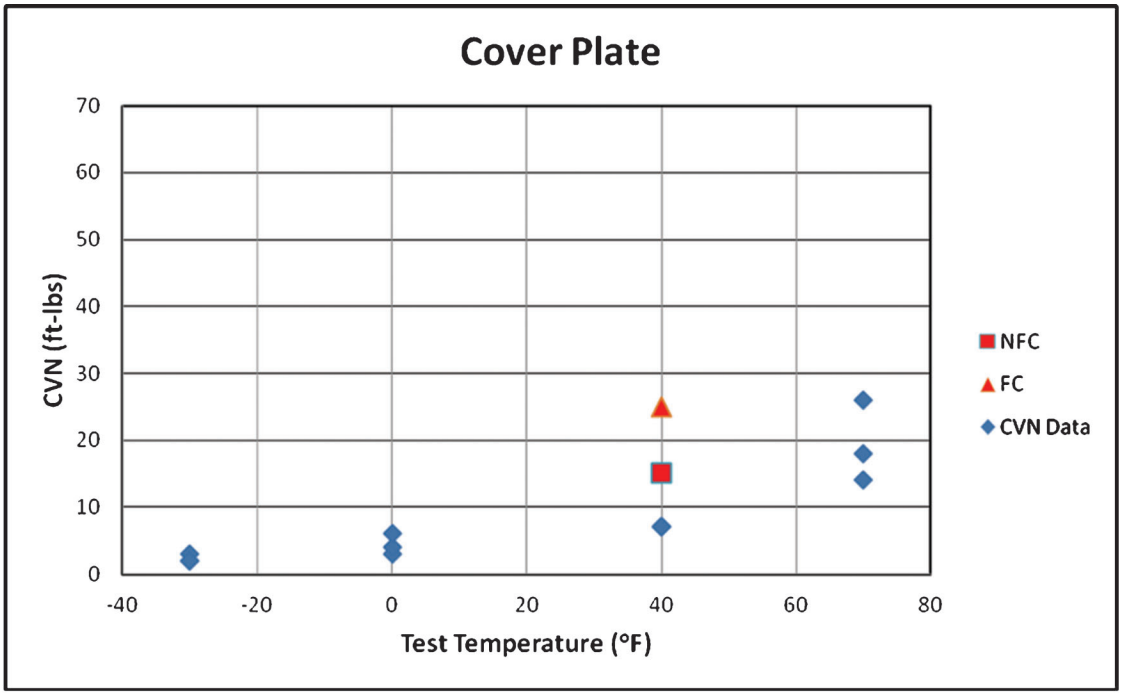

Figure 6.3: Cover plate angle plot of CVN data

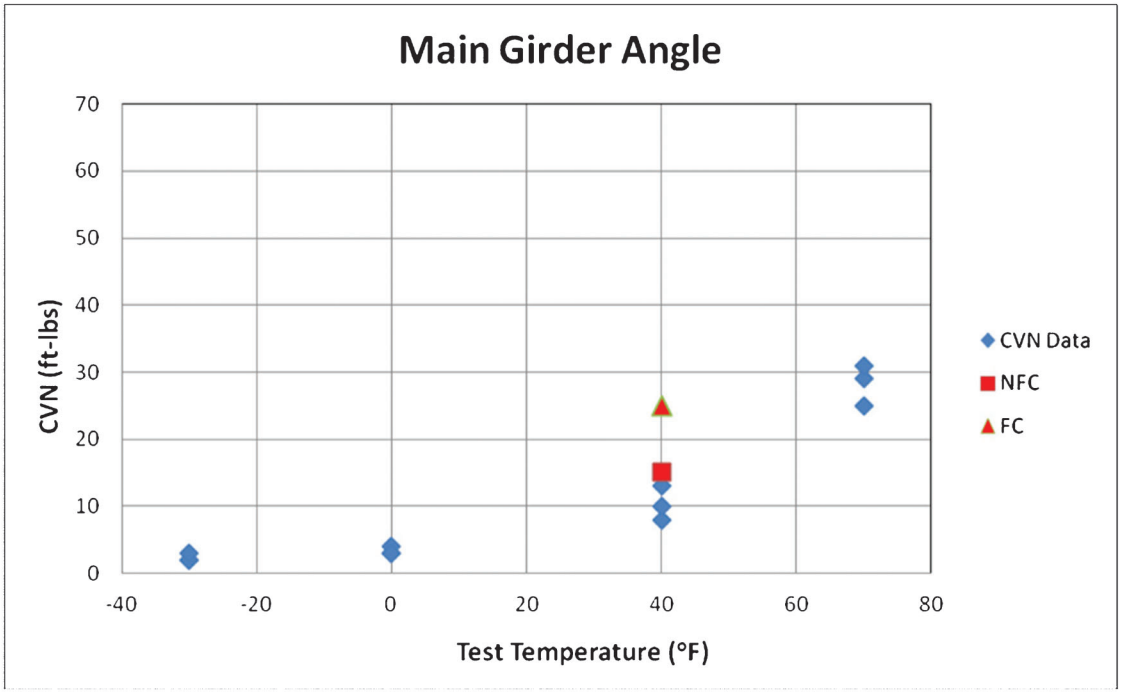

Figure 6.4: Main girder angle plot of CVN data

crack will have the same result. Furthermore, this makes no attempt to quantify the size of crack an inspector would be able to detect visually; rather, it simply identifies the length of crack that is impossible to find. Thus, the smallest sized crack an inspector could detect would need to be added to the 3/8″ flaw. For example, if it is assumed that the smallest crack a typical inspector could visually detect is 3/8″ the actual smallest detectable crack is 3/4″).

To determine if brittle fracture was a concern for a 3/8 inch flaw due to the low CVN values, the stress intensity factor was calculated. A standard K_I solution for a plate with a hole having a crack at the edge (Figure 6.7) was used for the stress intensity factor

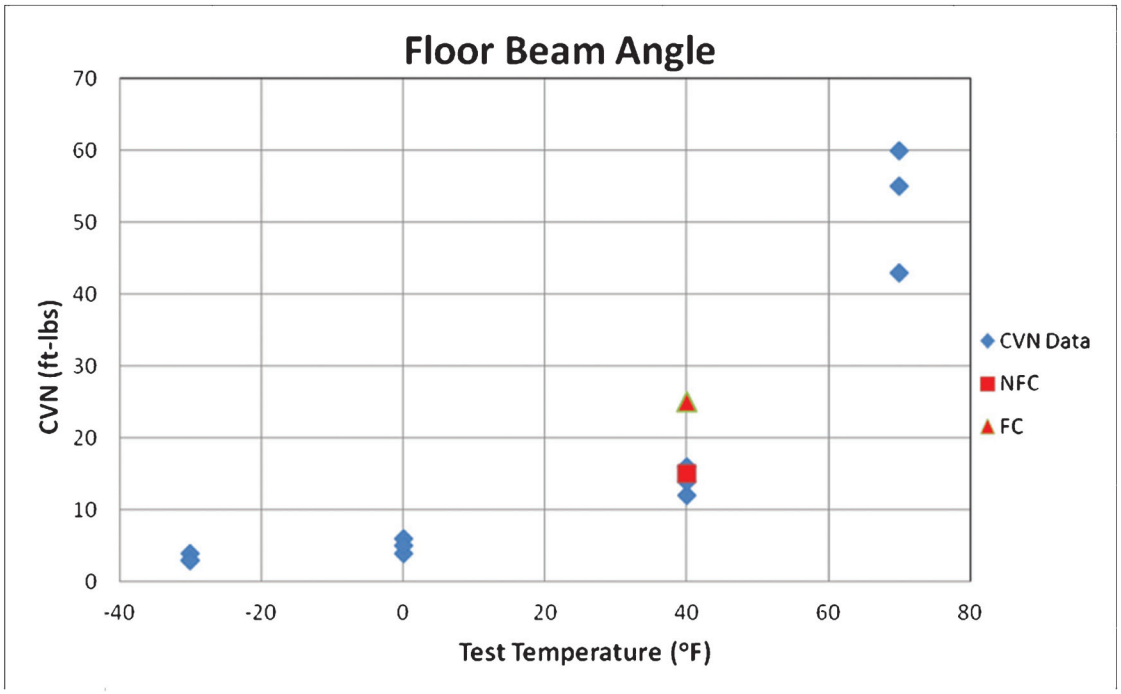

Figure 6.5: Floor beam angle plot of CVN data

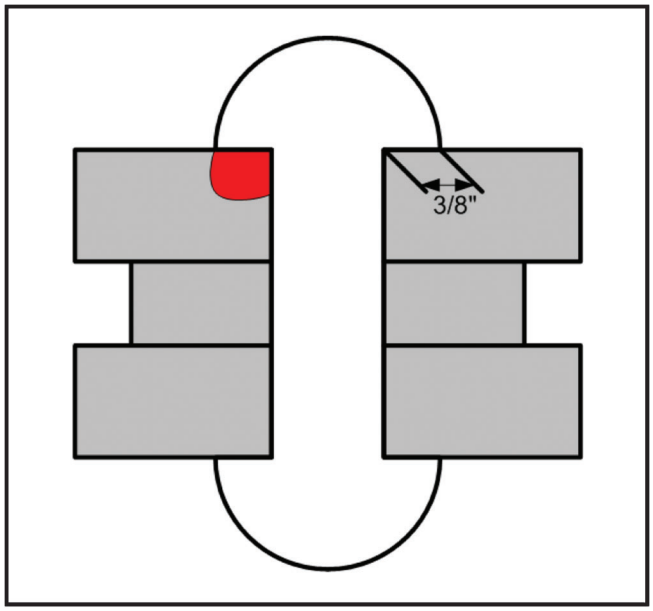

Figure 6.6: Critical crack length versus rivet head

calculation. The calculation performed is presented in Equation 6.1 where '*a*' is the crack length measured from edge of the hole, 'R' is the radius of the hole, and 'σ' is the applied stress. Equation 6.1 was taken from *Fundamentals of Structural Integrity: Damage Tolerant Design and Nondestructive* Evaluation by A. F. Grandt, Jr. (2004). The results from K_I equation in this book were quite comparable to other solutions presented by both D. Broek (1988) and A. Shukla (2005).

$$K_I = \left(\frac{.8733}{0.3245 + \frac{a}{R}} + 0.6762\right)\sigma\sqrt{\pi a}$$

Equation 6.1: Calculation used to determine K_I

The stress intensity factor was computed for the maximum stress caused by the combined total of the bridge: dead load stresses, field measured live load stresses recorded during the passage of the 1 million pound superload, and some assumed residual stresses. The total estimated stresses were on the order of the allowable stress used for the bridge design; thus, for the calculation of the stress intensity factor the allowable stress of 18 ksi was used. Using the dimensions found in Figure 6.7 and the allowable stress of 18 ksi a stress intensity factor of 28.4 ksi*(in)$^{0.5}$ was calculated using Equation 6.1. This stress intensity factor represents the load required to be resisted by the bridge material. Therefore, the amount of resistance in the material needed to be computed and compared to the stress intensity factor of 28.4 ksi*(in)$^{0.5}$.

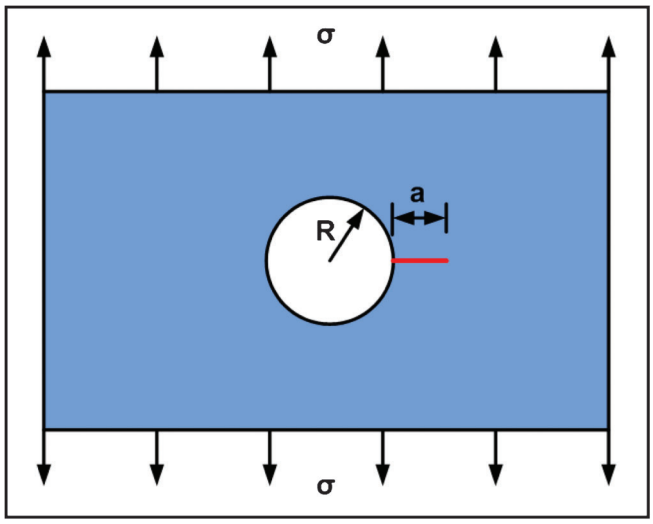

Figure 6.7: Standard K_I solution used for analysis

Using the Master Curve approach as outlined in BS7910 (2005) and the CVN data collected during the material testing, the stress intensity factor for the material was calculated. At −40° Fahrenheit with a 95% probability of survival the stress intensity factor for the material was determined to be 31 ksi*(in)$^{0.5}$. While the stress intensity factor for the material was greater than the stress intensity factor for a 3/8 inch crack scenario, indicating fracture should not occur, the proximity of the values was alarming.

The equation used to calculate the required stress intensity factor is a general solution and does not account for additional factors which play into the stress intensity factor such as the width and thickness of the plate or geometry of the crack. Each of these factors can increase the stress intensity factor beyond the general solution presented in Equation 6.1. Furthermore, assumptions were made during the calculation of the required stress intensity factor, such as the magnitude of stress to be used in the calculation, which could also impact the results. Therefore, due to the proximity of the two values a more refined calculation of the required stress intensity factor was performed. The new required stress intensity factor was calculated using Equation C.120 in API 579-1 Fitness for Service Manual. API Equation C.120 is a solution for a plate with a hole having a semi-elliptical corner crack at the hole. Using API Equation C.120 a required stress intensity factor of 33.9 ksi*(in)$^{0.5}$ was calculated (the full calculation of API Equation C.120 for this value can be found in Appendix C). This value is greater than the resistance stress intensity factor of 28.4 ksi*(in)$^{0.5}$. Thus, if a 3/8 inch flaw did exist under a rivet head fracture could potentially initiate from the flaw.

Due to the very low live-load stresses measured during routine traffic, fatigue stress ranges may not have been large enough to propagate cracks to the 3/8 inch critical crack length. However, it would not be appropriate to simply assume such cracks do not exist somewhere on the bridge when performing a fracture assessment. Thus, to evaluate the true status of cracking at the rivet holes further inspection was required. This involved removing a significant number of rivets and inspecting the holes for any defects. (It should be noted in the interim between the critical crack determination and rivet hole inspection results the Purdue Research Team advised INDOT to enact temporary temperature restrictions.

These included no significant superloads, above 250,000 pounds, be allowed to cross the bridge until the steel temperature on the shady side of the bridge exceeds 32 °F and no superloads at all should cross the bridge if the temperature of the steel is below 20 °F.)

6.2.2 Rivet Hole Inspection

The results of the critical crack length evaluation indicated a defect large enough to result in brittle fracture could potentially be hidden under a rivet head (as shown in Figure 6.6). Even though very low live-load stresses were measured during daily traffic, further evaluation was required to verify no such defects were present. Thus, rivets at selected critical locations of the US-41 White River Bridge were removed to check for the presence (or absence) of fatigue or even fabrication-induced cracks.

A total of 214 rivets were removed from several spans in the northern half of the northbound and southbound bridge superstructures (exact locations of all rivets removed can be found in the rivet removal plan attached to this report in Appendix B). The rivets were removed by shearing off the top rivet head and then driving the rivet out of the hole with a pneumatic chisel. All 214 rivet holes were inspected both visually and with magnetic particle testing. No cracks or defects were found in any of the 214 inspected holes. Once the inspection was complete and the condition documented the rivet was replaced with a fully pretensioned high-strength bolt. If the area around the rivet hole or the rivet hole itself was damaged at all during the removal process it was properly ground smooth as to not negatively impact the fatigue performance of the member. Lastly, all the new bolts were painted to reduce the potential for corrosion. All rivet removal and inspection work was performed by Wiss, Janney and Elstner, Inc. (WJE) from Northbrook, IL between December 14 and 16, 2009. Photographs taken during the rivet removal and inspection work can be seen in Figure 6.8 through Figure 6.10. (It should be noted

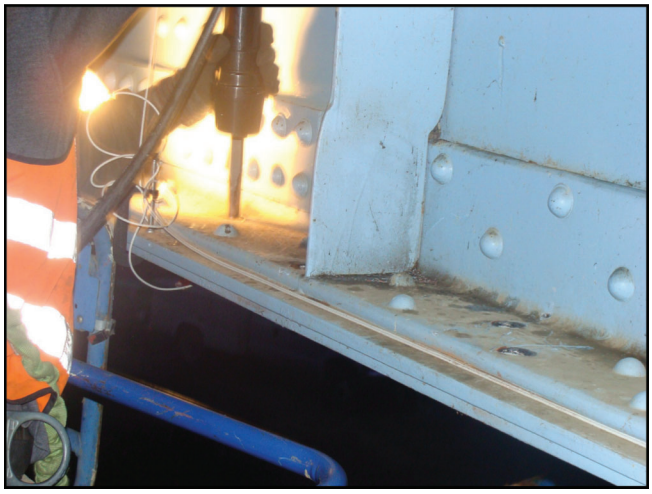

Figure 6.9: Driving the rivet out

that Figure 6.10 is only used to illustrate an example sample location of rivet holes and is not the final condition of the pretensioned bolts.)

6.2.3 After Fracture Member Redundancy

The US-41 White River Bridge is a riveted built-up structure comprised of multiple elements; therefore, fracture of any one element would not necessarily lead to fracture of the entire girder. Rather, fracture would most likely locally increase the stresses in the region of the girder around the girder and subsequent inspections would identify such a fracture prior to failure of the entire girder. Thus, to determine the effect of a plate or angle fracturing a redundancy analysis was performed. This analysis was intended to estimate the effect on the performance of the main girders should a fracture occur in one of the cover plates or angles compromising the flange.

A major advantage of built-up riveted members over welded plate girders is the fact the individual elements are isolated and separate components; therefore, a

Figure 6.8: Shearing off the rivet head

Figure 6.10: Example rivet hole sample location

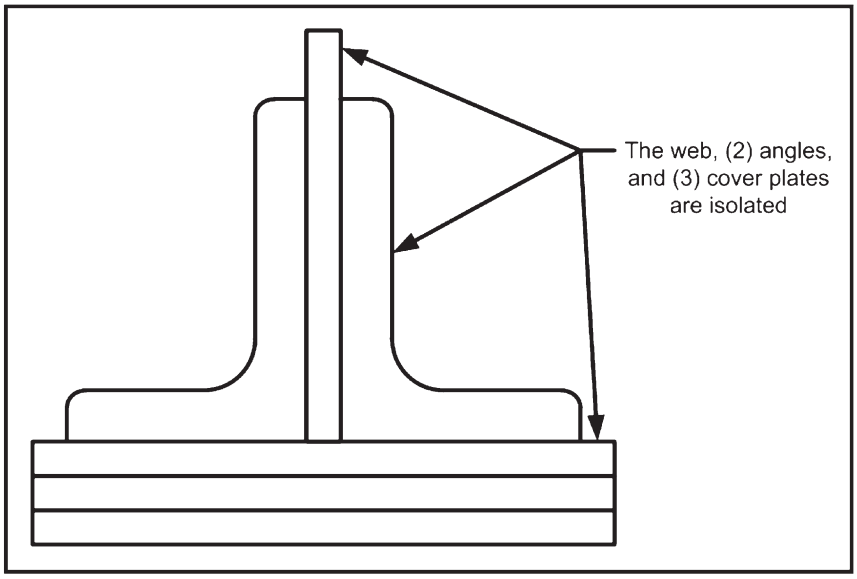

Figure 6.11: Example of redundancy in a built-up member

crack in one element has no direct path into another. This is not the case with welded built-up members in which fractures can propagate directly from a flange into a web (see Figure 6.11). There are many examples found in literature where individual components of riveted members have failed, while the overall integrity of the member was maintained. The redundancy analysis to follow did not attempt to determine the cause of the fracture, it simply assumes a fracture occurred.

There are two assumptions used for this simplified redundancy analysis. These include the following:

1. Either one cover plate or one of the flange angles fractures completely, while all other elements remain in place.
2. There is no composite action between the girders and the concrete slab. This assumption reflects how the bridge was originally designed. However, the field instrumentation indicated significant composite action developed between the girders and slab subjected to service loads and the permit loads for which data were obtained.

The results of this analysis indicated in the worst case, if a cover plate at midspan fails, the resulting increase in stress would be on the order of 27% above the as-designed stress. Likewise, if an angle at midspan were to fail, the increase in stress would be on the order of 22% above the as-designed stress. Therefore, the increase in stress used for the after fracture redundancy study will be assumed to be for the worst case scenario, thus 27% above the as-designed stress.

According to the design drawings, the allowable stress was 18 ksi. Assuming the worst location crack was at the full design allowable stress of 18 ksi, the resulting increased stress can be approximately calculated as $(1 + 27\%) \times 18$ ksi, or 23 ksi. The US-41 White River Bridge steel is identified as ASTM A7 which typically has a yield strength of 33 ksi. Thus, assuming a plate fractured, the cross-section would not be expected to yield. However, it should be noted this estimated increase in the applied stress is very conservative based on the assumptions listed above.

This calculation can be viewed in a tabular format in Table 6.6 and Table 6.7 for Pier 14 and midspan of Span R, respectively. The tables look at fracture occurring at different elements of the built-up section at both a pier and midspan location. It should be noted that the "no damage state" stress was calculated based on a moment producing a stress on the order of the allowable design stress of 18 ksi. This was done to show the worst case scenario should any of the design stresses be near the allowable stress. Also, all stresses were calculated at the bottom of each element. As mentioned above, if an element fails in the worst case (bottom cover plate at midspan) there is only a 27% increase in stress resulting in an after fracture stress of 23 ksi. This after fracture stress is still well below the yield stress of 33 ksi for the material.

One important note about the after fracture redundancy calculations is they were performed assuming a non-composite section. Field measurements indicated composite action was developed between the main girder and concrete deck, even though the structure was not designed in this fashion. Consequently, to understand the conservatism of the non-composite assumption, the after fracture redundancy analysis was also conducted to evaluate the change in stress when composite action was present. To compare the composite and non-composite results, the same bending moment was used for both analyses. It was found the increase in stresses for the fracture of a cover plate at midspan on a composite section produced a slightly greater increase as compared to a non-composite section: 30% versus the 27%, respectively. However, the actual stress after fracture for the composite case was still only 66% of the stress value for the corresponding non-composite case.

TABLE 6.6:
Increase in stress due to fracture at Pier 14

PIER 14							
		Fractured Component					
		20 × 7/16 Cover Plate		20 × 11/16 Cover Plate		8 × 8 × 7/8 Angle	
Element	No Damage State (ksi)	Damaged State (ksi)	% Increase	Damaged State (ksi)	% Increase	Damaged State (ksi)	% Increase
20 × 7/16 CP	17.9	18.3	2.1%	18.5	3.2%	18.3	2.4%
20 × 1/2 CP	17.7	18.1	2.0%	18.3	3.2%	18.2	2.4%
20 × 11/16 CP	17.6	17.9	2.0%	18.1	3.1%	18.0	2.3%
8 × 8 × 7/8	17.4	17.7	1.9%	17.9	3.0%	17.8	2.2%
116.5″ × 1/2 (Web)	17.4	17.7	1.9%	17.9	3.0%	17.8	2.2%
8 × 8 × 7/8	17.4	19.7	13.5%	21.2	22.2%	20.8	19.4%
20 × 11/16 CP	17.6	20.0	13.4%	21.5	22.1%	21.0	19.3%
20 × 1/2 CP	17.7	20.1	13.4%	21.6	22.0%	21.2	19.3%
20 × 7/16 CP	17.9	20.3	13.3%	21.8	21.9%	21.3	19.2%

Although these results are positive, a few other factors must be considered in the assessment. These include the following:

1. If a plate did fracture, the girder would then be in a 'faulted' state. Since the fracture would need to have originated from a rivet hole having some defect (e.g., crack), it may be possible other holes also have the same defect. This is especially true if the initial crack were primarily due to fatigue stress ranges since the applied live-load stress range would be the same. In other words, it is likely fatigue cracks at the edge of nearby or even the same hole (*in other components*) may exist. It should be noted this is unlikely given the rivet hole inspection results.
2. If fracture occurred, there would likely be local yielding at adjacent rivet holes due to the increase in shear transfer demands. Since the steel has rather low toughness, it is not known if adjacent holes or plates would tolerate the additional demand. This is especially the case at low temperatures.
3. As stated, after a fracture the girder would be in a faulted state and the stress demands on the adjacent components would be increased. Hence, it is essential in-service inspection identify the fracture prior to one of the remaining adjacent components failing, possibly compromising the entire girder.

6.2.4 Conclusion

The live load stresses measured by the Purdue Research Team in the main girders and the floor beams of the US-41 White River Bridge were observed to be quite low. Maximum stresses from trucks under routine traffic seldom exceed 2 ksi with only a very few trucks, or combinations of trucks, causing a maximum live load stresses of about 3.5 ksi. The million pound superloads spread out their load over many axles and were observed to cause a maximum live load stress level of roughly 7 ksi. Thus, all of these loadings cause a correspondingly low live-load stress range.

No cracks were found in the US-41 White River Bridge during a rivet hole inspection. A large and statistically significant number of rivet holes (214) were inspected both visually and with magnetic particle techniques as part of the inspection. Since the rivet holes inspected were located in the most critical

TABLE 6.7:
Increase in stress due to fracture at midspan of Span R

MIDSPAN of SPAN R							
		Fractured Component					
		20 × 11/16 Cover Plate (Bottom)		20 × 11/16 Cover Plate (Mid)		8 × 8 × 7/8 Angle	
Element	No Damage State (ksi)	Damaged State (ksi)	% Increase	Damaged State (ksi)	% Increase	Damaged State (ksi)	% Increase
20 × 11/16 CP	17.8	18.2	2.4%	18.2	2.1%	18.0	1.0%
20 × 11/16 CP	17.5	17.8	2.2%	17.8	1.9%	17.6	0.8%
8 × 8 × 7/8	17.1	17.5	1.9%	17.4	1.6%	17.2	0.6%
70.5″ × 1/2 (Web)	17.1	17.5	1.9%	17.4	1.6%	17.2	0.6%
8 × 8 × 7/8	17.1	21.7	27.0%	21.6	26.1%	20.8	21.7%
20 × 11/16 CP	17.5	22.1	26.8%	22.0	25.8%	21.2	21.5%
20 × 11/16 CP	17.8	22.5	26.5%	22.4	25.6%	21.6	21.3%

locations, it is reasonable to expect if fatigue cracking has not occurred at the inspected locations it has not likely occurred at the other rivet hole locations. Thus, even though the steel exhibits fairly low fracture toughness, if no cracks exist, then there is not a firm fracture mechanics reason to expect fracture.

Another factor considered during the fracture study is the redundancy of the riveted members. If any element of the riveted girder were to experience a brittle fracture, it would have most likely resulted in fracture of the given element only. This is because the riveted girder consists of several elements attached (i.e., riveted) together. Full connectivity of the girder does not exist as it does for a welded girder, and thereby providing a pathway for a crack to propagate over the entire depth of the girder. Approximate estimates indicated if any one part were to fracture (such as a single cover plate or angle) then the bending stress in the remaining intact elements would increase by as much as 50 percent. However, this increased stress value is based upon two extremely conservative assumptions. If these factors are taken into account, then it is believed the stresses will increase by a fairly small percentage in the un-fractured, and still intact, elements of the girder.

The final suggestion provided to INDOT was that some conservatism in terms of operating temperature would certainly not be unreasonable. Selecting a temperature, such as 10°F, below which no superloads should be ran would be an extra safeguard against the reduced fracture toughness values at lower temperatures. Also, the selection of a lower limit temperature addresses other issues not considered as part of the fracture evaluation. For example, the quality of inspection which can be conducted at low temperatures is unknown. Also, the performance of the pin and hanger assemblies and bearings, for which no fracture toughness testing was performed, is unknown. It was also recommended as part of the fracture evaluation that INDOT continue to inspect the bridge after significant superloads pass over the bridge. Specifically, the inspection should watch for fracture of any element, such as a cover plate or bottom flange angle.

7. SUPERLOADS

Over a period from June 2009 to July 2010 a series of super-heavy loads were transported approximately 120 miles by road from the port at Mount Vernon, IN to Edwardsport, IN. The super-heavy loads were moved in support of the construction of a power plant facility by Duke Energy. Approximately 100 super-heavy loads were moved in total ranging in weight from 200,000 lbs. up to over 1,000,000 lbs. The route between the port and power plant facility required the loads to cross a number of bridges. The influence of the super-heavy loads on most of the bridges was monitored by INDOT to assess the long-term performance of these bridges. Specifically, the effects on the US-41 White River Bridge were of particular interest. Therefore, instrumentation was installed on the US-41 White River Bridge to monitor load effects over time and to ensure that no negative long-term effects were sustained due to this loading.

7.1 Superload Description

Super-heavy loads or 'superloads' are classified by the Indiana Department of Transportation (INDOT) as vehicles having a width exceeding 16 feet, height exceeding 15 feet, length exceeding 110 feet, and a gross weight (weight of load and vehicle) greater than 108,000 pounds. Vehicles exceeding the size limitations and weighing more than 200,000 pounds, such as the ones involved in this study, require a permit from INDOT. Additionally, a police escort is required if the vehicle must slow down for bridges crossings. In the case of the US-41 White River Bridge all superloads were required to travel at a speed less than five miles per hour.

All superloads were transported by Bigge Crane and Rigging Company headquartered in San Leandro, CA. The most common superload vehicle configuration used was the beam and dollie transporter. Other superload vehicle configurations were used as well; however, the heaviest of the loads were moved by the beam and dollie transporter. The beam and dollie transporter uses large steel beams to carry the weight of the payload out to two supporting dollies. These dollies consist of multiple axles having four tires. Hauling the load in this fashion spreads the weight out over a large area, thereby reducing the impact on any single concentrated area. Example photographs of a beam and dollie transporter can be found in Figure 7.1 and Figure 7.2. As seen in the photographs two trucks or 'prime movers' were often required to transport the super-heavy loads. It should also be noted that the weight of the moving equipment alone (i.e., prime movers and beam and dollie transporter) was by no means negligible and substantially contributed to the gross weight of the superloads.

Figure 7.1: Photograph of beam and dollie transporter from the front

Figure 7.2: Photograph of beam and dollie transporter from the rear

7.2 Effects of Superloads

One way to evaluate any long-term effects of the superloads on the US-41 White River Bridge is to compare two similar loading events from different periods of time. Both loading events should be of a similar weight and configuration to appropriately make such a comparison. However, with that said, every load is unique. Thus, there are bound to be some differences in the loading response. Additionally, other factors play into the response measured by the strain gages. For instance, the transverse location of the load on the bridge will impact the stress measured by a given strain gage. Therefore, it should not come as a surprise if the two selected events do not match identically. The general bridge response is what should be compared between these events and not the specific measurement from a given gage. For example, it should be noted if composite action between the concrete deck and main girders is suddenly lost after the series of loads and not whether a given strain gage produces the same exact stress measurements for both events.

Both of the events selected for comparison were on different ends of the time spectrum. The first event occurred in the early going of the hauls. It was a 17′-6″ high, 22′-10″ wide, 280′-10″ long, 989,040 lbs. superload that crossed the US-41 White River Bridge on October 31, 2009. This was the first 'one million pound' superload to cross the bridge. Likewise, the second event was an 18′-6″ high, 23′-0″ wide, 280′-10″ long, 989,040 lbs. superload. However, it was the final superload to cross the US-41 White River Bridge on July 23, 2010. As mentioned above, these two loads are not exact copies; however, they are similar. Most importantly their weight and length are nearly identical. Therefore, comparing the global bridge behavior between the two events will shed light on any long-term effects of the superloads. It should be noted that the second event discussed occurred after the number of strain gages was reduced from forty-eight (48) channels to twenty-four (24) channels for long-term monitoring. Thus, these channels will be used for the comparison with some additional comments based on the complete number of strain gages available during the October 31, 2010 move.

7.2.1 Main Girder Response

Seven main girder strain gages remained for the long-term monitoring of the US-41 White River Bridge. Of the seven remaining strain gages, all but one was located on the bottom flange of the main girder. Due to the composite action developed between the concrete deck and steel girder, the top flange strain gages measurements were very small. Therefore, with the exception of the Pier 13 location, none of the main girder top flange strain gages were included in the long-term monitoring. The response of the seven remaining strain gages to the passage of two superloads, one from the beginning of the hauls and one near the end, will be used to evaluate any changes in the performance of the bridge.

Included in Table 7.1 is a summary of the seven main girder strain gages included in the long-term monitoring. For each of the two superload crossings the maximum and minimum stress values measured by each strain gage are presented as well as the resulting maximum stress range. It should be noted that the stress range given in Table 7.1 might not be the algebraic difference between the maximum and minimum values due to rounding all stresses in the table to the nearest tenth. Also, a general location for each strain gage is given in the table.

Keeping in mind that the two loads were not identical, the October 31, 2009 and July 23, 2010 hauls

TABLE 7.1:
Primary girder maximum stresses and stress range comparison

		Location		October 31, 2009			July 23, 2010		
Channel	Girder	Global	Local	Min (KSI)	Max (KSI)	S_r (KSI)	Min (KSI)	Max (KSI)	S_r (KSI)
CH_2	G2	Maximum positive moment Span N	Bottom	−1.9	5.5	7.4	−2.0	5.7	7.7
CH_4	G2	Inflection point Span N	Bottom	−7.1	6.2	13.3	−7.3	6.1	13.4
CH_5	G2	Maximum negative near Pier 13	Top	−0.1	1.7	1.8	−0.2	3.1	3.3
CH_6	G2	Maximum negative near Pier 13	Bottom	−6.0	0.5	6.5	−5.9	0.5	6.4
CH_12	G1	Maximum negative near Pier 13	Bottom	−5.8	0.5	6.3	−6.9	0.4	7.3
CH_24	G2	Maximum positive moment Span P	Bottom	−1.4	6.9	8.3	−1.5	7.0	8.5
CH_26	G1	Maximum positive moment Span P	Bottom	−1.3	6.1	7.4	−1.3	6.6	7.9

agree quite well in terms of measured stresses. With the exception of one strain gage, all the maximum measured stress ranges had a difference of 1.0 ksi or less between the two moves. The only exception to 1.0 ksi difference occurred at CH_5 where the difference was 1.5 ksi. A more detailed look at this location will follow in the coming paragraphs. Table 7.1 is not the only way to compare the load response between the two superloads. Comparing plots of the measured data also can give insight on any notable differences between the moves.

CH_4 was the location of the greatest stress range for the main girder strain gages. Plotted in Figure 7.3 is the measured data from CH_4 for both the October 31, 2009 move (teal trace) and July 23, 2010 move (blue trace). As can be seen in the figure, both moves have nearly identical traces. The shape of these traces is what was commonly observed for those loads close to three hundred feet long and one million pounds.

Also plotted in Figure 7.3 is CH_3 (yellow trace) during the October 31, 2009 move. This strain gage was not included in the long-term monitoring; hence, why it is not shown for the July 23, 2010 superload. However, plotting CH_3 for the earlier event can help determine if any composite action exists between the concrete deck and steel girders during a superload event. As can be seen from the plot, composite action is being developed. The response of CH_4 is always of a larger magnitude than that of CH_3. Looking specifically at the instant in time during the maximum tensile response of CH_4 (between time of 320 seconds and 380 seconds), the neutral axis is calculated using the field measured stress values. A plot of the resulting neutral axis location can be found in Figure 7.4.

The neutral axis of the composite section determined from the strain gage measurements is once again nearly identical to the computed neutral axis location. Since the measured neutral axis is above the one determined from the AASHTO calculation, full composite behavior is being developed between the two elements. Another interesting thing to note is that there was very little change in the position of the neutral axis calculated from the field measured stresses between the controlled load tests and this one million pound superload. During the superload, the load on the US-41 White River Bridge was approximately five times the load during controlled testing. Therefore, the fact that little to no change was noted in the position of the neutral axis

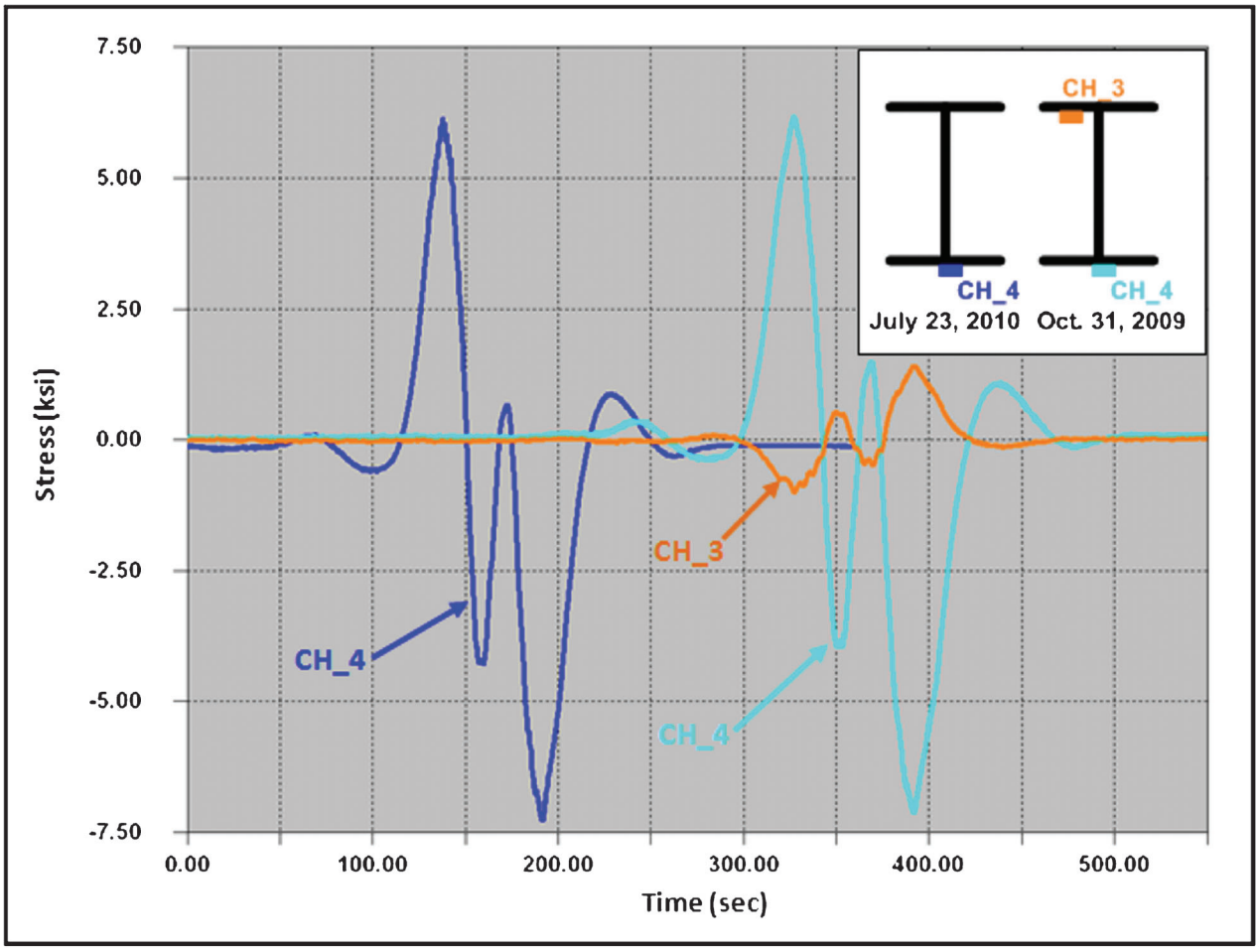

Figure 7.3: Dead load inflection point superload comparison

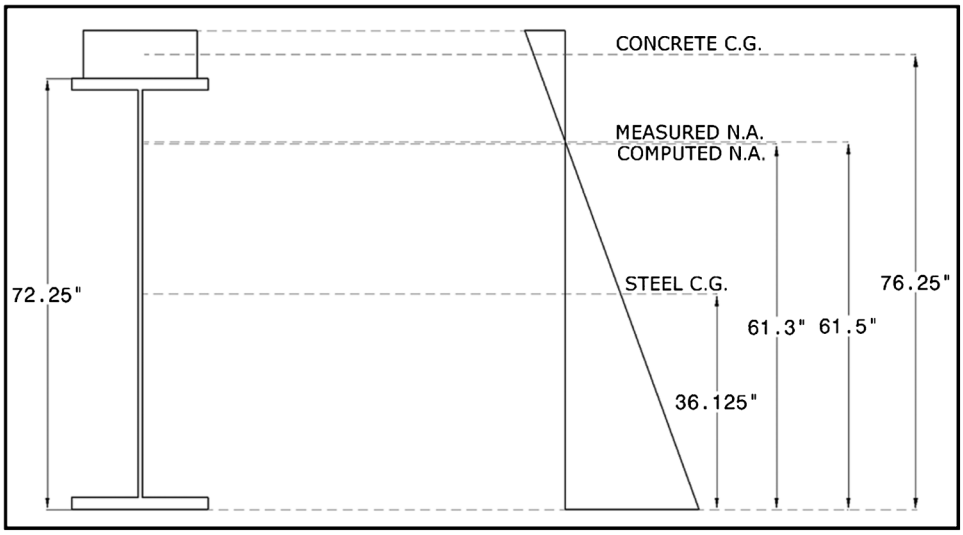

Figure 7.4: Neutral axis comparison for the October 31, 2009 move at inflection point

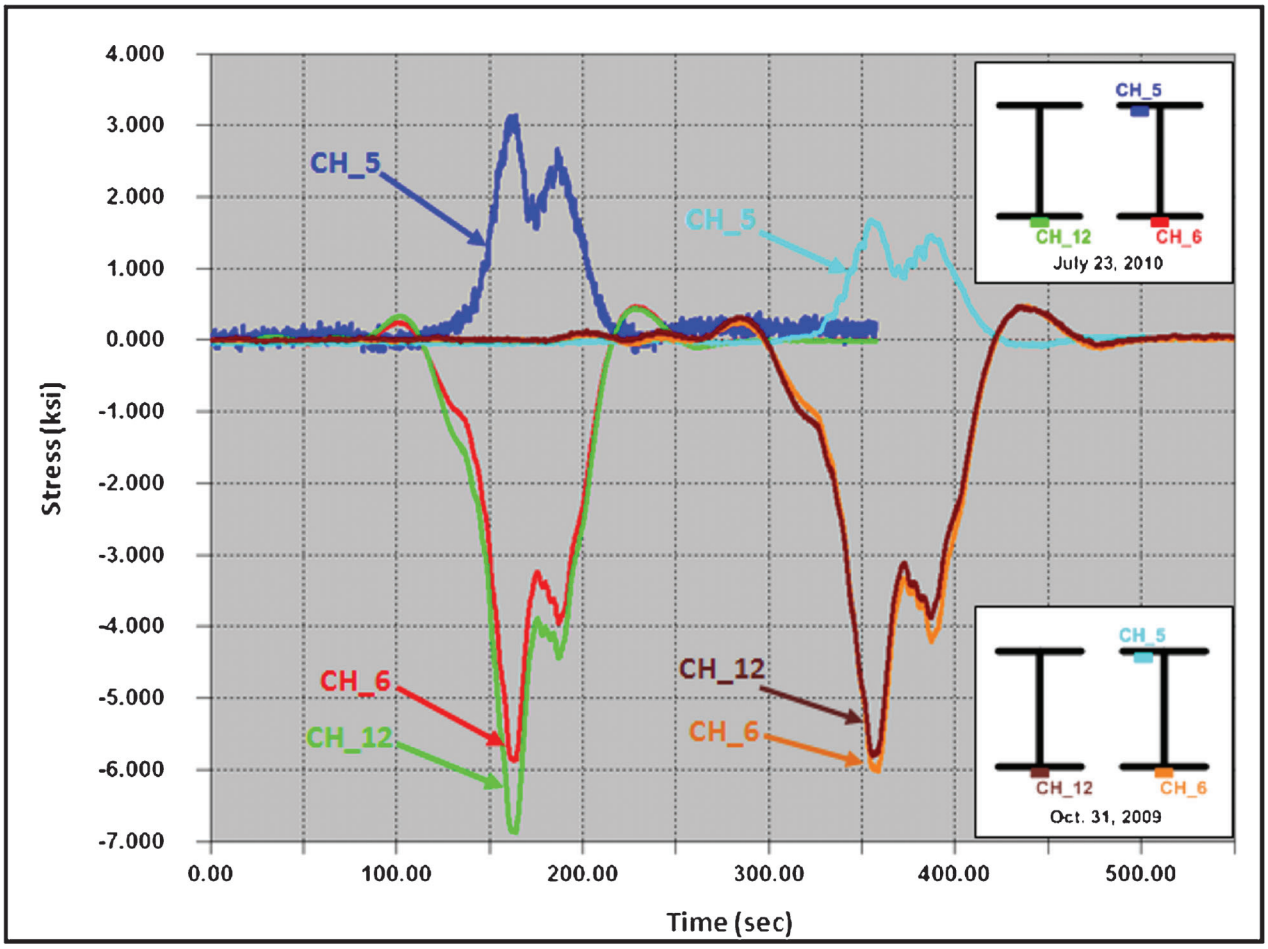

Figure 7.5: Pier 13 superload comparison

indicates there is great consistency and reliability in the composite action between the concrete deck and steel girders.

General agreement between the two hauls was also found at the Pier 13 main girder strain gage location. Plotted below in Figure 7.5 are the three strain gages that remained after the reduction for long-term monitoring. These include CH_5, CH_6, and CH_12. The US-41 White River Bridge experienced slightly smaller stresses during the October 31, 2009 superload. This difference can be due to a variety of reasons; however, the most likely reasons are the minor variations between the two vehicle payloads and the transverse location of the vehicle on the bridge. As mentioned above, the two moves selected for comparison were similar but not identical. It is expected to see variations in the stress measurements, similar to those plotted in Figure 7.5, due to minor load variations. Additionally, the transverse location of the vehicle may not have been exactly the same during both moves. Thus, the difference between the responses at the Pier 13 main girder strain gage location is not unexpected and of little concern to the Research Team.

Since both main girders are instrumented, load distribution can be evaluated at the Pier 13 main girder strain gage location. As seen in the figure, the load distribution between the two girders during the early move (orange and brown traces) was nearly identical. On the other hand, the load distribution during the later move (red and green traces) was not as uniform. This is not to say the load distribution during the later move was bad; rather, it was just not as uniform as the earlier haul. The most likely reason for variation in the load distribution during the July 23, 2010 move was the transverse location of the truck. Based on the data, the superload was most likely favoring the west side of the bridge during the later passage in turn loading Girder G1 heavier than Girder G2. Hence, why the peak stress in Girder G1 (green trace) was approximately 1.0 ksi greater than Girder G2 (red trace). Had the truck been more centered on the bridge the difference between the two moves would have been substantially less.

The response at both maximum positive moment strain gage locations was also compared. Between the two instrumented locations of maximum positive moment, a total of three strain gages remained during long-term monitoring. These strain gages included CH_2, CH_24, and CH_26. Plotted in Figure 7.6 and Figure 7.8 are the measured responses from the two superloads. Figure 7.6 plots CH_2 and Figure 7.8 plots CH_24 and CH_26.

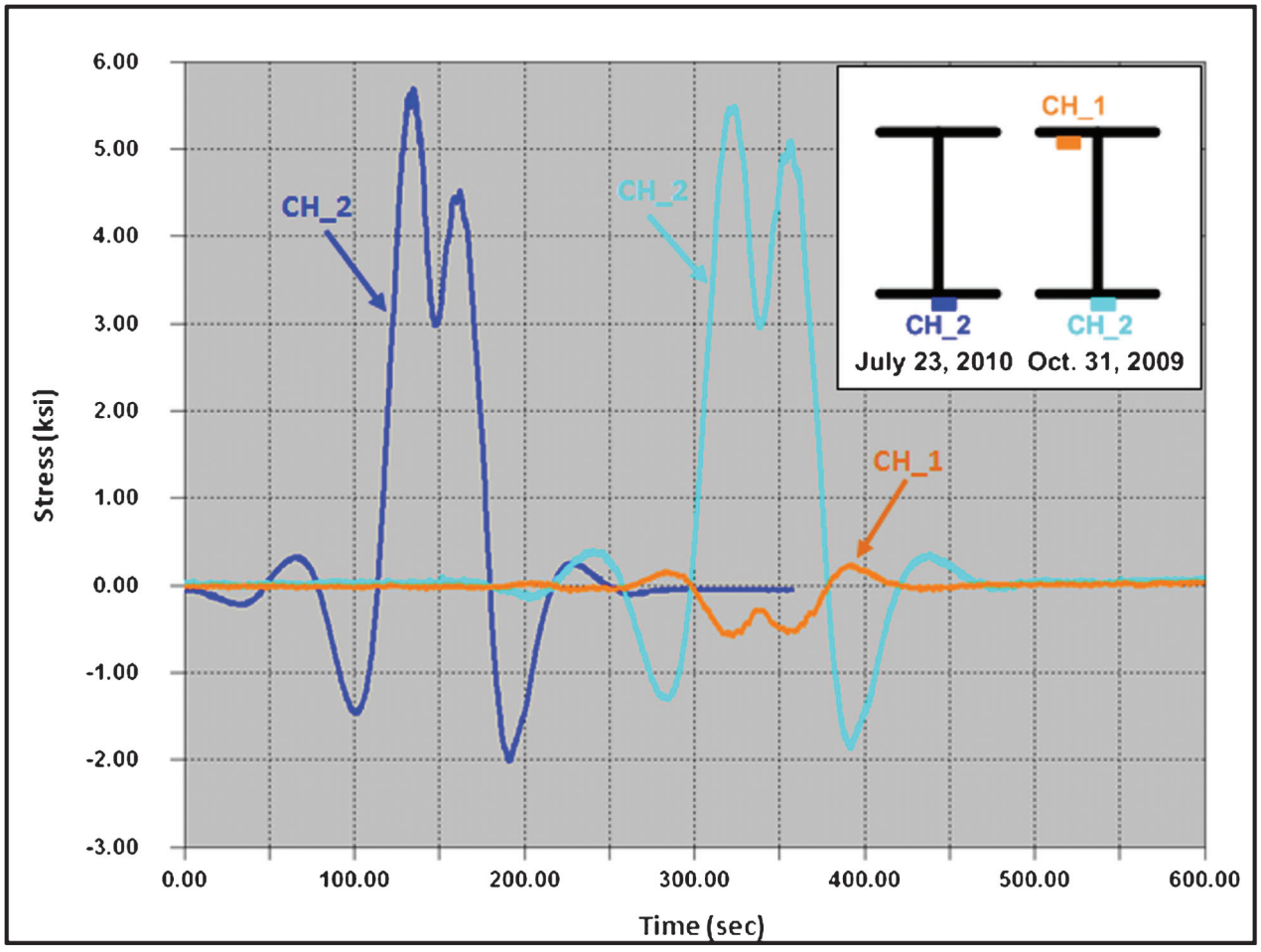

Figure 7.6: Positive moment Span N superload comparison

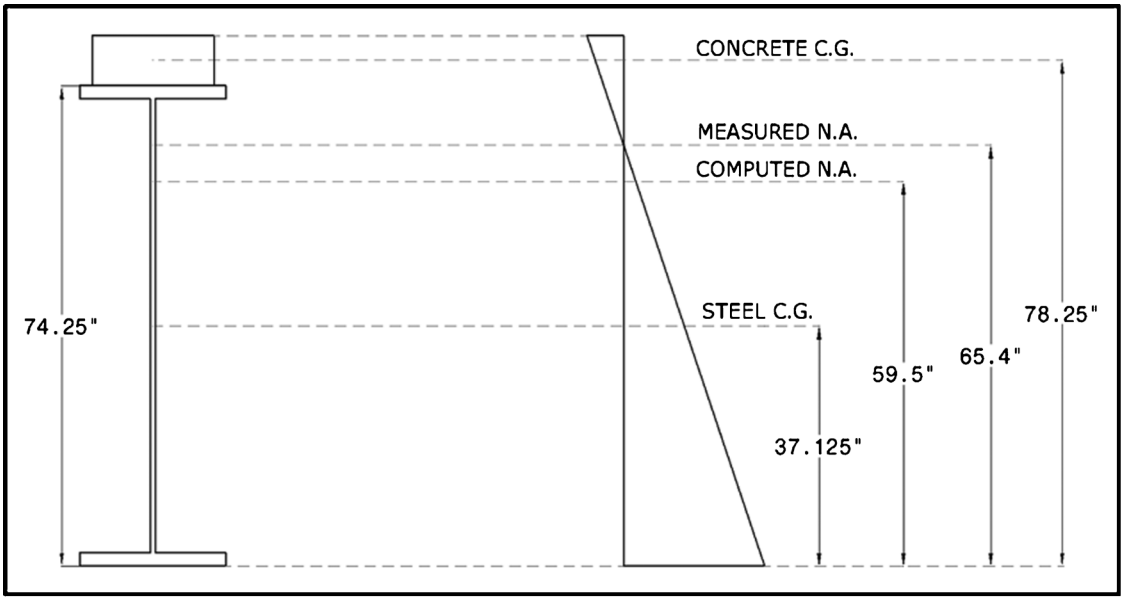

Figure 7.7: Neutral axis comparison for the October 31, 2009 move at midspan Span N

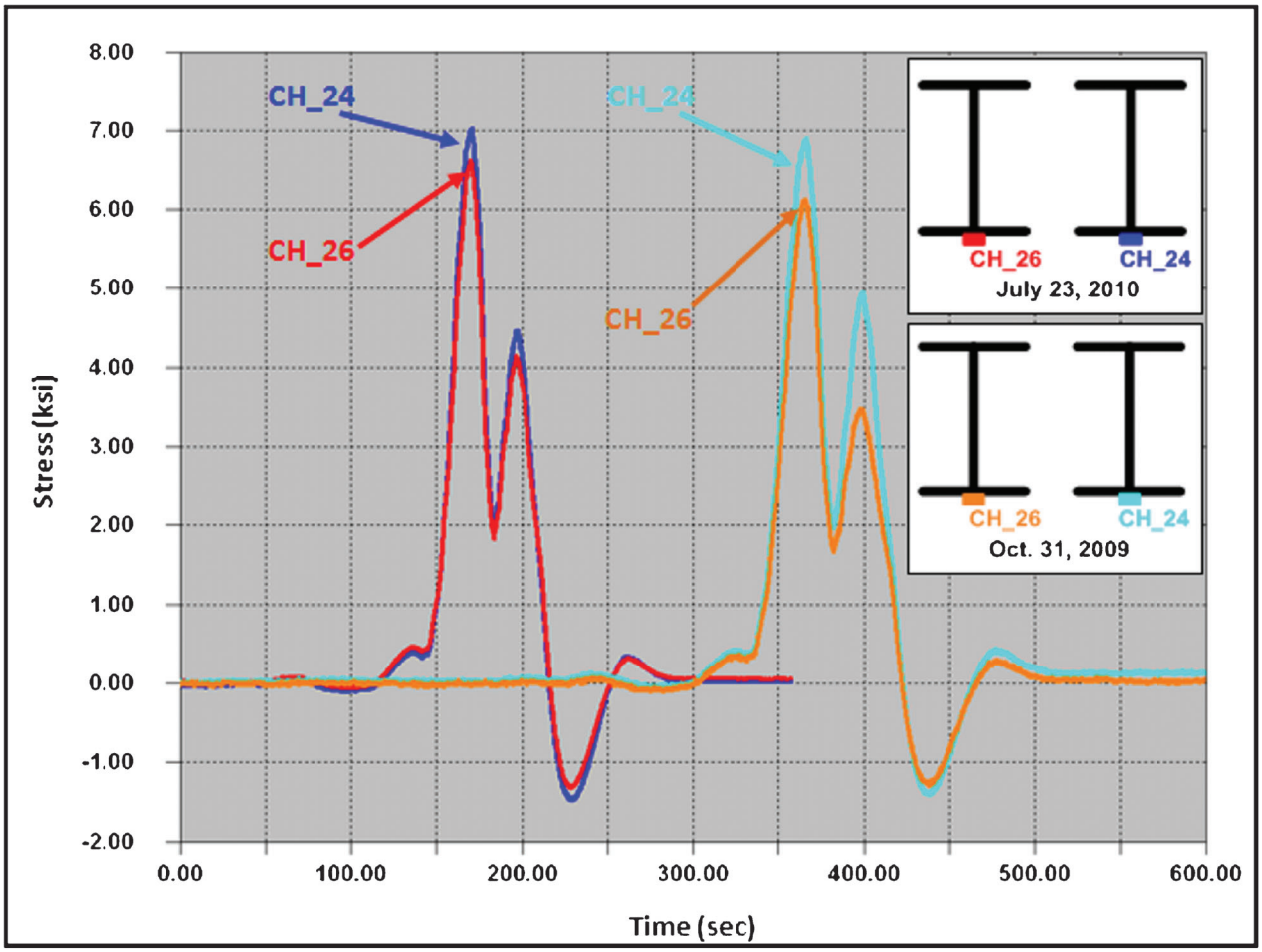

Figure 7.8: Positive moment Span P superload comparison

Overall, the response of all three strain gages agrees remarkably well between both of the passages.

Figure 7.6 plots CH_2 for both moves. Additionally, this figure includes CH_1 during the October 31, 2009 crossing. Plotting CH_1 allows for the composite action at the positive moment location to be analyzed. It is clear in Figure 7.6 that some element other than the main girder is carrying a portion of the compressive load. This element is once again the concrete deck. To determine if full composite action is developed, the neutral axis was calculated using field measured stresses and compared to the computed value. The resulting values are presented in Figure 7.7. As can be seen in the figure, the neutral axis determined from the field measured stress values is greater than the computed value indicating that full composite action is being developed between the steel girder and concrete deck. Interestingly, the position of the neutral axis as calculated from the field measured stresses only changed by 0.3″ between the controlled load testing and the October 31, 2009 million pound move. Thus, the composite action is very consistent and reliable; therefore, it can be relied upon during the analysis of the US-41 White River Bridge.

Looking at Figure 7.8, similar agreement between the loads is found. CH_24 and CH_26 have nearly identical plots during both crossings. Figure 7.8 can also be used to evaluate the load distribution between the two primary girders. The plot indicates that Girder G2 is carrying slightly more load than Girder G1. This is indicated by the higher stress in CH_24 than CH_26. Most likely, the cause for different stress levels between the two girders is the transverse location of the superload on the bridge. Based on Girder G2 having a greater stress than Girder G1, the truck is favoring the east side of the structure during both moves. Thus, the plotted load distribution is acceptable for both moves.

In comparing the response from the seven remaining strain gages at the four primary girder locations, little variation is seen between the October 31, 2009 crossing and the July 23, 2010 crossing. Different response characteristics were compared at each of these locations. These response characteristics included the load distribution, composite interaction, neutral axis location, and the global response. Based on the analyzed long-term data, it is the belief of the Research Team that the primary girders sustained no noticeable negative long-term effects from the passage of the multiple super-heavy loads.

7.2.2 Floor Beam Response

The floor beam response during the October 31, 2009 and July 23, 2010 hauls were quite similar. During the long-term monitoring, two floor beams were instrumented, each with one strain gage located on the bottom flange at midspan to measure the maximum positive stress. Table 7.2 lists the maximum and minimum stress values measured at the two floor beam strain gage locations during the passage of both the October 31, 2009 and July 23, 2010 superloads. The maximum resulting stress range is also included in Table 7.2. Additionally, the table specifies the location of the two floor beams instrumented.

Plots of CH_10 and CH_22 comparing both moves are shown in Figure 7.9 and Figure 7.10, respectively. Both floor beams have similar general responses including two large peaks and two small peaks. The two larger peaks are due to the front and rear trailer dollies whereas the smaller peaks are due to the primary movers. Between the two large peaks is a sudden large reduction in stress. This is from when the open space between the front and rear dollie of the hauler was over the floor beam. As expected, virtually no negative bending was measured at either floor beam strain gage. The only time the strain gages indicated negative bending was for CH_22 during the sudden drop in stress between the front and rear dollies. This was of little concern to the Research Team.

Overall the floor beam response from the October 31, 2009 move and the July 23, 2010 move compare remarkably well. Furthermore, both hauls agree with the response from controlled load tests only with larger magnitudes. The general shape of the response measured during the side-by-side controlled load test consisted of two large positive stress peaks with a sudden reduction in stress between the peaks. Thus, based on the analyzed long-term data, it is the belief of the Research Team that the floor beams sustained no noticeable negative long-term effects from the passage of the multiple super-heavy loads.

7.2.3 Stringer Response

Five stringer locations were originally instrumented with a total of ten strain gages. After the controlled load testing, those ten strain gages at the five locations were reduced to seven strain gages at four locations for long-term monitoring. It is worth noting that as a percentage of the original strain gages remaining for

TABLE 7.2:
Floor beam maximum stresses and stress range comparison

		Location		October 31, 2009			July 23, 2010		
Channel	Floor Beam Type	Global	Local	Min (KSI)	Max (KSI)	S_r (KSI)	Min (KSI)	Max (KSI)	S_r (KSI)
CH_10	Over Pier 13	Maximum positive moment	Bottom	0.0	3.7	3.7	0.0	4.0	4.0
CH_22	3rd FB north of hanger	Maximum positive moment	Bottom	−0.2	3.7	3.9	−0.3	3.7	4.0

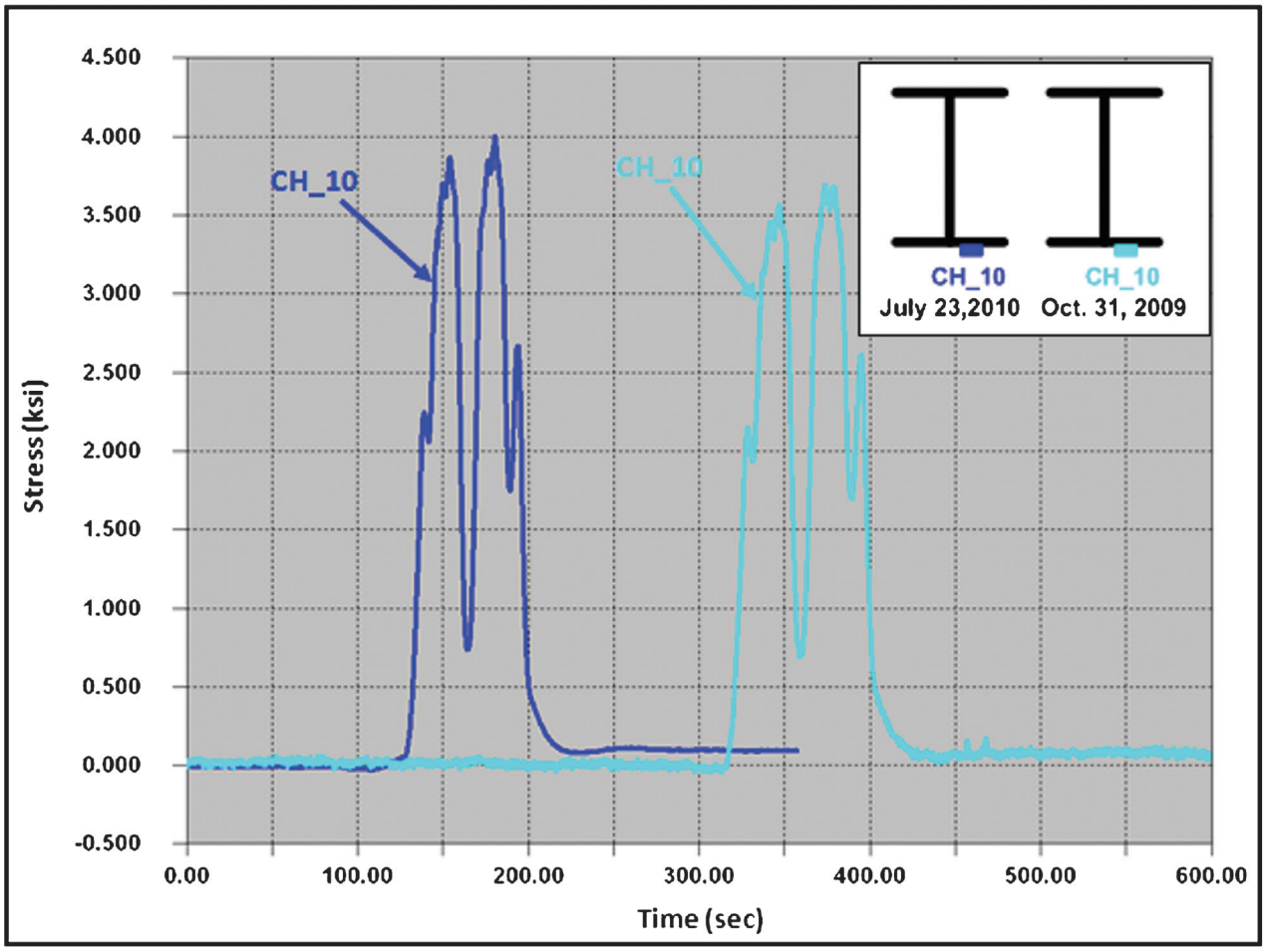

Figure 7.9: CH_10 superload comparison

long-term monitoring, the stringers on the US-41 White River Bridge were the element with the highest percentage.

A summary of the seven long-term strain gages can be found in Table 7.3. The table includes the maximum and minimum stress from both the October 31, 2009 and July 23, 2010 passages as well as the resulting maximum stress range. Additionally, Table 7.3 includes a brief description of the location for each of the seven remaining strain gages. It should be noted that the stress range given in Table 7.3 might not be the algebraic difference between the maximum and minimum values shown due to rounding all stresses in the table to the nearest one-tenth.

By far, the greatest stringer stresses were measured at the Pier 13 strain gage location. In turn, the largest stress ranges were also measured at these same strain gages. Figure 7.11 plots the data measured at the Pier 13 strain gage location for the October 31, 2009 and July 23, 2010 moves. As seen in the figure a similar general response is recorded for both crossings. As would be expected for a negative moment location, tension is measured in the top flange and compression is measured in the bottom. Slightly greater stresses were measured during the later move; however, the difference is of little concern as the majority of comparisons have indicated slightly greater stress during the July 23, 2010 superload.

Slightly greater stresses were also measured during the July 23, 2010 crossing for the positive moment strain gages. This can be seen numerically in Table 7.3 for CH_14 through CH_18. Figure 7.12 and Figure 7.13 plot the data for these four channels during both moves. CH_15 and CH_16 are presented in Figure 7.12 and CH_17 and CH_18 in Figure 7.13. Both plots do an excellent job illustrating how the general response between the October 31, 2009 and July 23, 2010 crossings are very similar. Like the negative moment stringer strain gages, there are four peaks. The first and last peaks are from the primary movers are of smaller magnitude. The middle two stress peaks due to the superload front and rear dollies. Separating the two largest peaks in stress is a large sudden drop in stress. This again is due to the space between the front and rear dollies of the superload.

The two largest stress peaks in the response of the positive moment stringer strain gages are made up of several small stress spikes. Like the controlled load test these little spikes are due to the individual axles of the superload. A magnified plot of CH_15 in Figure 7.12 is shown in Figure 7.14. Zooming in on the data clearly

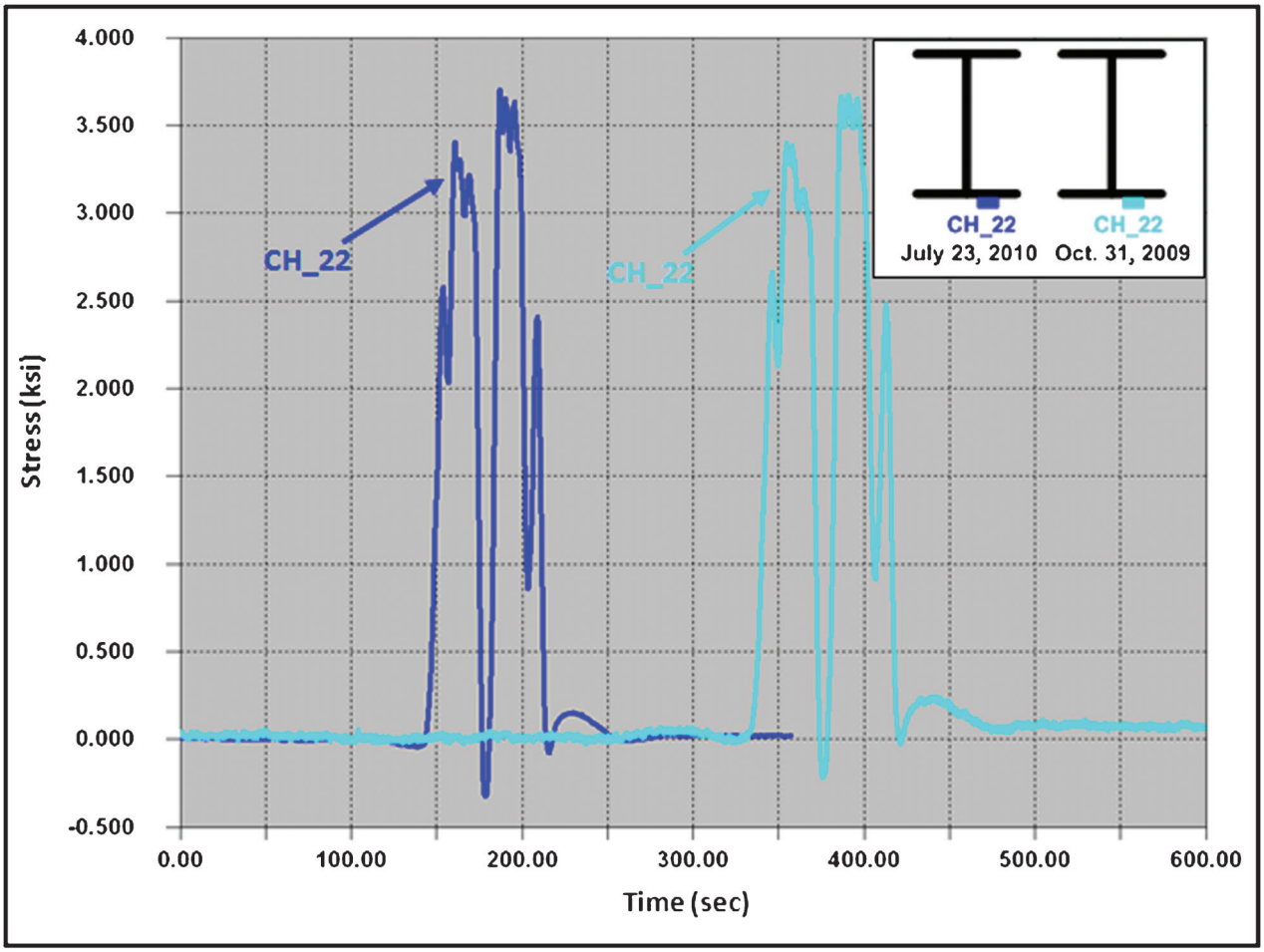

Figure 7.10: CH_22 superload comparison

TABLE 7.3:
Stringer maximum stresses and stress range comparison

		Location		October 31, 2009			July 23, 2010		
Channel	Stringer	Global	Local	Min (KSI)	Max (KSI)	S_r (KSI)	Min (KSI)	Max (KSI)	S_r (KSI)
CH_13	Center stringer Pier 13	Maximum negative moment	Top	−0.2	5.0	5.3	−0.2	6.0	6.3
CH_14	Center stringer Pier 13	Maximum negative moment	Bottom	−5.8	0.1	6.0	−6.6	0.2	6.8
CH_15	East stringer Simple span	Maximum positive moment	Top	−0.1	3.5	3.6	−0.1	3.9	4.1
CH_16	East stringer Simple span	Maximum positive moment	Bottom	−2.8	0.0	2.9	−3.2	0.1	3.3
CH_17	East stringer 0.4 point	Maximum positive moment	Top	−2.7	0.3	3.0	−3.1	0.4	3.4
CH_18	East stringer 0.4 point	Maximum positive moment	Bottom	−0.2	3.8	4.0	−0.3	4.3	4.5
CH_28	Center stringer 4th FB north of hanger	Maximum negative moment	Bottom	−2.6	0.4	3.0	−3.2	0.2	3.4

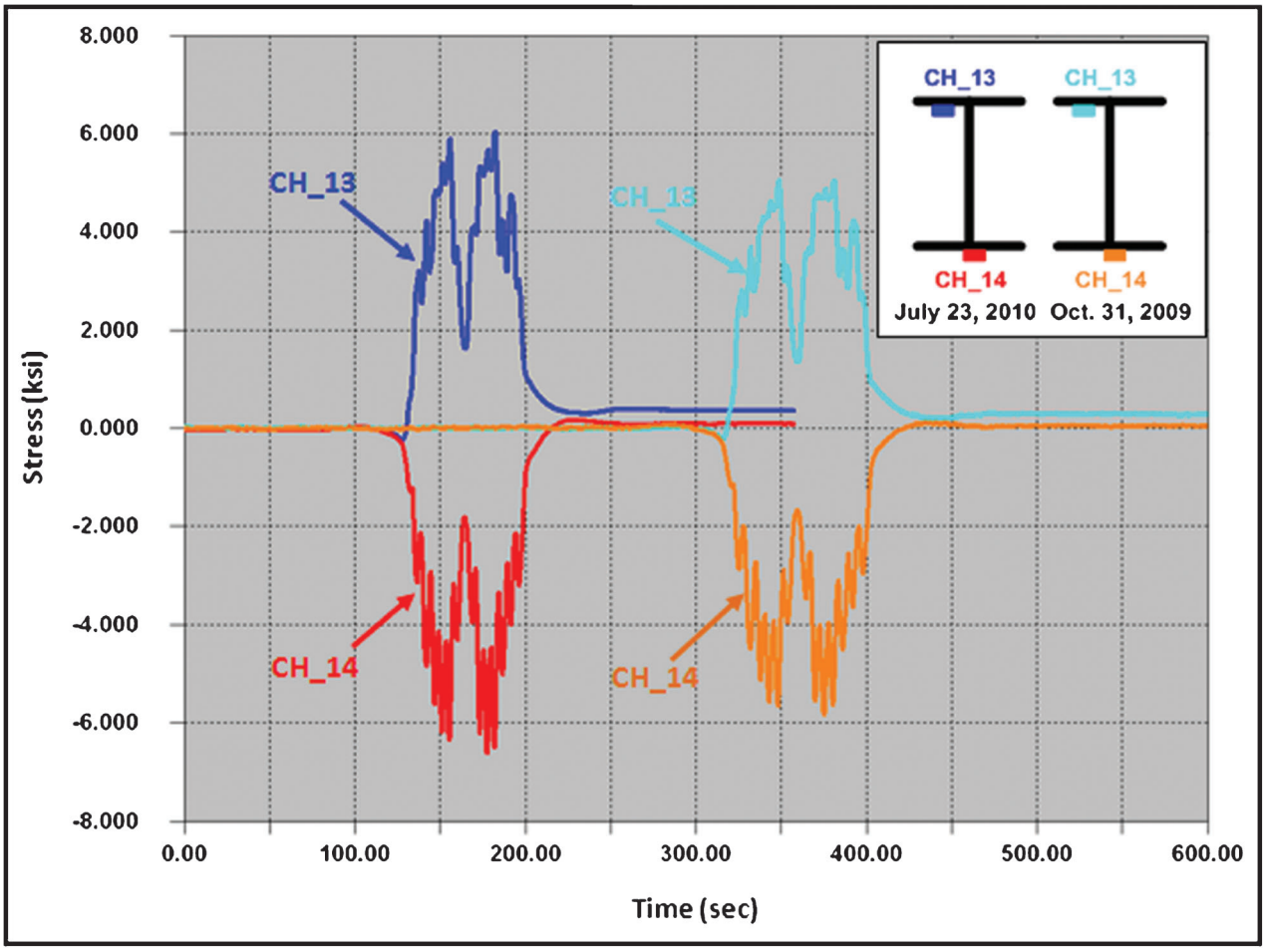

Figure 7.11: Pier 13 stringer superload comparison

shows the result of the individual axles. As can be seen in Figure 7.14, both the October 31, 2009 move and the July 23, 2010 move had a front primary mover pulling and a rear primary mover pushing the load. The actual load for both hauls was supported by a front and rear dollie consisting of four sets of axles each. It is worth mentioning that each spike is not necessarily due to a single axle. This is occasionally the case, such as the steer axle for the primary movers (first and eleventh spike). However, the spike from the drive axles of the primary mover could be from two or three individual axles. Likewise, the spikes from the axles of the front and rear dollies are typically due to multiple individual axles.

During the controlled load testing a small amount of composite action was noted between the concrete deck and steel stringers. This was determined by calculating the position of the neutral axis from the field measured stresses and comparing it to the non-composite neutral axis. After analyzing the controlled load test data the conclusion was reached that the amount and consistency of composite interaction was not sufficient to rely upon. Based on the three plots of data above (Figure 7.11 through Figure 7.13), the same conclusion was reached for these superloads. In Figure 7.11 both the tensile and compressive responses are nearly identical in magnitude indicating that no interaction is present. Conversely, in Figure 7.12 and Figure 7.13 the tensile response is greater than the compressive response; thus, indicating the concrete deck is carrying a portion of the compressive force. Combining all three data sets, it was concluded that the amount and consistency of composite interaction for the stringers is not enough to rely upon for analysis of the US-41 White River Bridge.

The general response from the stringers on the US-41 White River Bridge compared quite well between the October 31, 2009 and July 23, 2010 moves. As expected for the stringers, local bending was measured from individual axles of the superloads. Also, some composite action was observed at the positive moment strain gage locations; however, the amount and consistency of this interaction is not sufficient to rely upon for analysis. In conclusion, based on the analyzed long-term data and the comparison made between the October 31, 2009 and July 23, 2010 moves, it is the belief of the Research Team that the stringers sustained no noticeable negative long-term effects from the passage of the multiple super-heavy loads.

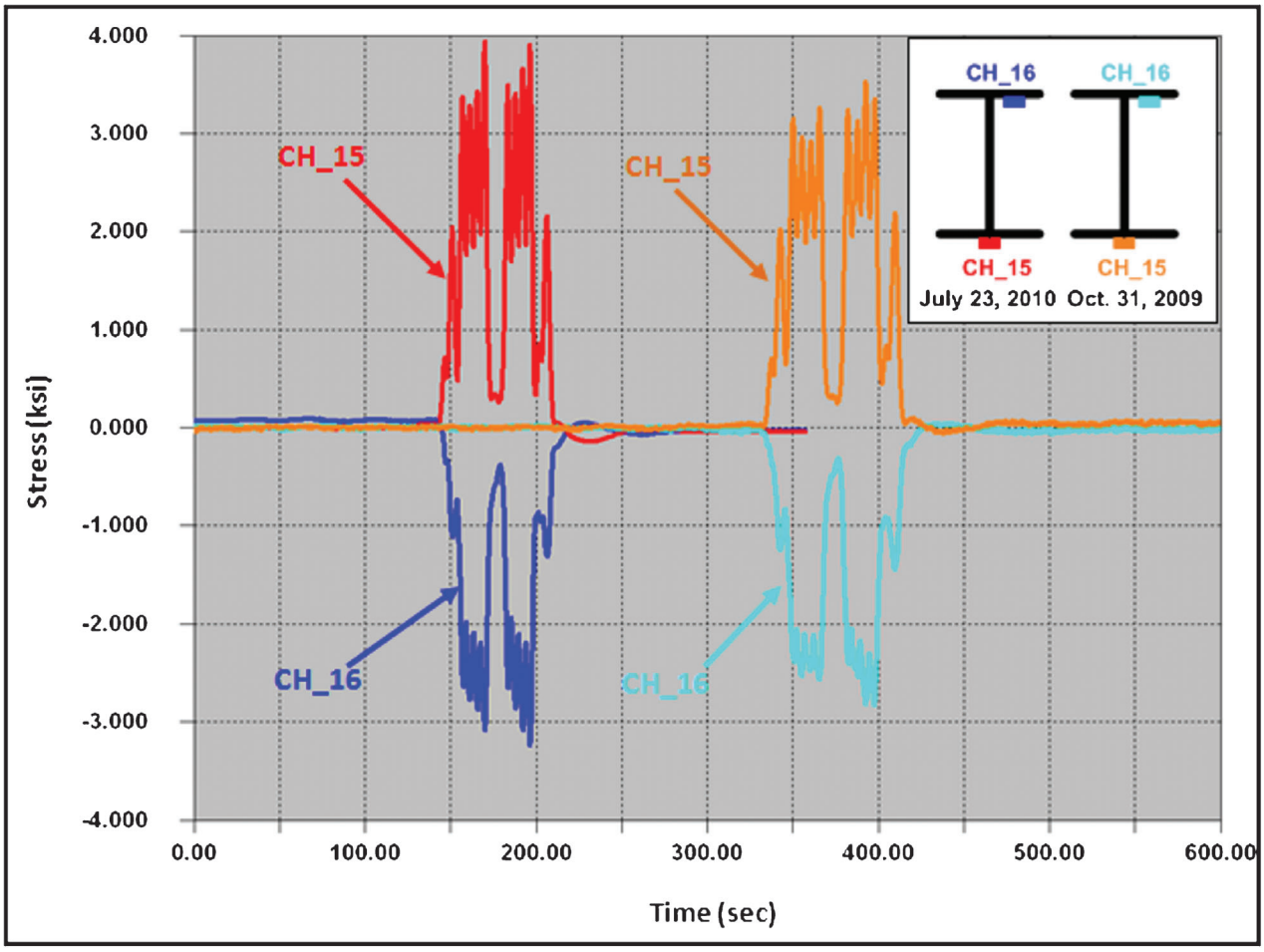

Figure 7.12: Simple span stringer superload comparison

7.2.4 Pin and Hanger Response

Bi-axial bending in the pin and hanger assemblies was an area of concern when the monitoring of the US-41 White River Bridge began. Therefore, based on the results of the controlled load testing seven pin and hanger strain gages on three different hangers were included in the long-term monitoring. The maximum and minimum stress recorded during the October 31, 2009 and July 23, 2010 moves are presented in Table 7.4 along with the resulting maximum stress range. Additionally, the specific hanger and face of hanger for each strain gage location is detailed in the table. It should be noted that the stress range given in Table 7.4 might not be the algebraic difference between the maximum and minimum values shown due to rounding all stresses in the table to the nearest one-tenth.

Four of the seven remaining strain gages were installed on Girder G2 east hanger. This specific hanger was the most heavily instrumented of all the hangers. During the controlled load testing some minor bending was observed when looking at CH_32 and CH_34. Thus, the data measured during the October 31, 2009 and July 23, 2010 moves is plotted in Figure 7.15 to evaluate any changes in the behavior of the hanger.

It can be seen that during both the October 31, 2009 move and the July 23, 2010 move bending occurs. This is signified by the alternating stresses as the load moves through successive spans. As can be seen in the plot, neither one of the moves clearly demonstrates more bending than the other. Additionally, the maximum responses, both tensile and compressive, are less than 0.5 ksi different between moves. However, one difference worth noting is the temporary displacement. The July 23, 2010 crossing has a greater remaining stress than the October 31, 2009 crossing. Approximately an additional 0.5 ksi remained after the superload exited the bridge. The remaining stress signifies some sort of displacement has occurred. From data collected over longer monitoring periods, it was observed that the pin and hangers vibrate back to their original position (i.e., zero stress) over time. Nevertheless, the remaining stress indicates that the pin and hanger movement is restricted to some degree.

Less bending was measured in the Girder G1 west hanger than Girder G2 east hanger for both superload passages. This was also the case during the controlled load testing. A plot of CH_43 and CH_44 for the October 31, 2009 and July 23, 2010 moves can be found in Figure 7.16. As can be seen in the plot, neither one of

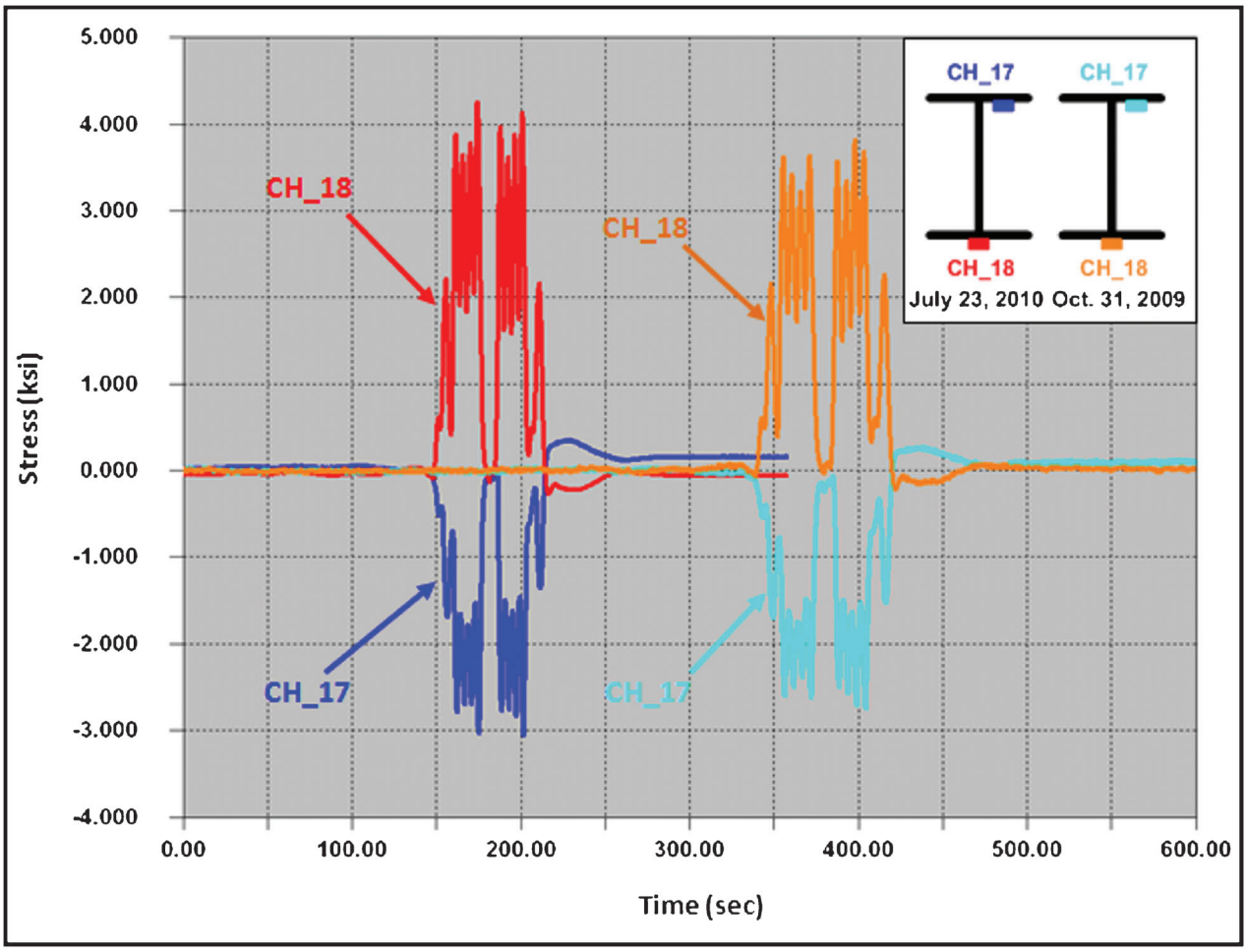

Figure 7.13: 0.4 point stringer superload comparison

the crossings clearly exhibits more bending than the other. However, the July 23, 2010 stress ranges are greater than the October 31, 2009 stress ranges by approximately 0.5 ksi. Such a minor difference is of little concern; especially, considering all the data presented above shows the later move producing larger stresses.

A final observation taken from Figure 7.16 is the stress remaining in the hangers after the superloads have exited the bridge. Less than 0.25 ksi remains in the Girder G1 west hanger after both moves. It should be noted that when looking at the CH_44 plot of the October 31, 2009 haul (orange trace) has a stress of 0.5 ksi; however, this trace as well as CH_43 from the same event (teal trace) should be shifted downward and centered at zero. Regardless, the amount of stress remaining in the Girder G1 west hanger after the passage is over 1.0 ksi less than Girder G2 east hanger. This indicates that the Girder G1 west hanger is moving much more freely than the Girder G2 east hanger.

Girder G2 west hanger had the largest remaining stress of all the pin and hangers included in the long-term monitoring. During the October 31, 2009 move a stress of approximately 2.7 ksi remained after the superload exited the US-41 White River Bridge. Conversely, a stress of approximately 3.7 ksi remained after the July 23, 2010 crossing. Figure 7.17 plots the measurements taken during each event. The remaining stress indicates that this pin and hanger is experiencing resistance to movement. Unfortunately, the opposite strain gage to CH_38 (CH_37) was not included in the long-term monitoring. Thus, it is difficult to determine the amount of bending that occurred during both crossings. However, based on the cycling stress, the hanger experienced some amount of bending during the hauls. One other interesting point to note is that CH_38 had the greatest stress range of all pin and hanger strain gages included in the long-term monitoring.

The general response of the pin and hangers on the US-41 White River Bridge compared quite well between the October 31, 2009 and July 23, 2010 moves. Bending of some degree was observed for all pin and hangers included in the long-term monitoring. However, most importantly, the bending did not worsen over time as more superloads crossed the bridge. The data indicates that the hangers on Girder G2 experienced worse bending than those on Girder G1. This suggests that Girder G2 is not moving completely freely. Based on the analyzed long-term data and the comparison made between the October 31,

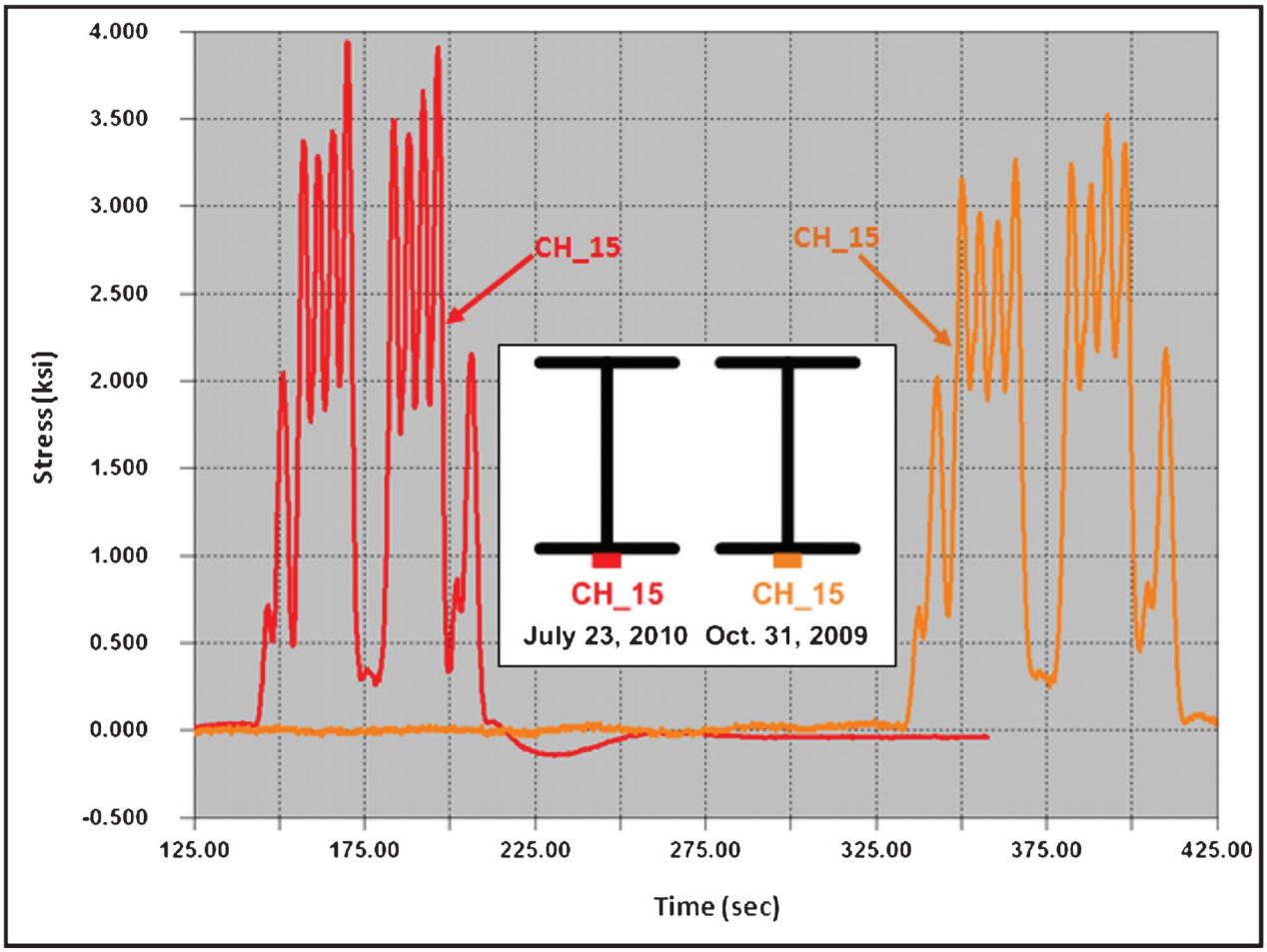

Figure 7.14: Zoomed in view of CH_15 for superload comparison

2009 and July 23, 2010 moves, it is the belief of the Research Team that the pin and hangers sustained no noticeable negative long-term effects from the passage of the multiple super-heavy loads. However, it is suggested that all pin and hangers should be lubricated to allow them to move more freely. This in turn should help reduce the bi-axial bending measured during long-term monitoring.

7.3 Maximum Loading Event

A number of the superloads crossing the US-41 White River Bridge in support of the new power plant facility had a gross vehicle weights (GVW) of approximately one million pounds. The GVW of the largest two superloads was 1,117,000 lbs. Dimensions of this vehicle as it traveled down the highway were a length of

TABLE 7.4:
Pin and hanger maximum stresses and stress range comparison

			October 31, 2009			July 23, 2010		
Channel	Girder	Face	Min (KSI)	Max (KSI)	S_r (KSI)	Min (KSI)	Max (KSI)	S_r (KSI)
CH_29	G2	East	−0.8	3.8	4.6	−0.8	3.3	4.1
CH_31	G2	East	−0.5	4.5	5.0	−0.6	4.3	4.9
CH_32	G2	East	−2.7	3.3	5.9	−3.0	3.3	6.3
CH_34	G2	East	−0.9	3.7	4.6	−0.7	4.1	4.8
CH_38	G2	West	−4.0	3.4	7.4	−4.9	2.3	7.2
CH_43	G1	West	−0.3	3.6	3.9	−0.5	3.8	4.3
CH_44	G1	West	−0.6	4.5	5.0	−1.2	4.3	5.5

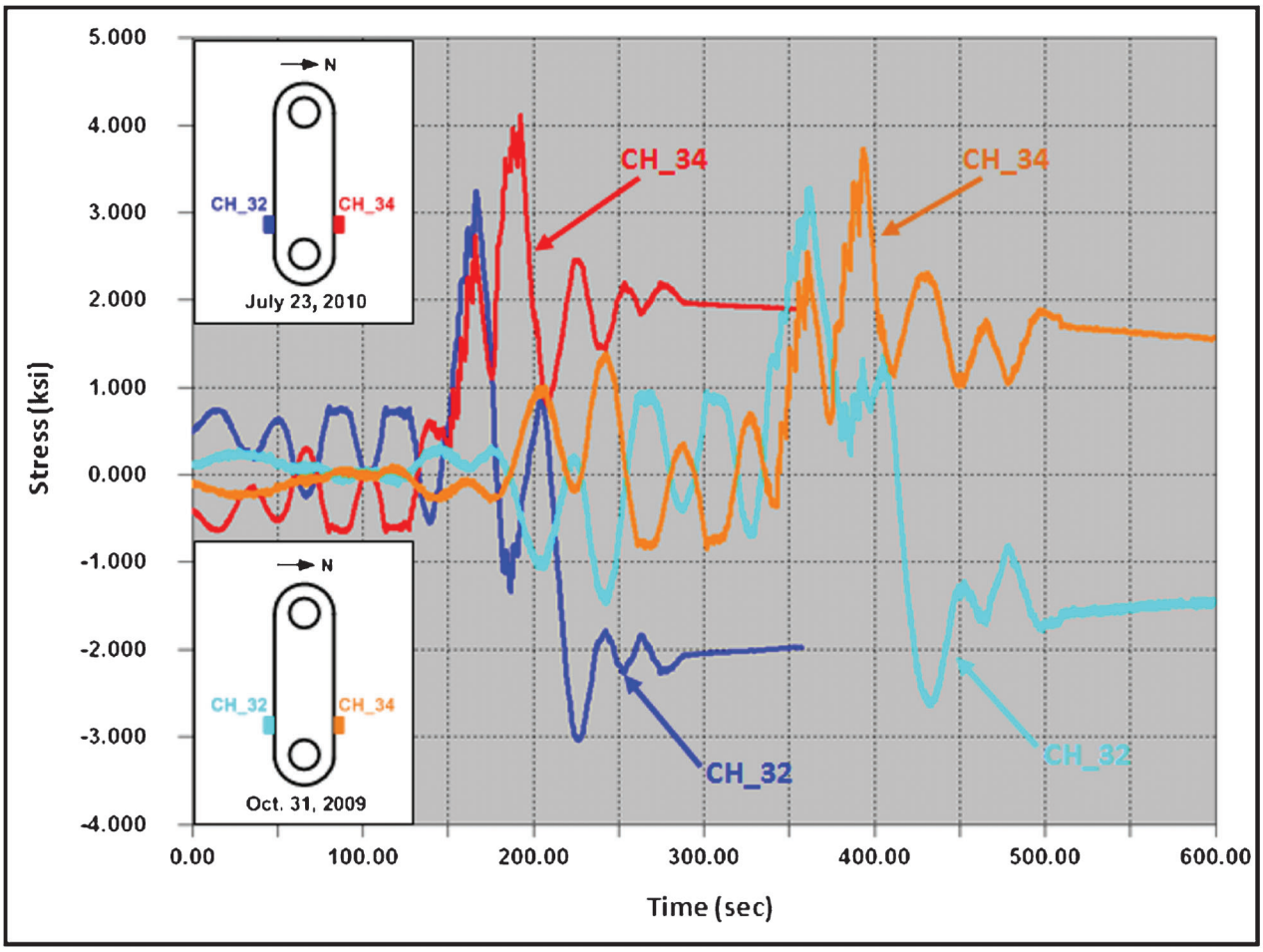

Figure 7.15: Girder G2 east hanger superload comparison

300 feet, width of 23 feet, and height of 23 feet. Also, it is worth mentioning, to further distribute the load when crossing the US-41 White River Bridge the prime movers were repositioned to approximately 100 feet out from the load. The first of these largest loads crossed the US-41 White River Bridge on May 23, 2010. Approximately two weeks later the second of these heaviest loads crossed on June 3, 2010. The following sections present data recorded from the four primary strain gage elements (main girder, floor beams, stringers, and pin and hanger expansion joints) for the June 3, 2010 move. As these moves occurred after the controlled load testing, the data reported will only be from the critical twenty-four (24) strain gages included in the long-term monitoring. Both of the heaviest moves resulted in similar strain gage responses; therefore, the June 3, 2010 move was selected for the discussion because it had slightly larger stresses.

7.3.1 Main Girder Response

Overall, the response of the US-41 White River Bridge to the heaviest superloads was very consistent with other super-heavy moves. The largest stresses (both tensile and compressive) were measured in the primary girders. Additionally, the greatest stress range was also calculated for the main girders. A summary of the maximum and minimum stresses as well as the maximum stress range from the June 3, 2010 move can be found in Table 7.5. Additionally, the location of each main girder strain gage can be found in the table.

As shown in Table 7.5, the peak stress range occurred at the dead load inflection point strain gage location (CH_4). This location had a maximum tensile response of 7.4 ksi and a maximum compressive response of −9.6 ksi during the June 3, 2010 passage, resulting in a stress range of 17.0 ksi. This was the largest stress range measured during the entirety of the superload monitoring.

Figure 7.18 is a plot of the response from CH_4 at the inflection point strain gage location as the heaviest superload crossed the US-41 White River Bridge. As can be seen in the figure, the general response is typical for this location; however, the magnitude of the response is larger than normal. A large tensile response is first measured, followed by a large compressive response. Similar behavior was observed at this location during the controlled load testing and during both superloads used in the comparison.

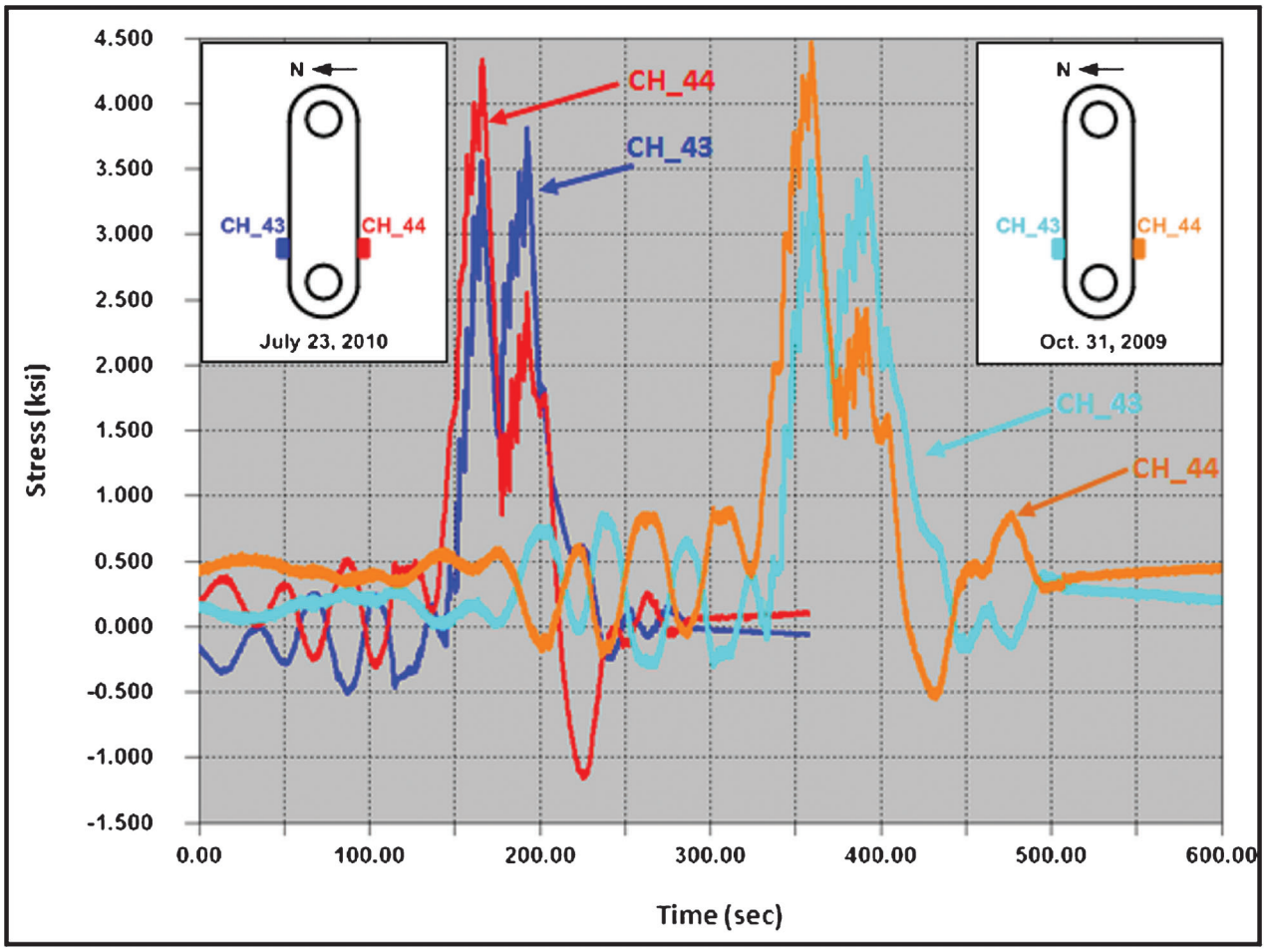

Figure 7.16: Girder G1 west hanger superload comparison

The Pier 13 strain gage location is an excellent one to examine when evaluating the effects of a given loading. This location has strain gages installed on both main girders; thus, the load distribution between the two girders can be examined. Additionally, Girder G2 has stain gages on both the top and bottom flanges; therefore, the effects of composite action can be analyzed. The Pier 13 strain gage location is the only main girder strain gage location with both the top and bottom flange stresses recorded for the long-term monitoring. This location was selected to have both strain gages recorded because if composite action was to be lost it would most likely to be here where the concrete would be put into tension. Figure 7.19 is a plot of the response from the three main girder strain gages to the heaviest superload.

The first thing observed in the figure is the nearly identical responses of the two bottom flange strain gages (CH_6 and CH_12). Both of these strain gages have a tensile response of approximately 0.6 ksi before and after the primary compressive response. The compressive response of both strain gages is very similar as well. A difference of only 0.3 ksi is measured (−7.3 for CH_6 and −7.0 for CH_12). Similar results were observed during the dual-lane controlled load tests. Since, as the US-41 White River Bridge is only a two girder bridge an equal load distribution is expected. Short of the vehicle being off center transversely, the load should be equally split between the two main girders.

When looking at the composite action developed during the crossing of the superload, it is quite apparent the concrete deck and steel girder were acting together. The stress measured at the top flange strain gage on Girder G2 was approximately half that of the bottom flange strain gage. Therefore, some other element is carrying the additional tensile load. As in the case of the controlled load test, the deck is the element carrying this load. Plotted in Figure 7.20 is a comparison of the neutral axis location calculated from the strain gage measurements taken during the passage of the heaviest superload and the computed neutral axis. The figure indicates that full composite action exists between the concrete deck and the steel girder. This is signified by the neutral axis from the field measured stresses being located between the neutral axis of the concrete deck and the computed neutral axis. Interestingly, once again the measured neutral axis agrees much better with

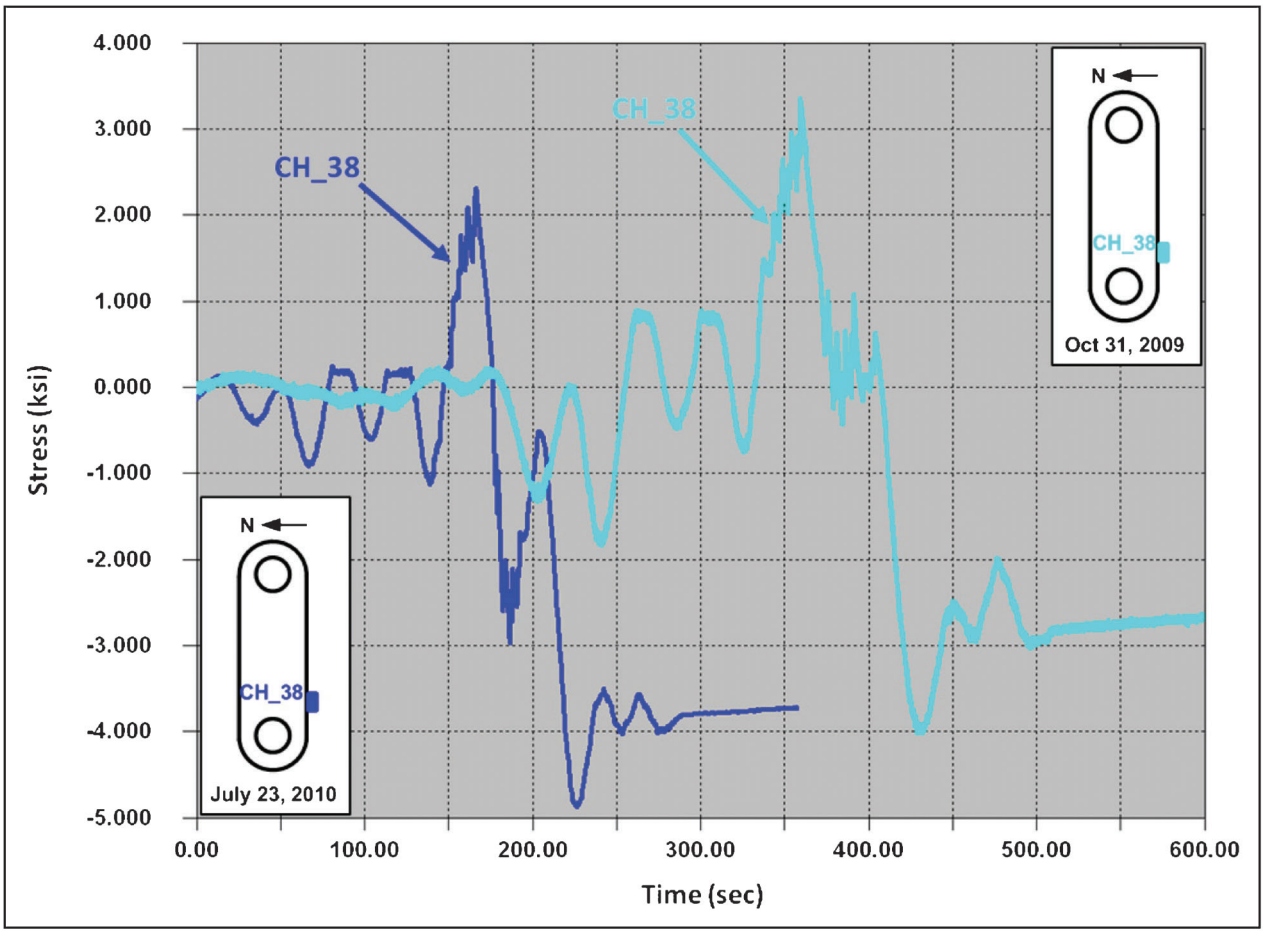

Figure 7.17: Girder G2 west hanger superload comparison

the computed neutral axis for the positive moment. It should also be noted that linear interpolation was used to calculate the stress at the top of the top flange due to the strain gage being located on the bottom side of the flange.

There also appears to be a downward shift in the measured neutral axis during the heaviest superload. The shift is noted when comparing Figure 7.20 of the heaviest superload to Figure 4.10 of the controlled load testing. Regardless, full composite action is still developed at this location when compared to the computed neutral axis.

Three strains gages remained connected on the primary girder at the location of maximum positive moment after the controlled load testing. These included channels CH_2, CH_24, and CH_26. All three strain gages were located on the bottom flange. CH_2 is at the location of maximum positive moment in Span N on Girder G2. CH_24 and CH_26 are at the location of maximum positive moment in Span P on Girder G2

TABLE 7.5:
Primary girder maximum stresses and stress range for the heaviest superload

		Location				
Channel	Girder	Global	Local	Min (KSI)	Max (KSI)	S_r (KSI)
CH_2	G2	Maximum positive moment Span N	Bottom	−2.6	7.3	9.9
CH_4	G2	Inflection point Span N	Bottom	−9.6	7.4	17.0
CH_5	G2	Maximum negative near Pier 13	Top	−0.1	3.8	3.9
CH_6	G2	Maximum negative near Pier 13	Bottom	−7.3	0.6	7.9
CH_12	G1	Maximum negative near Pier 13	Bottom	−7.0	0.6	7.6
CH_24	G2	Maximum positive moment Span P	Bottom	−2.0	7.8	9.8
CH_26	G1	Maximum positive moment Span P	Bottom	−1.7	6.6	8.3

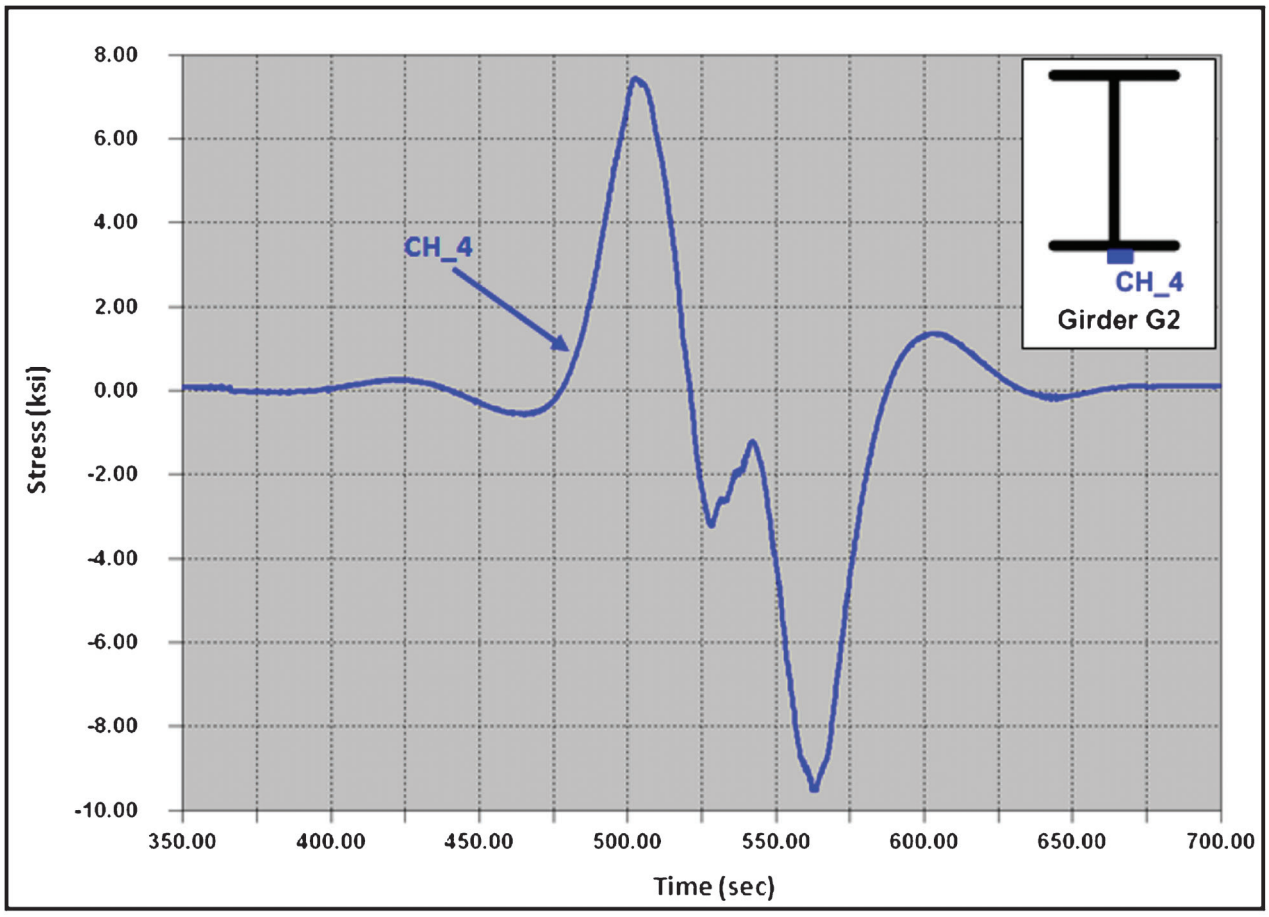

Figure 7.18: Response from heaviest superload at dead load inflection point

and Girder G1, respectively. Figure 7.21 is a plot of the response of CH_2 (blue trace), CH_24 (red trace), and CH_26 (green trace) during the heaviest superload. As expected, the general response of all three strain gages was very similar. This response was also similar to the response measured during the side-by-side crawl controlled load test with one exception. Due to the length of the superload, there are two peaks in the stress of the superload data. Conversely, the controlled load test only had a single peak. Nevertheless, the overall general response of the structure is the same between the two data sets.

Load distribution between the two primary girders can also be evaluated in Figure 7.21. At the midspan of Span P both primary girders are instrumented. Comparing the strain gage measurements at these two locations will give an indication of the load distribution. As can be seen in figure, Girder G2 (CH_24) carries slightly more load than Girder G1 (CH_26). This is signified by the measured stress in each girder. Similar load distribution was observed during the controlled load testing; likely, this is due to the transverse location of the superload. Based on the data, the truck is favoring the east side of the bridge. Thus, as expected, the increased weight of the superload has little effect on the load distribution at this location. One final note about the main girder positive moment strain gages, composite action cannot be evaluated because no top flange strain gages were included in the long-term monitoring.

7.3.2 Floor Beam Response

Two floor beam strain gages remained after the controlled load testing. Both of these were located at the position of maximum positive moment. The maximum and minimum stresses measured from both floor beam strain gages during the heaviest superload were recorded. Additionally, the resulting stress range for each strain gage was tabulated. All of these values can be found in Table 7.6. Also found in the table is a brief description of where these two floor beam strain gages are located. The response of the floor beam strain gages as the truck crossed the US-41 White River Bridge was plotted and can be seen in Figure 7.22.

The general response of the positive moment floor beam strain gages agrees quite well with both the controlled load test results and the data from the superload comparison. Both bottom flange strain gages measured a tensile stress as the truck crossed the bridge. The major difference between the controlled load test

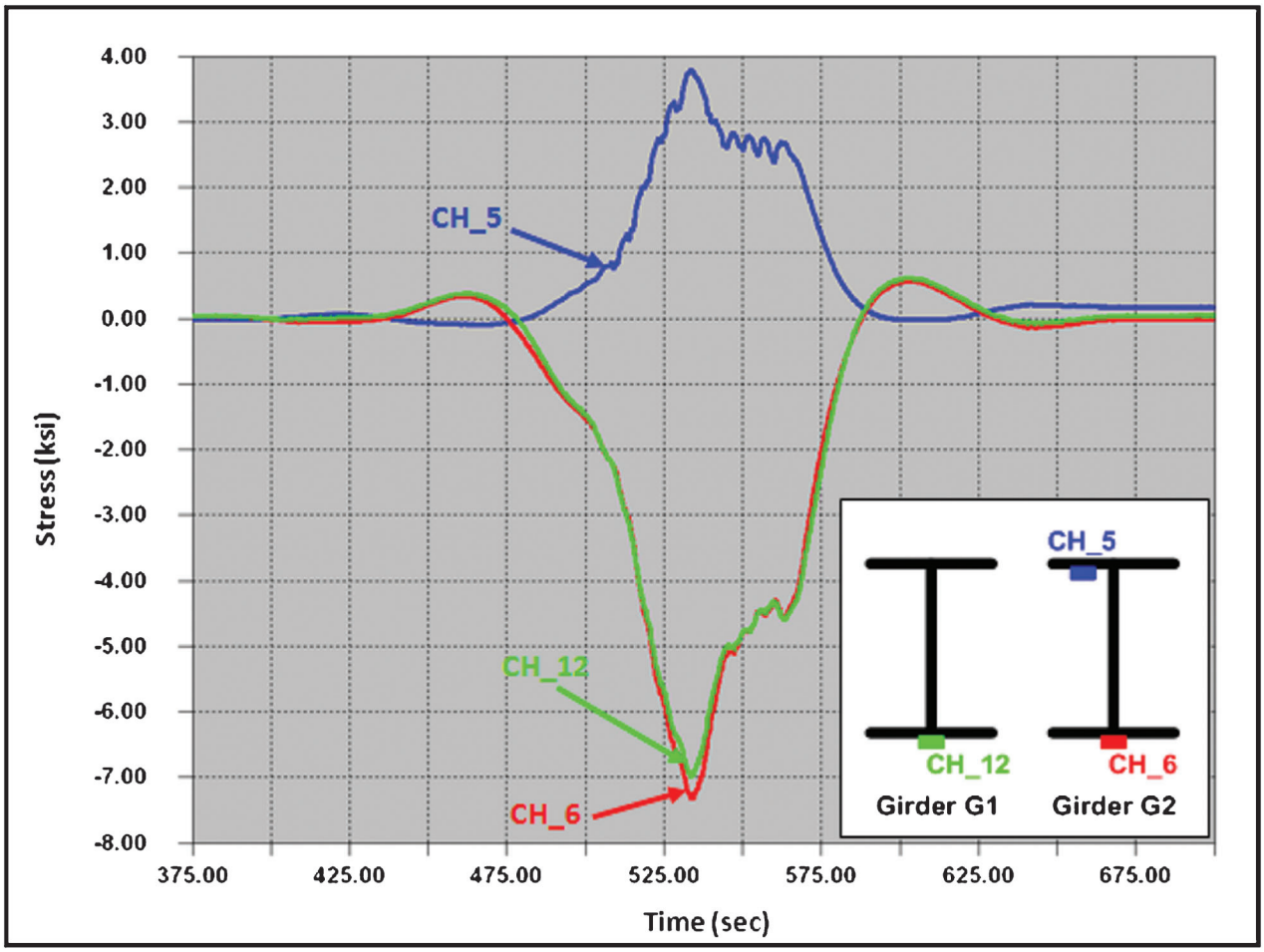

Figure 7.19: Response from heaviest superload at Pier 13

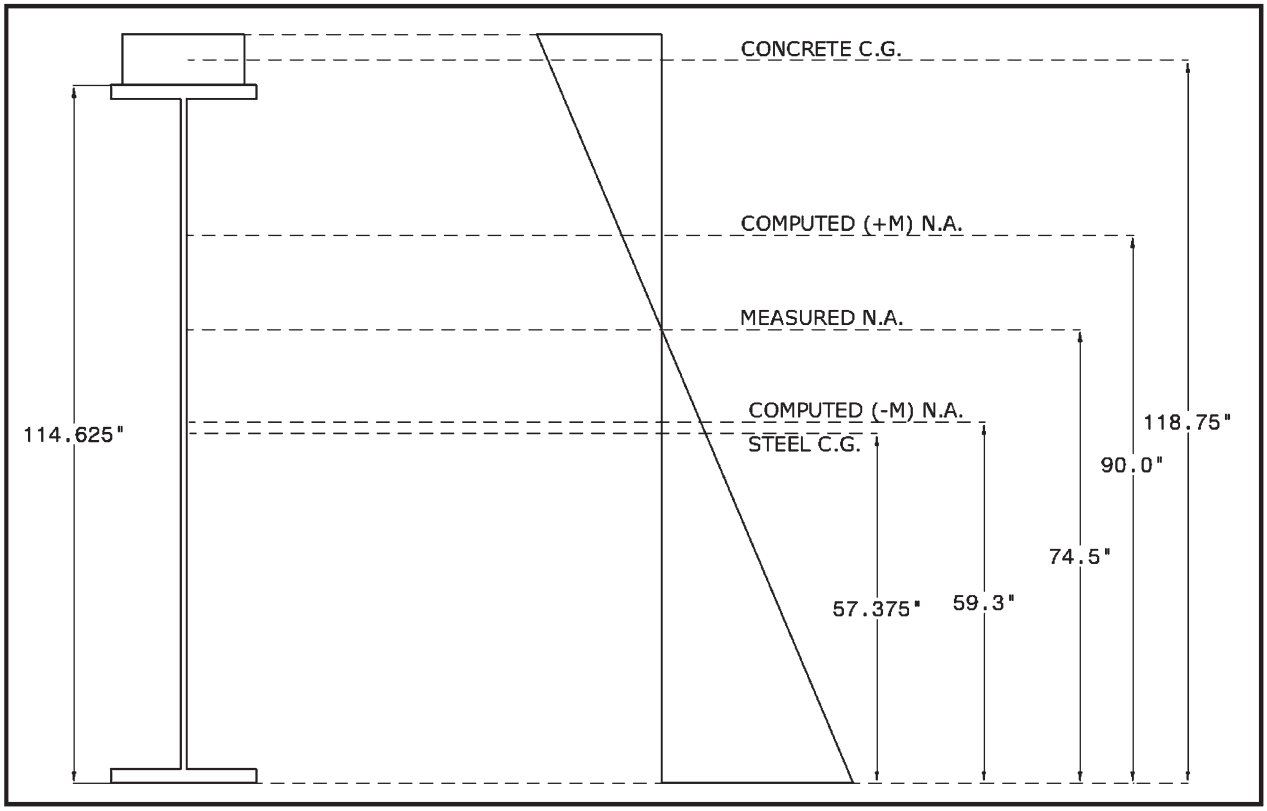

Figure 7.20: Neutral axis comparison for the heaviest superload at Pier 13 Girder G2

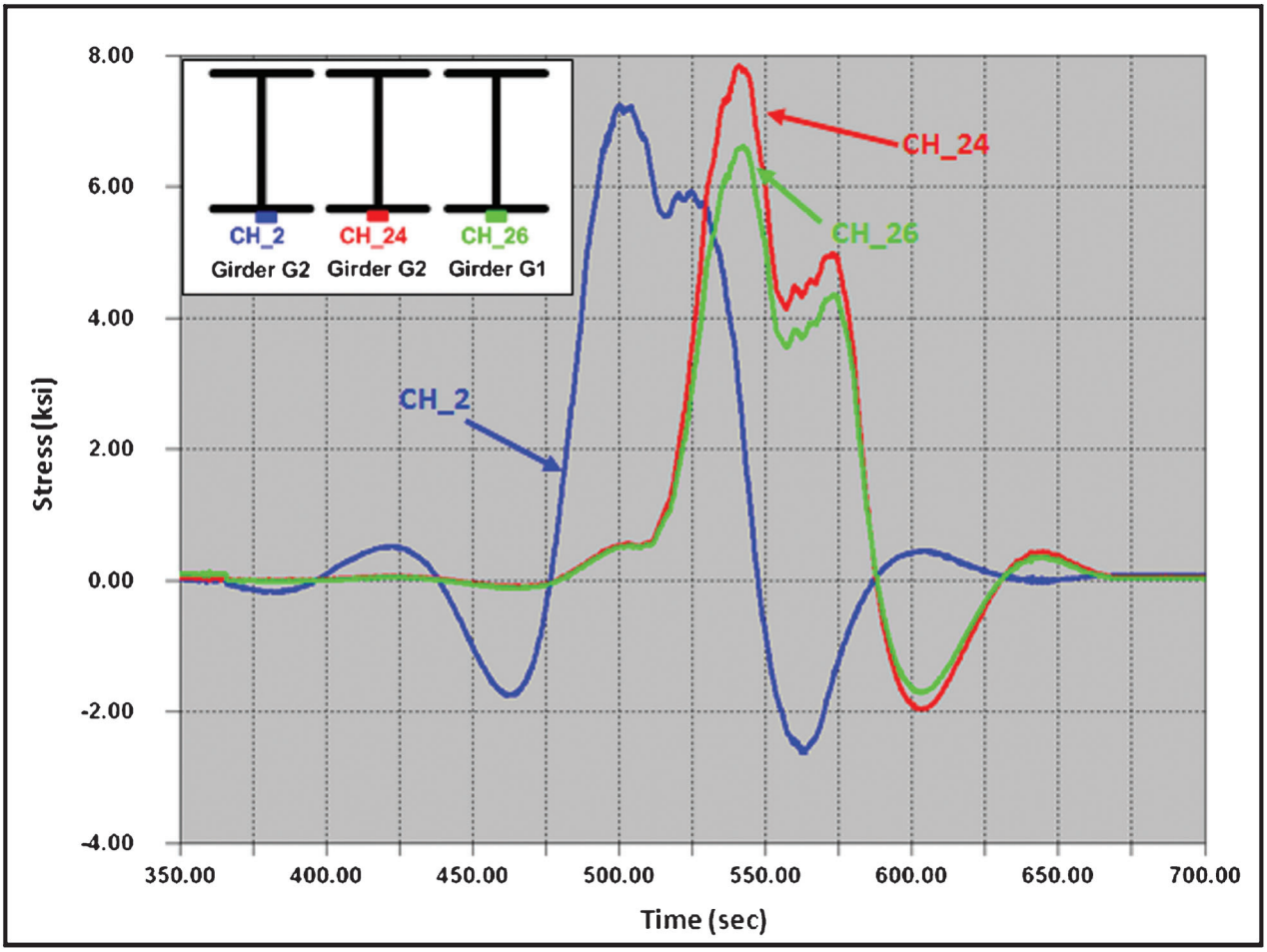

Figure 7.21: Response from heaviest superload at positive moment locations

results and these is the magnitude of the response. This is obviously due to the difference in load between the two loading events. One thing that should be noted is that CH_22 had a greater response than CH_10 during the controlled test; whereas, during the passage of this superload CH_10 had the larger response. This is of little concern because the load configuration varied greatly between the two loading events. The superload was much longer than the side-by-side crawl test configuration. Thus, it would not be expected to see perfectly scaled responses but rather general similarities between the two events.

Another interesting comparison is the plot from the side-by-side crawl controlled load test was much 'smoother' having only two defined peaks in stress. On the other hand, Figure 7.22 has multiple smaller stress spikes making up the two large peaks in stress. These smaller stress spikes are the direct result of individual axle lines crossing over the floor beams. Both superloads used for the comparison had similar stress spikes.

7.3.3 Stringer Response

Some of the highest stress measurements were recorded at various stringer locations. Therefore, seven stringer strain gages were included in the long-term monitoring to evaluate the effects of the super-heavy loading. The maximum positive and negative stresses at

TABLE 7.6:
Floor beam maximum stresses and stress range for the heaviest superload

Channel	Floor Beam Location	Location		Min (KSI)	Max (KSI)	S_r (KSI)
		Global	Local			
CH_10	Over Pier 13	Maximum positive moment	Bottom	0.0	4.3	4.3
CH_22	3rd FB north of hanger	Maximum positive moment	Bottom	−0.1	3.6	3.7

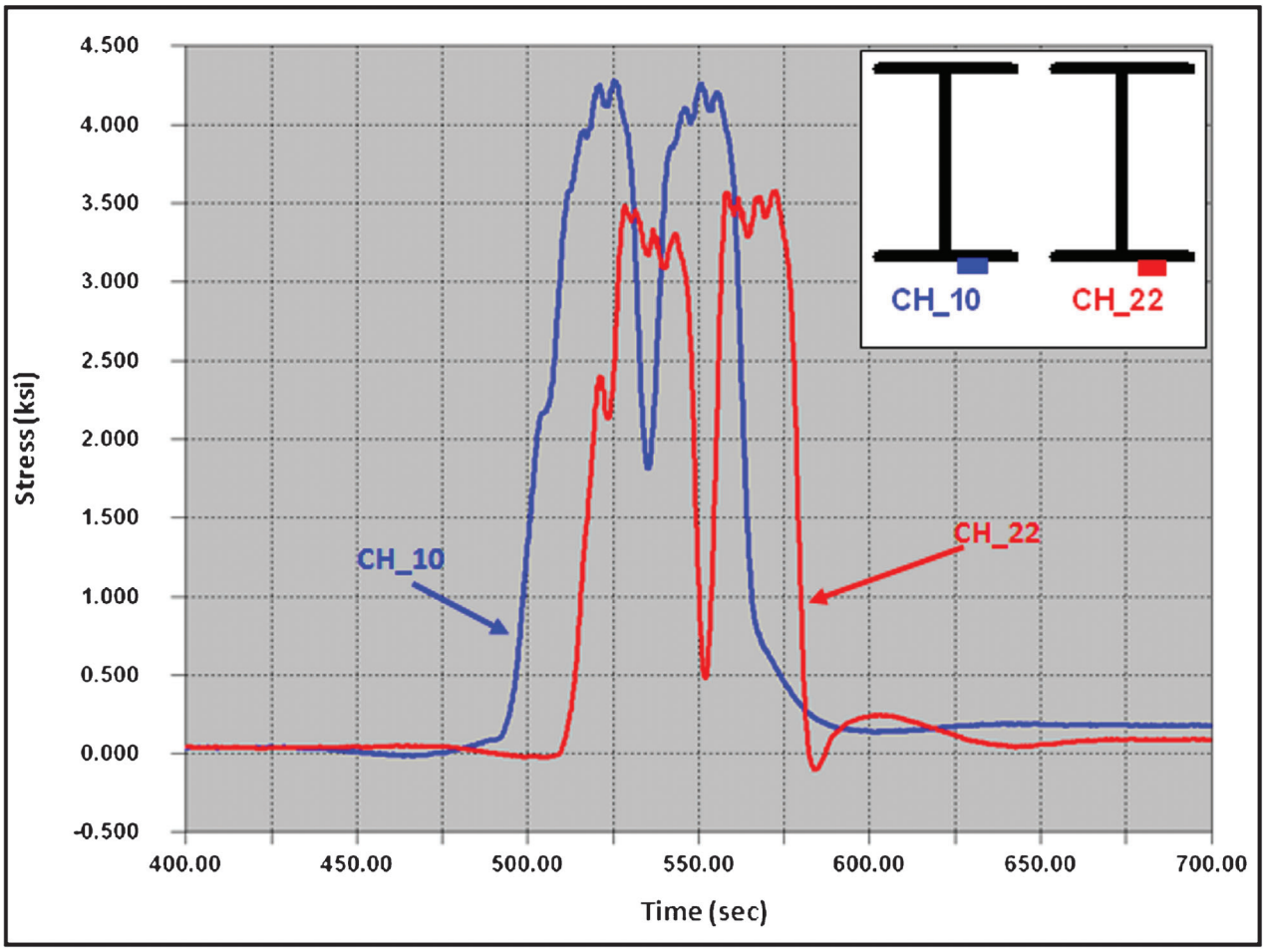

Figure 7.22: Floor beam response to heaviest superload

these locations were recorded from the heaviest superload. Using the peak stresses the maximum stress range was calculated. All of these values can be found in Table 7.7. Additionally, the table gives a brief description of where the remaining seven stringer strain gages are located. It should be noted that the stress range given in Table 7.7 might not be the algebraic difference between the maximum and minimum values shown due to rounding all stresses in the table to the nearest one-tenth.

The maximum stress ranges recorded in the stringers varied between 3.3 ksi and 7.3 ksi, depending on the strain gage location. However, it should be noted that the majority of the stringer strain gages had maximum stress ranges between 3.3 ksi and 4.4 ksi. It was only at the stringer location over Pier 13 (CH_13 and CH_14) that larger stress ranges were measured. The stringer at the Pier 13 position was continuous over the floor beam; therefore, it was a negative moment location. A

TABLE 7.7:
Stringer maximum stresses and stress range for the heaviest superload

		Location				
Channel	Stringer	Global	Local	Min (KSI)	Max (KSI)	S_r (KSI)
CH_13	Center stringer Pier 13	Maximum negative moment	Top	−0.2	6.5	6.7
CH_14	Center stringer Pier 13	Maximum negative moment	Bottom	−7.0	0.2	7.3
CH_15	East stringer Simple span	Maximum positive moment	Top	−0.1	3.9	4.1
CH_16	East stringer Simple span	Maximum positive moment	Bottom	−3.2	0.1	3.3
CH_17	East stringer 0.4 point	Maximum positive moment	Top	−3.3	0.4	3.7
CH_18	East stringer 0.4 point	Maximum positive moment	Bottom	−0.2	4.2	4.4
CH_28	Center stringer 4th FB north of hanger	Maximum negative moment	Bottom	−3.2	0.2	3.5

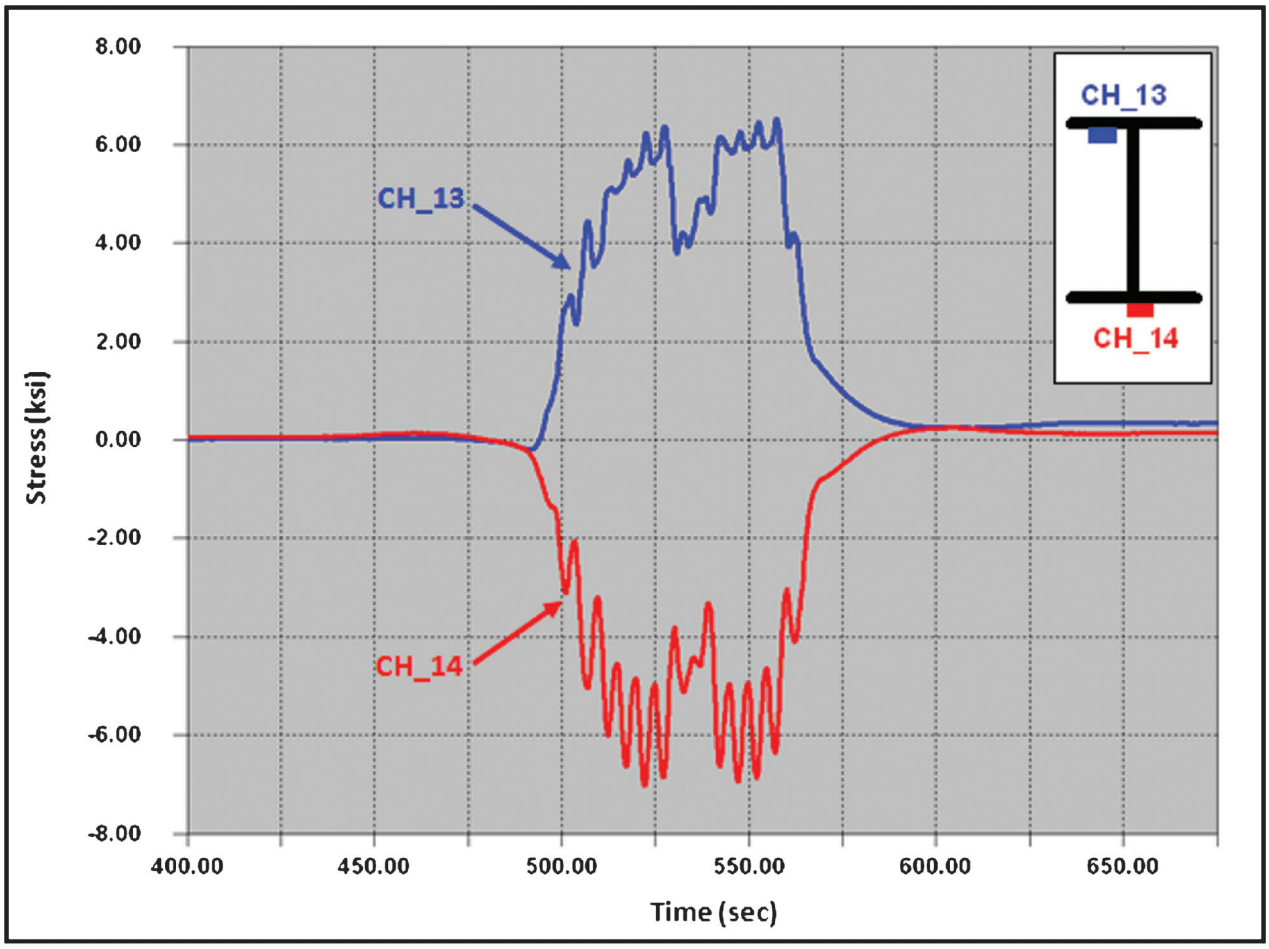

Figure 7.23: Stringer of Pier 13 response to heaviest superload

plot of the CH_13 and CH_14 data during the heaviest superload is presented in Figure 7.23.

The stringer response plotted for the strain gage location over Pier 13 is typical for a negative moment location. Tension is measured in the top flange (CH_13) and compression in the bottom flange (CH_14). As can be seen in the plot both the tensile and compressive responses are approximately the same magnitude, indicating they are equal and opposite. Having equal and opposite stresses signifies that no composite action is being developed between the concrete deck and steel stringers at this location.

Another observation displayed extremely well in Figure 7.23 is the local bending effect as each individual axle crosses over the strain gage location. Since the stringers are in direct contact with the deck, local bending effects are often captured at the stringer strain gage locations. Local bending effects similar to those found in this plot were measured during the controlled load testing and superload comparison as well. Thus, such effects are completely normal for a stringer and were expected during the passage of the heaviest superload.

During the controlled load testing and superload comparison, minor composite action between the concrete deck and steel stringers was observed in the positive moment regions. These include the east stringer in the simple span (CH_15 and CH_16) and the east stringer at the 0.4 point (CH_17 and CH_18). From the controlled load tests it was determined that the amount of composite interaction between the elements and consistency of this behavior was not enough to consider it during the analysis. For the heaviest superload these locations were once again evaluated to determine if any composite action existed. Plotted below in Figure 7.24 and Figure 7.25 is the measured response for these same two locations. Figure 7.24 plots channels CH_15 and CH_16 and Figure 7.25 plots channels CH_17 and CH_18. It should also be noted that these figures illustrate well the stress spikes from each axle. Additionally, the plots reveal minor composite action between the concrete deck and steel stringers still exists during the heaviest superload. Once again, the composite action is signified by the compressive response at both stringer locations being less than the tensile response. The compressive stress is three quarters of the tensile stress.

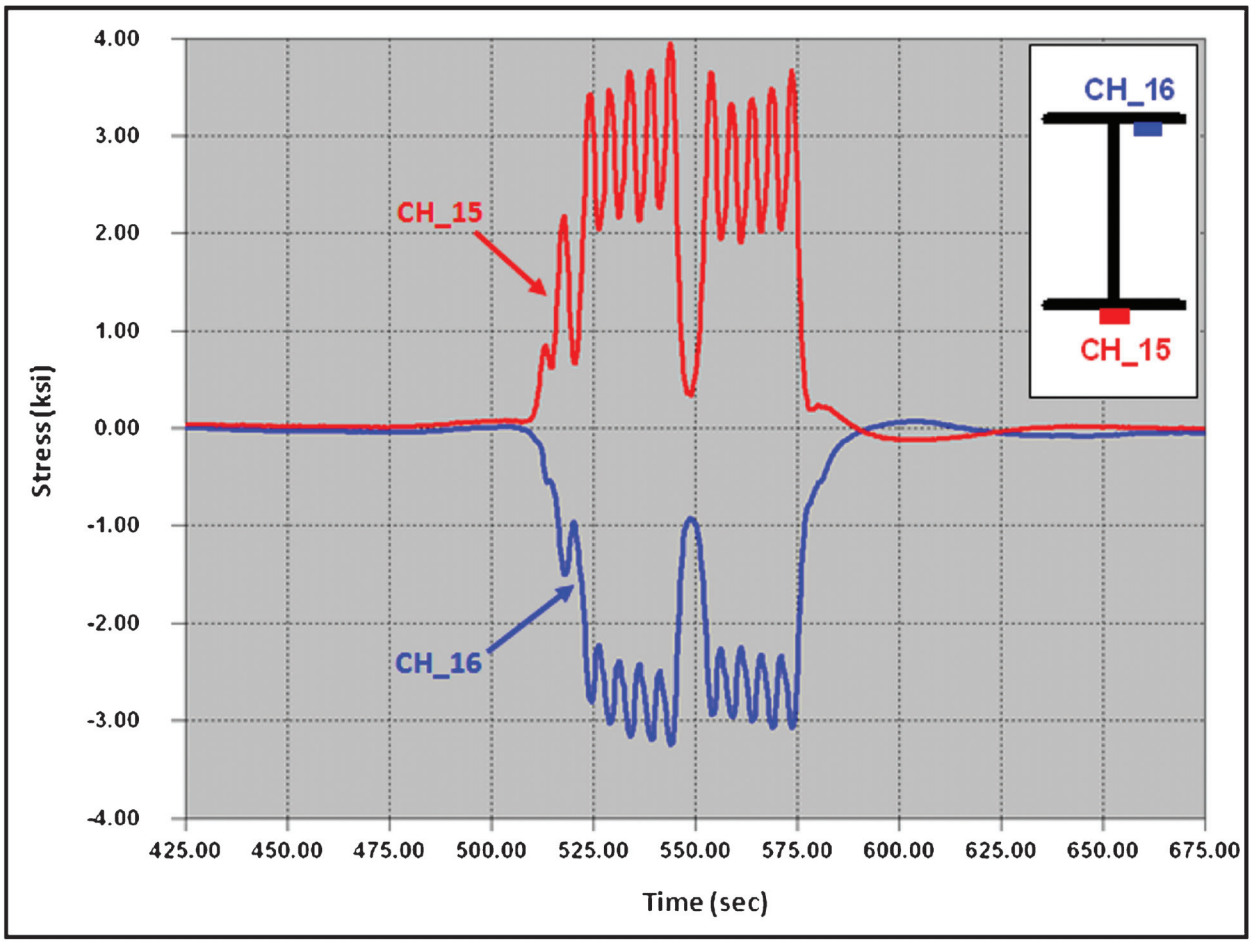

Figure 7.24: Maximum stress at CH_15 and CH_16 for heaviest superload

Using the maximum field measured stress values the neutral axis was computed and compared to the neutral axis of the steel section alone. A plot of the resulting values is shown in Figure 7.26. As can be seen in the figure, the neutral axis resulting from the strain gage measurements is slightly greater than the neutral axis of the steel stringer alone. This confirms that some composite action is being developed between the concrete deck and steel stringer. Comparing the locations of the neutral axis from the heaviest superload to those calculated from the controlled load test it is found that more slip has occurred. The additional slip is signified by the lower neutral axis for the superload than the controlled load tests. Thus, as in the case of the controlled load test, some minor composite action is developed between the concrete deck and steel stringers; however, it is not great enough or consistent enough to rely on in the analysis of the bridge.

7.3.4 Pin and Hanger Response

Bi-axial bending in pin and hanger assemblies has been known to lead to fatigue cracks of other bridges in the past. Therefore, three of the four hangers at the expansion joint north of Pier 13 had strain gages included in the long-term monitoring of the US-41 White River Bridge. These three hangers included the Girder G1 west hanger, Girder G2 east hanger, and Girder G2 west hanger. The maximum and minimum stress measured from each of the remaining strain gages on these three hangers due to the heaviest superload was recorded. From the peak stress values the maximum stress range was tabulated. Each of these three values can be found in Table 7.8. It should be noted that the stress range given in Table 7.8 might not be the algebraic difference between the maximum and minimum values shown due to rounding all stresses in the table to the nearest one-tenth.

The east hanger on Girder G2 had the most instrumentation of all the hangers monitored. Originally, eight strain gages were installed on this hanger. During the long-term monitoring four strain gages remained. The response of two of these strain gages (CH_32 and CH_34) is plotted in Figure 7.27. CH_32 and CH_34 were used to evaluate any bending that might be occurring in the hangers during the side-by-side controlled load tests and during the superload comparison.

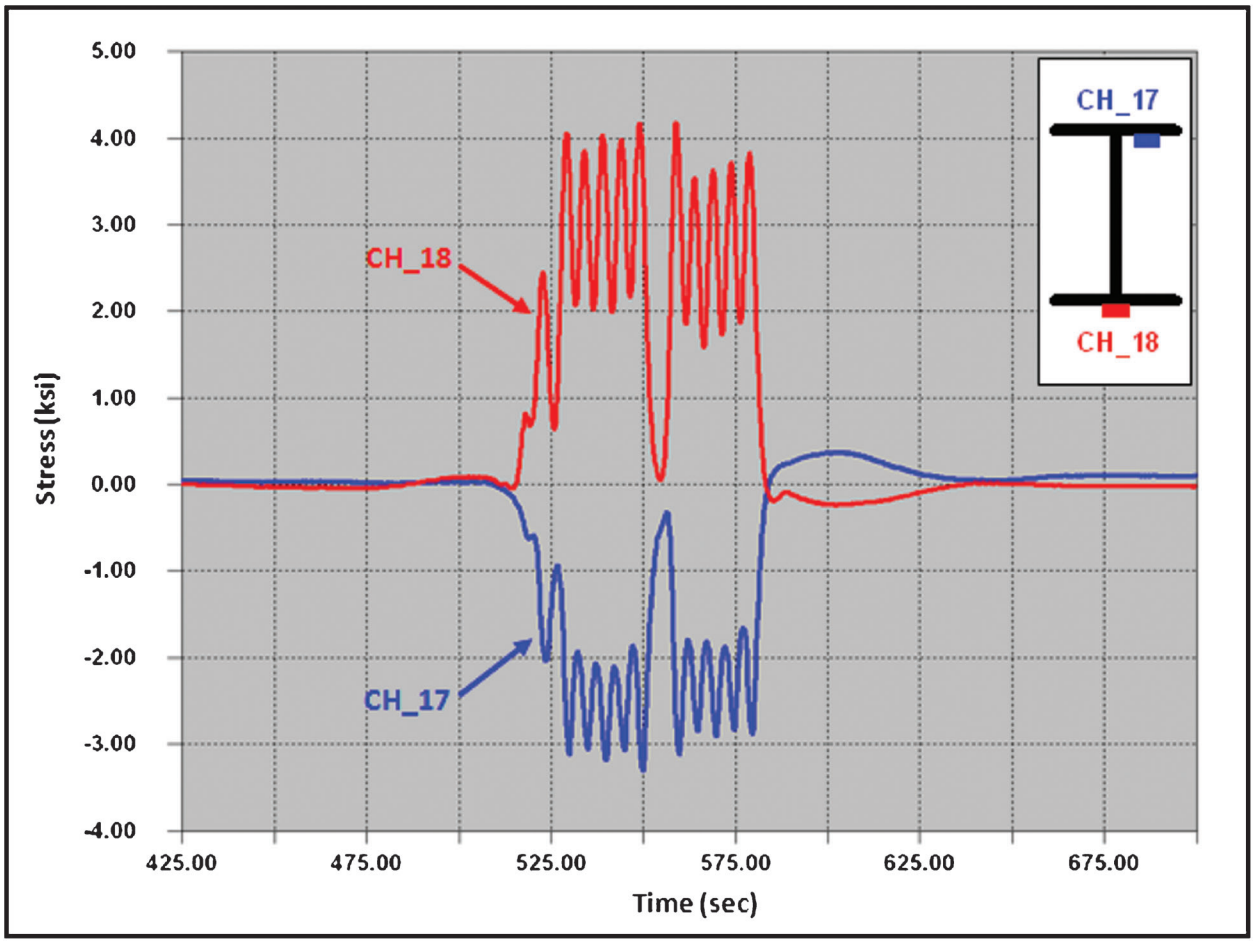

Figure 7.25: Maximum stress at CH_17 and CH_18 for heaviest superload

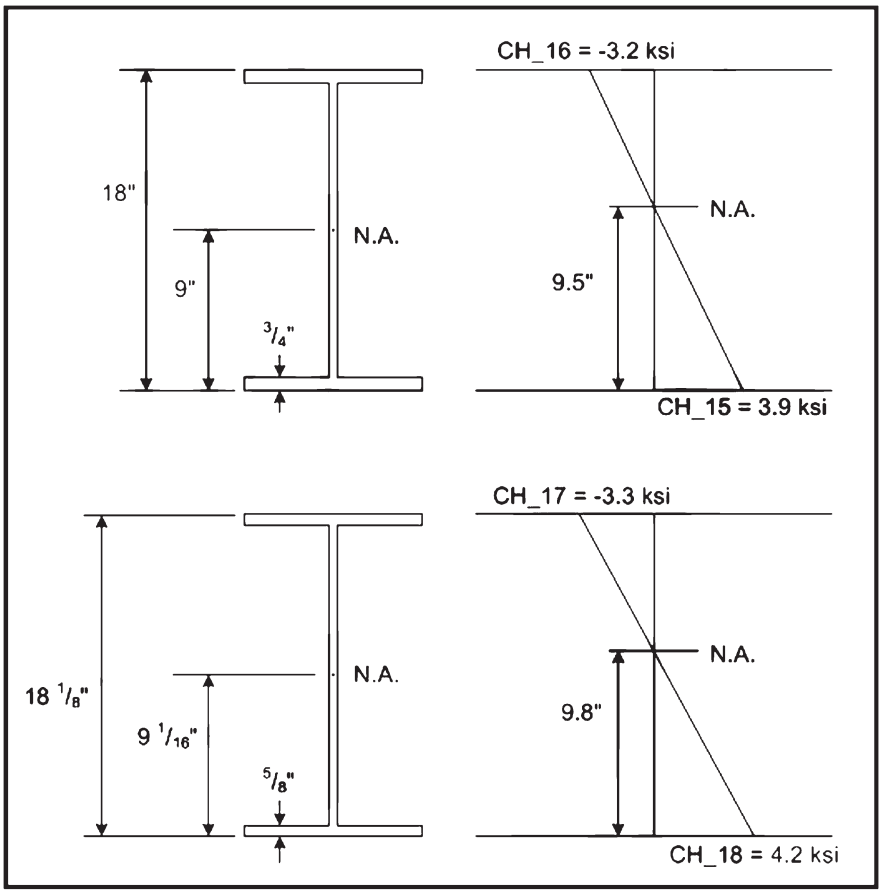

Figure 7.26: Neutral axis for positive moment region stringer locations from heaviest superload

TABLE 7.8:
Pin and hanger maximum stresses and stress range for the heaviest superload

Channel	Girder	Face	Min (KSI)	Max (KSI)	S_r (KSI)
CH_29	G2	East	−0.5	4.1	4.6
CH_31	G2	East	−0.7	4.9	5.6
CH_32	G2	East	−1.8	2.4	4.2
CH_34	G2	East	−0.5	5.2	5.7
CH_38	G2	West	−3.1	2.3	5.4
CH_43	G1	West	−0.3	4.3	4.7
CH_44	G1	West	−1.3	4.1	5.4

During both the controlled load tests and superload comparison, bi-axial bending regularly occurred as the vehicle(s) crossed through successive spans. Bending was signified by the alternating equal and opposite stresses measured by the strain gages. A similar behavior can be observed in Figure 7.27. It should be noted that the amount of bending occurring in the hanger prior to the load crossing the assembly appears to be less during the side-by-side controlled load tests. This is likely due to the length of the superload spreading the load out over many spans. Thus, the forces causing bending counteract each other as continuous spans are loaded. Conversely, once the superload crossed the pin and hanger assembly and began exiting the bridge, significantly more bending occurred than did during the side-by-side controlled load test. This increased bending is best noted in Figure 7.27 between 550 and 575 seconds.

One final observation made from the above plot is the amount of stress remaining in the hanger as the superload exited the bridge. During the controlled load test a stress of approximately 0.6 ksi remained after the test trucks crossed the bridge. When looking at the passage of the heaviest superload, a stress of approximately 0.8 ksi remains. This suggests that a larger displacement remained after the passage of the superload. As discussed in the section on the controlled load test, this type of behavior would be a concern if the displacement was permanent. However, over longer periods of monitoring it was found that the pin and hangers consistently vibrated back to their original position. Therefore, this temporary displacement is not of great concern.

Girder 1 west hanger had two strain gages remaining during the long-term monitoring (CH_43 and CH_44). These gages were used during the analysis of the

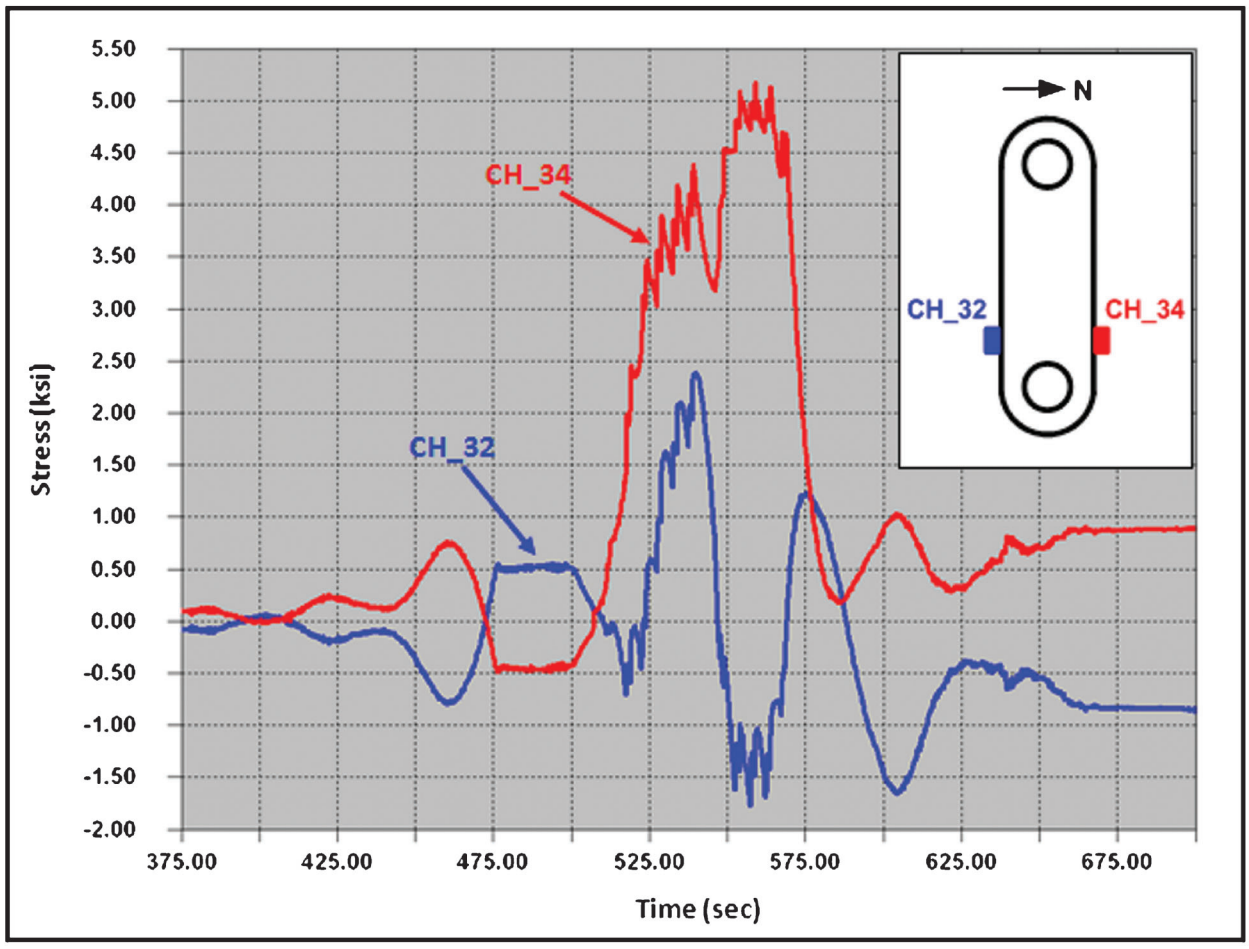

Figure 7.27: Girder G2 east hanger response to heaviest superload

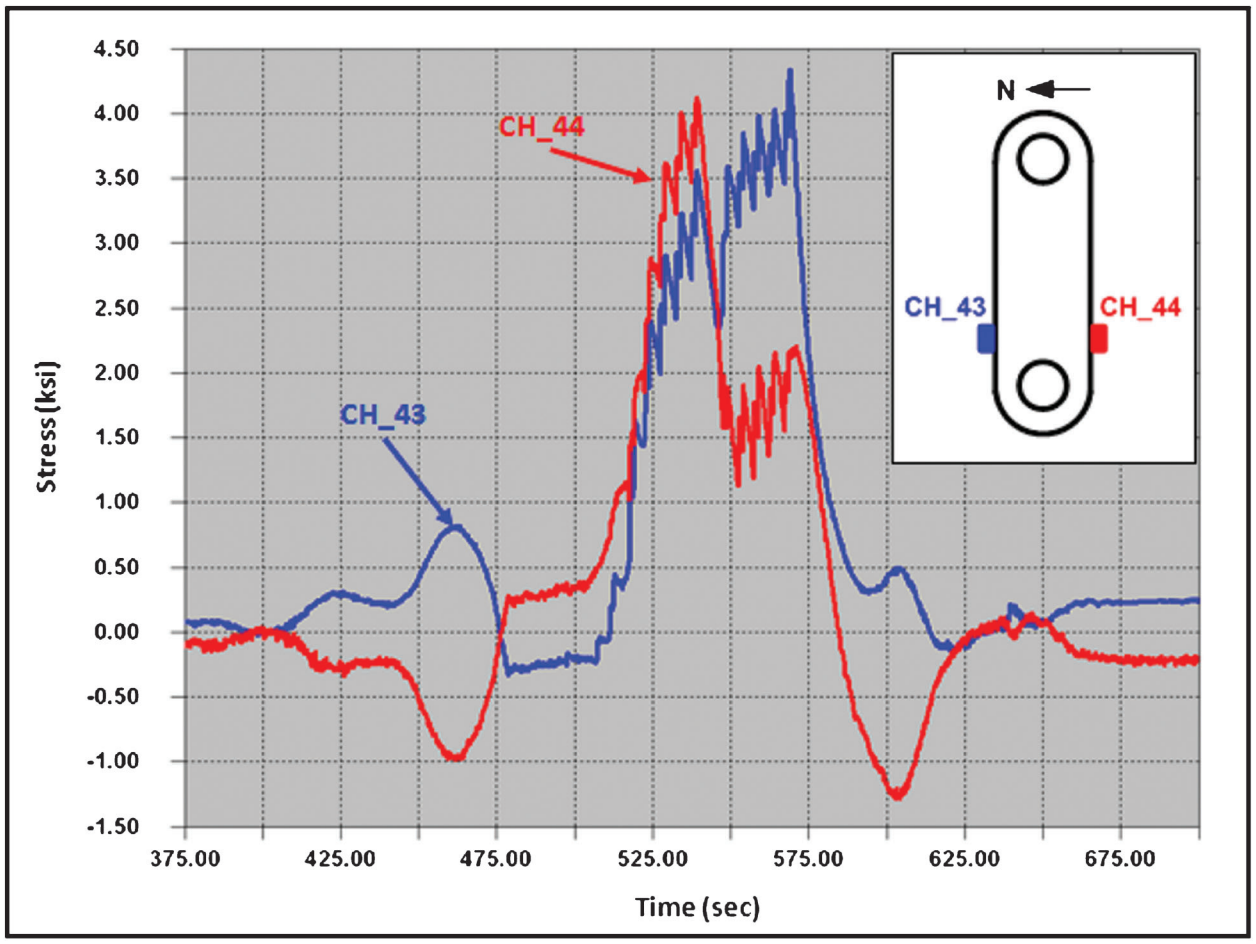

Figure 7.28: Girder G1 west hanger response to heaviest superload

controlled load test to determine if any bi-axial bending was occurring in the hanger. Plotted in Figure 7.28 is the response of CH_43 and CH_44 to the heaviest superload.

Girder G1 west hanger exhibits very minor bending as shown in Figure 7.28. However, like in the case for the controlled load test and superload comparison, much less bending is occurring in this hanger than Girder G2 east hanger. Very minor opposite alternating stresses are observed before and after the superload crosses the pin and hanger assembly. As is typical for a hanger, when the load crossed into the hung span a large tensile response is measured by both stain gages. One final indication that less bending is occurring at this hanger is the amount of stress remaining at the strain gages after the truck has exited the bridge. This stress is an indication of how much temporary displacement remains after the crossing. Less stress suggests that the pin and hangers were moving much more freely; hence, bending less.

7.4 Summary of Superloads

Based on information received from Bernardin, Lochmueller & Associates, Incorporated (BLA) a summary of all the superloads that crossed the US-41 White River Bridge is provided in Table 7.9. The summary includes the date of the crossing, dimensions of the vehicle, and GVW of each superload. It is important to note that the table only includes those loads over 300,000 lbs. Other heavy loads up to 300,000 lbs. crossed the bridge in conjunction with the power plant construction as well. In total seventy-four (74) superloads over 300,000 lbs. were moved across the US-41 White River Bridge over a period from June 18, 2009 to July 23, 2010.

The heaviest two superloads crossed the US-41 White River Bridge on May 23, 2010 and June 3, 2010 and had a GVW of 1,117,000 lbs. Fifteen other superloads of nearly one million pounds also crossed the bridge during the construction period. Based on the analyzed long-term monitoring data of all bridge elements, the Purdue Research Team believes that no negative long-term effects were sustained due to the series of super-heavy loads. Nevertheless, as noted earlier, it is recommended that all pin and hanger assemblies be lubricated to help ensure free rotation and minimize bending effects.

TABLE 7.9:
Summary of all superloads crossing the US-41 White River Bridge (curtsey of BLA)

DATE OF MOVE	HAUL VEHICLE	GROSS WEIGHT (per permit)	DATE OF MOVE	HAUL VEHICLE	GROSS WEIGHT (per permit)
6/18/09	17′-6″ H, 22′-10″ W, 182′-10″ L	553566 lbs.	1/23/10	18′-6″ H, 23′ W, 280′-10″ L	989,040 lbs.
6/23/09	17′-6″ H, 22′-10″ W, 182′-10″ L	553566 lbs.	1/31/10	18′-6″ H, 23′ W, 280′-10″ L	989,040 lbs.
6/29/09	17′-6″ H, 22′-10″ W, 182′-10″ L	553566 lbs.	2/7/10	18′-6″ H, 23′ W, 280′-10″ L	989,040 lbs.
7/7/09	17′-6″ H, 22′-10″ W, 182′-10″ L	553566 lbs.	2/13/10	18′-6″ H, 23′ W, 280′-10″ L	989,040 lbs.
8/21/09	17′-6″ H, 22′-10″ W, 259′-9″ L	697740 lbs.	2/19/10	16′-3″ H, 18′ W, 127′-8″ L	448,000 lbs.
8/29/09	17′-6″ H, 22′-10″ W, 259′-9″ L	697740 lbs.	2/21/10	16′-3″ H, 18′ W, 127′-8″ L	448,000 lbs.
9/21/09	12′-0″ H, 20′-0″ W, 186′-1″ L	471,830 lbs.	2/26/10	18′-6″ H, 23′ W, 280′-10″ L	989,040 lbs.
9/25/09	12′-0″ H, 20′-0″ W, 186′-1″ L	471,830 lbs.	2/28/10	22′-0″ H, 18′-9″ W, 157′-0″ L	531,600 lbs.
10/11/09	17′-6″ H, 22′-10″ W, 280′-10″ L	989,040 lbs.	2/28/10	22′-0″ H, 18′-9″ W, 157′-0″ L	531,600 lbs.
10/24/09	17′-6″ H, 22′-10″ W, 280′-10″ L	884,040 lbs.	3/3/10	18′-6″ H, 23′ W, 280′-10″ L	989,040 lbs.
10/28/09	14′-2″ H, 18′-0″ W, 162′-1″ L	549,600 lbs.	3/6/10	18′-0″ H, 18′-0″ W, 127′-8″ L	448,000 lbs.
10/31/09	17′-6″ H, 22′-10″ W, 280′-10″ L	989,040 lbs.	3/13/10	24′-0″ H, 23′-6″ W, 280′-10″ L	989,040 lbs.
11/7/09	18′-6″ H, 22′-10″ W, 280′-10″ L	989,040 lbs.	3/18/10	24′-0″ H, 23′-6″ W, 280′-10″ L	989,040 lbs.
11/14/09	18′-6″ H, 22′-10″ W, 280′-10″ L	989,040 lbs.	3/23/10	22′-6″ H, 18′-0″ W, 127′-8″ L	370,000 lbs.
12/1/09	14′-2″ H, 18′-0″ W, 162′-1″ L	549,600 lbs.	3/23/10	22′-0″ H, 18′-0″ W, 120′-0″ L	302,000lbs
12/4/09	19′H, 12′-6″ W, 122′ L (Load 1)	540,000 lbs.	3/25/10	23′-0″ H, 18′-0″ W, 128′-8″ L	378,000 lbs.
12/4/09	19′H, 12′-6″ W, 122′ L (Load 2)	540,000 lbs.	3/29/10	23′-0″ H, 18′-0″ W, 128′-8″ L	378,000 lbs.
12/5/09	18′-6″ H, 22′-10″ W, 280′-10″ L	989,040 lbs.	4/1/10	23′-0″ H, 18′-0″ W, 127′-8″ L	370,000 lbs.
12/12/09	19′-6″ H, 20′ W, 163′ L (Load 1)	549,600 lbs.	4/8/10	19′-6″ H, 18′-0″ W, 138′-10″ L	413,000 lbs.
12/12/09	19′-6″ H, 20′ W, 163′ L (Load 2)	549,600 lbs.	4/8/10	19′-6″ H, 18′-0″ W, 131′-2″ L	395,000 lbs.
12/12/09	23′ H, 20′ W, 225′ L (Load 3)	483,830 lbs.	4/12/10	19′-6″ H, 18′-0″ W, 138′-10″ L	413,000 lbs.
12/13/09	14′ H, 18′ W, 108′-7″ L	451,600 lbs.	4/12/10	19′-6″ H, 18′-0″ W, 131′-2″ L	395,000 lbs.
12/15/09	14′ H, 18′ W, 108′-7″ L	451,600 lbs.	4/14/10	19′-6″ H, 18′-0″ W, 138′-10″ L	413,000 lbs.
12/17/09	14′ H, 18′ W, 181′-6″ L (Load 1)	581,000 lbs.	4/14/10	19′-6″ H, 18′-0″ W, 131′-2″ L	395,000 lbs.
12/17/09	23′ H, 20′ W, 225′ L (Load 2)	483,830 lbs.	4/16/10	24′-0″ H, 20′-0″ W, 129′-9″ L	403,000 lbs.
1/4/10	14′ H, 18′ W, 174′-10″ L (Load 1)	563,000 lbs.	4/26/10	17′-0″ H, 21′-6″ W, 126′-5″ L	471,600 lbs.
1/4/10	14′ H, 18′ W, 162′-1″ L (Load 2)	549,600 lbs.	4/27/10	19′-6″ H, 21′-6″ W, 166′-2″ L	531,600 lbs.
1/5/10	14′ H, 18′ W, 108′-7″ L (Load 1)	451,600 lbs.	5/6/10	24′-0″ H, 19′-0″ W, 174′-10″ L	618,000 lbs.
1/5/10	14′ H, 18′ W, 162′-1″ L (Load 2)	549,600 lbs.	5/23/10	23′-0″ H, 23′-6″ W, 299′-0″ L	1117000 lbs.
1/9/10	14′ H, 18′ W, 117′-8″ L	471,600 lbs.	6/3/10	23′-0″ H, 23′-6″ W, 299′-0″ L	1117000 lbs.
1/11/10	14′ H, 18′ W, 174′-10″ L	563,000 lbs.	6/9/10	17′-0″ H, 21′-6″ W, 126′-5″ L	471,600 lbs.
1/13/10	14′ H, 18′ W, 174′-10″ L	563,000 lbs.	6/10/10	19′-6″ H, 21′-6″ W, 166′-2″ L	531,600 lbs.
1/15/10	14′ H, 18′ W, 174′-10″ L	563,000 lbs.	6/16/10	18′-9″ H, 18′-0″ W, 115′-3″ L	380,000 lbs.
1/16/10	18′-6″ H, 18′ W, 280′-10″ L	989,040 lbs.	6/16/10	18′-9″ H, 18′-0″ W, 115′-3″ L	380,000 lbs.
1/17/10	14′ H, 18′ W, 117′-8″ L	471,600 lbs.	6/21/10	18′ H, 18′ W, 181′-6″ L	620,000 lbs.
1/18/10	14′ H, 18′ W, 174′-10″ L	563,000 lbs.	6/23/10	18′ H, 18′ W, 181′-6″ L	620,000 lbs.
1/20/10	14′ H, 18′ W, 117′-8″ L	471,600 lbs.	7/23/10	18′-6″ H, 23′-0″ W, 280′-10″ L	989,040 lbs.

8. LONG-TERM MONITORING

Upon the completion of the controlled load testing, the measured data were evaluated to determine critical strain gage locations on the US-41 White River Bridge to be included in the long-term monitoring. Twenty-four (24) strain gages were identified from the original forty-eight (48) installed to be included. Long-term monitoring was conducted over a period from December 12, 2009 to September 10, 2010. During the period two primary types of data were collected: stress range histograms and triggered time-history data.

Stress range histograms were compiled by the data logger every ten minutes for the duration of the long-term monitoring period. The stress range histograms were created via the rainflow cycle counting method. An algorithm for the rainflow cycle counting method was programmed in the data logger. The algorithm would break ten minutes of time-history data into individual stress cycles and place them in the appropriate bin, automatically creating the histograms. Once the data were analyzed the data logger would flush the actual time-history data and only store the updated histograms. These histograms were then used to perform a fatigue analysis of the US-41 White River Bridge.

To limit the amount of data collected and transmitted back to Purdue, time-history data were initiated by trigger events. Based on the trigger, data collection would start and stop at predefined stress levels. Specifically, when strain in CH_24 reached a predefined threshold limit the data logger was ‘triggered’ and began recording and storing data for a predetermined amount of time. The data logger was also capable of buffering pre-trigger data. Thus, data prior to the trigger event were able to be included in the trigger data file as well.

Two separate triggers were used for the US-41 White River Bridge. The more common of the two triggers captured a heavily loaded truck found in normal daily

traffic. This trigger was tripped when the stress at CH_24 exceeded 1.8 ksi. (*Note: Stress was computed by multiplying the measured strain by the modulus of elasticity of the steel. This calculation was automatically performed internally by the data logger. Thus, all values report in the data files were in ksi.*) Once triggered, the data logger recorded data for four seconds before and after the event. Using a trigger event that captures heavily loaded daily traffic is extremely common practice for long-term monitoring. This because the captured time-history data can be used to verify the large stress cycles found in the stress range histograms. The second, less common, trigger event was designed to meet the needs of the US-41 White River Bridge monitoring of super-heavy loads. Hence, it was tripped when the stress at CH_24 exceeded 4.0 ksi. Also, since these loads moved much slower than normal daily traffic the pre and post trigger was set to 160 seconds and 180 second respectively. All trigger durations and stress thresholds were established by the Research Team based on a preliminary review of the initial data collected in the early going of long-term monitoring.

As stated above, the triggered time-history data served several purposes. These included limiting the amount of data collected and transmitted from the site as well as validation of the high stress cycles in the rainflow histograms. An additional purpose for the trigger events, specifically the high-stress triggers, was to evaluate the effects of the superloads. Much of the superload data was presented above in Chapter 5; therefore, it will not be discussed in great deal during this chapter. Rather, presented below is a brief discussion of some data collected from the triggered time-history. This data includes video images captured by a camera installed onsite by the Research Team. Furthermore, a fatigue analysis is presented during this chapter that includes stress range histograms and remaining fatigue life calculations for all strain gage locations included in the long-term monitoring.

8.1 Triggered Time-History Data and Video Images

Collecting time-history data based on trigger events is the best way to efficiently gather the most useful data. As great as it would be to collect and analyze live time-history data for every vehicle that crosses the US-41 White River Bridge, it is simply not a realistic goal when considering the amount of data involved from both a time perspective as well as data transfer viewpoint. Thus, based on preliminary monitoring the Research Team selected a given stress at one location to trigger data collection. The trigger stress value was set such that several trigger events would occur each day. Obviously, the number of events varied daily based on traffic patterns, season, weather, and other various factors.

To further compliment the triggered time-history data the Research Team installed a video camera on the US-41 White River Bridge. The data logger was programmed to simultaneously trigger the video camera when the time-history data was triggered. Once triggered, the video camera stored a predefined number of images before and after the trigger event. The number of stored pre and post trigger images was set such than an entire loading event was captured. Unfortunately, unlike the triggers on the data logger, the camera only had a single trigger. Therefore, the number of images recorded was selected to capture an entire daily traffic event or a significant portion of a superload event.

8.1.1 Single Truck

It was not uncommon for a standard tractor-trailer semi to trigger data collection. Figure 8.1 is a photograph taken by the video camera during a single tractor-trailer semi trigger event. As mentioned above, the trigger stress value was set such that only heavily loaded vehicles would cause a trigger event. Thus, it is likely that the tractor-trailer pictured was fully loaded. The selected trigger event pictures a semi having a standard box trailer; however, other types of single standard tractor-trailer vehicles also commonly triggered data collection. These other standard vehicles commonly triggering the daily traffic trigger included grain trucks, logging trucks, and gravel trucks.

When the standard tractor-trailer vehicles triggered data collection, the maximum stress of the trigger channel (CH_24) was near the trigger value of 1.8 ksi. In the case of the single truck trigger pictured above the maximum stress at CH_24 (pink trace) was approximately 1.8 ksi. This can be seen in Figure 8.2 which plots the data file for the single tractor-trailer event. The plot also includes several of the other main girder strain gages including CH_2, CH_4, CH_6, and CH_26. A maximum stress range of approximately 3.7 ksi at CH_4 (red trace) was recorded for this event. Lastly, the photograph in Figure 8.1 shows the truck is in the right lane, this can also be seen in the data plot. CH_24 and CH_26 are located at identical locations on opposite girders; therefore, these channels can be used

Figure 8.1: Single truck trigger video image

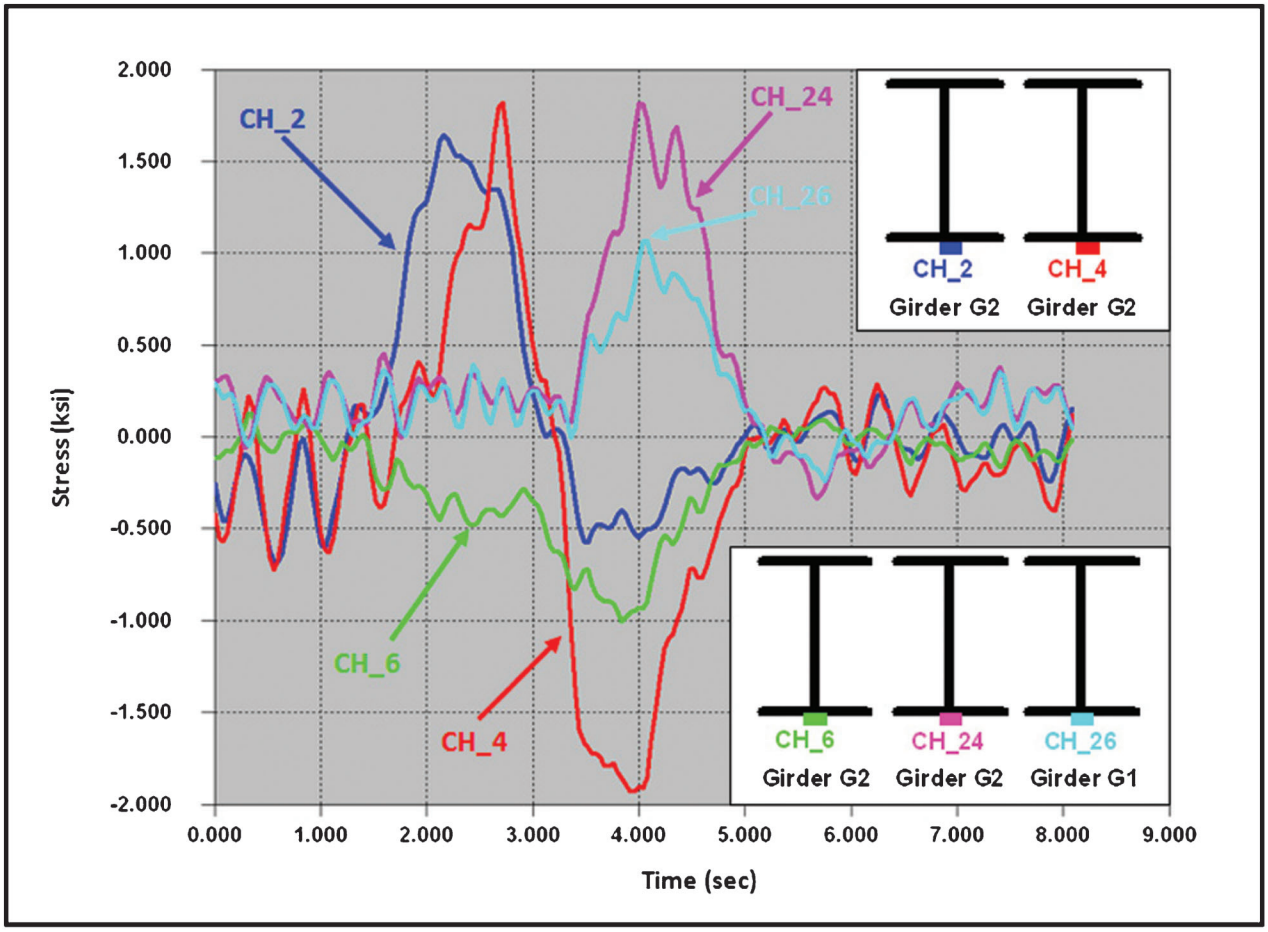

Figure 8.2: Single truck trigger data file

to evaluate the load distribution. CH_24 measures a larger stress by approximately 1.7 ksi indicating the truck is in the right lane. In this same fashion, the data plots can be used to determine the location and type of truck crossing the bridge.

8.1.2 Double Trucks

A more commonly occurring trigger was due to a double truck event. Figure 8.3 shows a video image captured by the video camera mounted on the US-41 White River Bridge during the double truck_1 event. Typically the double truck events consisted of two standard tractor-trailer semi trucks; however, other combinations were also observed to trigger data collection. The plot for the double truck_1 event is shown in Figure 8.4. As expected, the double truck_1 event results in greater stresses than the single standard tractor-trailer. The trigger channel, CH_24 (pink trace), had a maximum stress of approximately 2.8 ksi. CH_4 again had the greatest stress range; however, for the double truck_1 event it increased to 6.8 ksi. Another notable feature of the plot is the load distribution. It would be expected that CH_24 and CH_26 would have identical stresses if both lanes are loaded; however, this is not the case in Figure 8.4. CH_24 has a greater maximum stress by approximately 0.5 ksi. This is likely because the truck in the right lane is heavier. Looking at the photograph, the right truck is a grain truck which was commonly found to trigger data collection themselves. Thus, the most likely reason for the difference in peak stress is the varying weights of the two trucks.

Figure 8.3: Double truck_1 trigger video image

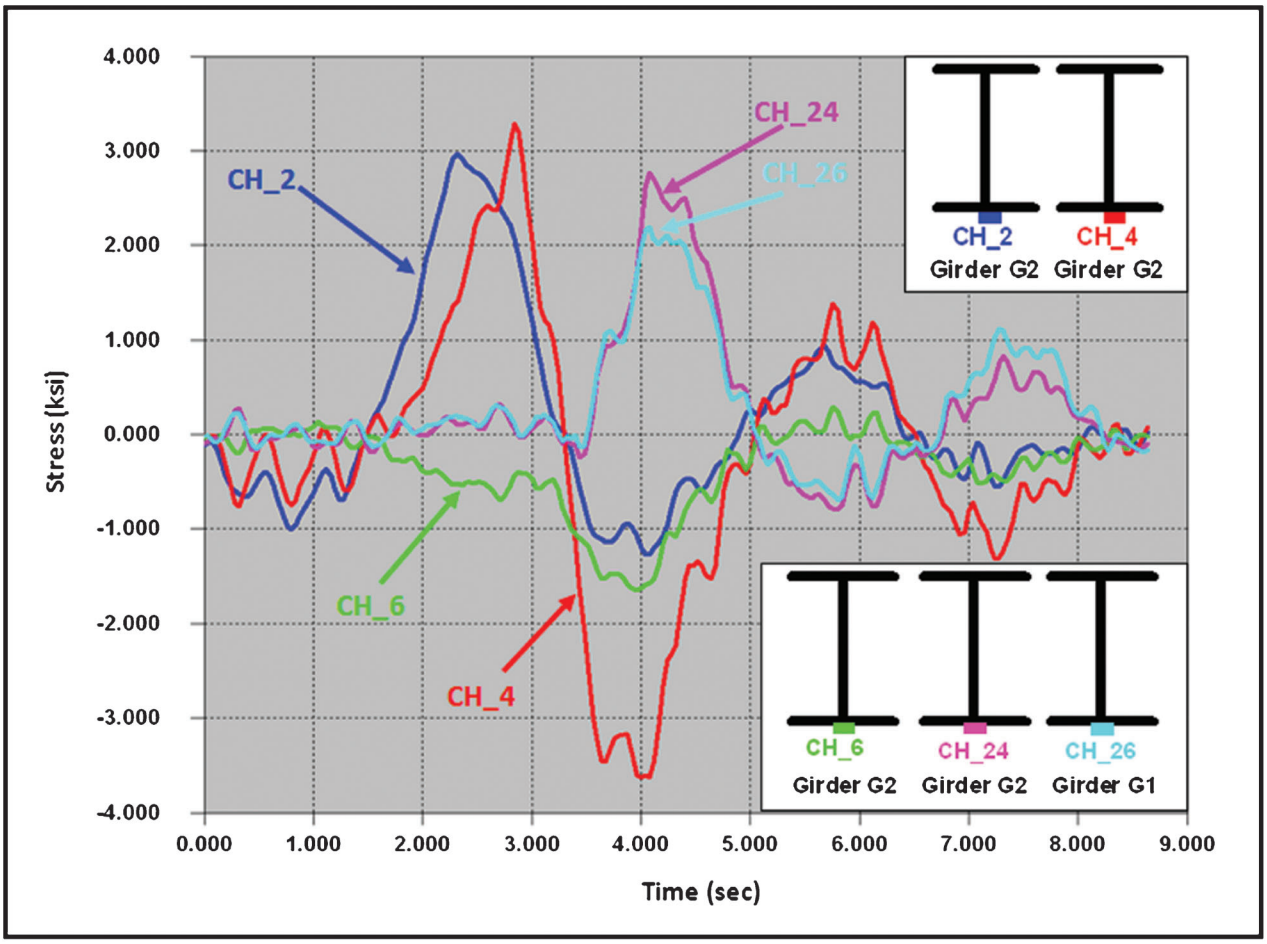

Figure 8.4: Double truck_1 trigger data file

A second double truck event was also included for comparison. Figure 8.5 is a photograph of the double truck_2 trigger event. This event features a standard tractor-trailer box truck in the left lane and a standard tractor-trailer tanker truck in the right lane. The maximum stress for CH_24 during this event was approximately 2.5 ksi as shown in Figure 8.6. This was slightly less than the double truck_1 trigger event. Likewise, the maximum stress range was less as well. CH_4 had a maximum stress range of 6.1 ksi versus 6.8 ksi during the double truck_1 event. However, during the double truck_2 trigger event a more uniform load distribution was observed when comparing CH_24 and CH_26. A difference of less than 0.1 ksi in the maximum stresses was measured. This would suggest that they two trucks captured during the double truck_2 event were of similar load intensity.

Figure 8.5: Double truck_2 trigger video image

8.1.3 Other non-standard vehicles

Beyond standard vehicles, other non-standard vehicles triggered data collection. One such vehicle was the drill unit pictured in Figure 8.7. The drill unit produced stresses greater than a standard tractor-trailer trigger event but less than the double truck trigger events. A plot of the data measured during the drill rig trigger event is shown in Figure 8.8. As can be seen the maximum stress at the trigger channel, CH_24 (pink trace), was approximately 2.3 ksi. As expected, this was between the stress produced during a standard single and double trigger event. Likewise, the maximum stress

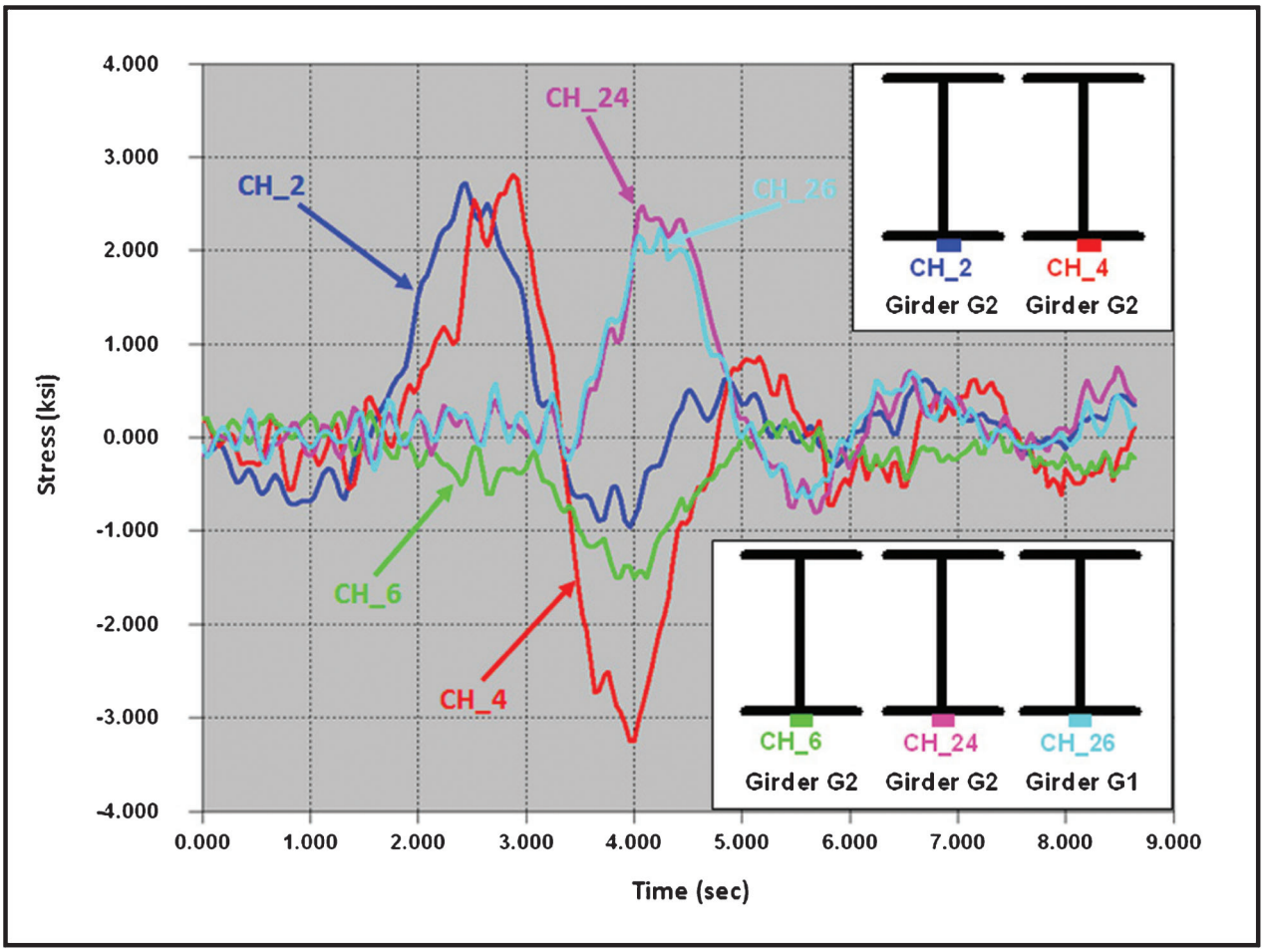

Figure 8.6: Double truck_2 trigger data file

range was also between the two standard events, CH_4 measured a maximum stress range of 5.9 ksi. The load distribution for the drill rig trigger event was similar to the single truck event. Since the drill rig was driving in the right lane, CH_24 measured a greater stress than CH_26.

Figure 8.7: Drill rig trigger video image

Another non-standard trigger event included the off-road crane pictured in Figure 8.9. The crane trigger event produced stresses very similar to the drill rig. This is not surprising as most non-permit vehicles have various restrictions making them conform to similar weights and axle loads. A plot of the data measured during the crane trigger event is included in Figure 8.10. As can be seen, CH_24 (pink trace), had a maximum stress of approximately 2.2 ksi during the crane trigger event versus 2.3 ksi during the drill rig trigger event. The maximum stress range at CH_4 during the crane event was 5.7 ksi versus 5.9 during the drill rig event. Also, as expected, the load distribution was typical for a single vehicle in the right lane (i.e., CH_24 had a greater stress than CH_26).

8.1.4 Superload

Another attractive feature of the video camera was that images from the superload events could also be captured. Figure 8.11 is a photograph taken during the passage of a superload. The data measured for this superload is also included in Figure 8.12. For comparison to normal daily traffic, the maximum stress at the trigger channel, CH_24 (pink trace) was approximately

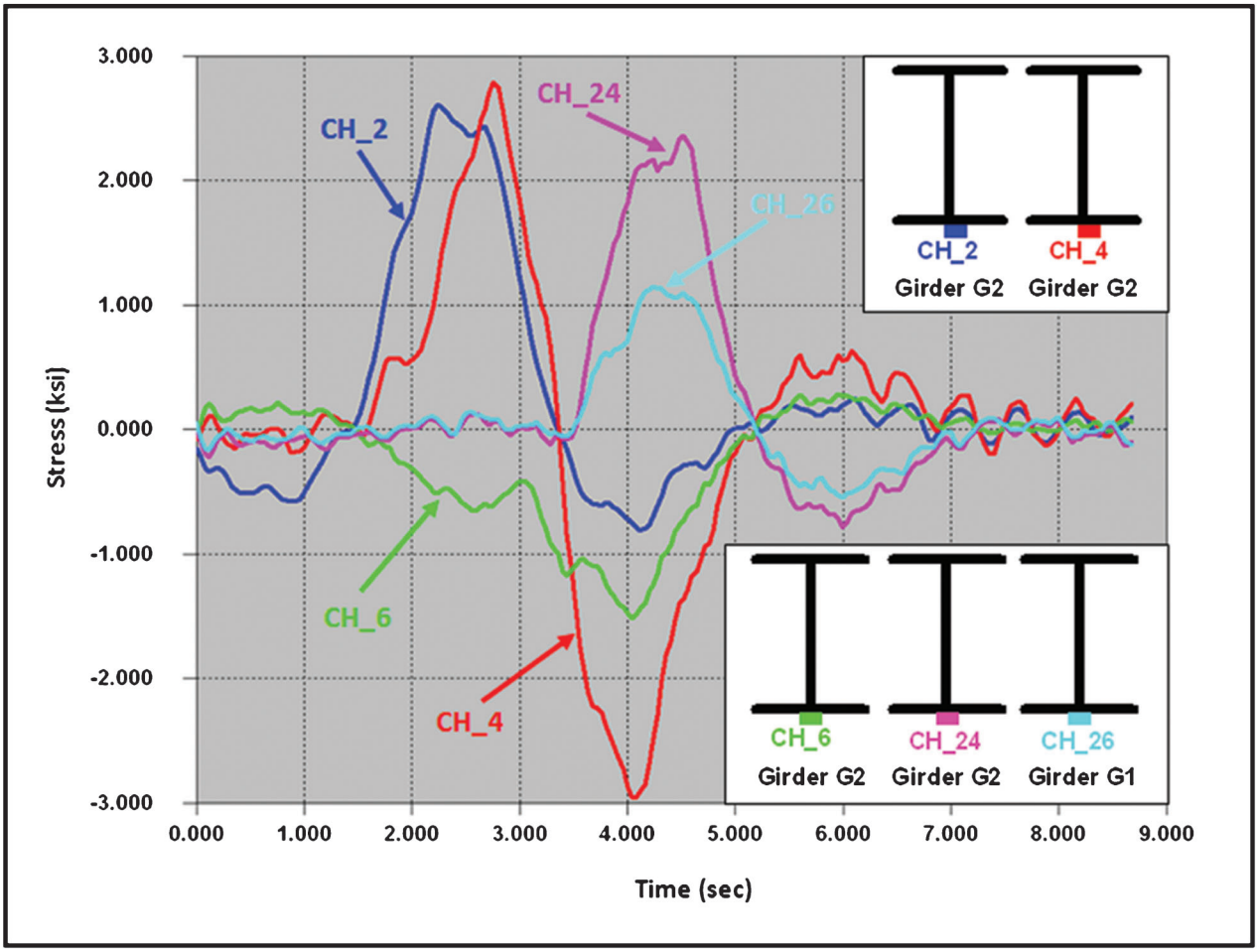

Figure 8.8: Drill rig trigger data file

5.8 ksi. This is over twice as much as a double truck trigger event. The stress range at CH_4 during this superload was just shy of 14.0 ksi which is again over twice that measured during a double truck trigger event. The superload events were discussed in detail during Chapter 5; however, this brief comparison helps to shed some light on how much greater the loading was during a superload event versus standard traffic.

Figure 8.9: Crane trigger video image

8.2 Stress-Range Histograms and Cyclic Evaluation

A fatigue analysis was also performed as part of the long-term monitoring. Rainflow cycle counting was used to create stress range histograms for the twenty-four (24) strain gages included in the long-term monitoring. Combining the stress range histograms with Miner's Rule, the effective stress range was calculated for each strain gage. The effective stress range is commonly used as a single stress range value to compute the expected fatigue life for a variable stress range histogram record. Equation 8.1 shows the equation used to calculate the effective stress range. Lastly, the remaining fatigue life was calculated for each of the long-term monitoring strain gage locations.

$$S_{reff} = \sum \left(f_i * S_{ri}^3\right)^{1/3}$$

Equation 8.1: Effective stress range

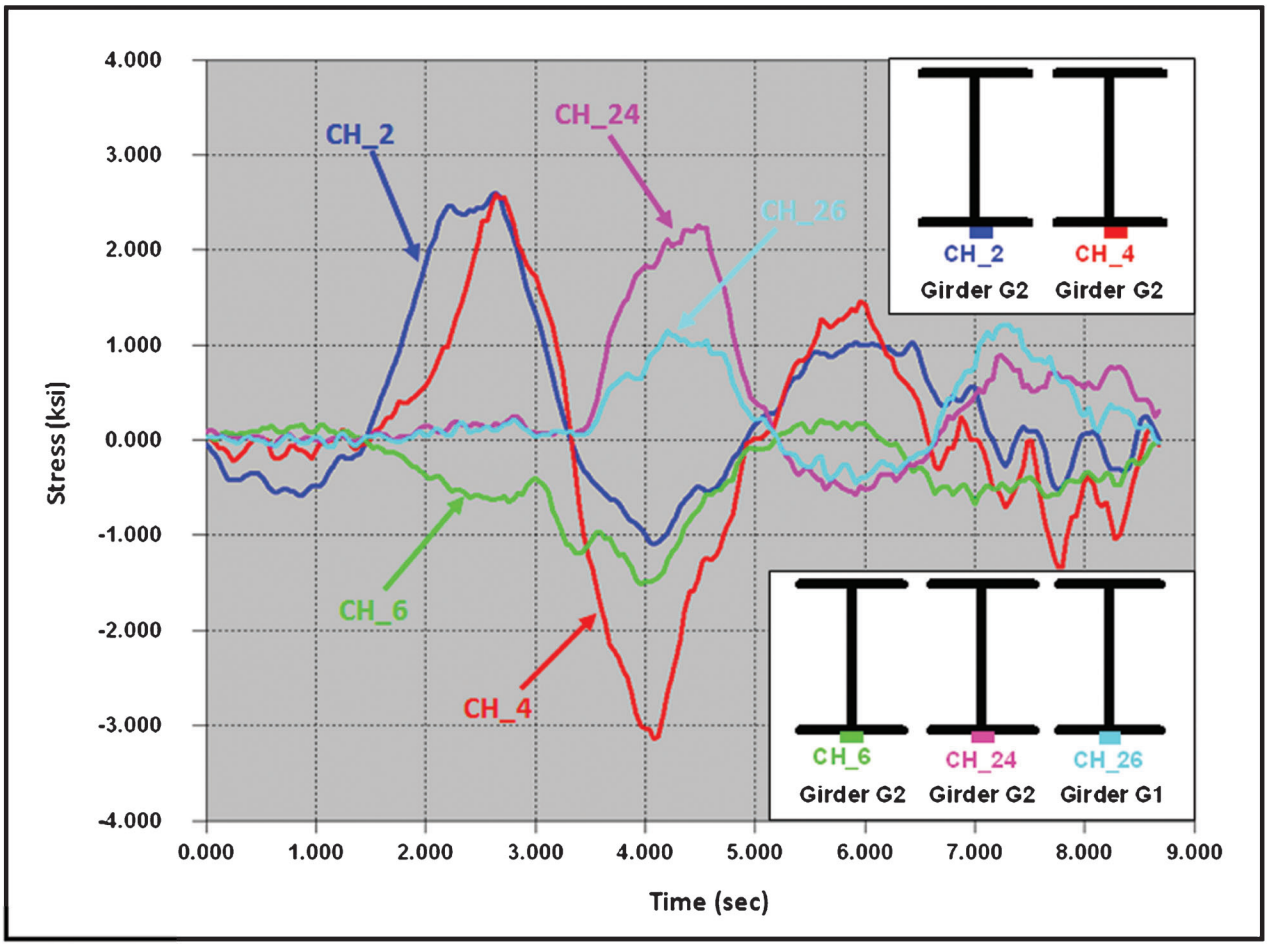

Figure 8.10: Crane trigger data file

Prior to presenting the results from the fatigue evaluation it is important to briefly discuss how the data were analyzed. The data logger used for the US-41 White River Bridge study was capable of creating histograms based on the rainflow cycle counting method. When the stress range histograms were created all bins were equally sized at 0.5 ksi. This is true except for the first bin which disregards all cycles less than 0.25 ksi (i.e., the first bin ranges from 0.25 ksi to 0.5 ksi). The data logger was programmed to perform the rainflow algorithm once every ten minutes and place all cycles in their respective bins for each channel.

Figure 8.11: Superload trigger video image

Once the final histograms were compiled for each strain gage, a truncation was performed based on the AASHTO fatigue category appropriate for the structure detail being monitored. The truncation disregarded all cycles below a given bin. Disregarding the lower bins of a histogram is common practice in a fatigue analysis. This is typically done so the effective stress range is not falsely "pulled down" by the high number of very small stress range cycles. A cutoff value that corresponds to approximately one-eighth up to one-third of the CAFL of a detail is often used. For example, a Category D detail with a CAFL of 7.0 ksi might be truncated such that all cycles less than 1.5 ksi (approximately 20% of the CAFL) are disregarded. The effective stress range for each strain gage was then calculated using Miner's Rule based on the truncated histograms. It should be noted that when calculating the effective stress range the average stress range for the bin is used.

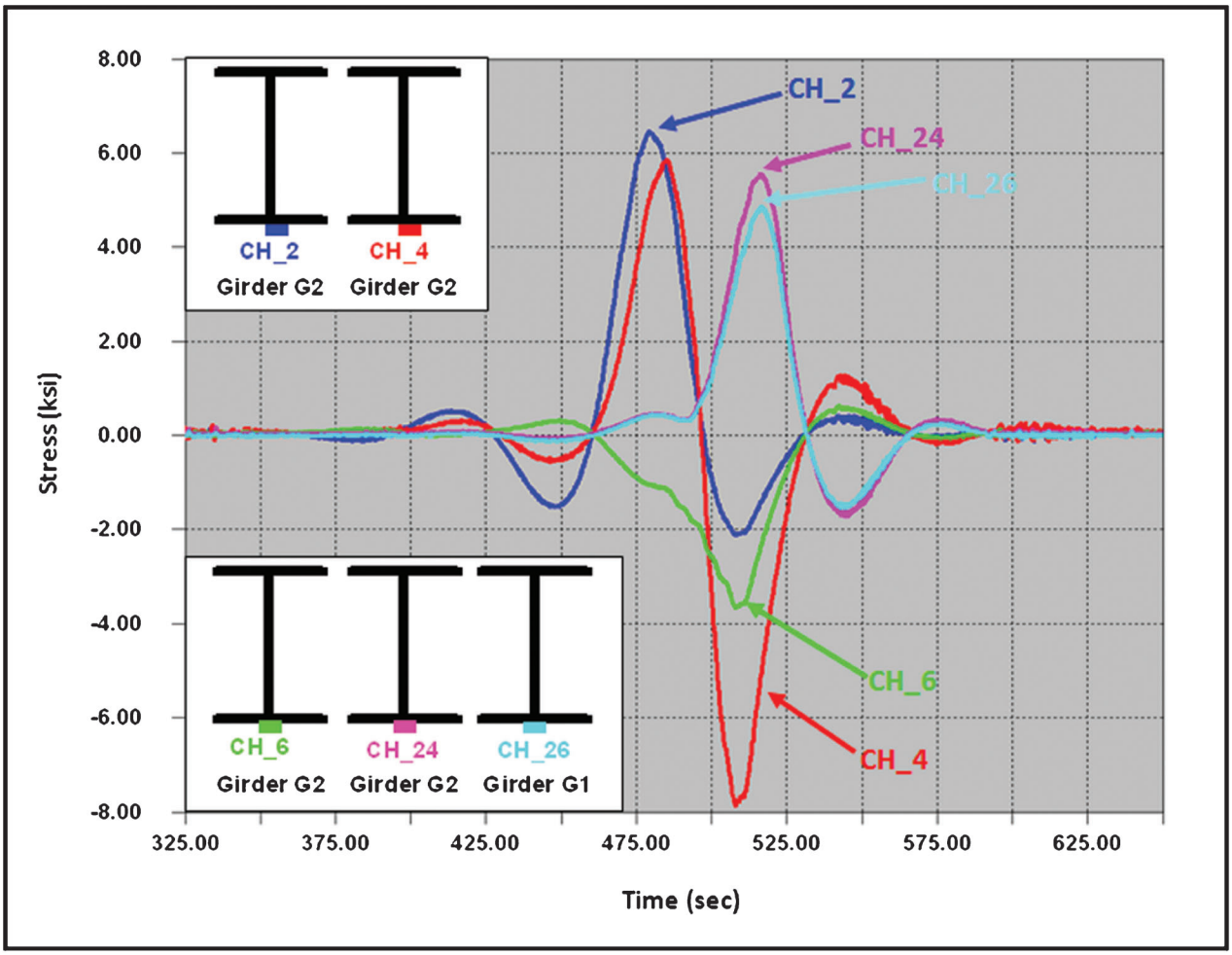

Figure 8.12: Superload trigger data file

Fatigue life estimates were also made for each of the strain gage locations using the effective stress range and truncated histograms. Based on detail category and the truncated histogram of each strain gage the percent of cycles exceeding the CAFL was computed. If the percent of cycles exceeding the CAFL was less than 1:10,000 the detail was determined to have infinite fatigue life; however, if more than 1:10,000 cycles exceeded the CAFL the detail was determined to have finite fatigue life. Dividing the detail constant for a given fatigue category, A, by the stress range, S_r, cubed of a given detail generates the number of cycles to failure as shown in Equation 8.2.

$$N_f = \frac{A}{S_r^3}$$

Equation 8.2: Number of cycles to failure

Combining the daily cycle count, calculated from the total cycle count from the histograms and length of the monitoring period, with the age of the structure, the amount of fatigue life used to date can be tabulated. The difference between the total fatigue life and the amount of fatigue life used to date is the amount of remaining fatigue life as shown in Equation 8.3.

$$N_r = N_f - Age$$

Equation 8.3: Number of cycles remaining

One final important note is that fatigue life estimates can range anywhere from negative years (i.e., the amount of used fatigue life is greater than the available fatigue life) up to thousands of years. Since, no one can accurately predict what will happen to a structure in 100 years, let alone over 1000 years, one of three conclusions is expressed for the remaining fatigue life of a given detail: numerical value up to 100 years, $>$ 100 years, or infinite. As traffic patterns and loading changes over time, it would be advisable to perform another fatigue analysis in approximately 25 years to re-evaluate the life estimates calculated during this study.

8.2.1 Fatigue Evaluation of Main Girders

Seven main girder strain gage locations were included in the long-term monitoring and fatigue

TABLE 8.1:
Stress range histogram for main girders

STRESS RANGE (KSI)	AVERAGE STRESS RANGE (KSI)	CH_2 220.7 Days	CH_4 220.7 Days	CH_5 220.7 Days	CH_6 220.7 Days	CH_12 220.7 Days	CH_24 220.7 Days	CH_26 220.7 Days
0.25 – 0.5	0.375	0	0	0	0	0	0	0
0.5 – 1.0	0.75	0	0	0	0	0	0	0
1.0 – 1.5	1.25	0	0	0	0	0	0	0
1.5 – 2.0	1.75	53,449	70,740	33	1,121	1,214	64,641	6,643
2.0 – 2.5	2.25	60,443	44,917	25	89	102	26,623	1,364
2.5 – 3.0	2.75	8,010	29,851	9	25	20	1,218	207
3.0 – 3.5	3.25	814	40,323	8	11	7	214	27
3.5 – 4.0	3.75	233	30,978	4	11	8	41	6
4.0 – 4.5	4.25	43	3,432	2	9	13	13	3
4.5 – 5.0	4.75	13	852	0	3	9	7	2
5.0 – 5.5	5.25	8	313	0	2	2	1	5
5.5 – 6.0	5.75	7	138	0	1	6	8	11
6.0 – 6.5	6.25	1	55	0	3	5	6	7
6.5 – 7.0	6.75	9	25	0	1	2	10	9
7.0 – 7.5	7.25	9	12	0	0	3	7	4
7.5 – 8.0	7.75	7	10	0	1	0	6	4
8.0 – 8.5	8.25	7	2	0	0	0	3	1
8.5 – 9.0	8.75	5	7	0	0	1	4	1
9.0 – 9.5	9.25	1	1	0	0	0	2	1
9.5 – 10.0	9.75	2	0	0	0	0	0	0
10.0 – 10.5	10.25	0	3	0	0	0	0	0
10.5 – 11.0	10.75	0	6	0	0	0	0	0
11.0 – 11.5	11.25	0	4	0	0	0	0	0
11.5 – 12.0	11.75	0	6	0	0	0	0	0
12.0 – 12.5	12.25	0	4	0	0	0	0	0
12.5 – 13.0	12.75	0	8	0	0	0	0	0
13.0 – 13.5	13.25	0	3	0	0	0	0	0
13.5 – 14.0	13.75	0	11	0	0	0	0	0

evaluation. These include the locations of maximum positive and negative moment as well as the dead load inflection point. The main girder strain gage locations were all AASHTO Category D fatigue details and subsequently have a CAFL of 7.0 ksi. These members were classified as Category D due to the rivets connecting the various members in the built-up section. As discussed above, truncation was performed based on the CAFL. For the main girder all stress cycles less than 1.5 ksi were not included in the fatigue analysis. The histograms presented in Table 8.1 for the main girder strain gages indicate a zero count for these bins. It is important to note that the zero shown in the figure was for the calculation of the effective stress range and the remaining fatigue life; however, the raw data for each of these bins still exists in the actual data files. Also included in the table is the total number of days data were collected at each location.

Using the histograms shown in Table 8.1 fatigue life calculations were performed. Results from the fatigue life calculation can be found in Table 8.2. Table 8.2 includes the detail category, maximum stress range, number of cycles exceeding the CAFL, effective stress range, number of cycles per day, and the remaining

TABLE 8.2:
Summary of fatigue evaluation for main girders

Strain Gage	Detail Category	S_{rmax} (ksi)	Cycles > CAFL #	Cycles > CAFL %	S_{reff} (ksi)	Cycles/day	Remaining Life (years)
CH_2	D	10	31	0.03%	2.1	558	> 100
CH_4	D	17.0*	77	0.03%	2.8	1,005	> 100
CH_5	D	4.5	0	0.00%	2.5	0	Infinite
CH_6	D	8	1	0.08%	2.1	6	> 100
CH_10	D	5.5	0	0.00%	2.1	4	Infinite
CH_12	D	9	4	0.29%	2.2	6	> 100
CH_24	D	9.5	22	0.02%	2.0	421	> 100
CH_26	D	9.5	11	0.13%	2.0	38	> 100

*Determined from time-history results

TABLE 8.3:
Stress range histogram for floor beams

STRESS RANGE (KSI)	AVERAGE STRESS RANGE (KSI)	CH_10 220.7 Days	CH_22 220.7 Days
0.25 – 0.5	0.375	0	0
0.5 – 1.0	0.75	0	0
1.0 – 1.5	1.25	0	0
1.5 – 2.0	1.75	688	2,399
2.0 – 2.5	2.25	79	236
2.5 – 3.0	2.75	37	57
3.0 – 3.5	3.25	24	24
3.5 – 4.0	3.75	11	14
4.0 – 4.5	4.25	12	5
4.5 – 5.0	4.75	1	1
5.0 – 5.5	5.25	1	0
5.5 – 6.0	5.75	0	0
6.0 – 6.5	6.25	0	0
6.5 – 7.0	6.75	0	0
7.0 – 7.5	7.25	0	0
7.5 – 8.0	7.75	0	0
8.0 – 8.5	8.25	0	0
8.5 – 9.0	8.75	0	0
9.0 – 9.5	9.25	0	0
9.5 – 10.0	9.75	0	0
10.0 – 10.5	10.25	0	0
10.5 – 11.0	10.75	0	0
11.0 – 11.5	11.25	0	0
11.5 – 12.0	11.75	0	0
12.0 – 12.5	12.25	0	0
12.5 – 13.0	12.75	0	0
13.0 – 13.5	13.25	0	0
13.5 – 14.0	13.75	0	0

fatigue life. Sufficient fatigue life remains for main girder strain gage locations. CH_4 had the shortest remaining fatigue life of all location monitored; however, it was still well over 100 years. Furthermore, these life estimates are very conservative as the number of super-heavy loadings over this monitoring period is much greater than normal. Therefore, based on the analyzed histograms, it is believed that the main girders of the US-41 White River Bridge will not develop any major fatigue problems in the foreseeable future.

8.2.2 Fatigue Evaluation of Floor Beams

Two floor beam strain gage locations were included in the long-term monitoring and fatigue evaluation. Both strain gages were located at the region of maximum positive moment. Specifically, they were installed at midspan of each floor beam on the bottom flange. Due to the rivets in the area of the floor beam strain gage locations, these locations are classified as an AASHTO Category D fatigue detail; thus, having a CAFL of 7.0 ksi. Like the main girders which also were Category D details, all cycles less than 1.5 ksi were truncated and hence omitted from the fatigue analysis. However, the raw data for the truncated bins is archived in the original data file. Table 8.3 is the resulting histogram for both floor beam strain gage locations including the manually entered zero count for the first three bins. Also included in the table is the total number of days data were collected at each location.

After performing the fatigue life calculation discussed above, it was found that the floor beam has infinite remaining fatigue life. No cycles greater than the CAFL of 7.0 ksi were ever measured as shown in Table 8.3; thus, infinite fatigue life would be expected. Table 8.4 presents the remaining fatigue life and various parameters related to the fatigue life calculations. These include the detail category, effective stress range, percentage of cycles exceeding the CAFL, and number of cycles per day. Also included in the table is the maximum stress range found in the histogram. Based on the stress range histograms collected for the floor beams from the US-41 White River Bridge the floor beams are not believed to have any major fatigue problems in the foreseeable future.

8.2.3 Fatigue Evaluation of Stringers

Seven stringer strain gage locations were included in the long-term monitoring. These included locations of both maximum positive and negative moment. Since the maximum moment stringer strain gages were installed at the center of the stringer away from any fatigue sensitive details and the stringers were rolled sections, these locations were classified as AASHTO Category A fatigue details having a CAFL of 24.0 ksi. Conversely, in the negative moment locations the stringers were connected to the floor beams with bolts. As it is unknown whether or not these bolts are fully pretensioned, it would be conservative to classify them as AASHTO Category D fatigue details with a CAFL of 7.0 ksi. In terms of truncation, the Category D details (CH_13, CH_14, and CH_28) were again truncated at 1.5 ksi. On the other hand, the Category A details (CH_15, CH_16, CH_17, and CH_18) was not truncated because if the standard truncation of one quarter the CAFL was performed no cycles would have remained. The histograms showing the various levels of truncation for each stringer location is presented in

TABLE 8.4:
Summary of fatigue evaluation for floor beams

			Cycles > CAFL				
Strain Gage	Detail Category	S_{rmax} (ksi)	#	%	S_{reff} (ksi)	Cycles/day	Remaining Life (years)
CH_10	D	5.5	0	0.00%	2.1	4	Infinite
CH_22	D	5	0	0.00%	1.9	12	Infinite

TABLE 8.5:
Stress range histogram for stringers

STRESS RANGE (KSI)	AVERAGE STRESS RANGE (KSI)	CH_13 220.7 Days	CH_14 220.7 Days	CH_15 220.7 Days	CH_16 220.7 Days	CH_17 220.7 Days	CH_18 220.7 Days	CH_28 220.7 Days
0.25 – 0.5	0.375	0	0	234,526	163,412	154,047	256,186	0
0.5 – 1.0	0.75	0	0	232,618	137,267	187,943	222,887	0
1.0 – 1.5	1.25	0	0	113,719	38,733	93,255	111,308	0
1.5 – 2.0	1.75	7,389	7,044	90,927	1,584	27,976	105,755	8,687
2.0 – 2.5	2.25	570	461	6,079	186	885	24,729	269
2.5 – 3.0	2.75	75	61	446	24	66	976	37
3.0 – 3.5	3.25	29	27	73	17	20	117	10
3.5 – 4.0	3.75	19	18	17	5	4	30	3
4.0 – 4.5	4.25	16	18	7	3	2	20	0
4.5 – 5.0	4.75	10	15	1	1	1	7	0
5.0 – 5.5	5.25	8	4	2	2	0	1	0
5.5 – 6.0	5.75	4	8	1	0	0	0	0
6.0 – 6.5	6.25	1	4	0	0	0	0	0
6.5 – 7.0	6.75	2	1	0	0	0	0	0
7.0 – 7.5	7.25	0	3	0	0	0	0	0
7.5 – 8.0	7.75	0	0	0	0	0	0	0
8.0 – 8.5	8.25	0	0	0	0	0	0	0
8.5 – 9.0	8.75	0	0	0	0	0	0	0
9.0 – 9.5	9.25	0	0	0	0	0	0	0
9.5 – 10.0	9.75	0	0	0	0	0	0	0
10.0 – 10.5	10.25	0	0	0	0	0	0	0
10.5 – 11.0	10.75	0	0	0	0	0	0	0
11.0 – 11.5	11.25	0	0	0	0	0	0	0
11.5 – 12.0	11.75	0	0	0	0	0	0	0
12.0 – 12.5	12.25	0	0	0	0	0	0	0
12.5 – 13.0	12.75	0	0	0	0	0	0	0
13.0 – 13.5	13.25	0	0	0	0	0	0	0
13.5 – 14.0	13.75	0	0	0	0	0	0	0

Table 8.5. Also included in the table is the total number of days data was collected at each location. It should be noted that the raw data for the zeroed bins has been archived in the original data file.

All the stringer strain gage locations were determined to have sufficient life. Interestingly, only one of the seven strain gages monitored, CH_14, had any cycles greater than the CAFL. Additionally, this was the only stringer location determined to have finite life. Table 8.6 presents a summary of the important parameters from the fatigue life calculation. The table includes the detail category, maximum stress range, effective stress range, percentage of cycles exceeding the CAFL, number of cycles per day, and calculated fatigue life. From the stress range histograms and fatigue life calculations, it is believed that the stringers of the US-41 White River Bridge will not have any major fatigue problems in the foreseeable future.

8.2.4 Fatigue Evaluation of Pin and Hanger

The pin and hanger assemblies were of great interest throughout the monitoring of the US-41 White River Bridge. Seven strain gages were included in the long-term monitoring to determine if bi-axial bending was occurring in the hangers and evaluate the fatigue performance of the hangers. The AASHTO Specification considers a hanger to be a Category E

TABLE 8.6:
Summary of fatigue evaluation for stringers

Strain Gage	Detail Category	S_{rmax} (ksi)	Cycles > CAFL #	Cycles > CAFL %	S_{reff} (ksi)	Cycles/day	Remaining Life (years)
CH_13	D	7	0	0.00%	1.9	37	Infinite
CH_14	D	7.5	3	0.04%	1.9	35	> 100
CH_15	A	6	0	0.00%	1.1	3,074	Infinite
CH_16	A	5.5	0	0.00%	0.8	1,546	Infinite
CH_17	A	5	0	0.00%	1.0	2,104	Infinite
CH_18	A	5.5	0	0.00%	1.2	3,272	Infinite
CH_28	D	4	0	0.00%	1.8	41	Infinite

TABLE 8.7:
Stress range histogram for pin and hanger assembly

STRESS RANGE (KSI)	AVERAGE STRESS RANGE (KSI)	CH_29 220.7 Days	CH_31 220.7 Days	CH_32 220.7 Days	CH_34 204.6 Days	CH_38 220.7 Days	CH_43 220.7 Days	CH_44 220.7 Days
0.25 – 0.5	0.375	0	0	0	0	0	0	0
0.5 – 1.0	0.75	0	0	0	0	0	0	0
1.0 – 1.5	1.25	144,280	86,189	204,859	115,376	224,818	12,728	89,347
1.5 – 2.0	1.75	88,924	30,205	64,681	14,447	69,621	1,152	9,726
2.0 – 2.5	2.25	20,902	1,561	14,285	4,354	21,286	109	1,888
2.5 – 3.0	2.75	499	109	1,647	927	3,293	21	104
3.0 – 3.5	3.25	60	30	206	120	619	16	11
3.5 – 4.0	3.75	19	21	47	59	128	12	6
4.0 – 4.5	4.25	16	14	18	27	35	10	12
4.5 – 5.0	4.75	7	14	11	23	16	4	10
5.0 – 5.5	5.25	3	8	13	6	11	2	12
5.5 – 6.0	5.75	0	3	14	7	9	0	4
6.0 – 6.5	6.25	0	4	5	0	13	0	1
6.5 – 7.0	6.75	0	0	1	0	10	0	0
7.0 – 7.5	7.25	0	0	1	0	10	0	0
7.5 – 8.0	7.75	0	0	0	0	6	0	0
8.0 – 8.5	8.25	0	0	0	0	2	0	0
8.5 – 9.0	8.75	0	0	0	0	0	0	0
9.0 – 9.5	9.25	0	0	0	0	0	0	0
9.5 – 10.0	9.75	0	0	0	0	0	0	0
10.0 – 10.5	10.25	0	0	0	0	0	0	0
10.5 – 11.0	10.75	0	0	0	0	0	0	0
11.0 – 11.5	11.25	0	0	0	0	0	0	0
11.5 – 12.0	11.75	0	0	0	0	0	0	0
12.0 – 12.5	12.25	0	0	0	0	0	0	0
12.5 – 13.0	12.75	0	0	0	0	0	0	0
13.0 – 13.5	13.25	0	0	0	0	0	0	0
13.5 – 14.0	13.75	0	0	0	0	0	0	0

fatigue detail. In all actuality a hanger is nothing more than a plate with a hole when considering stress concentration. AASHTO classifies a plate with a hole as a Category D detail. Nevertheless, for this evaluation, the AASHTO designation of Category E with a CAFL of 4.5 ksi was used. Therefore, all cycles less than 1.0 ksi are truncated during the fatigue analysis.

Table 8.7 shows the histograms for the seven hanger strain gage locations. The table shows the truncation performed for each of these channels. Also included in the table is the total time in days data were collected at each location. It should also be noted that the data from the truncated channels has been archived in the original data file should this data be required in the future.

Following the procedure outline at the beginning of the fatigue discussion, the remaining fatigue life for each hanger was calculated. Table 8.8 presents calculated remaining fatigue life as well as several important parameters used during the fatigue life calculation. These include the detail category, effective stress range, percentage of cycles exceeding the CAFL, and number of cycles per day. The table also includes the maximum stress range measured. The calculations indicated all seven hanger locations have sufficient fatigue life. Interestingly, only one hanger was determined to have infinite fatigue life. However, it should again be noted that these calculations are very conservative for a couple of reasons: the larger number of super-heavy

TABLE 8.8:
Summary of fatigue evaluation for pin and hanger

Strain Gage	Detail Category	S_{rmax} (ksi)	Cycles > CAFL #	Cycles > CAFL %	S_{reff} (ksi)	Cycles/day	Remaining Life (years)
CH_29	E	5.5	10	0.00%	1.6	1,154	Infinite
CH_31	E	6.5	29	0.02%	1.4	535	> 100
CH_32	E	7.5	45	0.02%	1.5	1,295	> 100
CH_34	E	6	36	0.03%	1.4	662	> 100
CH_38	E	8.5	77	0.02%	1.5	1,450	> 100
CH_43	E	5.5	6	0.04%	1.4	64	> 100
CH_44	E	6.5	27	0.03%	1.4	458	> 100

TABLE 8.9:
Stress range histogram for cross-bracing

STRESS RANGE (KSI)	AVERAGE STRESS RANGE (KSI)	CH_48
		220.7 Days
0.25 – 0.5	0.375	0
0.5 – 1.0	0.75	0
1.0 – 1.5	1.25	0
1.5 – 2.0	1.75	44,460
2.0 – 2.5	2.25	2,141
2.5 – 3.0	2.75	236
3.0 – 3.5	3.25	35
3.5 – 4.0	3.75	10
4.0 – 4.5	4.25	3
4.5 – 5.0	4.75	10
5.0 – 5.5	5.25	8
5.5 – 6.0	5.75	8
6.0 – 6.5	6.25	7
6.5 – 7.0	6.75	5
7.0 – 7.5	7.25	3
7.5 – 8.0	7.75	2
8.0 – 8.5	8.25	0
8.5 – 9.0	8.75	0
9.0 – 9.5	9.25	0
9.5 – 10.0	9.75	0
10.0 – 10.5	10.25	0
10.5 – 11.0	10.75	0
11.0 – 11.5	11.25	0
11.5 – 12.0	11.75	0
12.0 – 12.5	12.25	0
12.5 – 13.0	12.75	0
13.0 – 13.5	13.25	0
13.5 – 14.0	13.75	0

events as well as the conservative use of a more severe fatigue category. Based on the measured and calculated data, the pin and hanger assemblies on the US-41 White River Bridge are believed to not have any major fatigue problems in the foreseeable future.

8.2.5 Fatigue Evaluation of Cross-bracing

During the long-term monitoring, the response from only one of four strain gages on the cross-bracing of the US-41 White River Bridge was measured. Based upon a preliminary review of strain data, the Research Team determined the cross-bracing was acting as expected; thus, it was decided to keep channels on more critical details during the long-term monitoring phase. Nevertheless, one strain gage was included to monitor any long-term changes of the cross-bracing. The stress range histogram from this remaining strain gage can be found in Table 8.9.

As can be seen in the table all cycles less than 1.5 ksi were truncated. This was based on the bolted connection at the gusset plate near the cross-bracing strain gages. Typically, AASHTO classifies fully pretensioned bolts as a Category B fatigue detail; however, since it is unknown whether these bolts are fully pretensioned or not Category D was conservatively assumed. All the truncated bins have been archived in the original data file should this data be required at a later time. Additionally, the total monitoring period in days is included in the table.

Using the stress range histogram and Category D assumption, the remaining fatigue life was calculated for the cross-bracing. A summary of key values used for this calculation can be found in Table 8.10. The remaining fatigue life can also be found in this table. Sufficient fatigue life was calculated for this detail. Thus, it is believed that the US-41 White River Bridge will not have any major fatigue problems with the cross-bracing in the foreseeable future.

9. SUMMARY AND CONCLUSIONS

The following section provides a summary of the project and results from the controlled load testing, analytical work, super-heavy loading evaluation, and fatigue assessment conducted as part of a study of the US-41 White River Bridge in Hazelton, IN over a period from August 2009 to September 2010. Finally, this section concludes with some suggested action items to be performed on the US-41 White River Bridge based on the results obtained during this study.

Instrumentation Plan

1. The primary intent of the monitoring was to capture live load stress ranges in predetermined areas of interest:

a. Main girder locations of maximum positive and negative moment
b. Main girder dead load inflection point
c. Pin and hanger assemblies
d. Other non-fracture critical primary members (i.e., floor beams and stringers)
e. Cross-bracing

2. Original instrumentation consisted of forty-eight (48) uni-axial, weldable, resistance-type strain gages installed on the northbound superstructure in Spans N and P. The strain gages were distributed as follows:

a. Main girders – 12 strain gages
b. Floor beams – 6 strain gages
c. Stringers – 10 strain gages

TABLE 8.10:
Summary of fatigue evaluation for cross-bracing

Strain Gage	Detail Category	S_{rmax} (ksi)	Cycles > CAFL		S_{reff} (ksi)	Cycles/day	Remaining Life (years)
			#	%			
CH_48	D	8	5	0.01%	1.8	213	> 100

d. Pin and hangers – 16 strain gages
e. Cross-bracing – 4 strain gages

3. For the long-term monitoring, the original forty-eight (48) strain gages were reduced to the twenty-four (24) most critical strain gages. The strain gages were distributed as follows:

a. Main girders – 7 strain gages
b. Floor beams – 2 strain gages
c. Stringers – 7 strain gages
d. Pin and hangers – 7 strain gages
e. Cross-bracing – 1 strain gages

4. All data were originally collected and stored at the bridge. At predefined intervals the data were automatically downloaded to a server residing at Purdue University.
5. Video monitoring was also used in conjunction with the strain measurements to observe the type of vehicle(s) causing a given response.

Controlled Load Testing

1. Four fully loaded plow trucks were used during the controlled load testing, with a total combined weight of 237,000 pounds.
2. Four static park tests and two crawl tests (~5 mph) were performed.
3. Full composite action was developed between the steel main girders and the concrete deck. It is believed that the rivet heads of the main girder were effective in reducing the slip at the contact surface between the two materials.
4. Excellent load distribution was observed at the locations on the main girder where both primary girders were instrumented. As expected for a two girder bridge, approximately half the load was distributed to each girder for both lanes loaded, and more load was to be distributed to the closest adjacent girder than the opposite girder when one lane was loaded.
5. The steel stringers showed signs of some partial composite interaction with the concrete deck. However, the interaction was not significant or consistent enough to rely upon during analysis.
6. Local bending effects were measured at the stringer strain gage locations due to individual axles crossing over the strain gage.
7. Bending was observed in all four of the instrumented hangers. However, each of the hangers demonstrated a different degree of bending during the tests.
8. Temporary displacement was noted in the pin and hangers once the trucks exited the bridge. Like the bending, the temporary displacement varied depending on the freedom of each individual hanger.
9. Based on the results from the controlled load testing the most critical strain gages from the original forty-eight (48) strain gages were identified and the inventory of active strain gages was reduced to twenty-four (24) critical strain gages for long term monitoring.

Analytical Studies

1. A simple two-dimensional frame section model was constructed of the east-most primary girder of the US-41 White River Bridge. The model was used for an influence line analysis and to predict stresses based on the controlled load testing
2. The influence line analysis was performed to determine the optimal locations for the test trucks during the controlled load testing. The intent was to maximize the response at the strain gage locations of interest.
3. Stresses computed based on the analytical model were compared to those measured during the field testing. It was found that the model typically over predicted the stress at any given location. The explanation for this behavior is that the model does not account for other load carrying elements of the bridge such as the stringers and parapets.

Fracture Evaluation

1. CVN and hardness testing were performed on material samples removed from the US-41 White River Bridge. The CVN testing revealed that the bridge has very low material toughness; thus, an in-depth fracture evaluation was undertaken.
2. A critical crack size of approximately 3/8″ was calculated based on the CVN results, loading measurements, and assumed dead load stresses.
3. The critical flaw size was nearly identical to the amount of material covered by a rivet head. Thus, Wiss, Janney, Elstner, Inc. (WJE) was contracted to remove 214 rivets from selected areas of high stress and inspect the base metal for any cracks or defects using magnetic particle inspection techniques. No cracks were found as a result of the investigation performed by WJE.
4. Results of the fracture evaluation suggest fracture is not likely to occur for the US-41 White River Bridge.
5. A minimum operating temperature of 10° Fahrenheit was established for the passage of superloads after the evaluation.

Super-Heavy Loading Evaluation

1. Many of the same conclusions reached during the controlled load testing were echoed during the super-heavy loading evaluation. In most cases, the response for the superloads was simply a scaled response of the controlled load testing. This suggests two things:

a. The US-41 White River Bridge is very stiff and the measured stresses were very small. In no case was a maximum stress induced that was large enough to cause inelastic response of the bridge elements.
b. The super-heavy loads were well distributed over a long length and with many axles. This in turn greatly reduced the local impact at any specific location.

2. The composite action measured between the main girders and concrete deck during the passage of normal daily traffic and controlled load tests was also present during the passage of all superloads. Thus, it was not lost as a result of the multiple super heavy loadings.
3. Consistent composite action between the steel stringers and concrete deck was not measured during the super-heavy loads. Therefore, the intermit interaction at this location was not considered during analysis.

4. The pin and hanger assemblies continued to demonstrate bending and temporary displacement throughout the super-heavy passages. No noticeable difference was observed as multiple superloads crossed the bridge.

Long-Term Monitoring

1. Using a rainflow cycle counting algorithm, stress range histograms were computed for all twenty-four (24) long-term monitoring strain gages. From these histograms the effective stress range at each location was tabulated. Based on the effective stress range and cycle count the remaining fatigue life for each detail was calculated.
2. All twenty-four (24) long-term monitoring strain gage locations were determined to have sufficient or infinite fatigue life. Consequently, it is believed that the US-41 White River Bridge will have no major fatigue problems in the foreseeable future.
3. As traffic patterns and loading changes over time and the condition of the structure deteriorates, it is advisable to perform another fatigue analysis in approximately 25 years to re-evaluate the life estimates calculated during this study.

Suggested Future Actions

1. Inspect all pin and hanger assemblies for cracks using an appropriate inspection and evaluation technique.
2. Bending and temporary displacement of the pin and hanger assembly was consistently measured throughout the monitoring period. Consequently, all pin and hanger joints should be thoroughly greased to promote free movement and minimize bending stress effects.

APPENDIX A – INSTRUMENTATION PLANS

APPENDIX B – RIVET REMOVAL PLAN

APPENDIX C – API 579-1 EQUATION C.108

REFERENCES

American Petrolium Institute (API). (2007). *Fitness-For-Service Manual.* API 579-1/ASME FFS-1. Washington, D.C.

British Standards Institution. (2005). *Guide to Methods for Assessing the Acceptability of Flaws in Metallic Structures.* BS 7910:2005. The British Standards Institution, London

Broek, D. (1988). *The Practical Use of Fracture Mechanics.* Dordrecht, Netherlands

Grandt Jr., A.F. (2004). Fundamentals of Structural Integrity: Damage Tolerant Design and Nondestructive Evaluation. Hoboken, NJ.

Shukla, A. (2005). Practical Fracture Mechanics in Design: Second Edition, Revised and Expanded. New York, NY.